Modeling landslide hazard in the Esino River Valley

(central Italy)

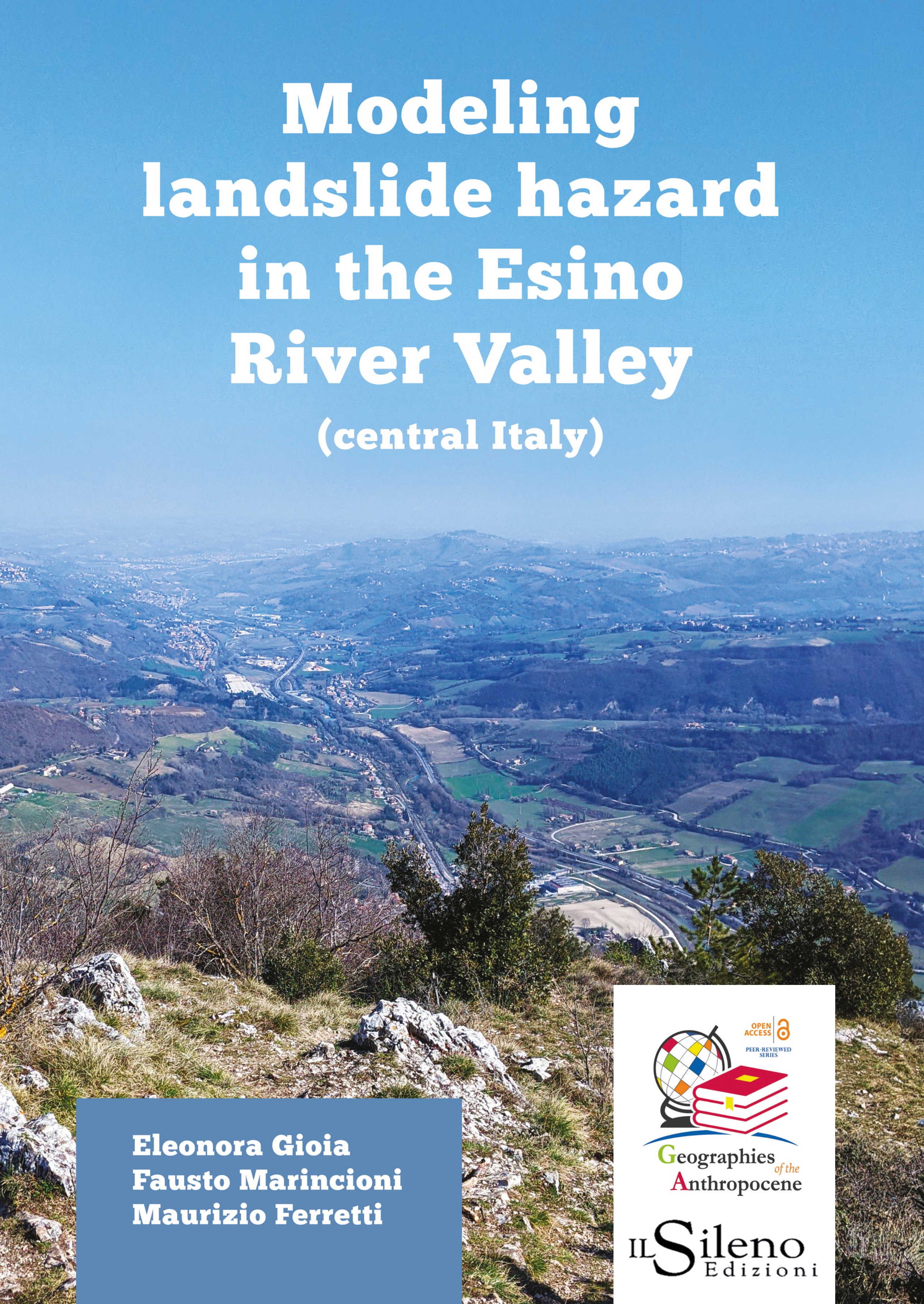

Eleonora Gioia
Fausto Marincioni
Maurizio Ferretti

OPEN ACCESS
PEER-REVIEWED SERIES
Geographies of the Anthropocene

IL Sileno Edizioni

Modeling landslide hazard in the Esino River Valley (central Italy)

Eleonora Gioia[1]
Fausto Marincioni[1]
Maurizio Ferretti[2]

[1]Department of Life and Environmental Sciences,
Università Politecnica delle Marche, Ancona, Italy
[2]P.F. Sistema Integrato delle Emergenze ARS,
Regione Marche, Ancona, Italy

E-mail: e.gioia@univpm.it / f.marincioni@univpm.it /
maurizio.ferretti@regione.marche.it

Corresponding author: Eleonora Gioia

OPEN ACCESS
PEER-REVIEWED SERIES
Geographies of the Anthropocene

IL Sileno Edizioni

Modeling landslide hazard in the Esino River Valley (central Italy)

Eleonora Gioia, Fausto Marincioni, Maurizio Ferretti

is a monographic volume of the Open Access and peer-reviewed series "Geographies of the Anthropocene"

(Il Sileno Edizioni), ISSN 2611-3171.

www.ilsileno.it/geographiesoftheanthropocene/

Cover: Esino River Valley view from Monte Murano, Marche, Italy
(photo: Eleonora Gioia; graphic design: Camilla Ninivaggi)

ISBN 979-12-80064-11-0
March 2021
(First Edition)

OPEN ACCESS
PEER-REVIEWED SERIES
ISSN 2611-3171

Geographies of the Anthropocene

Open Access and Peer-Reviewed series

Website: www.ilsileno.it/geographiesoftheanthropocene;

The book series "Geographies of the Anthropocene" edited by Association for Scientific Promotion "Il Sileno" (Il Sileno Edizioni) will discuss the new processes of the Anthropocene epoch through the various worldviews of geoscientists and humanists, intersecting disciplines of Geosciences, Geography, Geoethics, Philosophy, Socio-Anthropology, Sociology of Environment and Territory, Psychology, Economics, Environmental Humanities and cognate disciplines.

Geoethics focuses on how scientists (natural and social), arts and humanities scholars working in tandem can become more aware of their ethical responsibilities to guide society on matters related to public safety in the face of natural hazards, sustainable use of resources, climate change and protection of the environment. Furthermore, the integrated and multiple perspectives of the Environmental Humanities, can help to more fully understand the cultures of, and the cultures which frame the Anthropocene. Indeed, the focus of Geoethics and Environmental Humanities research, that is, the analysis of the way humans think and act for the purpose of advising and suggesting appropriate behaviors where human activities interact with the geosphere, is dialectically linked to the complex concept of Anthropocene.

The book series "Geographies of the Anthropocene" publishes online volumes, both collective volumes and monographs, which are set in the perspective of providing reflections, work materials and experimentation in the fields of research and education about the new geographies of the Anthropocene.

"Geographies of the Anthropocene" encourages proposals that address one or more themes, including case studies, but welcome all volumes related to the interdisciplinary context of the Anthropocene.
Published volumes are subject to a review process (**double blind peer review**) to ensure their scientific rigor.

The volume proposals can be presented in English, Italian, French or Spanish.

The choice of digital Open Access format is coherent with the flexible structure of the series, in order to facilitate the direct accessibility and usability by both authors and readers.

Abstract

Modeling landslide hazard is among the forecast activities of the Civil Protection system. Usually, scientific literature that aims to determine rainfall thresholds for the possible occurrence of landslides, tends to rely on two main separate approaches: empirical and physical models. This research contributes to such debate by adopting both the approaches, after integrating some of the each other features. This novel methodology has been applied to the landslides affecting the eastward Esino River Valley, located in the Marche region (central Italy). Post-orogenic quaternary sediments, with approximatively similar hydrogeological properties and prone to rainfall-induced shallow landslides, characterize this 550 km2 wide area.
This volume is divided in four sections focusing on: i) the validation of the correlation between historical landslides and rainfall series; ii) the application of empirical models, namely the cumulative event – duration, the maximum intensity – duration, the mean intensity – duration, and the Bayesian methods; iii) the application of the US Geological Survey’s Transient Rainfall Infiltration and Grid-based Regional Slope-stability (TRIGRS) physical model; iv) the testing of all the above models, during a rainfall event that affected the study area on 2-4 May 2014 and triggered several landslides.
Results of this research are proposed as possible decision support tools for landslide warning.

Keywords

Landslides, landslide forecast, empirical model, physical model, Italy.

CONTENTS

1 Introduction

1.1 Landslide hazard

The general term “landslide” is used to describe a wide variety of processes that result in the downslope movement of soil, rock, organic material or artificial fill, or a combination of these, under the effect of gravity (Cruden, 1991; Cruden and Varnes, 1996). “Landslide hazard” is defined as the probability, for a potentially damaging landslide of a given magnitude, to occur within a given area and within a given period of time (Varnes, 1984). This definition refers to (i) the dimension and destructive power of the phenomenon, (ii) the geographical location where it may occur, and (iii) the time recurrence of the event (Guzzetti et al., 1999).

TYPE OF MOVEMENT		**TYPE OF MATERIAL**		
		BEDROCK	**ENGINEERING SOILS**	
			Predominantly coarse	**Predominantly fine**
FALLS		Rock fall	Debris fall	Earth fall
TOPPLES		Rock topple	Debris topple	Earth topple
SLIDES	ROTATIONAL	Rock slide	Debris slide	Earth slide
	TRANSLATIONAL			
LATERAL SPREADS		Rock spread	Debris spread	Earth spread
FLOWS		Rock flow (deep creep)	Debris flow (soil creep)	Earth flow (soil creep)
COMPLEX: Combination of two or more principal types of movement				

Table 1 Types of landslides. Simplified version of Varnes (1978) classification (EU-FP7, 2012).

Landslides can be classified into different types based on the slope movement mechanism and rate, the material involved, the mechanical behavior, or the movement stage. Among all the classifications proposed in literature (e.g. Varnes 1978; Hutchinson 1988; Leroueil 2001; Hungr et al. 2013), the most widespread is the work of Varnes (1978), modified in Cruden and Varnes (1996). They proposed a taxonomy that mainly considers the types of movement at the initial stage of the motion and the material (Table 1).

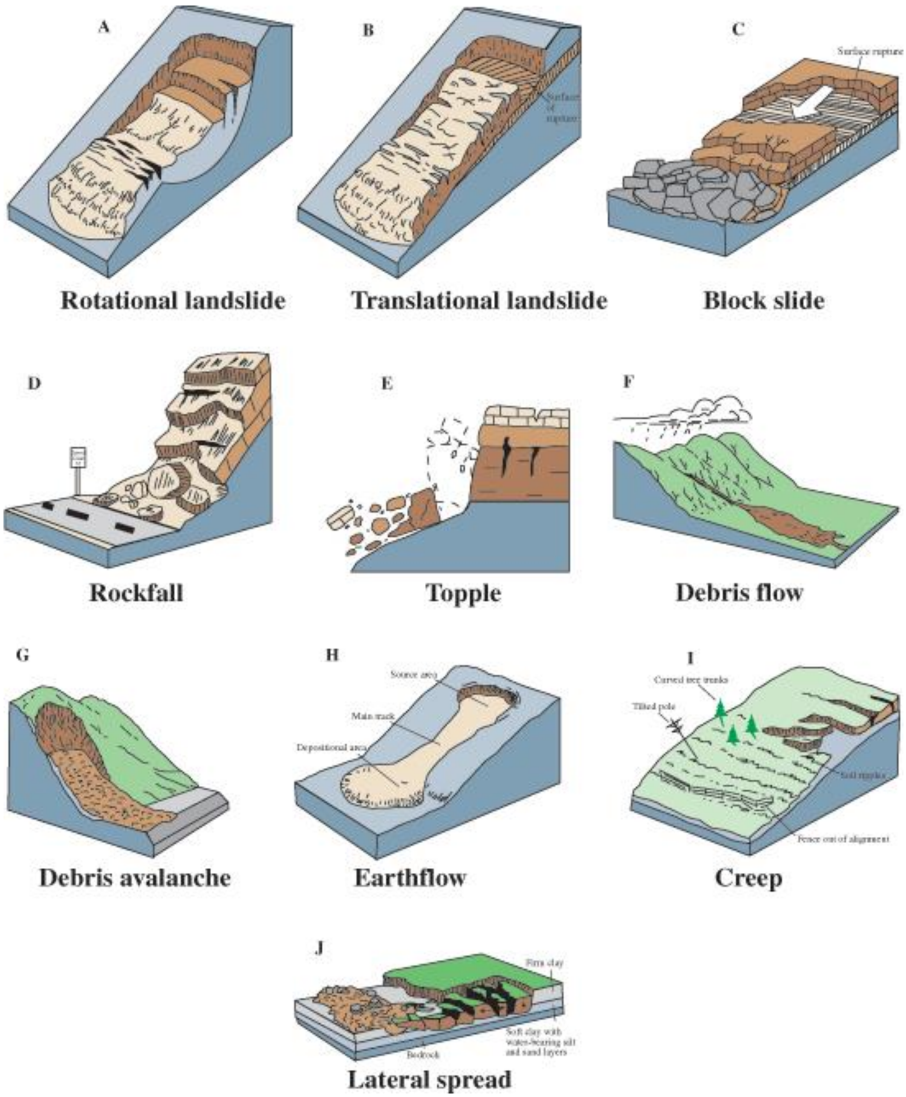

Figure 1 These schematics illustrate some of the most common types of landslide movements (U.S. Geological Survey, 2004).

The type of movement is governed by the mechanical internal behavior of the material involved and by the displacement of the landslide mass: fall, topple, slide, spread, or flow. The material in a landslide mass is considered either rock or soil (or both); the latter is described as debris if composed of coarse fragments and earth if mainly composed of sand-sized or finer particles. Thus, landslides are described using two terms that refer respectively to material and movement (i.e., rock fall, debris flow, and so forth) (Figure 1). A combination of two or more types of movement is called a complex landslide.

The traditional viewpoint that landslides are restricted to extremely steep slopes and inhospitable terrain does not reflect the real nature of the problem. Slope failures affect both dry and humid areas, and most important, steep slopes are not a prerequisite for landslides to occur. In fact, landslides affect most countries in the world (International Geotechnical Societies UNESCO Working Party on World Landslide Inventory (WP/WLI), 1993). The reason for such wide geographic coverage has to do with the many different triggering mechanisms.

Landslides are caused by different processes and characteristics that can be arranged in four groups: (i) geological causes (weak, sensitive, weathered, or sheared materials, contrast in permeability or in stiffness); (ii) morphological causes (fluvial, glacial or wave erosion of slope toe, tectonic or volcanic uplift, erosion of lateral margins; (iii) physical causes (intense rainfall, snowmelt, prolonged or exceptional precipitation, rapid drawdown of floods and tides, earthquake, volcanic eruption, thawing); and (iv) human causes (deforestation, irrigation, mining, artificial vibration, water leakage, land use changes) (Alexander, 1992; Cruden and Varnes, 1996; Leroueil, 2001). The predisposing factors of a landslide are intrinsic of the local specific conditions such as slope angle, soil thickness, slope exposure, slope curvature, land use, hydraulic conditions, historical landslides, geomorphological units, lithology, tracks and man-made cuts (Di Crescenzo et al., 2008; Pereira et al., 2012). A different meaning assumes the term “trigger” which commonly refers to “an external stimulus that causes a near-immediate response in the form of a landslide by rapidly increasing the stresses, or by reducing the strength of slope materials” (Wieczorek, 1996). Landslide main natural triggering factors are:

i. rainfall, in many cases particularly intense or prolonged thunderstorms, or a combination of both;
ii. erosion, caused by the undercutting of the slope due to a river, especially during a flood, by bank and lateral erosion in coastal settings, especially within clay slopes and fissured material, or by surface erosion due to water flow;
iii. snowmelt, caused by a sudden increase of temperature, that leads to rapid melting of the snow pack, infiltration of the water into the ground and a rather rapid increase of soil pore pressure;

iv. weathering of the bedrock, causing the reduction of material strength and the creation of a regolith layer, weaker than the parent rock, which may slide;
v. earthquake, which increases the likelihood of landslides occurrence, due to the ground shaking itself or to the induced dilation of soil materials, allowing rapid infiltration of water right afterwards;
vi. volcanism, usually magmatic intrusions and phreatic explosions in volcanic edifices or volcanic debris flows (also known as lahars) constituted by a deluge of rock, soil, ash, and water.

As mentioned, each of these factors can cause decrease in shear strength of the slopes or increase in driving shear stress (Leroueil, 2001). The processes pertaining to the first category are e.g. infiltration due to rainfall, snowmelt, irrigation, leakage, and weathering. The processes pertaining to the second category are e.g. erosion or excavation at the toe of the slope, surcharging at the top, rapid drawdown, impulsive loading, and earthquakes.

The wide variety of geosystems and geomaterials, the intrinsic difficulty in obtaining complete and reliable knowledge of the initial conditions of the slope, the complex behavior of materials over time and space, and the numerous possible climate conditions make extremely complex the discipline of landslide forecasting. However, the identification and modelling of the processes that may trigger failures of natural slopes form an essential part of landslide hazard and risk assessment studies.

1.1.1 Landslide hazard in Italy

Landslide hazard is an extremely widespread problem throughout Italy. The increasing incidence of catastrophic events corresponds to a progressive increase of the built environment and expansion of the urban settlements, which affected the country after the World War II, often in hazardous areas (APAT - Dipartimento Difesa del Suolo, 2007; Consiglio Nazionale dei Geologi, 2010). For this reason, the interest in such issue has constantly grown, leading to several studies and surveys.

In Italy, the first systematic study on landslides performed by Almagià (1910) for the Italian Geographic Society dates back to 1910, but in the eighties the research experiences a major boost.

In 1987, the National Agency for New Technologies, Energy and Sustainable Economic Development (ENEA) commissioned to a research group the three-year project GIANO, regarding the collection, analysis, processing, and

interpretation of historical information on the effects produced by extreme natural events in Italy, from the year 1000 to 1985. The GIANO project resulted in more than 350 records related to landslides (ENEA, 1990).
In 1989, the National Group for Defence from Hydrogeological Disasters (Gruppo Nazionale per la Difesa dalla Catastrofi Idrogeologiche - GNDCI), a section of the National Research Council (Consiglio Nazionale delle Ricerche – CNR), started an official inventory of the areas historically affected by landslides and floods between 1918 and 1990. The so-called project AVI (Italian Vulnerated Areas) collected 22000 landslide records from 18500 localities by the consultation of newspapers, scientific publications, and interviews (Guzzetti et al., 1994).
In 1992, the National Geological Survey published a major study on "Geological and geoenvironmental instability in Italy since World War II to 1990", edited by V. Catenacci (1992), which collected qualitative and quantitative information on the main catastrophic events in the national territory. The study reported hydrogeological phenomena occurred in about 4570 Italian municipalities (56.5% of the total) involving 195000 km^2 (65% of the total). However, a large part of the landslides data were considered unreliable because of the lack of an authority in charge of data collection and the publication.
In 1998, after a catastrophic landslide event in Sarno (Campania region), the need to have a complete and homogeneous distribution of landslides records throughout the country has strengthened, in terms of both the storage of information and the cartographic representation of the phenomena. The national Agency for Environmental Protection and Technical Services (APAT) and the Autonomous Provinces started the IFFI project (Inventory of Landslides in Italy) that provided a detailed and updated picture of the landslides in the Italian territory. This project surveyed 470000 landslides affecting an area of 20000 km^2, the 6.6% of the national territory (updated to December 2006) (APAT - Dipartimento Difesa del Suolo, 2007). The IFFI project represented both at national and regional levels the opportunity to achieve two important goals never faced before: (i) homogenization of the geographical, geological and geothematic archives, and (ii) construction of a detailed quantitative and qualitative inventory of the landslides distribution. The inventory is based on research of historical data, photo interpretation and field survey, regularly updating. Data analysis shows that between 1985 and 2001 approximately 13500 landslides were triggered, with a significant peak in the second half of the nineties.

Most of the landslides considered had an impact on the built environment, namely those who have caused damages and losses to people, properties and infrastructures.
Recent reports showed that, in the period 2002-2010, 196 landslides affected about 18500 people, including victims, wounded and displaced persons (Consiglio Nazionale dei Geologi, 2010). Furthermore, Guzzetti et al. (2012) highlighted that, between 2005 and 2011, all the regions have suffered at least one major landslide event, confirming the geographical spread of the hydrogeological risk.

1.1.2 Landslide hazard in the Marche region

The Marche region is one of the Italian regions most affected by landslides. In 2008, the Ministry of the Environment (Ministry of Environment Territory and Sea, 2008) identified 245 municipalities with areas of high landslide risk, corresponding to 99.6% of the total municipalities of the Region. The study carried out in 2008 did not take into account the change in the number of municipalities inside the region, due to the passage of some administrations to the Emilia Romagna region in 2009 and the merge of others in 2013. The areas defined at high hydrogeological criticality (i.e. risk level 3 or 4 out of 4; hazard level of 3 or 4 out of 4) by the National Plan for the governance of Hydrogeological Hazard - PAI (Regione Marche - Autorità di Bacino Regionale 2004 and updates) are 955 km^2, corresponding to 9.9% of the entire Region. The 9.0% of these zones are subject to landslides and the 0.9% are subject to flood.
A first update of the IFFI project was realized after the signing of a new agreement between APAT and the Marche region in 2005 (Principi et al., 2007). The analysis of geomorphological data derived from the Marche IFFI project allowed to register for the entire region 42522 landslides, 39788 of which were considered “mappable” (landslide area > 1600 m^2) and 2735 “non-mappable” (landslide area < 1600 m^2). The total area affected by landslides is 1882 km^2, covering the 19.4% of the entire Region.
Considering the density of landslides, i.e. the number of events identified in relation to the surface, on a national scale there are 1.56 landslides per square kilometer. The Marche region greatly exceed with 4.4 landslides per square kilometer (Consiglio Nazionale dei Geologi, 2010).
Among the provinces, Pesaro-Urbino is seventh in Italy and first in the Region for number of recorded events (17317 landslides and 629 km^2)

(Consiglio Nazionale dei Geologi, 2010; Principi et al., 2007) (Table 2). The other records for the provinces existing in that moment (Fermo was not operational yet) are Ancona with 8220 landslides and 422 km^2, Macerata with 9118 landslides and 421 km^2, and Ascoli Piceno with 7867 landslides and 410 km^2.

PROVINCE	LANDSLIDES	AREA (km^2)
Pesaro-Urbino	17317	628.53
Ancona	8220	421.97
Macerata	9118	420.95
Ascoli Piceno	7867	410.34

Table 2 Summary of the landslides data of the IFFI project divided by province (Principi et al., 2007)

Considering the landslide index, defined as the percentage ratio between the landslide area and the total area, the provinces with the highest index in the Region are Pesaro-Urbino and Ancona (22%), which are among the highest in Italy as well (Consiglio Nazionale dei Geologi, 2010).
Landslide distribution is related to the various lithological, structural and morphological characteristics peculiar to the Marche region (Principi et al., 2007). Mountain areas are affected by landslides often fast and large but with sporadic frequency. These phenomena mainly consist of (i) rock falls, located in correspondence of the sub-vertical walls of limestone and calcareous marl of the Marchean and Umbro-Marchean ridges or in arenaceous-pelitic formations (e.g. Laga Formation), and (ii) Deep Seated Gravitational Slope Deformations (DSGSD), recognizable by the characteristics scarps, counterscarps, trenches, and the irregular pattern of the rocky slopes. The first are typical of the province of Ascoli Piceno, while the second type is common in the inland areas of Pesaro-Urbino. Moreover, slides are widespread in the mountain and the adjacent hilly area, especially in the provinces of Macerata and Pesaro-Urbino (each counts more than three thousand phenomena). The lithologies involved are the marly interior Marche Basin, the arenaceous exterior Marche Basin and the smaller basins consisting of alternating arenaceous-pelitic terrains (e.g. Camerino, Pietrarubbia-Peglio-Urbania etc.). Moving eastward, the Plio-Pleistocene marine clay soils are mainly interested by both flows and slides involving the substrate or the eluvio-colluvial cover. Flow is the most frequent type of movement, especially in the Pesaro-Urbino province. The two types of landslide mentioned above (flows and slides), often in association, can reach considerable sizes and cause serious damage to entire towns. From the analysis of the inventory data, landslide index

reaches the maximum values in this Plio-Pleistocene hilly area, which extends from the east of the ridges to the Adriatic coast (Principi et al., 2007).

Furthermore, data obtained by the IFFI project correlated with the land use map, show that the land use class more characterized by landslides is the permanent crops (vineyards, fruit trees, etc...), namely crops not subject to rotation that occupy the soil for a long period (Figure 2). Arable lands and heterogeneous agricultural areas have also high landslide indexes (> 20%). This shows the negative influence that human activity has on the stability of slopes in the Marche region. In fact, in recent decades, agricultural soils have been used in order to increase the annual production with the introduction of mechanized farming techniques and the modification of the characteristics of the slopes (removal of plants, removal of hedges and rows). This resulted in the transformation of the runoff system and sometimes in the disappearance of the drainage network leading to increasing levels of erosion (Principi et al., 2007).

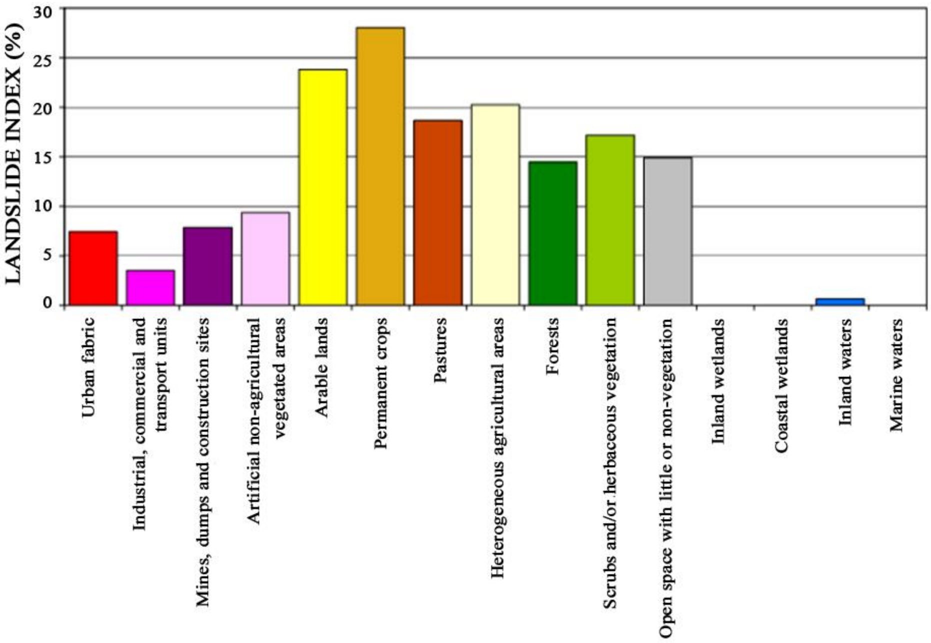

Figure 2 Landslide index representative of each land use class (Principi et al., 2007).

1.2 Rationale for this study

This study originated from the need of the Civil Protection Department of the Marche region (central Italy) to improve the ability of landslides forecasting in the pertaining area. The research intended to propose an innovative approach for the development of rainfall thresholds for shallow landslides, which could be useful as a support tool for decision making in the procedures of the Marche Civil Protection.

Based on the L. 24 February 1992, n. 225, on the "establishment of the National Service of Civil Protection", the activities regarding this service are those aimed at the forecast and prevention of various scenarios of risk, the rescue of disaster victim population and all other activities needed to overcome the emergence.

The *forecast* consists of activities directed to the study and determination of the causes of hazardous events, the identification of risks and the identification of areas subject to the risks.

The *prevention* consists of activities designed to prevent or minimize the possibility of damage subsequent to natural or human-induced events, based on the knowledge acquired during the prevision phase.

The *rescue* consists in the implementation of actions aimed at ensuring the people affected by the calamitous events of all forms of first aid.

The *overcoming of the emergency* consists in the application of the steps required to the emergency management, recovery and restoration of normal life, in coordination with the pertinent institutional bodies.

Particularly, the L.R. 11 December 2001, n. 32, on the "Regional system of Civil Protection", regulates all activities for the risk prediction, the prevention of life and properties damages, the rescue and the overcome of the emergency in the Marche region. In order to pursue these tasks the regional structure may avail itself of the Regional Functional Center (CFR) as determined by the Prime Minister Directive DirPCM 27 February 2004, on the "Civil protection operational guidelines for managing organization and functioning of the national and regional warning system for hydrogeological and hydraulic risk". Based on the DirPCM 27 February 2004, the CFRs represent the technical-scientific structure of reference and support for the emergency management of meteorological, hydrological and seismological risks. They are responsible for:

a) a forecast phase involving the evaluation of the weather, hydrological, hydraulic and geomorphological situation expected, supported by appropriate numerical modeling, and the estimation of the effects that this situation may lead to the integrity of life, property, settlements and the environment;

b) a phase of monitoring and surveillance, divided into: (i) qualitative and quantitative, direct and instrumental observation of the current event, (ii) short-term prediction of its effects through the weather nowcasting and/or hydrogeological models initialized from measurements collected in real time.

The fragility of the Italian territory and in particular of the Marche region (see chapters 1.1.1 and 1.1.2) to the landslide hazard, has directed the research on the triggering causes of the slope failures to be an important part of the activities concerning the Marche Civil Protection Department and, definitely, the CFR. Specifically, the underlying motivation for this particular project was threefold.

First, the identification of rainfall amounts that lead to landslides may help mitigate the loss of life and property damages, therefore the hydrogeological risk. When a storm is expected or is passing over a territory, monitoring meteorological, hydrological or geotechnical parameters (e.g. rainfall duration, soil moisture conditions, or groundwater pore pressure), coupled with initiation thresholds defined with statistical or deterministic methods, may allow the identification of potentially hazardous (Guzzetti et al., 2005). The adoption of rainfall thresholds should lead to anticipate landslide occurrence with sufficient confidence to alert agencies who can issue warning or alarm messages to civil protection authorities and the population. As an example, based on rainfall forecasts, a preliminary assessment of the probability that the triggering thresholds will be exceeded can be made. If the forecast outlines a potentially critical hydrogeological situation, the alert phase can be activated and, in landslide-prone areas, a risk assessment procedure can be initiated in real time (Aleotti, 2004). In a few places in the world rainfall thresholds are part of operational landslide warning systems in which rainfall measurements are compared with established thresholds, and when pre-established values are exceeded alarm messages are issued (Guzzetti et al., 2005). The activation of a warning system would empower individuals and communities exposed to landslides to act in sufficient time and in an appropriate manner to reduce the possibility of personal injury, loss of life and damage to property and the environment (UNISDR, 2010).

Second, developing models for rainfall induced landslide forecasting may provide insights into the process of landslide initiation in the Marche region.

The literature on the subject of rainfall triggered mass movements is vast and scattered within journals, books, proceedings, internal and technical reports pertaining to the realm of different sciences (De Vita and Reichenbach, 1998; Wieczorek and Guzzetti, 2000). Every existing predicting method presents advantages and limitations in the framework of early warning systems for civil protection (Guzzetti et al., 2005). However, each model allows a different perspective to successfully define the key input parameters that control slope failures, both from the landscape and the climate. For example, deterministic models may highlight the role of the slope angle, the infiltration rate or the soil storage capacity in decreasing the stability of a hillslope. On the other hand, empirical models possibly help in understanding the contribution of definite ranges of rainstorm features (e.g. rainfall duration, rainfall intensity, critical rainfall, antecedent rainfall, rainfall frequency), in activating one or more landslides. Moreover, the combination of these key parameters is characteristics of a specific area, or even a single slope, depending on its morphological, hydrological, geological, and climatic conditions. Therefore, the design of landslide predictive models, calibrated and applied in the Marche region, is fundamental to correctly simulate the potential unstable areas and to individuate the local threshold settings that could be responsible or slope failures within the region.

Third, predicting landslides triggered by rainfall it is important to understand and measure how the landscape evolves for the purposes of a proper territorial planning. With recent improvements of both rainfall forecasts and digital techniques for accurately depicting the topography and modelling the hydrologic response, rainfall thresholds could become more useful for identifying not only the time, but also the location of potentially damaging landslides resulting from intense rainfall (Guzzetti et al., 2005). The threshold analysis results can be used as input to estimate the landslide spatial probability. The spatial estimation of the consequences of the triggering factors, could led to a more adequate construction of susceptibility maps to effectively define the landslide hazard of an area. However, this is not the ending point of the process. The ultimate objective of a good forecasting activity is the landslide risk reduction with a correct territorial planning, which takes place when the activities and behavior of populations at risk are changed so the consequences of a landslide event result in no or low losses (DeGraff, 2012). The susceptibility map represents thus the beginning of an educational practice requiring a change in how the affected society behaves. Typically, this takes place by translating the information embodied in the rainfall thresholds and consequently in a landslide hazard map, into some change in policy and regulation applying to the affected area.

In summary, the landslide forecasting is one of the main role of the Marche CFR given the high predisposition of the territory to such hazard. The importance of this activity is highlighted by the potential contained in the predictive model, such as enhanced knowledge of the mechanisms of landslide triggering and mitigation of the hydrogeological risk.

2 State of the art on landslides forecast

Rainfall is a recognized trigger of landslides, and researchers have long attempted to determine the amount of precipitation needed to trigger slope failures, a problem of scientific and societal interest. The literature on the subject of rainfall-triggered mass movements is vast and scattered in journals, books, proceedings, internal and technical reports pertaining to the field of different sciences: geomorphology, hydrology, hydrogeology, soil science, geography, pedology, agronomy, and forestry among others (De Vita and Reichenbach, 1998). Some of the most investigated topics are: (i) types, patterns, and causes of widespread landsliding; (ii) modelling slope groundwater response to rainfall; (iii) significance, role, extent, and availability of thresholds; (iv) usefulness of thresholds for the evaluation and mitigation of landslide hazard and risk (De Vita and Reichenbach, 1998).

Landslides triggered by rainfall are caused by the buildup of water pressure into the ground (Campbell, 1975; Wilson, 1989). Groundwater conditions responsible for slope failures are related to rainfall through infiltration, soil characteristics, antecedent moisture content, and rainfall history (Wieczorek, 1996). Campbell (1975) postulated that infiltration of intense rainfall creates temporarily perched aquifers with positive pore water pressures, which reduce the effective strength of the superficial soils and initiate the landsliding. However, these phenomena are poorly understood, and prediction of rainfall-induced landslides is problematic (Campbell, 1975; Crozier and Glade, 1999; Larsen and Simon, 1993; Montgomery and Dietrich, 1994; Wieczorek et al., 2000). Moreover, the properties of earth materials and the slope conditions may vary greatly over short distances, and the timing, location and intensity of triggering events are generally difficult to forecast. This heterogeneity is but one of the complicating factors that makes difficult to analyze the mechanics of groundwater flow and the development of instability with simple stability models (Wieczorek and Guzzetti, 2000). For this reason, the relationship between rainfall, water table fluctuations and landslide movement is often difficult to establish and the prediction of place and time of landslide occurrence is still a challenging issue.

The key words in rainfall-induced landslides forecasting are rainfall and threshold.
Rainfall is defined as “the total amount of rain that falls in a given area in a given period” (Guzzetti et al., 2005). The “critical rainfall” is the rainfall measured from the beginning of the event (zero point), i.e. from the time when rainfall intensity increases sharply, to the time of the occurrence of the (first) landslide (Figure 3). The rapid increase in rainfall intensity results in a sharp change in the slope of the rainfall cumulative curve. Duration of the critical rainfall event is “the time that elapses from the beginning of critical precipitation to activation of the landslides” (Aleotti, 2004).

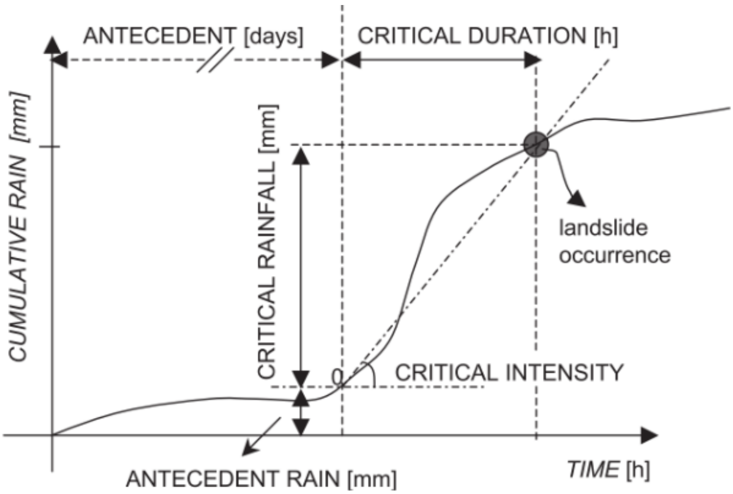

Figure 3 Definition of rainfall parameters (Aleotti 2004)

On the other hand, a “threshold” is defined as “the minimum or maximum level of some quantity needed for a process to take place or a state to change” (White et al., 1996). A minimum threshold outlines the lowest level below which a process does not occur. A maximum threshold represents the level above which a process always occur, i.e. there is a 100% chance of occurrence whenever the threshold is exceeded (Crozier, 1996).
For rainfall-induced landslides, a threshold may represent the minimum intensity or duration of rain, the minimum level of pore water pressure, the soil moisture, the slope angle, the reduction of shear strength, or the displacement required for a landslide to take place (e.g. Crozier 1996; Reichenbach et al. 1998; Guzzetti et al. 2007). Thresholds can also be defined

for other parameters controlling the occurrence of landslides, such as the antecedent hydrogeological conditions or the (minimum or maximum) soil depth required for failures to take place (Reichenbach et al., 1998). If only the triggering rainfall events are considered, most of the authors (including Caine 1980; Guzzetti et al. 2007) define the threshold as the lower limit beneath which landslides never occurs. Others, e.g. Crozier (1999), define the threshold as the upper limit above which landslides always occur. If the rainfall events that do not cause landslides are also considered, the threshold is the limit that best separates triggering from non-triggering rainfall events (e.g. Jibson 1989; Corominas et al. 2002; Giannecchini 2005).

Certainly, individual mass movements respond to specific local conditions, yet the rainfall threshold methods describing the mechanisms linking rainfall patterns and mass movements can be grouped into: (i) empirical (statistical, historical) models, and (ii) physical (deterministic, process-based, conceptual) models (Aleotti, 2004; Busslinger, 2009; EU-FP7, 2012; Guzzetti et al., 2007).

The *empirical rainfall threshold models* (statistical approach) assess relationships between rainfall characteristics (storm mean and maximum hourly intensity, storm duration, rainfall amount, and antecedent rainfall) and landslides through statistical analysis of historical records (Guzzetti et al., 2008). The definition of the most critical rainfall conditions depends on the soil characteristics and initial state (soil moisture content). In particular, shallow landslides and debris flows often occur during, or suddenly after, short intense rainfall. Shallow landslides are defined as failures of low cohesive soil or regolith, few meters thick (Cruden and Varnes, 1996; Sidle and Ochiai, 2006). Data necessary for these models can be obtained from a network of weather stations and records of occurred landslides.
Different types of empirical rainfall thresholds for the possible initiation of landslides have been proposed in the literature (Berti and Simoni, 2005; Caine, 1980; Cancelli and Nova, 1985; Cannon and Ellen, 1985; Chien-Yuan et al., 2005; Coe et al., 2004, 2008; Giannecchini, 2005; Godt et al., 2006a; Guzzetti et al., 2007; Larsen and Simon, 1993; Staley et al., 2013; Vennari et al., 2014; Wieczorek, 1987). The published thresholds can be classified by (Guzzetti et al., 2007): (i) the extent of the geographical area for which they were defined, and (ii) the type of rainfall measurement used to establish the thresholds.
Based on their geographical extent, rainfall thresholds can be subdivided as (a) global, (b) regional, or (c) local thresholds (Guzzetti et al., 2008). A *global*

threshold attempts to establish a general ("worldwide") minimum level below which landslides do not occur, independently of local morphological, lithological, and land-use conditions and of local or regional rainfall pattern and history. This threshold is obtained by using the available data from different countries. The easiest way to define a global threshold consists in tracing a lower limit line embracing all the recorded rainfall conditions that resulted in landslides. Global thresholds have been proposed by e.g. Caine (1980), Innes (1983), Clarizia et al. (1996), Crosta and Frattini (2000), Guzzetti et al. (2005). A regional threshold is defined for areas extending from a few to several thousand square kilometers of similar meteorological, geological, and physiographic characteristics. Regional thresholds have been proposed by e.g. Caine (1980), Larsen and Simon (1993), Jakob and Weatherly (2003), Aleotti (2004), Chien-Yuan et al. (2005). These thresholds are potentially suited for landslide warning systems based on quantitative spatial rainfall forecasts, estimates, or measurements (Guzzetti et al., 2008). A local threshold considers the local climatic regime and geomorphological setting and is applicable to single landslides or to groups of landslides in areas extending from few to some hundreds of square kilometers. Local thresholds have been proposed by e.g. Corominas and Moya (1996), Giannecchini (2005), Godt et al. (2006b). Regional and local thresholds perform reasonably well in the area where they were developed, but cannot be easily exported to neighboring areas (Crosta, 1989). Global thresholds are relevant where local or regional thresholds are not available, but may result in (locally numerous) false positives, i.e. prediction of landslides that eventually do not occur.
Based on the type of rainfall measurement, rainfall thresholds can be subdivided in (Guzzetti et al., 2008): (a) thresholds that combine rainfall characteristics of specific events (Brunetti et al., 2010; Cannon et al., 2011; Dahal and Hasegawa, 2008; Staley et al., 2013; Vennari et al., 2014), (b) thresholds that consider the antecedent conditions (Aleotti, 2004; Chleborad et al., 2006; Crozier, 1999; Martelloni et al., 2011; Papa et al., 2013; Terlien, 1998) and (c) other thresholds, including hydrological thresholds (Jakob and Weatherly, 2003; Reichenbach et al., 1998) (see chapter 2.1).

The *physical rainfall threshold models* (deterministic approach) usually combine local geotechnical, hydrological and geomorphological features of the slope, such as slope angle, with a steady or transient groundwater flow model (Baum et al., 2002; Chen and Zhang, 2014; Crosta and Frattini, 2003; Montgomery and Dietrich, 1994; Raia et al., 2014; Segoni et al., 2009). These models integrate hydrological models for a simplified description of the dynamics of infiltration and saturation phenomena, together with

geotechnical approaches for the stability analysis. Physical models usually attempt to account for infiltration and vertical movement of water into the ground surface, for modelling the longitudinal trend of groundwater.
The aim of physical models is quantifying (i) the rainfall conditions at which shallow landslides can be triggered (e.g. Frattini et al., 2004), (ii) the extent of landslides occurrence (i.e., the number of events, the area involved by landsliding) (e.g. Crozier and Glade, 1999), and (iii) the time-dependent slope stability of potentially sliding surfaces (e.g. Baum et al., 2002). Other studies have considered the landslide initiation as a function of dynamic variables as the land use changes (e.g. Montgomery and Dietrich, 1994) or slope deformation.
Physically based thresholds are calibrated using rainfall events for which the rainfall measurements and the location and time of slope failures are known. Physical thresholds are not as widely developed as the empirical thresholds and, generally, they require detailed knowledge of the boundary conditions, which are seldom available outside specially equipped (with e.g. rain gauges, piezometers, tensiometers) test fields. Therefore, the geographical extent of physically based thresholds links local or sometimes regional rainfall measurements to local terrain characteristics. Recent and sporadic attempts towards the definition of physical regional thresholds have been proposed using distributed hydrological models (Frattini et al., 2004; Raia et al., 2014).

The availability of data has a key role in the definition of the rainfall thresholds as well as the quality (e.g. proximity to study area, spatial and temporal resolution, etc.) and the quantity (e.g. number of historical information, covered period, etc.), which overall influence the results of the analysis (Guzzetti et al., 2005). All these factors ultimately condition the choice of the model to be applied to the study area.

2.1 Empirical models

Empirical rainfall thresholds are defined by analyzing past rainfall events that have resulted in landslides. The methodology applied is a “black box” model, in which the complex physical processes involved in landslide initiation are ignored and a more simple and functional empirical correlation is found between the primarily cause (rainfall) and the effect (landslide) (Martelloni et al., 2011). It is assumed that the mathematical relationship that represents the threshold, beyond which landslides have occurred in the past, will also trigger landslides in the future.

The thresholds are usually obtained by drawing lower-bound lines to the rainfall conditions that resulted in landslides, plotted in Cartesian, semi-logarithmic, or logarithmic coordinates. The curves can be drawn visually or by statistical techniques. Frequently, the thresholds are defined using ill-formalized, poorly documented, or non-reproducible methods (Guzzetti et al., 2007). Where information on rainfall conditions that did not result in slope failures is available (e.g. Lumb 1975; Jibson 1989; Corominas and Moya 1999; Marchi et al. 2002; Giannecchini 2005), thresholds are defined as the best separators of rainfall conditions that resulted and did not result in slope instability. The number of the triggered slope failures (e.g., single vs. multiple events) can also be considered to construct a threshold.

Review of the literature (Busslinger, 2009; Guzzetti et al., 2007, 2005; Wieczorek and Guzzetti, 2000) reveals that no unique set of measurements exists to characterize the rainfall conditions that are likely (or not likely) to trigger slope failures. The most commonly investigated rainfall parameters and climate variables used in the literature for the definition of empirical thresholds are (Guzzetti et al., 2008):

(i) *rainfall duration* (D), first introduced by Caine (1980) and defined as the duration of the rainfall event (in h or days);

(ii) *rainfall intensity* (I), first introduced by Caine (1980) and defined as the total rainfall amount divided by the duration of the rainfall event (in mm/h);

(iii) *maximum hourly rainfall intensity* (I_{MAX}), first introduced by Onodera et al. (1974) (in mm/h), defined as the hourly peak of precipitation during the rainfall event;

(iv) *cumulative event rainfall* (E), first introduced by Innes (Innes, 1983) and defined as the total rainfall measured from the beginning of the rainfall event to the time of failure (in mm);

(v) *critical rainfall* (C), first introduced by Govi and Sorzana (1980) and defined as the total amount of rainfall from the time of distinct increase in rainfall intensity to the time of the triggering of the first landslide (in mm);

(vi) *daily rainfall* (R), first introduced by Crozier and Eyles (1980) and defined as the total amount of rainfall for the day of the landslide event (in mm);

(vii) *antecedent rainfall* (A_D), first introduced by Govi and Sorzana (1980) and defined as the total precipitation measured before the landslide triggering rainfall event (in mm); D indicates the considered period in days;

(viii) *mean annual precipitation* (MAP), first introduced by Guidicini and Iwasa (1977) and defined as the long term yearly average precipitation measured in a rain gauge, obtained from historical rainfall records (in mm);

(ix) *average number of rainy days in a year* or *rainfall frequency* (RD_S), first introduced by Wilson and Jayko (1997) and defined as the long term yearly average of rain days (i.e. a day with at least 0.1mm of rain) measured in a rain gauge, obtained from historical rainfall records.

Many authors use different definitions and combinations of these parameters, specific and calibrated for the studied area. Thresholds were defined in literature considering for example (Guzzetti et al., 2005): (a) mean rainfall intensity for the event; (b) maximum rainfall intensity for the duration of the event; (c) rainfall intensity at the time of the slope failure; (d) duration above a pre-defined intensity level; (e) cumulative rainfall, with or without the exact indication of the time of the slope failure; (f) intensity or cumulative rainfall normalized to MAP; (g) rainfall intensity normalized to the ratio between MAP and the yearly number of rainy days; (h) antecedent rainfall, for different time intervals before the occurrence of the landslide or before the starting time of the event; and (i) daily rainfall versus antecedent soil water status index. Moreover, these very classifications may be subject to different interpretations. As an example, rainfall intensity is the amount of precipitation accumulated in a period, or the rate of precipitation in a period, most commonly measured in millimeters per hour. Depending on the length of the observation period, rainfall intensity may represent an “instantaneous” measure of the rainfall rate, or an average value of precipitation over hours (hourly intensity), days (daily intensity), or longer periods. For long observation periods, rainfall intensity represents an “average” value that underestimates the peak (maximum) rainfall rate occurred during the observation period. Hence, rainfall intensity measured over short and long periods have different physical meaning (Guzzetti et al., 2007). For this reason, language inconsistencies and disagreement on the requisite rainfall and landslide variables have negative consequences for the possible use of the thresholds, complicating the definition of rainfall models and making difficult the comparison.

As previously mentioned, empirical rainfall thresholds can be grouped in three categories (Guzzetti et al., 2007, 2005): (i) thresholds that consider rainfall characteristics of specific events, (ii) thresholds that consider the antecedent conditions, and (iii) other thresholds.

2.1.1 Thresholds that consider rainfall characteristics of specific events

The majority of the thresholds established using precipitation measurements, obtained from individual or multiple rainfall events, can be grouped in: (a) intensity – duration (ID) thresholds, (b) thresholds based on the cumulative event rainfall (E), (c) event rainfall – duration thresholds (ED), and (d) event rainfall – intensity (EI) thresholds.

The empirical models based on the **intensity-duration (ID)** approach are thoroughly documented in the literature (Aleotti, 2004; Brunetti et al., 2010; Cannon et al., 2011; Chleborad et al., 2006; Corominas et al., 2002; Giannecchini et al., 2012; Godt et al., 2006a; Guzzetti et al., 2008; Papa et al., 2013; Peruccacci et al., 2012; Rappelli, 2008; Staley et al., 2013; Wieczorek, 1987). The first study to relate these rainfall thresholds to landslide initiation was published by Caine (1980). In this landmark paper, Caine listed 73 rainfall duration and intensity conditions that had resulted in shallow landslides (< 3 m deep) and debris flows worldwide. Using local precipitation records, he defined an upper threshold for landslide initiation as:

$$I = 14.82D^{-0.21} \qquad (1)$$

where *I* is rainfall intensity (mm/h) and *D* is rainfall duration (h). These data fit for precipitation between 10 min and 10 days in duration, and poorly fit for longer or shorter durations. He suggested that the lack of fit for very short durations resulted from insufficient depths of water to change pore water pressure. Data were compiled from a variety of climatic and geologic conditions. As a result, the rainfall intensity-duration estimates are non-homogeneous. Moreover, Crozier (1996) pointed out that Caine's dataset does not include climatic events that did not trigger landslides, which is an equally important statistic. Despite this limitation, since the pioneering work of Caine, information on the rainfall ID conditions that have resulted in slope failures was collected at various sites or regions worldwide, and different rainfall ID thresholds were proposed at the local, regional, and global scales (for a reference list see Guzzetti et al. 2007). The threshold functions assumes now the form of the following equation:

$$I = c + \alpha D^{-\beta} \qquad (2)$$

where $c \geq 0$, α and β are empirical parameters of the specific site conditions. α is a scaling parameter (the intercept), and β is the shape parameter that controls the slope of the power law threshold curve.

Significant differences between the thresholds exists. The listed ID thresholds (Guzzetti et al., 2007) span a considerable range of rainfall durations and intensities. For the majority of the ID thresholds $c = 0$. When $c = 0$ equation (2) is a simple power law. Additionally, all the listed power laws have negative scaling exponents (β). The negative power law relation suggests a similar scaling behavior of the rainfall conditions that result in landslides. However, this simple trend has a conceptual limitation: for very long periods, even extremely small average rainfall intensities may result in landslides, a condition difficult to justify. The differences among the thresholds can be explained by the fact that they are based on data sets from areas with different geological, geomorphological, and climatic settings. As an example, Brunetti et al. (2010) defined ID thresholds for Italy and for the Abruzzo region, central Italy. The regional ID threshold for Abruzzo was found to be lower than the threshold defined for Italy, and lower than similar regional ID thresholds defined for areas in northern Italy (Aleotti, 2004; Ceriani et al., 1994) or in southern Italy (Calcaterra et al., 2000).

The ID approach can be further refined by normalizing the intensity value by the mean annual precipitation (MAP) (Govi et al., 1985). This emphasizes the regional character of a threshold, taking into account the local climate regime and the season of occurrence. Following Govi et al. (1985), several authors investigated the relationship between rainfall duration and rainfall intensity normalized by MAP (Aleotti et al., 2002; Bacchini and Zannoni, 2003; Cannon, 1988; Ceriani et al., 1994; Dahal and Hasegawa, 2008; Giannecchini, 2006).

The empirical models based on the **cumulative event rainfall (E)** approach have been attempted by few authors (Campbell, 1975; Cannon and Ellen, 1985; Cardinali et al., 2006; Corominas and Moya, 1999; Govi and Sorzana, 1980; Guidicini and Iwasa, 1977; Hong et al., 2005; Innes, 1983; Lumb, 1975; Terlien, 1998). These thresholds represents the minimum amount of rainfall necessary to trigger at least a landslide in the considered area. For example, for Nilsen and Turner (1975) a minimum precipitation of 177.8 mm is sufficient to initiate abundant shallow landslides in Contra Costa County (California, USA), whereas for Mark and Newman (1985) the threshold in San Francisco Bay region (California, USA) is 254 mm. Corominas and Moya (1999), differentiate the threshold depending on the time elapsed: E minimum is 180-190 mm if the event lasts 24-36 h or is 300 mm if the event lasts 24-48 h. The problem is identify the critical rainfall that define the rainfall event. In Canuti et al. (1985) the event is 1-3 days long, while in Bhandari et al. (1991) is always 3 days long.
Different rainfall variables have been combined to the E parameter for the definition of these thresholds, including: (i) daily rainfall (R) (Campbell, 1975; Corominas and Moya, 1996; Lumb, 1975), (ii) antecedent rainfall (A_D) (Lumb, 1975; Pasuto and Silvano, 1998; Sorriso-Valvo et al., 1994); and (iii) normalized cumulative event rainfall (E_{MAP}), often expressed as a percentage of the MAP. According to the last type of thresholds, if the total precipitation during a rainfall event exceeds an established percentage of the MAP, landslides are likely to occur, or to occur abundantly. As an example, Guidicini and Iwasa (1977), working in Brazil, determined that when the total event rainfall exceeded 12% of the MAP landslides were likely to occur independently of the antecedent conditions, whereas when the total event rainfall ranged from 8% to 12% of the MAP landslides initiation was dependent on rainfall history. Similarly, Govi and Sorzana (1980), working in the Piedmont region of NW Italy, discovered that areas characterized by large MAP required a higher amount of rainfall to trigger slope failures than areas characterized by lower MAP. Moreover, Bhandari et al. (1991), determined that in Sri Lanka when the precipitation is inferior to the 5% of the MAP, the probability of landslides is low.

On the other hand, numerous investigators have related measures of the cumulative event rainfall to the duration of the rainfall events, thus defining **event rainfall – duration (ED)** thresholds (Aleotti, 2004; Caine, 1980; Corominas and Moya, 1999; Giannecchini, 2006; Innes, 1983; Wilson, 1989). In general, the method assumes that the threshold curve is a power law:

$$E = \alpha D^{\gamma} \qquad (3)$$

where E is the cumulated event rainfall (mm), D is the duration of the rainfall event (h), α and γ are the equivalent of the α and β parameters of the ID thresholds ($\gamma = -\beta + 1$).
For example, Innes (1983) used information on 35 rainfall events that had resulted in debris flows worldwide to establish a first global minimum ED threshold for possible debris flow occurrence. The threshold was in the form of the power-law equation, valid for duration from 0.1 to 100 h:

$$E = 4.93 D^{0.504} \qquad (4)$$

More recently, Kanji et al. (2003) collected information on the rainfall conditions that resulted in landslides in several geographical areas worldwide, and proposed the global minimum ED threshold
$E = 22.4 \times D^{0.41}$.
Several other thresholds have been determined also in regional and local scales. Peruccacci et al. (2012) compiled a new catalogue of 442 rainfall events that triggered landslides in the Abruzzo, Marche, and Umbria regions, central Italy, between 2002 and 2010, and proposed ED thresholds for the entire study area, for the three administrative subdivisions, for the main lithological domains, and for different seasonal periods. The cumulated rainfall necessary to trigger landslides in the studied area was slightly larger for flysch deposits than for soft post-orogenic sediments (clay, silt, sand, gravel) and for sedimentary carbonate rocks. Vennari at al. (2014) adopted the procedure proposed by Brunetti et al. (2010) and modified by Peruccacci et al. (2012) to evaluate the uncertainty associated with the thresholds. They determined new regional ED thresholds for possible shallow landslide occurrence in Calabria (Italy) for the 1% and the 5% exceedance probability levels. Results showed that for short rainfall durations ($D \leq 24$ h), lower amounts of cumulated event rainfall are required to trigger landslides in the Tyrrhenian (western) alert region than in the Ionian (eastern) alert region.
The thresholds modeled in literature present similar ascending trends ($\gamma > 0$) and exhibit comparable fixed or changing gradients, but differ significantly in the minimum amount of rainfall required to trigger landslides. This is mainly attributable to the different climates of the considered regions.

Finally, the empirical models based on **event rainfall – intensity (EI)** thresholds and normalized EI thresholds have been pursued (Aleotti et al., 2002; Bacchini and Zannoni, 2003; Giannecchini, 2005; Govi et al., 1985;

Heyerdahl et al., 2003; Hong et al., 2005; Jibson, 1989; Onodera et al., 1974). The general form of the equation describing the relationship is a power law:

$$I = \alpha E^{-\beta} \qquad (5)$$

where I is the rainfall intensity (mm/h), E is the cumulated event rainfall (mm), and α and β are the equivalent of the α and β parameters of the ID thresholds.

Onodera et al. (1974) were the first to propose EI quantitative rainfall thresholds for the initiation of shallow landslides in Japan, suggesting a set of thresholds (upper, intermediate and lower) linking the maximum hourly rainfall intensity to the cumulative event rainfall. Govi and Sorzana (1980) adopted a slightly different approach and linked the average rainfall intensity during the final phase of the storm (i.e., the period when landslides occurred) to the critical event rainfall, normalized to the MAP. These authors found linear (in Cartesian coordinates) and complex relationships, depending on landslide abundance, on the season of the event, and on the antecedent rainfall conditions.

2.1.2 Thresholds that consider the antecedent conditions

Much of the scientific literature considers the antecedent conditions to define landslide empirical thresholds based on the amount of the antecedent rainfall (Aleotti, 2004; Chleborad, 2000; Crozier, 1999; Gabet et al., 2004; Glade et al., 2000; Jaiswal and van Westen, 2009; Kim et al., 1991; Lumb, 1975; Sengupta et al., 2010; Terlien, 1998). In fact, antecedent precipitation influences groundwater levels and soil moisture thus predisposing slopes to failure (Crozier, 1996; Wieczorek, 1996). However, the geographical pattern and the temporal evolution of groundwater and soil moisture are difficult to know precisely, as they depend on various mutable factors, including heterogeneity of soils (strength and hydraulic properties) and regional climate (Guzzetti et al., 2005). Because of this local variability, when using antecedent rainfall measurements to predict landslide occurrence, a key difficulty is the definition of the period to be taken into account for the accumulated precipitation (Guzzetti et al., 2007; Martelloni et al., 2011).

Very different methods and time intervals have been considered, ranging from a few days (Heyerdahl et al., 2003; Kim et al., 1991) to a few months (Cardinali et al., 2006; De Vita, 2000; Galliani et al., 2001).

A simple way of using antecedent precipitation measurements consists of establishing a threshold based on the amount of the antecedent rainfall, but more composite correlations have been proposed between the antecedent precipitation and the event or daily rainfall (Guzzetti et al., 2007).

In NW Italy, Govi et al. (1985) determined that the 60-day antecedent rainfall needed to trigger landslides varied seasonally with a minimum value of 140 mm, and that the sum of antecedent and event rainfall needed to initiate slope failures was at least 300 mm.

Kim et al. (1991) studied the correlation between daily rainfall at failure and the 3-day cumulative rainfall before the failure, in Korea. They showed that landslides plotted above the threshold were mainly governed by the rainfall intensity at failure, whereas landslides below the threshold were conditioned by cumulative antecedent rainfall. A diagonal line in a daily rainfall - 3-day cumulative rainfall chart, represented the threshold.

In 1986, Crozier proposed a formula to weight the antecedent rainfall:

$$CAR_X = KP_1 + K^2P_2 + \cdots K^n P_n \qquad (6)$$

where CAR_X is the calibrated antecedent rainfall for day x; P_1 is the daily rainfall for the day before day x; P_n is the daily rainfall for the nth day before day x. The constant K is an empirical parameter that accounts for the decreasing effect of a particular rainy event over time, usually considered between 0.8 and 0.9 depending on the draining capacity of the material and the hydrological characteristics of the area. This constant makes rainfall occurring more than 30 days before a landslide event to become negligible (Capecchi and Focardi, 1988). Therefore, this formula allow considering a maximum of 30-day period of antecedent rainfall.

Terlien (1998), working in Colombia, related the normalized daily rainfall to the normalized antecedent rainfall tested for 2-, 5-, 15- and 25-days. He found that antecedent rainfall of 25 days provided the best separation between days with and days without landslides. However, for those landslides triggered by high daily rainfall amounts (normalized daily rainfall exceeding 0.9, corresponding to a daily rainfall of 70 mm) a window of 15 antecedent rainfall days would be sufficient. The depth of the failure surface can partly explain the difference in the number of antecedent days. Precisely, the 15-day period window was related to shallow landslides with a maximum failure surface depth of ~2 m, whereas the 25-day period window was related to failure surface depth of ~6 m.

Chleborad (2006; 2000), in a study in the Seattle area (Washington), defined an antecedent rainfall threshold in a scattered plot showing 3-day precipitation amounts (P_3) that occurred immediately prior to the landslides and antecedent 15-day cumulative precipitation (P_{15}) that occurred prior to the 3 considered days. The approximate lower-bound precipitation threshold was defined by the equation: $P_3 = 0.67P_{15} + 3.50$.
De Vita (2000), studying an area in Campania (Southern Italy), correlated the total daily rainfall (R) to the antecedent rainfall for periods from 1 to 60 days. This author established that, for antecedent precipitation in the range between 1 and 19 days before the landslide event, the daily rainfall needed to trigger landslides decreases with the amount of the antecedent precipitation. If longer periods were considered, the daily rainfall required to initiate landslides first decreased and then flattened at about 50 mm.
In a proximal area, Aleotti (2004), investigated the correlation between critical rainfall and antecedent periods of 7 and 10 days by tracing curves separating the 90% of the rainfall events. However, throughout this study he could not identify a significant correlation between antecedent rainfall and critical rainfall.
Gabet et al. (2004) combined the daily rainfall with the total rainfall since the beginning of the monsoon season in Nepal. They found that a minimum seasonal rainfall (528 mm) must accumulate and a minimum daily rainfall (9 mm) must be exceeded to bring the regolith up to field capacity (the soil moisture beyond which gravity drainage ensues), so that future rainfall may produce positive pore pressures and trigger landslides.
Zêzere et al. (2005) performed the analysis in the Lisbon area (Portugal) calculating the cumulative absolute antecedent rainfall (CAR) (after Crozier 1986) for 1, 5, 10, 15, 30, 45, 60, 75 and 90 consecutive days prior to the dates of confirmed landslide activity during a 45 years period. The best results obtained for shallow landslide episodes correspond to an exponential law ($R = 167.28e^{-0.0355CAR}$) for the 5 days CAR, while deep landslide events are better discriminated by combined threshold of R=16mm and 30 days CAR=85mm.
Cardinali et al. (2006) found a correlation between landslides occurred in SW Umbria, central Italy, with antecedent rainfall exceeding 590 mm over a 3-month period, or 700 mm over a 4-month period.
Walker (2007) applied a method to data series from Australia, formed from the daily rainfalls and anterior cumulative totals for 2, 5, 10, 20, 30, 60 and 90 days. Days on which multiple landslides are likely to occur are often related with 30 to 60 day antecedent rainfall.

Martelloni et al. (2011) developed a decisional algorithm for the forecast of landslides in Emilia Romagna region (central Italy). This system considers the cumulative rainfall up to 2 days before the day of analysis (included) in case of shallow landslide, and the cumulative rainfall from 4 days up to 63-245 days before the day of analysis (included) in case of deep-seated landslide. The different intervals account for lithological and hydrogeological conditions of the study area. In permeable terrains, pore water pressure reacts rapidly to rainfall, while in the case of low-permeability terrains the antecedent rainfall is more important. In addition, hydrological response for deep-seated landslides and for terrains with low hydraulic conductivity is governed by more complicated mechanisms, which are quite difficult to model with a statistical black box approach. Martelloni verified that the long period of cumulative rainfall generated much more false alarms than the short period.
Tiranti et al. (2013) modified the Govi et al. (1985) diagram with new data and with the introduction of the snow melt as a fraction of antecedent rainfall. The importance of snow dynamics in the calculation of the antecedent precipitation has been demonstrated especially in sedimentary environments.

Some authors debated the importance of the antecedent precipitation for the initiation of landslides because the correlation between the antecedent rainfall and the occurrence of slope failures could not be found (Aleotti, 2004; Brand et al., 1984), or the antecedent precipitation had not significance for soils with large interparticle voids (Brand, 1992; Corominas and Moya, 1999). In fact, the relationship between antecedent rainfall and landslide occurrence assumes importance if only applied within a defined region with homogeneous geological and climatological features and cannot be exported to other regions (Pignone et al., 2005).

2.1.3 Other thresholds

Other types of thresholds, which may also combine the variables listed in the previous categories, have been proposed in the literature for the initiation of landslides (Guzzetti et al., 2005).
For example, Govi and Sorzana (1980) correlated the cumulative event rainfall (E) normalized by MAP to the severity of the event in terms of number of landslides triggered per km^2.

Ayalew (1999), working in Ethiopia, proposed a regional threshold called L_f, which is the likelihood of occurrence of failure. The L_f factor is so determined:

$$L_f = K\frac{X}{Y} \times 100\% \qquad (7)$$

where K is a ratio of the total number of days up to the date of analysis with a rainfall > 5mm and the mean annual number of rainy days in the area (or in the nearby recording station). Days with a rainfall ≤ 5mm are considered as if there was no precipitation because is assumed to be lost by evaporation. X is the cumulative precipitation recorded up to the date of analysis (E); Y is the mean annual precipitation in the area (MAP). The ratio between X and Y is used to address the effect of rainfall duration on the variation of the moisture content and the pore water pressure of soils. It is shown that when L_f < 15% landslides are not expected, when 15 < L_f < 30% cracks and other signs of slope movement are observed, while L_f > 30% indicates a much greater probability of landslide occurrence.
Wilson (2000) related the maximum 24-hour rainfall amount from storms that triggered debris flows in some U.S. countries to the maximum 24-hour rainfall expected in a 5-year return period. He proposed that the probability of debris flow occurrence was a function of the daily rainfall (R) normalized by the 5-year storm rainfall.
Aleotti et al. (2002) defined three regional logarithmic thresholds, for shallow landslides in the Piedmont region in Northern Italy, using the rainfall intensity normalized by MAP (NI) and the critical rainfall normalized by MAP (CN). They found (i) a threshold for high-magnitude events, (ii) a general critical threshold, and (iii) a threshold for low-magnitude events.
Bacchini and Zannoni (2003) proposed two local thresholds for debris flow (Dolomites, NE Italy), based on (a) the triggering rainfall normalized by MAP related to the mean intensity (I > 2mm/h), and (b) the rainfall intensity normalized by MAP related to the duration.
Jakob and Weatherly (2003) established hydroclimatic regional thresholds for the occurrence of slope failures in the British Columbia, following Reichenbach et al. (1998). The model presented attempted to predict landslide initiation by combining precipitation data with streamflow records from a small watershed that responds quickly to water input. They analyzed hydroclimatic variables from 25 storms that triggered shallow landslides on the study area, and an equal number of storms of comparable magnitude that failed to trigger shallow landslides. The three discriminant variables selected are: (i) total precipitation over a 4-week period prior to a storm, (ii) maximum

rainfall in a 6-h period during a storm, and (iii) the number of hours in which the basin discharge exceeded 1 m^3/s. Based on the three selected variables, Jakob and Weatherly (2003) established warning and initiation thresholds for debris flows and shallow landslides.
Cepeda et al. (2009), worked on a new local rainfall threshold function based on a generalization of the Caine (1980) power law:

$$I = \left[\alpha_1 A_n^{\alpha_2}\right] D^{\beta} \qquad (8)$$

where I and D are defined as Caine, the expression in parentheses is equivalent to Caine's α parameter, α_1, α_2 and β are parameters estimated for the threshold, A_n is the n-days cumulative rainfall. Equation (8) accounts for the effects of the antecedent precipitation and requires a calibration of the value of 'n'. Cepeda et al. (2011) proposed a local application of the IAD model for slides, whose improved performance is achieved with triggering rainfall from 3 to 17 h and antecedent rain of 50 days. They also found that, for debris flows with triggering rainfall from 1 to 9 h, a traditional ID threshold is sufficient with no need of antecedent rain.

2.1.4 A probabilistic approach

In a purely empirical definition of a threshold is implied that, when its value is crossed, a radical change of state within a system will occur and this change often manifests suddenly (Berti et al., 2012). Therefore, the state of the system can be predicted by comparing the input value (or a set of input values) with the threshold. This approach imply also that there is a binary possible output (above or below the threshold) since no randomness is involved in the development of future states of the system (Berti et al., 2012). Consequently, this method can be successfully used to define a rainfall threshold in the ideal conditions in which the activation mechanism is directly controlled by rainfall, such as debris flows in coarse granular material that are initiated by channel runoff (Aleotti, 2004; Berti and Simoni, 2005; Caine, 1980; Ceriani et al., 1994; Coe et al., 2008). In these cases, the separation between rainfall that triggered and rainfall that did not triggered landslides is clear.
However, although exceedance of the precipitation threshold is necessary for inducing movements, it is not sufficient to trigger a slide, especially when the model is applied to complex or deep-seated landslides (Floris and Bozzano, 2008; Guzzetti et al., 2005; Pignone et al., 2005). For these landslides,

stability conditions are controlled by a combination of hydrogeological and time-dependent driving forcing, such as the soil moisture near the surface, pores distribution of pressure, atmospheric agents, softening of the materials, and long-term changes in the field of stress (Aleotti and Chowdhury, 1999; Leroueil, 2001; Montgomery and Dietrich, 1994). In these cases, the distinction between critical and non-critical precipitation is not sharp. Hence, is necessary to estimate the uncertainty and to correlate a given rainfall event to the probability of landslide occurrence.

Empirically-based probability models are mathematical models that use historical records of landslide occurrence to predict the temporal probability of future landslides (Coe et al., 2004), dealing with the limitations to our knowledge of natural processes (Crovelli, 2000). In the attempt to reduce the subjectivity of the definition of a threshold, probability models are advantageous for several reasons. First, they incorporate variability and uncertainty, providing a quantitative assessment of threshold reliability (Bean, 2009). In fact, when a threshold is exceeded a purely empirical approach do not account for the possibility of non-landslide occurrence, whereas a probabilistic approach considers the distribution of non-triggering rainfall. Moreover, these models allow to estimate the probability of extreme events which correspond to the tail of probabilistic distributions (Berti et al., 2012). Finally, probability models are widely used for susceptibility assessment analysis, to determine the probability of occurrence of a landslide with a magnitude greater (or lower) than an arbitrarily chosen reference amount, within a specific time period and at a given location (Coe et al., 2004; Crovelli, 2000; Motamedi and Liang, 2013). The results of the empirically based analyses are typically portrayed using Geographical Information Systems (GIS) (J.W. Godt et al., 2008).

Several authors used probability method (e.g. binomial distribution, Poisson distribution) for the calculation of objective and reproducible rainfall threshold for the possible occurrence of rainfall-induced landslides (Ayalew, 1999; Berti and Simoni, 2012; Brunetti et al., 2010; Chleborad, 2000; Floris and Bozzano, 2008; Glade et al., 2000; Guzzetti et al., 2005; Motamedi and Liang, 2013; Reichenbach et al., 1998). One of the most applied approach is the statistical Bayesian inference. Bayesian inference is a method in which “Bayes' theorem is used to invert conditional probabilities” and “revise or update subjective probabilities consistent with new information” (Wilks, 2011).

The first to propose the application of the Bayesian inference method, to determine global and regional ID thresholds, were Guzzetti et al. (2005). Initially, they collected intensity-duration data of rainfall events that resulted in at least a landslide worldwide and they treated them as independent events. Then, they computed:

i. the *likelihood* as the probability that all the inventoried events would cause the observed landslides;
ii. the *a priori* idea of the parameter values distribution, then revised by the model looking at the observed data;
iii. the *posterior* probability distribution.

Guzzetti et al. (2005) hypothesized the Pareto distribution as the a priori distribution, suggesting a power law probability for the random event. The proposed global threshold is lower than Caine (1980) and Innes (1983), but similar to Crosta and Frattini (2000) in the range of rainfall durations between 20 and 60 h. They further computed new regional thresholds for different climatic scenarios using the Bayesian model, showing a link between climatic regime and rainfall thresholds.

In 2007, Guzzetti et al., proposed another Bayesian approach to define an ID threshold for Central and Southern Europe. First, they selected the threshold curve, in the form of the power law proposed by Caine (1980). Second, they used a probability model to find acceptable ranges of the prior probability distributions of the scale (intercept, α) and the shape (slope, β) of the curve. Hence, after some experimentation, prior probability distributions for α and β were chosen. Estimated values of α and β were then obtained through Bayesian inference of their posterior probability distributions, given the model results and the empirical data. The same procedure was used to infer global normalized-ID thresholds in Guzzetti et al. (2008) and regional ID thresholds in Brunetti et al. (2010).

Berti et al. (2012) proposed a new application of the Bayesian probability. In this approach the Bayes' theorem is applied to compute the *posterior probability* P(A|B), i.e. the conditional probability of occurrence of a landslide (A) given a rainfall episode of a fixed amount (B). The formulation of the theorem is:

$$P(A|B) = \frac{P(B|A) \cdot P(A)}{P(B)} \qquad (9)$$

where P(B|A) is the *likelihood*, i.e. the conditional probability of observing a certain rainfall event when a landslide occurs; P(A) is the *prior probability*, i.e. the probability that a landslide occurs independently of the rainfall event;

P(B) is the *marginal probability*, i.e. the probability of observing a rainfall event of a certain magnitude independently of the occurrence of a landslide. The method is computed in terms of relative frequencies and returns a value of landslide probability (from 0 to 1) for each combination of the selected variables (A and B).

2.1.5 Advantages and limitations of the empirical models

The main advantage of empirical rainfall thresholds lays in the fact that the approach is useful and practical. Therefore, empirical models are more suitable for the development of rainfall thresholds at regional, national, or global scale (Martelloni et al., 2011).
The calculation of this empirical landslide-triggering rainfall threshold requires both spatial and temporal information on landslide frequency and rainfall values. Rainfall necessary data can be obtained with a relatively simple and affordable network of weather stations, even over large areas. Where information on landslides and rainfall is available, plots can be prepared and threshold curves can be easily fitted as lower or upper bounds for the occurrence of slope failures (Guzzetti et al., 2005).
Moreover, a large and various number of threshold models exist in literature so that the current methodologies are widely tested (Wieczorek and Guzzetti, 2000).

On the other hand, several limitations for the application of empirical rainfall thresholds are evident. The main disadvantages refers mostly to the availability of data of adequate quality, resolution and recording length. Records of landslides demonstrate that rainfall thresholds are often exceeded without giving rise to any slope movement. Therefore, a detailed inventory of landslides must be compiled before and after the events to develop and calibrate the thresholds. Indeed, a single event may be so intense (“extreme” i.e., with a return period exceeding 100 years) as not to be representative of the local instability conditions. Thresholds based on extreme events can underestimate the probability of failures (Guzzetti et al., 2005). Hence, a long record of rainfall measurements and many events resulting from different meteorological conditions should be analyzed to define reliable rainfall thresholds. Unfortunately, information on an acceptable number of events is seldom available.

Another limit is the poor quality of accessible data on which the empirical methods are based (homogeneity and completeness, landslide timing, rainfall data resolution and rain gauge location). This issue may cause a degree of uncertainty that can be addressed by complementing the rainfall threshold information with probabilities of landslide occurrence (Jaiswal and van Westen, 2009).
Also, given that rainfall is not the only factor that causes landslides, the method used to identify and describe the rainfall event may increase uncertainty. Many authors either do not specify the criteria used for rainfall definition or generally refer to "the beginning of a rainfall event". However, qualitative criteria for rainfall identification leave room to subjectivity and impair comparison of results. Only few authors addressed the problem of rainfall identification (Aleotti, 2004; Berti et al., 2012; Brunetti et al., 2010).
Additionally, most of the proposed thresholds perform reasonably well in the region where they were developed, but cannot be exported to other areas, and their temporal accuracy remains largely untested (Crozier, 1996; Guzzetti et al., 2005).
Furthermore, empirical models frequently do not discriminate different landslide types. The choice of the right parameters for defining thresholds depends primarily on the landslide typology. There is a general agreement in recognizing that debris flows and shallow landslides are preferentially triggered by short and intense rainfalls (Campbell, 1974; Crosta, 1998), while deep-seated landslides are more commonly connected with prolonged and less intense rainfall events (Bonnard and Noverraz, 2001). In those areas affected by both shallow and deep-seated landslides, it is essential to define a methodology which could be flexible enough to encompass both of them (Martelloni et al., 2011).
Finally, the empirical threshold approach assumes the immutable state of both the trigger and the reacting system (Glade, 2012). Instead, we are living in a complex system defined by non-linearity, chaotic behavior, natural and human interference that modifies the triggering effects and the slope responses. However, empirical models with their limitations still represent challenging and valid methods to estimate landslide occurrence and support a landslide warning system.

2.2 Physical models

Beside statistical methods, deterministic models have been also widely used since the 1990s (Cervi et al., 2010; Montgomery and Dietrich, 1994; Wilcock et al., 2003), due to the increasing requirement of both spatial and temporal forecasting of landslides occurrence.

Physical rainfall threshold models generally aim to simulate the physical phenomena related to the water movement that proceed in the ground, as a result of meteorological inputs (Picarelli and Vinale, 2007). In fact, mechanical, hydraulic and physical properties of soils (Cancelli and Nova, 1985; Pierson, 1983; Wilson and Wieczorek, 1995), slope morphometry (Crosta, 1998), soil thickness (Corominas 2001), vegetation cover (Buchanan and Savigny, 1990), seepage conditions (Iverson and Major, 1986), antecedent soil moisture (Campbell, 1975), and bioactivity (Tao and Barros, 2014) are specific to the local geographic site and may lead to unstable conditions in response to rain. Additionally, rainfall regimes are typical and distinctive of a specific region. Physical models provide, therefore, the possibility of putting in relation the regional precipitation with the site-specific groundwater system, allowing to evaluate the role of these processes in the stability conditions (Baum et al., 2010; Crosta and Frattini, 2003; Montgomery and Dietrich, 1994; Picarelli and Vinale, 2007). To achieve this, physical models usually combine spatially variable geotechnical and geomorphological features (e.g., slope gradient, soil depth, and soil properties) with simplified hydrological models (Berti et al., 2012; Gabet et al., 2004; Terlien, 1998; Wilson and Wieczorek, 1995). This approach requires both time-invariant and time-dependent information (Raia et al., 2014). The assumed time-invariant information are for instance the mechanical, hydrological, and geometrical characteristics of the sliding material. The time-dependent information includes for example the groundwater flow. Due to lack of complete information and knowledge of the physical laws that control landslide initiation, only simplified conceptual models are currently available (Raia et al., 2014).

Finally, because process-based models may determine the location and the timing of the forecasted landslides, they can be successfully applied on landslide warning systems (Guzzetti et al., 2007).

2.2.1 General description of the physical phenomena

The *hillslope hydrology* is one of the most important issues in landslides activation. Water movement, from precipitation to discharge to streams or rivers, involves many physical processes such as overland flow, infiltration, interception, stem flow, evaporation, through flow, and groundwater flow (Lu and Godt, 2013). Rainfall that falls on the ground normally causes short-term and long-term responses. Short-term response begins at the surface of the soil, due to infiltration and runoff, and propagates downwards, leading the rise of water table and pore pressure (or pressure head) in the saturated zone (Baum et al., 2010). Long-term response affects the initial depth of the water table and the flow direction (Baum et al., 2010). The complexity of these processes, does not facilitate the modeling of slope instability (Sidle and Ochiai, 2006), even in idealized, smooth, homogeneous hillsides (Freeze, 1971). In fact, three-dimensional topographic forms, surface roughness, interactions of surface and subsurface water, and various kinds of heterogeneity (e.g. textural variations, stratifications, structural discontinuities, root holes, contrast in soil or rock properties) all exacerbate the complexity (Baum et al., 2010; Crosta and Dal Negro, 2003; Torres et al., 1998; Uchida et al., 2001).
Particularly, both at matric and hillslope scale, water movement is highly dependent on (Ali et al., 2014; Anderson et al., 1978; Cascini et al., 2006; EU-FP7, 2012; Feddes et al., 1976; Greco et al., 2013; Montgomery et al., 1997; Muzylo et al., 2009; Sidle et al., 2000; Sidle and Ochiai, 2006; Simoni et al., 2004):

a) climatic conditions, such as the rainfall characteristics (duration, intensity and pattern);
b) soil hydraulic and mechanical properties, such as thickness, permeability, conductivity, moisture content, porosity, presence of large macropores created by subsurface erosion, presence of preferential flow network, fractures and interstices, bedrock morphology, soil-bedrock interface, soil-water retention curve, initial conditions (suction), and boundary conditions;
c) vegetation cover, such as root water uptake and canopy interception.

These environmental variables (preparatory factors) affect the timing of the generation of surface runoff, the amount of water that infiltrates into the ground and the time to achieve the instability conditions (Della Sala and Cuomo, 2013; Reichenbach et al., 1998).

In fact, rainfall is not the primary cause of slope failures; it is the triggering agent (Simoni et al., 2004). Landslides are caused by the buildup of pore water pressure (triggering factor) into the ground (Campbell, 1975; Terzaghi, 1943; Wilson, 1989). Positive pore-water pressures, produced by percolating rainfall or by accumulation of water at a certain depth due to changes in permeability, decrease the shear strength (i.e. apparent cohesion) or increase the shear stress (i.e. driving forces) of the potential failure surface (Chen and Zhang, 2014; Terlien, 1998). Negative pore-water pressures in the unsaturated zone above the water table contribute towards its shear strength and thus help to maintain stability (Fredlund and Rahardjo, 1993).

The mechanisms transforming the rainfall regime into pore water pressure fluctuations are various and, sometimes, extremely complex to describe in actual slopes (Cascini et al., 2010; Dhakal and Sullivan, 2014). However, two hydrologic processes mainly control changes in pore pressure that may lead to failure: infiltration of water from the surface (saturation from above) and accretion of groundwater table levels (saturation from below) (EU-FP7, 2012; Terlien, 1998).

Infiltration is the portion of precipitation falling on the ground surface, that moves into surficial materials towards the stream (through flow) or the groundwater flow (Lu and Godt, 2013). Infiltration can occur because of rainfall, snowmelt, irrigation, or leakage from aqueducts. The infiltration of rainwater causes loss of suction (i.e. reduction in negative pore water pressure), during propagation of the wetting front, and rise of the groundwater table (i.e. generation of a positive pore water pressure), thus increasing pore water pressure with destabilizing effects (Ali et al., 2014; Collins and Znidarcic, 2004; Zhang et al., 2011).

Groundwater table response to rainfall is extremely variable and strictly connected to the before-mentioned preparatory factors (Cascini et al., 2010). Generally, when the saturated hydraulic conductivity is constant, a loss of suction causes a shallow failure while a rise in the water table causes a deep failure (Ali et al., 2014; Terlien, 1998). When the hydrological and geotechnical soil properties change vertically, the location of the potential failure surfaces can be determined by detailed analysis of the slopes or by monitoring pore-water pressure fluctuations on the potentially unstable slopes (Terlien, 1998).

Pore water pressure monitoring is fundamental to develop reliable models of hydrological processes responsible for rainfall-triggered landslides (Berti and Simoni, 2010). The pore pressure at the water table is zero by definition.

Above the water table, water flows up vertically in the overlying layer based on the water capillary-retention properties of the soil. Here, a tension-saturated zone extends where the pressure head is negative but the water content remains constant and saturated. This zone is called “capillary fringe” (Gillham, 1984). The height of the capillary fringe is equivalent to the air-entry value of the soil, which is the negative water pressure at which the largest soil pores begin to drain (Brooks and Corey, 1964; Godt and McKenna, 2008). The distributions of volumetric water content and pressure head above the water table are described by the soil-water characteristic curve (SWCC) (Godt and McKenna, 2008).
The pore pressure response to infiltration at depth is a transient process controlled by the hydraulic properties of the hillslope, the initial moisture content, and the rainfall characteristics (Godt et al., 2006a; Iverson, 2000; Savage et al., 2004). Freeze and Cherry (1979) showed observations of vertically downward infiltration above the water table, immediately after rainfall events, with an advance rate of the wetting front depending on antecedent wetness. An example in Washington state (Baum et al., 2005) shows that the response of initially dry soil is slow, whereas the increase of soil moisture results in much more rapid response. In both the cases, the response lag time increased with depth which is consistent with vertical flow assumption; significant lateral flow would tend to equalize response times or produce rapid responses at depth (Baum et al., 2010). Perched water and lateral flow commonly grow beneath the mantle where the permeability contrasts impede the downward percolation and lead to the rise of transient perched water tables and the downslope saturated flow of water over the impeding layer (Baum et al., 2010; Dhakal and Sullivan, 2014; Montgomery et al., 1997).

In literature, there are different hydrological models proposed for the estimation of the infiltration rates, which broadly can be divided in two main groups: a) empirical models, and b) physically based models (Cuomo and Della Sala, 2013). Among the empirical models, a commonly accepted one is the Curve Number (CN) method (USSCS - U.S. Soil Conservation Service, 1964) which is based on a simple mass balance equation between the runoff, the cumulative rainfall, the infiltration, and the maximum soil moisture retention. Among the physically based models, the most applied are the Green-Ampt models and the Richards equation models. The Green-Ampt method (Green and Ampt, 1911), based on the Darcy's law (1856), is a one-dimensional vertical infiltration process applied into an initially dry homogeneous soil with a uniform initial water content. The model assumes the presence of a continuous thin flux of water at the ground surface, causing a downward moving wetting front. The Richards equation method (Richards, 1931), describes an unsteady, variably saturated, percolating flow in response to rainfall, allowing the hydraulic conductivity to vary with water content. Several analytical solutions (e.g. Srivastava and Yeh 1991; Iverson 2000; Chien-Yuan et al. 2005) and approximate solutions (e.g. Cho 2009) to the Richards equation have been proposed in literature. Both classes of approach have significant limits, due to different generalizations that prevent a proper simulation of rainfall infiltration. For example, the CN method does not consider the hydraulic properties; the Green-Ampt method does not reflect the slope angle effect; and the Richards equation method requires the distribution of hydraulic conductivity and pressure head, which are not easy to measure.

To determine the critical pore water pressures, literature studies refer to the slope stability analysis. The *hillslope stability* is generally analyzed using the concept of "limit equilibrium", which allows to evaluate the conditions of equilibrium of a rigid-plastic body, whose soil mass tends to slide down an assigned area (of arbitrarily shape and choice) under the influence of gravity (Picarelli and Vinale, 2007). The limit equilibrium defines the limiting state of mechanical equilibrium between the shear stress and the shear strength of the slope material (Lu and Godt, 2013).
The stability is assessed through the introduction of a factor of safety (F_S), defined as the ratio between the resisting and the driving forces acting on a point along the potential failure plane (equation (10)):

$$F_S = \frac{Resisting\ forces}{Driving\ forces} \qquad (10)$$

The resisting force is the Coulomb shear strength of the soils, a combination of gravity, pore pressure and material properties. Thus, the knowledge of the groundwater regime is of fundamental importance in the analysis of slope stability (Cascini et al., 2006). The shear strength of the soil is given by the Mohr-Coulomb failure criterion (Skempton and DeLory, 1957). The driving force is the shear stress, i.e. the slope parallel component of gravity.
When the shear strength is grater then the shear stress (F_S>1), the slope is predicted stable. When the shear stress is grater then the shear strength (F_S<1), the slope is predicted unstable. F_S =1 is a state of equilibrium, but inherently unstable.

The local factor of safety is a value of a small part of the potential failure surface; the overall factor of safety is an average value taken over the entire potential failure surface (Baum, 1995).
When the failure surface is flat and parallel to the ground, the stability of the slope is analyzed through the simple 1-D limit equilibrium model called infinite-slope stability model (Taylor, 1948), whose stress conditions are repeated identically along any vertical (Picarelli and Vinale, 2007). It assumes that (a) each infinitely long slice of slope receives the same amount and intensity of rainfall, (b) the time required for infiltration normal to the slope is much less than for flow parallel to the slope (Collins and Znidarcic, 2004), (c) the wetting front propagates in a direction normal to the slope (White and Singham, 2012), and (d) the depth of failure is small compared to the length of the landslide mass (Ali et al., 2014). The infinite-slope stability model is frequently used to compute F_S under dry, saturated and variably saturated conditions. An alternative example of analytical solution for calculating F_S for failure surface geometries other than planar is the ordinary method of slices, in which the slope is divided into a number of slices separated by vertical boundaries. F_S is so computed for the n^{th} slice by summarizing the effect of the single shear strength and stress. A commonly used technique has developed by Bishop (1955), which improved the method of slices considering the inter-slice forces.

2.2.2 *Effects of rainfall in different soils*

Different behaviors can be expected in different geologic conditions. As described before, rainfall causes the buildup of pore water pressure into the ground and, consequently, the reduction of the effective strength (Campbell, 1975; Terzaghi, 1943). This mechanism is highly influenced by topographic and soil characteristics of the site (Cannon and Ellen, 1985).

Although nearly saturated conditions are often needed to reach the instability (Sidle and Swanston, 1982), landslides have been observed to occur in wholly or partly unsaturated conditions (Iverson, 1997; Lu and Godt, 2013; Rubin and Steinhardt, 1963). In unsaturated conditions, the contribution of capillary forces to the effective strength is of fundamental importance and depends on soil properties (especially the hydraulic conductivity), degree of saturation, matric suction and fluid interface properties (Ali et al., 2014; Bishop, 1959; Collins and Znidarcic, 2004; EU-FP7, 2012; Lee et al., 2014; Mitchell, 1976;

Torres et al., 1998). Unsaturated conditions are typical of steep and thin soils because the capillary forces allow the soil to remain stable at angles steeper than the friction angle (EU-FP7, 2012).
Since the 1970s, many hydraulic studies started to focus the attention on monitoring the pore pressure both in saturated and unsaturated soils. As example, Weymann (1973) indicated that saturated through flow can only develop within a surficial horizon with breaks in the vertical permeability which impede further vertical movement. Harr (1977), similarly, observed occasional saturation at soil-subsoil interface where the saturated hydraulic conductivity decrease of two order of magnitude, due to changes in pore-size distribution. Iverson and Mayor (1987), proved that the surficial groundwater flow, in different soil context, is mostly direct downward unregarding the degree of saturation. They also demonstrated that the increase in pore pressure propagates mainly from the surface through the unsaturated zone, attenuating with depth and dependently on the antecedent water content. The importance of the unsaturated zone dynamics in pore pressure response was stressed also by Torres et al. (1998). They hypothesized that, when the soil is close to saturation in the vadose zone (between capillary fringe and land surface), the pressure response is very quick, since any pulse of rain can quickly cause saturation.

Different types of rainfall can trigger both shallow and deep-seated landslides.
As said, shallow landslides are often triggered by short and high-intensity precipitation, whereas deep-seated landslides are triggered by prolonged and low-intensity rainfall (Campbell, 1975; Cancelli and Nova, 1985; Corominas, 2001; Crosta, 1998; Sidle and Swanston, 1982; Von Ruette et al., 2013). The subsurface flow and slope instability of shallow soils are controlled by several mechanisms such as (EU-FP7, 2012): (i) rapid accretion of pore water pressure, due to pulses of rainfall, infiltration and development of a wetting front in the unsaturated zone (Della Sala and Cuomo, 2013; Reid et al., 1997; Zimmermann et al., 1966); (ii) rapid rising of the water table (Matsushi and Matsukura, 2007; Wilson and Wieczorek, 1995); (iii) seepage forces (Iverson and Major, 1986); (iv) upwelling of pore pressure from fractured bedrock under a weathered regolith (Montgomery et al., 1997; Van Asch and Buma, 1997); (v) soil pipes in headscarps (Jenkins et al., 1988; Pierson, 1983); (vi) fluidization at the time of failure (Iverson and Lahusen, 1989). Crosta and Frattini (2003) grouped the factors governing the occurrence of shallow landslides in two categories: (a) the almost static variables, and (b) the dynamic variables. The first, such as soil properties, seepage in the bedrock

and topography, define the spatial susceptibility of the slopes. The second, such as the degree of saturation, assess the temporal triggering conditions along the susceptible slopes.
On the other hand, deep-seated landslides experience seasonal episodes of accelerated movements, due to seasonal rainy periods, rapid snowmelt, and regional climate perturbations (Bovis and Jones, 1992). Studies suggested that deep-seated landslides are initiated by the loss of negative pore water pressure or matric suction (Dahal et al., 2009). In these large complexes, complicated hydrogeological patterns can be found. Single or multiple water reservoirs can be identified (Malet et al., 2005), whose recharge can be supplied by deep circuits beside the infiltration rate (Tacher et al., n.d.). Moreover, pore pressure responds to large rainfall input within several days at moderate depth and within several weeks to several months at higher depth (Baum and Reid, 2000; Coe et al., 2003; Iverson and Major, 1987; Reid, 1994)

The rise of pressure head into the ground can be produced also by different soil textures (Tofani et al., 2006). Fine-grained soils, for example, are widely susceptible to rainfall-induced slope failures due to generally low shear resistances (Hutchinson, 1988). In fact, the response of the slope material relies primarily on ground permeability. The low permeability of fine-grained soils (e.g. clay-rich soils) impedes the flow of water thus reducing the soil suction and developing the pore pressure (Baum, 1995). These materials are normally more sensitive to precipitation with long duration and moderate intensity (Casagli et al., 2006), therefore antecedent rainfall have high influence. Baum and Reid (1995) documented that surface infiltration saturates clay-rich soils in few days, causing rapid pressure pulses, and lags behind with depth as rain attenuate, while gradients maintain a strong downward component. Matsushi and Matsukura (2007), highlighted that clayey soils are likely to maintain nearly-saturated conditions during the wet season, favoring the rapid buildup of positive pore pressures. Berti and Simoni (2010) measured in a clay cover relatively fast and transient responses to precipitation at 0.1-2.5m of depth, which can be well reproduced by a one-dimensional linear diffusion model.
On the contrary, course-grained soils are susceptible to rainfall-induced slope failures during periods of intense rainfall, due to increased pore pressure and seepage forces (Dahal et al., 2009). In these cases antecedent rainfall has little influence on landslide occurrence (Corominas, 2001)

2.2.3 Review of the existing models

In literature, two kinds of physically based approaches have been applied to explain the relationship between rainfall and slope failures: hydrological models and slope stability models (Caris, 1991; Crozier, 1986; Terlien, 1998).

Hydrological models are used to analyze the interaction between rainfall and soils (i.e. infiltration process, changes in the groundwater table and variations of the physical properties) and to obtain pore water pressure profiles for assessing the rainfall amounts that are required to build up critical pressure heads (Segoni et al., 2009). Various hydrological models have been proposed to:

(i) predict the accumulation of the infiltrated water into the ground (Collins and Znidarcic, 2004; Green and Ampt, 1911; Iverson, 2000; Iverson and Major, 1986; Montgomery and Dietrich, 1994; Wilson, 1989; Wu and Sidle, 1995);
(ii) calculate the soil moisture to assess the effect of antecedent rainfall (Crozier and Eyles, 1980; Crozier, 1999; Glade et al., 2000; Godt et al., 2006a; O'Loughlin, 1986; Ponziani et al., 2012; Rianna et al., 2014; USSCS - U.S. Soil Conservation Service, 1964);
(iii) monitor the groundwater and model seasonal water table changes (Baum and Reid, 1995; Haneberg, 1991; Hodge and Freeze, 1977; Iverson and Major, 1987);
(iv) estimate the temporal and spatial distribution of groundwater recharge (Dripps and Bradbury, 2007);
(v) reproduce the soil suction and water content fluctuations (Greco et al., 2013).

Slope stability models are used to determine critical pore water pressures with the aim to compute the slope factor of safety (F_S) (Chen and Zhang, 2014). These models extend spatially the simplified stability methods widely adopted in geotechnical engineering (Taylor, 1948; Wu and Sidle, 1995).
Many different techniques and methods have been developed in recent years for slope stability analysis. The infinite-slope stability model is one of the most commonly used, due to its simplicity (Ali et al., 2014; Baum et al., 2002; Collins and Znidarcic, 2004; J.W. Godt et al., 2008; Iverson, 2000; Montgomery and Dietrich, 1994; Raia et al., 2014; Salciarini et al., 2006; Savage et al., 2003; Wu and Sidle, 1995). However, Li et al. (2013)

demonstrated that besides the approximations it still maintain validity as a simplified framework to assess failures due to the infiltration of rainfall. Some application of the infinite-slope model are the Level I Stability Analysis (LISA) model (Hammond et al., 1992) that uses Monte Carlo simulation of the infinite-slope equation to estimate a probability of slope failure in relative stability assessment of natural slopes, and the PROBability of STABility (PROBSTAB) model (Van Beek and Van Asch, 2004) that compute the probability of failure for the entire soil column.

Much research has been done to *combine hydrological and slope stability models* to explain the relationship between rainfall and slope failures (Armaş et al., 2014; Baum et al., 2002; Borga et al., 1998; Casagli et al., 2006; Crosta and Frattini, 2003; Dahal et al., 2009; Montgomery and Dietrich, 1994; Raia et al., 2014; Salciarini et al., 2013; Terlien, 1998; Tofani et al., 2006; Torres et al., 1998; Wu and Sidle, 1995). Numerous techniques have been developed and implemented in GISs to evaluate the effects of topographic convergences and drainage areas on slope failures (D'Amato Avanzi et al., 2009). These physical methods generally rely on the application of one-, two- or three-dimensional hydrological models coupled with, usually, an infinite-slope safety factor equation by means of analytical, numerical, and hybrids mathematical tools (J.W. Godt et al., 2008).
The most adopted combinations are between the infinite-slope stability analysis and (Baum et al., 2010):

a) a steady-state shallow subsurface flow model (Montgomery and Dietrich, 1994; Pack et al., 1998);
b) a time-dependent or quasi time-dependent shallow groundwater flow model (Van Beek and Van Asch, 2004; Wu and Sidle, 1995);
c) a transient infiltration model (Baum et al., 2002; Crosta and Frattini, 2003; Iverson, 2000; Salciarini et al., 2006; Savage et al., 2004, 2003);
d) a distributed model of vertical suction and moisture (Rigon et al., 2006; Simoni et al., 2008);
e) a fully three-dimensional solution to the Richards equation (Mirus et al., 2007);
f) a one dimensional numerical solution for unsaturated and variably saturated flow (Godt and McKenna, 2008; Mercogliano et al., 2013)

A large number of coupled physical models have been proposed in literature. Here, the most common are presented.

One of the first successful examples of coupled models was the TOPography based hydrological MODEL (TOPMODEL) suggested by Beven and Kirkby

(1979). They introduced a topography index to analyze the influence of topography on the behavior of saturated slope materials. The index was then incorporated in a hydrological model that simulate the runoff in a spatial context.

Shortly after, the HYSteretic Water and SOlut transport in the Root zone (HYSWASOR) simulation model (Van Genuchten, 1980) was developed. It is a finite difference 1-D isothermal hydrological model for transport of water in saturated conditions, combined with a slope stability model using Bishop's method of analysis. This type of model evolved in numerous later examples such as the Combined Hydrology And Slope stability Model (CHASM) (Anderson and Lloyd, 1991) produced by Bristol University, the 2D Hillflow (Bronstert, 1994), and the GwFluct v 2.0 (Terlien, 1996).

Among the most diffused physical models there is the SHALlow slope STABility model (SHALSTAB) proposed by Montgomery and Dietrich (1994). It is based on a geometrically confined infinite slope model of the Mohr–Coulomb failure criterion coupled with a simplified steady state hydrologic model (O'Loughlin, 1981) based on Darcy's law. The main assumptions of this combined model are (D'Amato Avanzi et al., 2009): (i) infinite slope; (ii) parallel failure plane, water table and ground surface; (iii) failure plane at the colluvium-bedrock boundary; (iv) steady state shallow subsurface flow; (v) absence of deep drainage and flow in the bedrock. At each point of the slope SHALSTAB estimates the pressure head buildup, above an impermeable layer, assuming a constant infiltration rate which also includes the entire part of precipitation that has infiltrated atop (Picarelli and Vinale, 2007). Moreover, this model considers some material properties as input and can be used in the spatial assessment with GIS (Dahal et al., 2009; Grelle et al., 2013). However, the hydrologic approach suggested by Montgomery and Dietrich (1994), neglects moisture content above the water table and does not account for transient response to rainfall.

In 1995, Wu and Sidle, developed a Distributed SLope stability Model (dSLAM) for steep forested basins, long timescales and landscape management. They based the approach on a kinematic wave groundwater model, including vegetation impacts in terms of root strength and vegetation surcharge, and an infinite slope model. The method was intended to analyze rapid, shallow landslides and the spatial distribution of F_S in both temporal and spatial dimensions.

Pack et al. (1998), developed another model, the Stability INdex MAPping (SINMAP) which can be applied for slopes that have a shallow soil depth and impermeable underlying bedrock. SINMAP is similar to SHALSTAB and dSLAM, because they are all based on a geometrically confined infinite slope model that takes into account the dynamic regime of the pore pressures and they can be implemented in a GIS framework. These steady models are very useful for a preliminary stability assessment over areas particularly large, but have the limitation of ignoring the effect of the transient phenomena due to infiltration (Iverson, 2000). However, SINMAP is the more advanced because uses cohesion and root cohesion (Dahal et al., 2009).

Montrasio (2000) worked on a simplified model for the forecast of soil slip (Shallow Landslides Instability Prediction - SLIP), which has been widely applied at a local scale in Italy and implemented for a real-time monitoring at a regional scale (Quintavalla et al., 2009). This model is based on the limit equilibrium method applied to an infinite slope and is able to link the factor of safety with the seasonal, daily or hourly rainfall trend, taking into account the underground water flow.

Iverson (2000), extended the pore pressure distribution model of Reid (1994), including an infinite-slope stability model and a prediction of near-surface pore-pressure conditions, to assess short-term pore water response to rainfall in the hypothesis of vertical infiltration. The model helps to predict timing, depth, and acceleration of rainfall-induced landslides (Dahal et al., 2009). He used rational approximations of the Richards equation to develop a theoretical model that augments steady and quasi-steady models by requiring intensity-duration and hydraulic diffusivity as input parameters. The simplified model framework is valid for varying periods and for different hydrological conditions (Crosta and Frattini, 2003). Nonetheless, it cannot predict all complexities observed in the field (Iverson, 2000), but only under a restrictive and unrealistic set of conditions (i.e. very low intensity and long duration rainfall, small depth of the failure surface compared to the sliding mass, anisotropic saturated hydraulic conductivity) (Jonathan W Godt et al., 2008).

A large part of the literature is based on the U.S. Geological Survey’s Transient Rainfall Infiltration and Grid-Based Regional Slope-Stability (TRIGRS) model (Baum et al., 2008, 2002, 2010), which simulates the pore pressure response to rainfall infiltration. TRIGRS uses a distributed approach to model transient vertical groundwater flow over a digital landscape combined with an infinite slope-stability calculation after Iverson (2000). The model assumes a two-layer system that consists of an unsaturated zone above a saturated zone. The timing needed to reach potential instability in the unsaturated zone depends on the soil-water characteristics of the hillslope material (Godt et al., 2012). Both input variables and rainfall rate may vary in space and time. TRIGRS utilizes an approximate analytical solutions of the Richards equation for saturated (Iverson, 2000; Savage et al., 2003) and variably saturated conditions (Savage et al., 2004; Srivastava and Yeh, 1991) to determine a one-dimensional solution for pore pressure diffusion in a soil layer of finite depth and its spatial and temporal oscillations. The difference between TRIGRS and SHALSTAB is that the first uses analytical solutions of the infiltration both transient and stationary (Picarelli and Vinale, 2007). The variation of pore pressure following a rainfall event is a non-stationary process; it depends on the rainfall intensity and duration, and on the hydraulic characteristics of the soil. A proper simulation of the phenomenon requires therefore the stability analysis to be coupled with a transitional infiltration model. The transient solution for pore pressure response, considered in TRIGRS, can be applied on any steady state groundwater flow that is consistent with model assumption (Jonathan W Godt et al., 2008). Input data for the model include time-varying rainfall, topographic slope, colluvial thickness, initial water table depth, and material strength and hydraulic properties. Finally, TRIGRS computes factor of safety at any time during a rainstorm and is implemented in a GIS framework. Key limitations of the model are: (a) the assumption that near-surface soils are saturated or nearly saturated, (b) the assumption that soils are homogeneous and isotropic, and (c) the inability of the model to simulate flood response, which would require distributed routing capability (Tao and Barros, 2014).

TRIGRS has been widely applied in the international literature. For example, Keim and Skaugset (2003) used the model to characterize the effects of forest canopies on slope stability in the northeastern United States. Salciarini et al. (2006) analyzed susceptibility to shallow landslides in an area in the eastern Umbria (central Italy). Tan et al. (2008) adopted TRIGRS for shallow landslides in Taiwan with the support of GIS, GPS, and Remote Sensing framework (3S). Godt et al. (2008a) tested the model in an area of Seattle, Washington, and showed that is effective for shallow landslide hazard maps. Vieira et al. (2010) used TRIGRS in Brasil, introducing two indexes for back analysis: Scars Concentration index (i.e. the ratio between the number of output cells with scars and the total number of cells with scars within the catchment), and Landslide Potential index (i.e. the ratio between the number of cells with scars, in each defined class, and the total number of cells in that same class). Grelle et al. (2013) performed the analysis in southern Italy introducing an initial water table depth estimation model, a probabilistic analysis of rainfall, and some new indexes for back analysis validation. Raia et al. (2014), proposed a new probabilistic code of the model (TRIGRS-P) to overcome the problem of poor knowledge of terrain characteristics over large study areas.

Another example of a coupled hydrological-slope stability model is the Geo-Slope package (Geo-Slope, 2003a, 2003b). SEEP/W (Geo-Slope, 2003a) adopts an implicit numerical solution of Darcy's equation, for saturated and unsaturated flow conditions, to analyze the seepage and describe the pore-water pressure variations within porous materials over space and time. SLOPE/W (Geo-Slope, 2003b) performs the slope stability analysis adopting the limit equilibrium method and a variety of methods (e.g., a simplified Bishop's method, the Spencer method, a generalized limit equilibrium method) to solve the computational problems for the factor of safety. Coupled SEEP/W–SLOPE/W analyses have been adopted successively to evaluate the dynamic conditions of both the stability of riverbanks and slopes (Aleotti, 2004; Casagli et al., 2006; Collins and Znidarcic, 2004; Crosta and Dal Negro, 2003; Dahal et al., 2009; Rinaldi et al., 2004). Dahal et al. (2009) have applied an example of the SEEP/W–SLOPE/W analyses in Nepal, for the rainfall-triggered landslides that occurred during an extreme monsoon rainfall event on 23 July 2002, to understand the relationship of pore pressure variations in soil layers and to determine the spatial variation of landslide occurrence. Tofani et al. (2006) performed the SEEP/W-SLOPE/W analyses to investigate the instability mechanisms behind rainfall-triggered landslides that occurred during the storm of 20–21 November 2000 in Tuscany (Italy).

Numerous coupled models have attempted to include stochastic uncertainty analysis to account for heterogeneity and errors in specified soil properties (e.g., thickness, cohesion, friction angle) (Tao and Barros, 2014). For example, the distributed hydrological model with coupled water and energy budgets (GEOtop) (Rigon et al., 2006) was combined with an infinite-slope geotechnical model (GEOtop-FS) (Simoni et al., 2008) to simulate the probability of shallow landslide occurrence for saturated conditions. GEOtop-FS computes soil moisture and matric suction within individual soil layers by a numerical solution of the Richards equation in a 3-D scheme (Papa et al., 2013; Von Ruette et al., 2013). This model uses Gaussian distributions to describe the range of independent parameters and linear uncertainty analysis to estimate their combined effect on the factor of safety (Tao and Barros, 2014).

Mirus et al. (2007) estimated slope stability using a fully three-dimensional numerical solution to the Richards equation combined with the infinite-slope equation. They demonstrated that, without taking into account convergent subsurface flow, pore water pressures, and thus slope stability, are underestimated.

Lehmann and Or (2012) proposed a Landslide Hydromechanical Triggering (LHT) model, successively extended in Catchment-scale Hydromechanical Landslide Triggering (CHLT) model (Von Ruette et al., 2013). The CHLT model enables evaluation of the effects of soil type, mechanical reinforcement (soil cohesion and lateral root strength), and initial soil water content on landslide characteristics. The simplified model statistically predicts localized landslide patterns, volumes release, and wide landslide size frequency distributions.

Lanni et al. (2012) produced a simplified physical model named Connectivity Index-based Shallow LAndslide Model (CI-SLAM) for shallow landslide forecasting. In this method, a dynamic topographic index-based hydrological model is combined with an infinite slope stability model to describe the transient lateral flow. Such flow, initiates only if rainfall exceeds a threshold value determining hydrological connectivity.

Finally, Rossi et al. (2013), developed the HIgh REsolution Slope Stability simulator (HIRESS) that integrates a hydrological and a geotechnical model to provide the probability of slope failure, given an uniform Monte Carlo probability distribution for input parameters. The HIRESSS code is used for analyzing shallow landslide triggering in real time, on large areas, using parallel computational techniques. The hydrological model is based on an analytical solution of an approximated form of Richards's equation under the wet condition hypothesis. The geotechnical model is based on an infinite slope model and it takes into account the increase in strength and cohesion due to matric suction in unsaturated soils and the soil mass variation on partially saturated soil due to infiltration.

2.2.4 Advantages and limitations of the physical models

The main advantage of the physical models is that they can predict the slope failure accurately considering site specific conditions (Chen and Zhang, 2014). Being process-driven, they gain the benefit of considering the geotechnical parameters that characterize the material involved and the dynamic factors which affect the phenomenon (rainfall and soil characteristics) (D'Amato Avanzi et al., 2009). Thus, for both small and widespread areas with non-homogeneous soils, these models are particularly appropriate. Moreover, when a large data set on historical landslides and rainfall patterns is limited, the hydrogeological processes need to be studied in detail to describe the mechanisms that are responsible for rainfall-induced landslide (Terlien, 1998). In this case, the application of a deterministic approach is desirable to find critical rainfall amounts (Wilson and Wieczorek, 1995). Specifically, some models seems to be particularly valuable to take into account the heterogeneity of the land in a distributed manner and with a high level of detail (e.g. TRIGRS). Others, provides an optimal spatial distribution of critical rainfall (e.g. SHALSTAB). Finally, other models show to be suitable tools for stability analysis in nearly real time and for large scales (e.g. SLIP).

However, various limitations exist. The main constraint is that physically based models require and depend on detailed spatial information on the physical, mechanical, geotechnical, hydrological, lithological, and morphological properties that control the initiation of landslides (Berti et al., 2012; Guzzetti et al., 2007; Segoni et al., 2009). This information is difficult to collect precisely over large areas due to the high spatial variability (Cervi et al., 2010; Terlien, 1998), and is rarely available outside specifically equipped and onerous field investigations (Chen and Zhang, 2014). For this reason, they are more commonly applied at the slope or catchment scale (Baum et al., 2002; EU-FP7, 2012; Mercogliano et al., 2013; Segoni et al., 2009). Moreover, the calibration of physical models needs site-specific precipitation measurements and exact location and timing of slope failures, but such data are not usually available (Guzzetti et al., 2007). Another limitation for the application of these methods over large areas is the need for a relevant computational time which is not compatible with real-time applications (Rossi et al., 2013). Additionally, these models that compute F_S cell by cell, usually overestimate the potential instabilities because a single instable element do not slide if it is surrounded by stable elements (Papa et al., 2013). Furthermore, assumptions of these models are too restrictive, e.g. the pore water pressure responses very rapidly to transient rainfall and the pressure redistribution includes a large component normal to slope. Finally, the best performance of physically based models is achieved when attempting to predict shallow landslides (soil slides and debris flows), rather than predicting deep-seated landslides (Guzzetti et al., 2007). In fact, the characteristics of shallow landslides (e.g., modest thickness of terrain involved, almost planar sliding surface, water table almost parallel to the sliding surface) are often compatible with assumptions used by these models (Picarelli and Vinale, 2007).

3 Research framework

3.1 Research objective, hypotheses and questions

Rainfall induced shallow landslide forecasting is an issue of remarkable importance worldwide, which has been broadly deepened during the last decades. Much of the research have focused on the application of either empirical or physical models at various scales. The choice of the method and the scale is mostly determined by the availability of data and the purpose of the study.
Empirical models are commonly used at regional and global scale when historical rainfall and landslides inventories are available. On the other hand, physical models are generally applied at local and slope scale because they requires nearly real time hydrological and geotechnical data.
Landslide monitoring and forecasting in the Marche region, are carried out by the Civil Protection "Regional Functional Center" (CFR), in order to setting up the warning system and support the contingent emergency management activities. For this purpose, site-specific and calibrated rainfall thresholds are required. However, these agencies are responsible for large territories (e.g. hundreds or even thousands of square kilometers) and so they cannot usually rely on physically based models because of the difficulty of defining the exact spatial and temporal variation of the many involved factors. Conversely, empirical models, ignoring the physical processes, may oversimplify the real conditions of the territory and the correlation between the primarily cause (rainfall) and the effect (landslide).

The primary *objective* of this study is determining the potential landslide rainfall thresholds that could be useful as a decision tool for the Marche CFR. In order to achieve this, the research intended to apply different predictive models to enhance landslide forecasting in the Marche Region.

The entire research revolves around the *hypothesis* that the synergic use of empirical and physical approaches improves the ability to analyze the correlation involving landslides and rainfall. Particularly, the study investigates the possibility of merging empirical and physical methodologies to enhance the prediction of shallow landslides in a specific area of the Marche region. It is hypothesized that the use of different methods of analysis on a same area of study and the comparison between the results obtained can:

i) enhance the quality and reliability of each model, ii) identify the main triggering factors of the phenomena analyzed and neglect the less important, and iii) choose the most appropriate methodology for the forecasting activity in the study area.
The study area selected for this research is borderline-scale and therefore challenging for both the techniques: it is smaller than the area usually selected for the application of empirical models and bigger than areas selected for physically based studies. The reason of this choice is for reaching a compromise of the two models to allow a comparison and to take advantage of the benefits of both the approaches.

The process of hypothesis testing has been guided by several research questions.

First, is the correlation between rainfall and landslide initiation positive in the study area? This is the primary question to answer and the basis of the entire research. Indeed, is necessary to demonstrate that rainfall is one of the key triggering factor of shallow landslides within the selected field.

Second, how geologic factors can be considered as input in empirical rainfall thresholds models? Additionally, what are the most effective rainfall parameters (e.g. intensity, duration, cumulative rainfall, antecedent moisture…) for the definition of rainfall triggering thresholds within the study area? Moreover, are the trends of these parameters in agreement with the hydrogeological characteristics of the terrain? The assumption is that such methods can be calibrated, at the beginning of the analysis, using local hydrogeological properties, which should influence the modeled rainfall thresholds.

Third, how statistical analysis can be applied as input of a deterministic model? Furthermore, is it possible to use the physical TRIGRS model over a broad area, even where geotechnical and hydraulic properties data as well as temporal changes in topography or subsurface conditions are not available? Here, the postulation is that, when a detailed monitoring of physical properties is not feasible, a statistical approach may help in assessing the process-based model.

Finally, after a validation test, which is the best methodology for the study area? The hypothesis is that the integration of the approaches makes all of them stronger and valid. In addition, the concurrent application allows to overcome the limitations and to benefit of the advantages of both the models.

3.2 Study area

This chapter provides morphological, hydrographical, geological, lithological, and climatological description of the Marche region. Detailed description is given for the study area, which is situated in the eastward section of the Esino river basin.

3.2.1 Overview of the Marche region

The area selected for this study is located in the Marche region, on the East coast of central Italy.

The *morphology* of the Marche region can be summarized in two parts: the mountainous western portion (the Apennines) and the hilly eastern area (the Subapennine) that extends towards the Adriatic coast (Figure 4) (Bisci and Dramis, 1991). The Region is characterized by (i) a narrow coastal plain, which varies in width from a few hundred meters to a few tens of kilometers, (ii) preponderance of hills with an average height of 300-400 m, and (iii) a mountainous area. In the northern portion of the territory, the Apennine chain splits into two ridges: the inland Umbro-Marchean ridge, which is the watershed between the Adriatic and the Tyrrhenian tivers, and the eastern Marchean ridge, crossed by some of the major rivers (Figure 4). These chains unify in the south originating the Sibillini Mountains in which are sited the highest heights (Dramis, 1984).

The majority of the springs of the main *hydrographic network* (i.e. Foglia, Metauro, Esino, Potenza, Cienti and Tronto) are in the Umbro-Marchean ridge. The initial section of the main rivers, therefore, flows through the Apennines and towards the Adriatic Sea with E-NE direction (Figure 4). In the mountainous portion, characterized mainly by the action of linear erosion carried by rivers, the valleys are narrow and deep (Coltorti and Nanni, 1987). In the hilly section, there is a significant change in the morphology of the river valleys, which are wider and with gentle slopes. Here, the action of the water is less aggressive and erosive due to the lower energy of the relief (Bisci and Dramis, 1991). The sea mouth of the rivers is via estuaries that do not protrude from the very general outline of the coast.

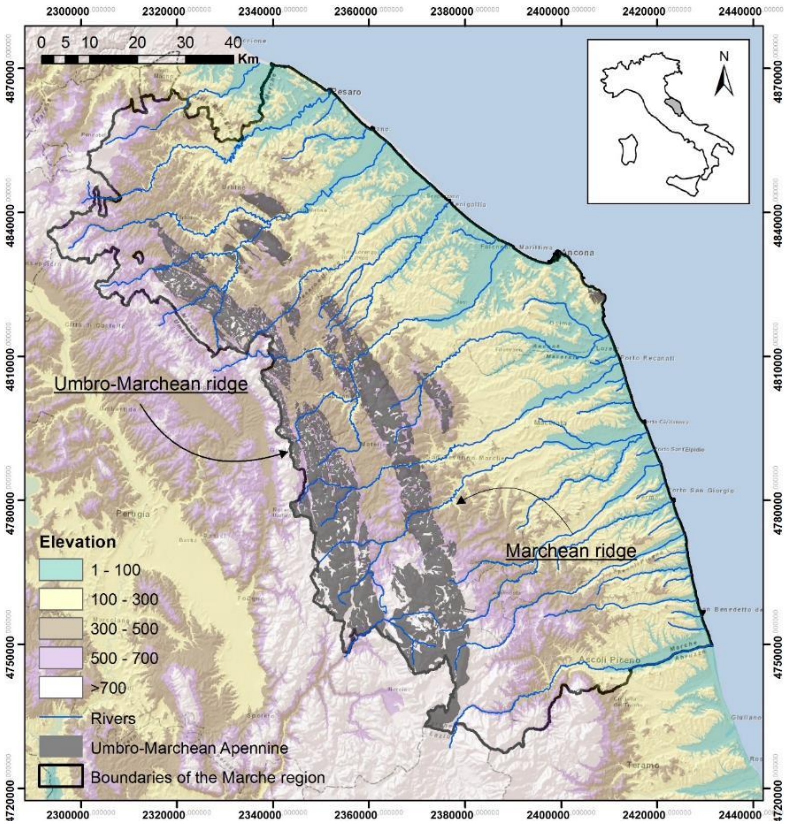

Figure 4 The morphology and hydrography of the Marche region. The figure highlights the E-NE direction of the regional rivers

From a *geological* point of view, the Umbro-Marchean Apennine is the most southern and external part of the Northern Apennines. It is the result of a complex history of deformation that has affected the entire stratigraphic succession of the African continental margin from the opening of the Tethys Ocean (Late Triassic) (Principi et al., 2007). The sedimentary succession, almost continuous from the Upper Triassic to the Neogene, has variations in thickness and facies that reflect the time-space oscillations of the sedimentary environments (Centamore and Micarelli, 1991). In the first Triassic stage, the deposition of sediments took place in correspondence of a basal carbonate platform that in the Jurassic was substituted by a pelagic basin with high subsidence (Figure 5). This basin, called the Umbro-Marchean basin, is mainly composed of calcareous and siliceous rocks. The next phase consisted of a more uniform marine system that was maintained for a long period of about 100 million years from Cretaceous to the end of Paleogene. The pelagic formations of Cretaceous and Paleogene of the Umbro-Marchean basin consist mostly of calcareous marl, marl and argillaceous marls (Figure 5). From the Early Neogene (Miocene), the basin started to be affected by the first compressive forces related to the genesis of the Apennines. As a result, it assumed the characteristics of a foreland with turbiditic sedimentation derived from the continental shelf (Centamore and Micarelli, 1991) (Figure 5). In this stage, three main morpho-structural units separated by the emerged ridges were outlined: (i) the Umbrian basin, (ii) the internal Marchean basin, and (iii) the external Marchean basin. Among the Miocene formations, the Chalky-Sulfurous is the most widespread. During the Plio-Pleistocene period, the gradual eastward migration of the foreland basin led to progressively lowering marine conditions (Fiorillo, 2004) (Figure 5). The Plio-Pleistocene marine sedimentary succession depicting the Marche region is mainly characterized by pelitic and pelitic-arenaceous sediments (Antonini et al., 2003).

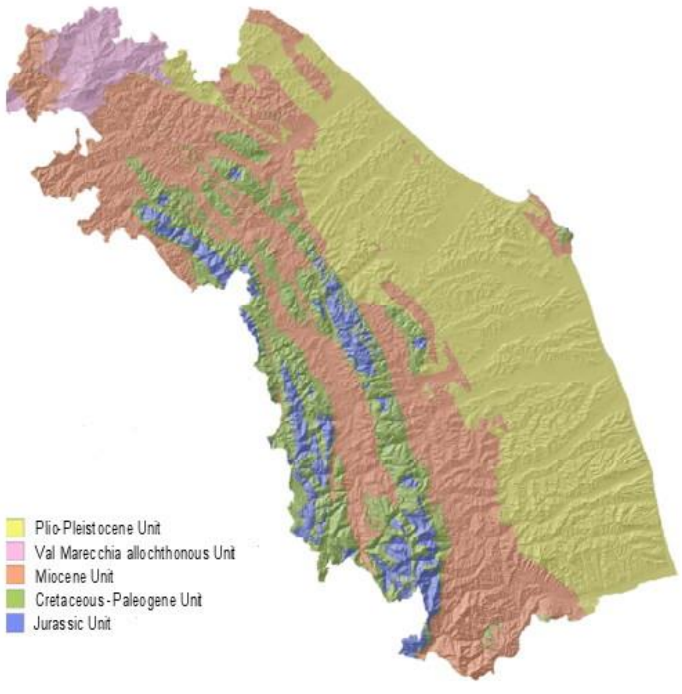

Figure 5 Geological map of the Marche region (modified after APAT - Dipartimento Difesa del Suolo 2007)

The continental deposits related to the Quaternary of Umbria-Marche consist of alluvial terraces and slope deposits (Principi et al., 2007). Finally, in the northern area of the Region emerges the complex of Val Marecchia, which is disconnected from the rest of the regional landscape for its specific structural characteristics, being a chaotic allochthonous complex slipped from the innermost parts of the Apennines (Figure 5).

The *lithologies* occurring in the Marche region are quite various, even if characterized by the exclusive presence of sedimentary rocks. These sediments have different physical, mechanical, structural, and disposition features, depending on their composition and grain size, which cause a different degree of erosion and propensity to failure. The lithotypes have been grouped in the following *hydrogeological classes* (Coltorti and Nanni, 1987) (Figure 6):

a) *limestone*, characterized by steep and averagely stable slopes typical of the Apennines, high reliefs, scarce erosion, falls and topples as types of failure, possible karst and freezing phenomena;
b) *marl and calcareous marl*, characterized by a percentage of clay that facilitates erosion and does not allow the maintenance of steep slopes, wider river valleys, low permeability;
c) *sandstone, conglomeratic sandstone and pelitic sandstone*, characterized by sharp relief and rugged morphology, resistance to erosion, good mechanical features but where they form steep slopes and in correspondence of the areas affected by tectonic phenomena may originate falls or slides, generally low permeability that causes a greater amount of water flowing on the surface;
d) *chalk*, characterized by materials poorly resistant to erosion and particularly soluble making them subject to karst phenomena, low and rounded reliefs;
e) *clay and sandy-clay*, characterized by hilly morphology and gentle slopes, very low permeability and easy erodibility (e.g. badlands), high susceptibility to landslides especially slides and flows, freeze-thaw cycles;
f) *alluvium and colluvium*, characterized by loose rocks, resistance to erosion and permeability directly proportional to the particle size.

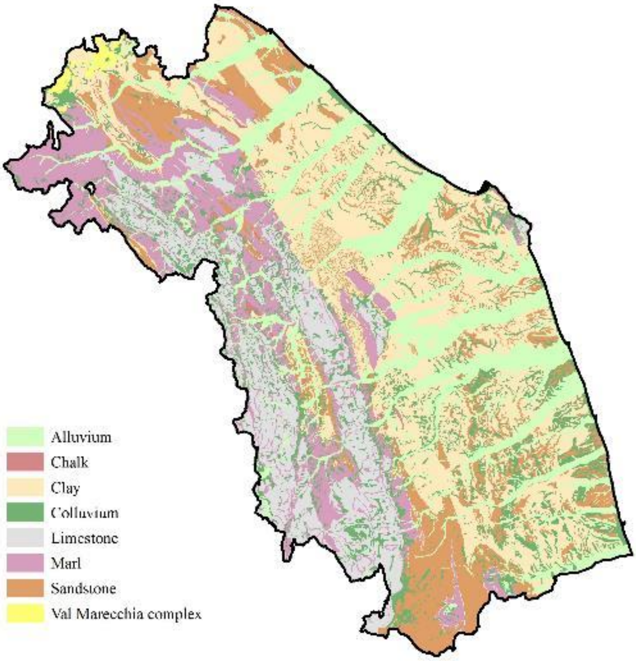

Figure 6 Lithology of the Marche region, grouped in hydrogeological classes

Climatic factors play a key role in the initiation of landslides, especially in climates where long dry seasons alternate with periods of intense and (or) prolonged rainfall. The climate characteristics of Marche are affected by the Adriatic Sea, which weakly mitigate the cold air mass coming from north and east, and by the presence of the Apennine chain, which hampers the mostly temperate and humid air masses from west (Bisci and Dramis, 1991). Consequently, the Region is characterized by two macroclimates: the mediterranean and the temperate. The mediterranean macroclimate belongs only to the coastal strip from the center (Ancona) to the southern boundary with Abruzzo region. The temperate macroclimate is distinguished in: (a) submediterranean, which includes the hilly portion and so most of the region, (b) mesotemperate, which characterize the Apennine ridge, and (c) criotemperate, which corresponds to the highest peaks of the Apennines.
The rainfall pattern (data from 1950 to 1989) can be divided in three longitudinal homogeneous zones (Figure 7): (i) a coastal belt with MAP of 600-850mm, (ii) a central belt with MAP of 850-1100mm, and (iii) a

mountain belt with values of MAP over 1100mm. However, the southern part of the Region is usually less rainy than the north.

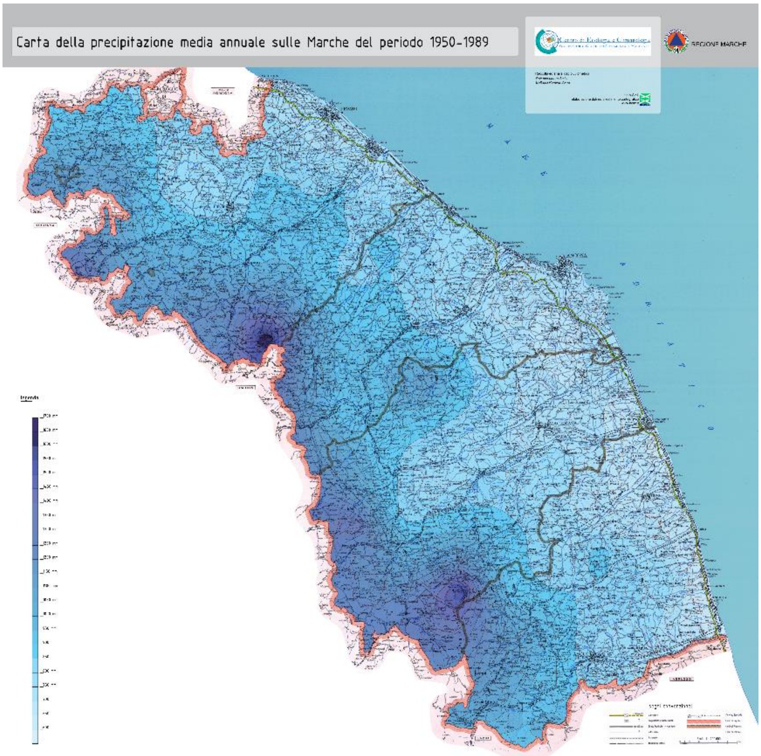

Figure 7 Map of the mean annual precipitation of the Marche region during the period 1950-1989 (Amici and Spina, 2002)

3.2.2 The post-orogenic complex of the Esino river basin

Surveys, data collection, and analysis of this research were carried out in the eastward section of the Esino river catchment, Marche region. The rational for this choice is that the Esino river basin is one of the largest and most inhabited (National Institute of Statistics - ISTAT, 2014) of the region. Therefore, the exposure to the hazard is higher and it is easier to gather information about past landslides.

The river extends for 85 km, from its natural spring located at 576m a.s.l. on Mount Cafaggio, near Esanatoglia (Macerata), to its mouth situated near

Falconara (Ancona) on the Adriatic coast (Boni and Mastrorillo, 1995) (Figure 8). As almost all the major rivers of the Marche region, the Esino have the springs in the Umbro-Marchean ridge and flows in E-NE direction toward the Adriatic Sea. The river has a medium slope of 1.2%, and its average discharge at the mouth is about 18 m^3/s, with value ranging from 5 m^3/s in the summer and 1400 m^3/s in the fall (Bisci and Dramis, 1991). The hydrographic network in the Esino basin is strongly controlled by the structures and the heterogeneous lithology of the Apennines and general morphology of the Marche territory (Coltorti and Nanni, 1987).

The catchment area of Esino covers 1223 square kilometers mainly included within the administrative boundaries of the province of Ancona, with an appreciable portion in the province of Macerata and only minor areas in the provinces of Pesaro and Perugia (the latest is in the Umbria region).
The Esino basin is located within the geological and morphological setting of the Umbro-Marchean Apennine, which in the studied basin splits into two ridges: the inland Umbro-Marchean ridge and the eastern Marchean ridge. In the catchment area, these ridges circumscribe a syncline fold, the core of which is constituted by a younger and easily erodible outcropping layer. Therefore, the concurrence between tectogenesis and morphogenesis caused the stream to cross perpendicularly the anticlines and have in some cases segmented trend (Coltorti and Nanni, 1987).
The geological setting of the Esino basin is a Quaternary sedimentary sequence that resulted from compressional tectonic forces started during the Neogene (Bisci and Dramis, 1991; Principi et al., 2007).
Almost exclusively sedimentary rocks, roughly divided into the following hydrogeological complexes, characterize the area: (i) carbonatic, (ii) terrigenous, and (iii) post-orogenic sediments. Carbonate rocks prevail in the basin's westward section, terrigenous sediments dominate the central area, and a post-orogenic complex covers the basin's eastward section, from the Subapennine hills to the Adriatic coast (Gentili and Dramis, 1997) (
Figure 8). Every material determines different levels of slope erosion and different mass movement mechanisms (Bisci and Dramis 1991). For example, the carbonate complex is principally composed of calcareous rocks susceptible to falls and topples. In contrast, the terrigenous and post-orogenic complexes of the study area are more susceptible to slides and flows (Antonini et al., 2003; Bisci and Dramis, 1991).

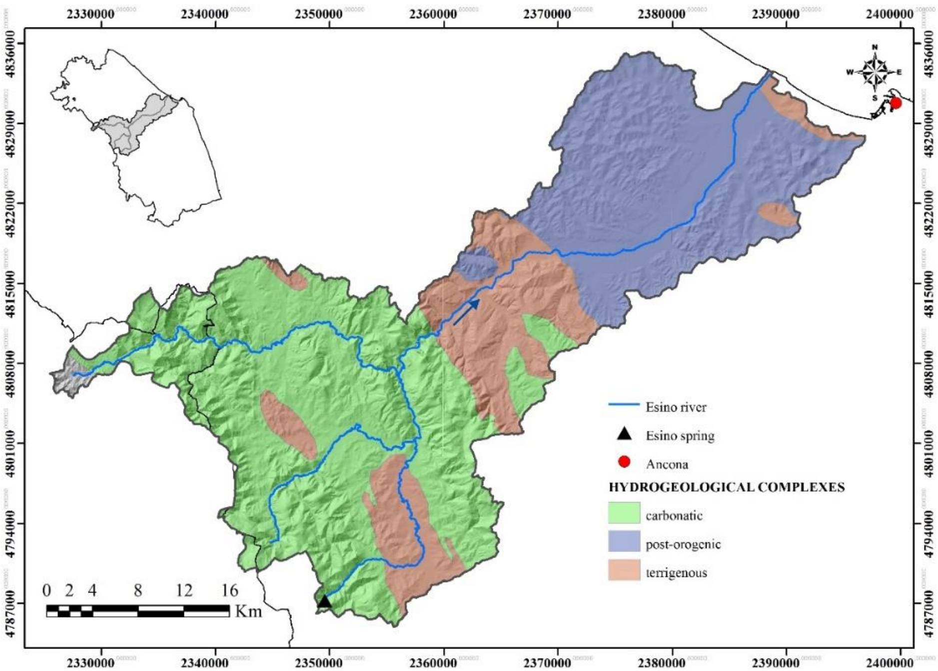

Figure 8 Hydrogeological map of the Esino river basin

The study area covers about 550km^2 and is located in the post-orogenic sedimentary complex of the Esino river basin. It contains abundant marine post-orogenic sediments of the Pliocene and Pleistocene, also known as blue clay deposits (Fiorillo, 2004). These deposits constitute a clastic succession formed by grey-blue silty and marly clays, interspersed with fine sands and conglomerates of various thickness marking the bedding (Fiorillo, 2004; Gentili and Dramis, 1997) (Figure 9). The origin of the post-orogenic slopes can be considered as the nearly simultaneous result of the process that caused the scarps and the geomorphological modelling, because of the high erodibility of the materials. Upon the hillsides, a colluvial yellowish cover, produced and removed by weathering and degradation of the substratum, defines the slope profiles and, therefore, the slope angles (Fiorillo, 2004).

The hydrogeological characteristics of the area can be considered relatively uniform, although distinguishable in 7 main units (Table 3 and Figure 9): alluvium, chalk, clay, colluvium, limestone, marl and sandstone.

UNIT	DESCRIPTION
Alluvium	Alluvial plain (recent and ancient) (Holocene – Middle and Upper Pleistocene)
Chalk	Chalk, chalky-sandstone and bituminous clay (Messinian)
Clay	Clay, clayey-marl and marly-clay (Pleistocene – Pliocene - Messinian)
Colluvium	Eluvio-colluvial, slope debris, morainic deposits (Holocene – Upper Pleistocene)
Limestone	White, red and varied sliver (limestone and flint) (Priabonian - Cenomanian)
Marl	Marl, calcareous marl and argillaceous marls (Miocene – Oligocene)
Sandstone	Sandstone, arenaceous-conglomeratic, arenaceous-pelitic units interposed with clays (Pleistocene – Pliocene - Messinian)

Table 3 Main hydrogeological units in the study area

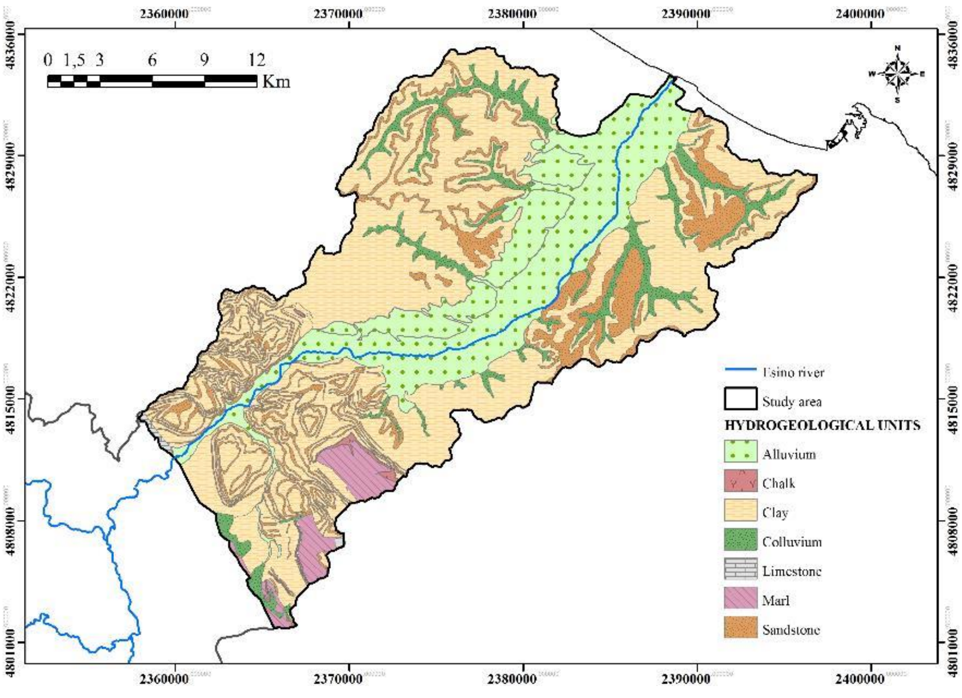

Figure 9 Study area: the post-orogenic sediments of the Esino river basin.

One reason of the selection of the Plio-Pleistocene hilly zone for the research, is that the landslide index reaches the maximum values in this area (Principi et al., 2007)
The propensity of the study area to shallow slides is an additional motivation of its choice. Even though deep-seated landslides can occurs, the post-orogenic complex is particularly affected by numerous and variably sized shallow landslides (flows and slides), especially involving the transitional layer between the weathered material and the substrate (Bisci and Dramis, 1991).
To understand the relationship between landslides and precipitation in post-orogenic complex, the permeability (*K*) plays a very important role. Permeability indicates a measure of the ability of a porous material (often, a rock or unconsolidated material) to allow fluids to pass through it. Typically, the lithologies of this area have medium-low permeability, thus they have a discreet ability to store water. Given the aptitude of the soil at saturation, these landslides are often attributed to the cumulated rainfall over the area. However, literature review demonstrated the predominant influence of high intensity and short duration precipitation, for initiation of shallow landslides, due to infiltration processes (J. Zêzere et al., 2005). In conjunction with intense rainfall events, the partially saturated surficial covers, face numerous problems related to two triggering mechanisms: i) landslide initiation involving few meters of soil (typically 1-3 m), and ii) erosion involving thicknesses much more modest (a few centimeters) (Della Sala and Cuomo, 2013).
Indeed, shallow landslides are suitable with both empirical and physical prediction models for several reasons (Cervi et al., 2010): (a) the small sizes allow to represent landslides with a point at a regional scale, (b) the failures generally consist of relatively uniform geotechnical characteristics and constant thickness, (c) simplified models may deduct hydrological conditions, and (d) the complexity of the phenomena is lower than in larger landslides.

3.3 Methodology

The methodology of this study aimed at answering the above-mentioned research questions (Chapter 3.1), in order to achieve the primary objective of determining the potential landslide rainfall thresholds with both empirical and physical methods. The analysis has been divided into four parts as explained in the following outline.

The *first part* examined the correlation between rainfall and landslide in the post-orogenic complex of the Esino river basin. The very first step consisted of a thorough review and analysis of the input databases, which is the catalog of historical landslides and the time series of precipitation.
For what concerns the catalog of historical landslides, information was gathered from different sources, among which the Marche CFR, managing reports about landslides events and ensuing landslide damage claims of local authorities. Other data were collected from a national catalog of landslide and flood sites. This catalog, called Vulnerable Areas of Italy (AVI) and available from the National Research Council (http://avi.gndci.cnr.it/), was commissioned in 1989 and kept updated until 2001. Moreover, the local Fire Department provided reports of technical actions regarding landslides. Finally, local newspaper articles were considered and subsequently were verified on-site for extension and entity. Data collected were georeferenced in the Gauss-Boaga coordinates and digitalized into a Geographical Information System (GIS).
Time series of precipitation are daily collected through the local mechanical (MR) or telemetric (TR) rain gauges distributed in the study area or in the proximity. Rainfall data were extracted using the Sirmip On-Line (SOL) database, made available by the CFR and publicly accessible though the Marche Region's Civil Protection website (http://84.38.48.145/sol).
Landslides and rainfall data were compared to verify a potential correlation both in their mean annual and monthly trends.

The *second part* consisted in the application of the empirical models on the study area. The aim of this section was to consider the hydrogeological properties in the calibration of empirical rainfall thresholds. The main novelties of this chapter lie in the selection of the area and the scale of analysis. The statistical approach here is applied at local scale (550 km^2 are considered "local" for empirical models), to a peculiar study area with relatively uniform hydrogeological characteristics. Based on this assumption, cumulative event rainfall (E), rainfall duration (D), rainfall intensity (I), daily

rainfall (R) and antecedent rainfall (A_D) has been computed for landslides events collected in the post-orogenic section.
Three empirical rainfall thresholds models were applied: (i) the cumulative event rainfall – duration (ED) method, (ii) the intensity – duration (ID) method, and (iii) the Bayesian probabilistic method.
For the first method, the cumulative precipitation and the duration of the rainfall events that triggered at least one landslide in the study area were plotted on a logarithmic graph. The distribution of data was then compared with some existing regional, national, and global thresholds in which the study area is included. In this chart, the number of landslides activated by each event was also taken into account to compare the values of the measured ED couples.
The same technique was adopted for the intensity – duration method. Moreover, in this case, a local ID threshold that represents a greater than 10% likelihood of landslide initiation was computed. Additionally, based on the ID data dissemination, a probability graph was shown. This graph displays a cluster of lines, each of which represents, for any specific rainfall duration, the probability that a percentage of the known landslides lays below the line.
Finally, the Bayesian statistical technique has been applied to analyze the most effective rainfall parameters and to draw probabilistic thresholds. The Bayesian investigation was initially used to find the probability of observing a landslide when a rainfall event of given magnitude occurs. This approach has been applied individually with daily, cumulated event, and antecedent rainfall. At a later stage, Bayes analysis has been employed by coupling the two variables of daily and antecedent rainfall.

The *third part* involved the application of a physical model, the U.S. Geological Survey's Transient Rainfall Infiltration and Grid-Based Regional Slope-Stability (TRIGRS) model (Baum et al. 2002), to simulate the pore pressure response to rainfall infiltration for the post-orogenic sediments of the Esino catchment. The aim of this section was to use a deterministic method, particularly the TRIGRS program, over a large area where data required are not always available. TRIGRS was chosen because the study area lithology tend towards saturation after rainfall, thus it is particularly suited for the model's demand for saturated, tension-saturated, or nearly saturated initial conditions. TRIGRS also allows the computation of F_S without requiring physical parameters that are very difficult to obtain in such large areas, i.e. the evapotranspiration index or multiple dimensions infiltration fluxes.
The main novelties of this chapter lie in the use of a statistical process as input and, again, in the scale of the analysis. The physical model here is applied at

regional scale (550 km^2 are considered "regional" for physically based models) in the same area of the previous section, which have relatively uniform hydrogeological features, and combined with a Geographic Information System (GIS).
Hydrogeological and topographic (20m Digital Elevation Model) data for this spatial analysis have been obtained from the Civil Protection CFR. On the other hand, requirements as soil depths, groundwater conditions, or hydrologic and strength properties of the materials (i.e. cohesion c, unit weight of soil γ, angle of internal friction φ, volumetric water content θ, hydraulic diffusivity D_0, saturated hydraulic conductivity K_S, and the inverse of capillary fringe height or inverse of the air entry pressure head α) were not accessible. These parameters were derived in the analysis and assumed time invariant, whereas the pressure-head response resulting from rainfall infiltration was considered transient.
Due to the lack of field data, mechanical and hydrological property values were assigned through a statistical analysis based on literature review of soils matching the local hydrogeological units. A soil texture class was identified for every hydrogeological unit found in the study area, namely clay, sandy-clay and loam. The model was then calibrated by computing the pressure head variation for a single 1-D profile over a range of hydrological property values typical of the soil texture classes identified. For the simulation, TRIGRS was ran assuming saturated conditions with infinite depth of basal boundary (SAT-INF) and unsaturated soils with an impermeable basal boundary at a defined depth (UNS-FIN). It is so highlighted the variation in pressure head with the variation of saturated hydraulic conductivity, saturated hydraulic diffusivity and initial depth of the water table.
Afterwards, the resulting variations of pressure head and factor of safety were compared with the landslides occurrence to identify the best fitting hydrogeological input conditions. Using calibrated inputs and a soil depth model, TRIGRS was ran for the entire study area. Finally, Receiver Operating Characteristic (ROC) analysis was applied to compare TRIGRS's output with a shallow landslides inventory.

The *fourth part* described the test of the models previously developed. The aim of this chapter was to compare the results and verify the effectiveness of the methodologies in a real case study. The validation was applied to the rainfall event that affected the study area, and most of the Region, from 2 to 4 May 2014. For the landslides activated during this storm, the rainfall variables was computed and plotted in both the ED and ID graphs. Particularly the validity of ID threshold developed in this study was tested.

Moreover, the likelihood of landslide initiation was established with the Bayes analysis. Finally, the TRIGRS model was run using the rainfall patterns of the May 2014 event and the hydrogeological properties calibrated in the above section. The ROC analysis was applied to compare the number of grid cell predicted as unstable from TRIGRS and those effectively resulted in landslides.

4 Application of predictive models on the Esino river basin

4.1 Landslide and rainfall patterns

This chapter describes the results of the first phase of the research, namely the review and analysis of landslides and rainfall data in the post-orogenic complex of the Esino basin. Furthermore, a comparison between their annual and monthly trends is proposed to verify a connection between the two series.

4.1.1 Historical landslides

Based on the review of historical landslides, the study area was affected by 234 landslides over the period 1953 to 2012. Although the meticulousness of the research, the review shows mainly shallow landslides (usually 1m of depth) triggered near transportation infrastructures, civil or industrial buildings. These failures have been reported to the authorities and the press because of the damage caused or the media exposure achieved in the territory. Therefore, the database obtained may not be completely exhaustive of the actual instability conditions of the area of interest.

The landslide time series was initially plotted on annual basis as shown in Figure 10. Landslides affected the study area in almost every year of the observation period, except for 1993, 2000, 2002, 2003 and 2012. However, the years before 1990 shows discontinuity in the availability of data. In fact, the amount of reports found in that period is not significant. On the other hand, the years characterized by a relatively large number of events were 1990 (30 landslides cataloged), 1996 (31), 1997 (18), 1998 (53), 2005 (20) and 2011 (19).

The time series was then observed considering the monthly distribution of landslides in the period 1953-2012 (Figure 11). Nearly half of these landslides (110) were triggered in December, 34 in January, and 21 in March. The months of June, July and August have been affected only by 1 o 2 landslides.

It has to be specified that many records were registered with uncertain date (Figure 12). Particularly, 155 landslides have been reported with certain day of initiation, whereas 31 have two days of uncertainty, 17 have three days of uncertainty, 11 have four days of uncertainty, 8 have five days of uncertainty, and 12 have three days of uncertainty. When the exact timing of the failure ranged from two dates, the landslide was considered as triggered in the last day of the period of uncertainty. For example, 24 landslides initiated between 30 November and 1 December 1998. In this case, all the events were classified as if they had occurred the 1 December. For this reason, November is represented as a month with low landslide rate, but a much higher number of events may have characterized it.

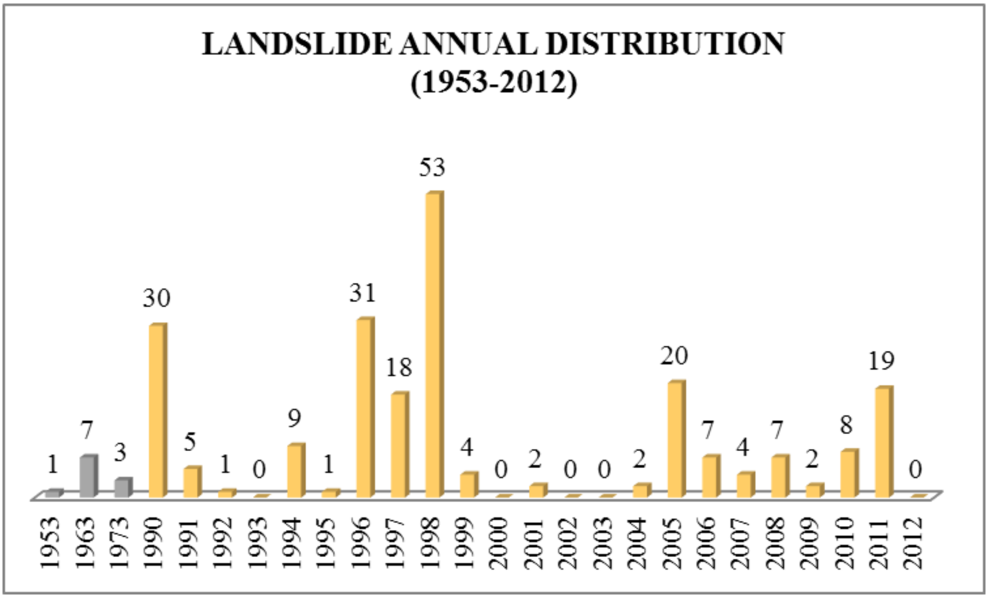

Figure 10 Landslide annual distribution from 1953 to 2012 in the study area.

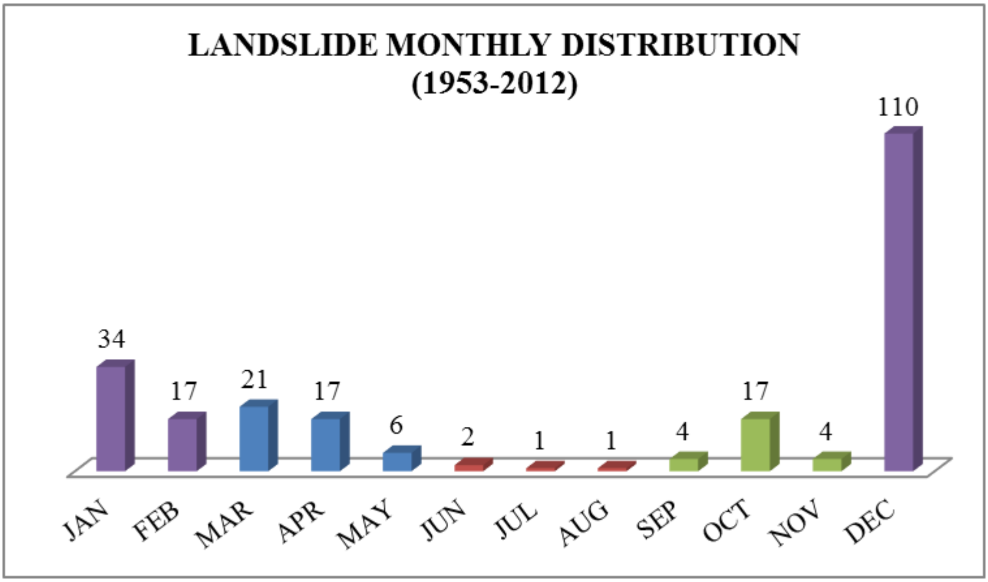

Figure 11 Landslide monthly distribution from 1953 to 2012 in the study area

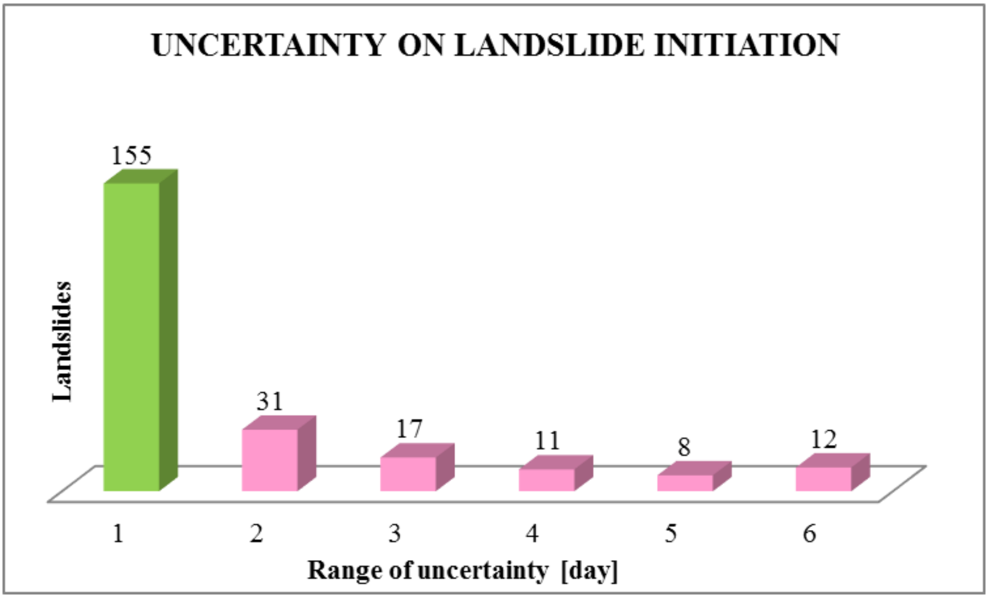

Figure 12 Number of landslides with certain or uncertain time of failure. Figure shows the range of uncertainty in days.

So far, some observations can be done considering the seasonal trend. In fact, (Figure 13):

(i) 161 (68.8%) landslides occurred in winter;
(ii) 44 (18.8%) landslides occurred in spring;
(iii) 25 (10.7%) landslides occurred in autumn;
(iv) 4 (1.7%) landslides occurred in summer.

Therefore, the large majority of events occurred in winter, followed by spring, autumn and lastly summer.

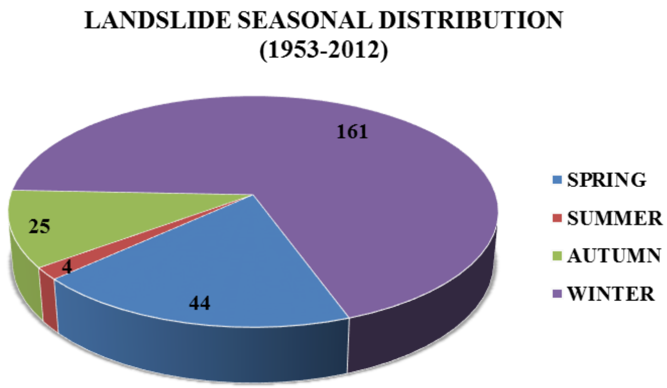

Figure 13 Landslide seasonal distribution from 1953 to 2012 in the study area

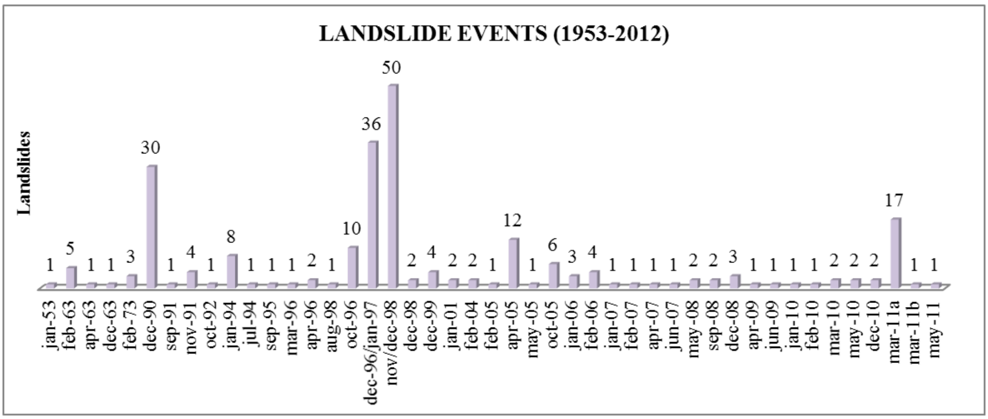

Figure 14 Landslides grouped per events from 1953 to 2012 in the study area

To have an overview of the temporal distribution, the landslides were also grouped into events, i.e. periods of subsequent days with slope failures (Figure 14). The analysis shows that the main periods with landslide are:

a) 10-15 December 1990, in which 30 landslides were triggered;
b) 7-10 October 1996, in which 10 landslides were triggered;
c) 26 December 1996 - 5 January 1997 in which 36 landslides were triggered;
d) 30 November - 4 December 1998, in which 50 landslides were triggered;
e) 10-13 April 2005, in which 12 landslides were triggered;
f) 1-9 March 2011 (mar-11a in Figure 14), in which 17 landslides were triggered.

In all the other periods, the number of landslides recorded was less than 10.

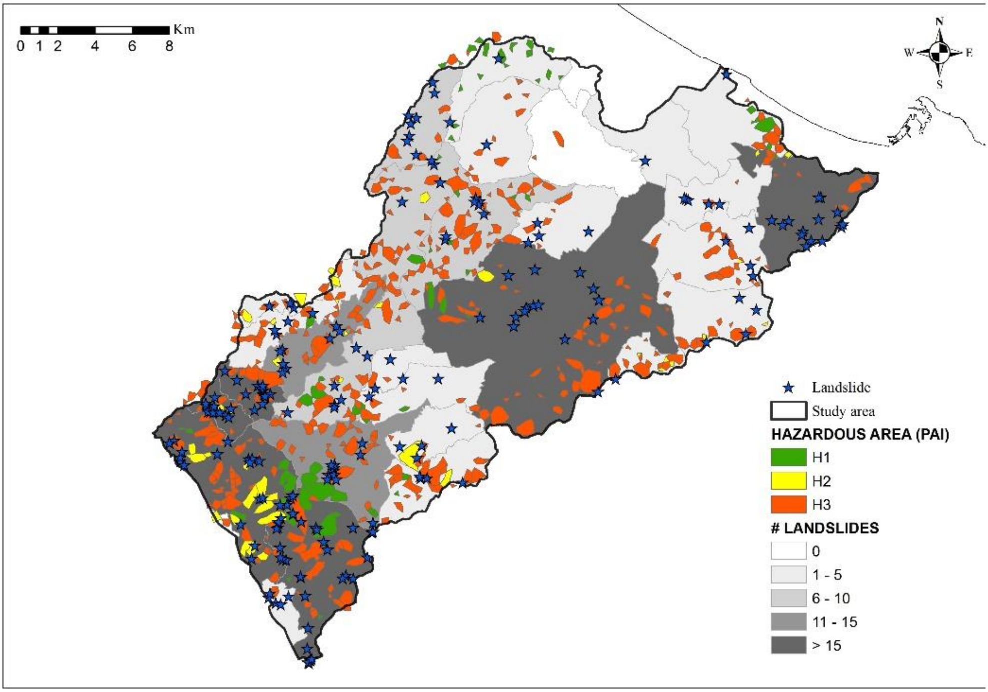

Figure 15 Landslides spatial distribution within the study area. Figure shows also the number of landslides collected per municipality and the hazardous areas from the PAI classification

Data collected were georeferenced in the Gauss-Boaga system and digitalized into a GIS to allow a spatial comparison with other layers such as for example the administrative boundaries (Figure 15).

GIS analysis shows that certain municipalities included in the study area are more prone to landslides, such as Ancona, Apiro, Jesi, Mergo, Rosora, and Serra San Quirico. Other municipalities, among those that fall entirely within the basin, were not affected by landslides between 1953 and 2012 (e.g., Montemarciano and Monte San Vito).

Furthermore, landslides were compared with the areas classified as hazardous by the National Plan for the governance of Hydrogeological Hazard - PAI (Regione Marche - Autorità di Bacino Regionale 2004 and updates) (Figure 15). The PAI assigns four level of hazard (from 1 to 4) to polygons corresponding to past surveyed landslides, depending on the type of phenomenon (e.g., debris flow, slide, complex) and the state of activity (active, inactive or quiescent).
Most landslides collected in this study are not located close to the areas classified hazardous by the PAI. Only 13% of the landslides is less than 50m from a H3 area (high hazard), 6% from a H2 area (medium hazard) and 2% from a H1 area (low hazard) (Figure 16). Moreover, only 21% of the landslides is less than 100m from a H3 area (high hazard), 5% from a H2 area (medium hazard) and 4% from a H1 area (low hazard) (Figure 17).

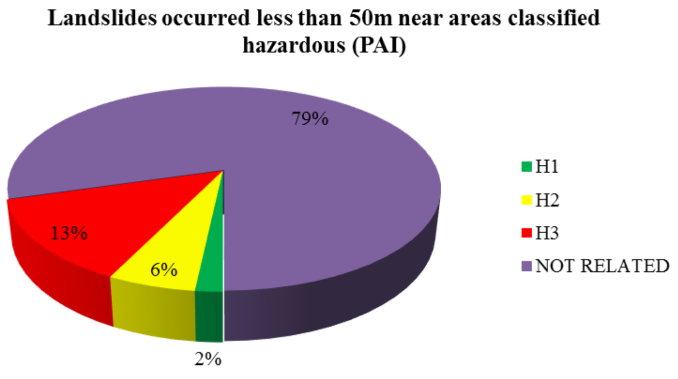

Figure 16 Landslides occurred less than 50m from areas classified hazardous (H1, H2, and H3) by the PAI

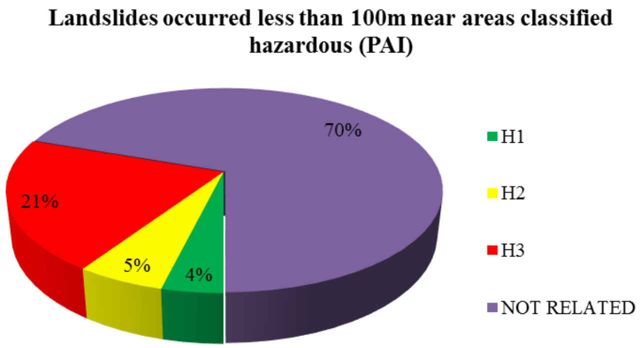

Figure 17 Landslides occurred less than 100m from areas classified hazardous (H1, H2, and H3) by the PAI

Finally, the 234 georeferenced landslides were analyzed based on the land use of the soil in which they have been triggered, following the methodology used in Carone et al. (2015). Data of land use were gained from the Corine Land Cover maps (1990, 2000, and 2006). Results shows that the majority of the landslides initiated in cultivated areas (162), followed by urbanized areas (43), and forested areas (19) (Figure 18).

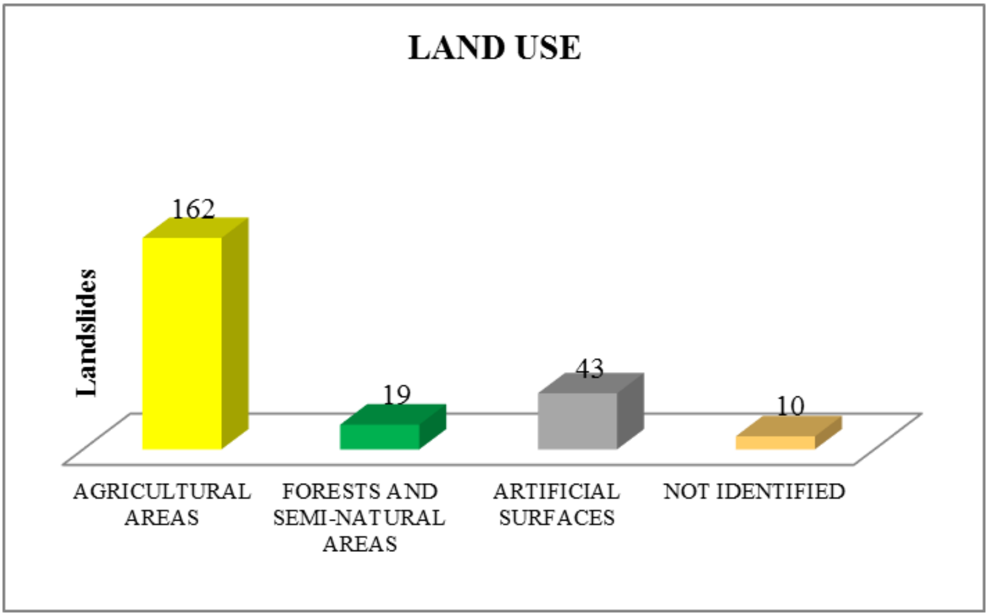

Figure 18 Land use of the soils affected by landslides from 1953 to 2012 in the study area

4.1.2 Rainfall patterns

Time series of precipitation are daily collected through the local mechanical (MR) or telemetric (TR) rain gauges network of the Marche Civil Protection. MR are apparatuses in which the rainfall amounts are read manually whereas in TR are read by automatic weather station (AWS).
Eleven rain gauges are located within and near the study area (Table 4 and Figure 19). Rainfall series of these stations were extracted using the Sirmip On-Line (SOL) database, made available by the Marche CFR. Table 4 lists the rainfall stations by name and reference code, type of network (mechanical or telemetric), and time of availability.
Table 4 illustrates that 5 rain gauges are part of the TR network, activated from 2003 or later and still operating, whereas 6 devices are part of the MR network, activated in 1951 and dismantled between 2007 to 2011. The rain gauge at Poggio San Romualdo is located at the highest elevation (926m asl). In fact, it is positioned in the mountainous portion of the basin, located further west of the area of interest (Figure 19). The rain gauge that is instead at the lowest altitude is Ancona (Torrette) (6m), which is located in the coastal portion between the Esino and Musone basins. The remaining rain gauges are well distributed for altitude and are located both in the hills and in the alluvial and coastal plains.

Thereafter, with the values acquired from the rain gauges, the average annual and monthly rainfall have been computed over the period observed. Usually, for climatological studies, the mean precipitations are computed over three decades (e.g., 1961-1990, 1981-2010). In this research, landslides were triggered over about 60 years. In order to cover six decades, the averages values of rainfall have been calculated for the years 1951-2011 (2012 was not affected by landslides).
Figure 20 shows the Mean Annual Precipitation (MAP) fell over the study area during the years subject to landslides, from 1953 to 2011. The values displayed have been averaged among the available rain gauges. The average MAP (red line) represents the mean yearly rainfall computed from 1951 to 2011 in every gauge. The graph indicates a fluctuation of the rainy and dry years. Particularly, the years 1996, 1998, 1999, 2002, 2005, and 2010 are considered rainy because their MAPs are higher than the six decades average. On the other hand, the years 1990, 1992, 1993, 1994, 2000, 2001, 2003, 2007, 2009, and 2011 are considered dry because the MAPs are lower than the mean.

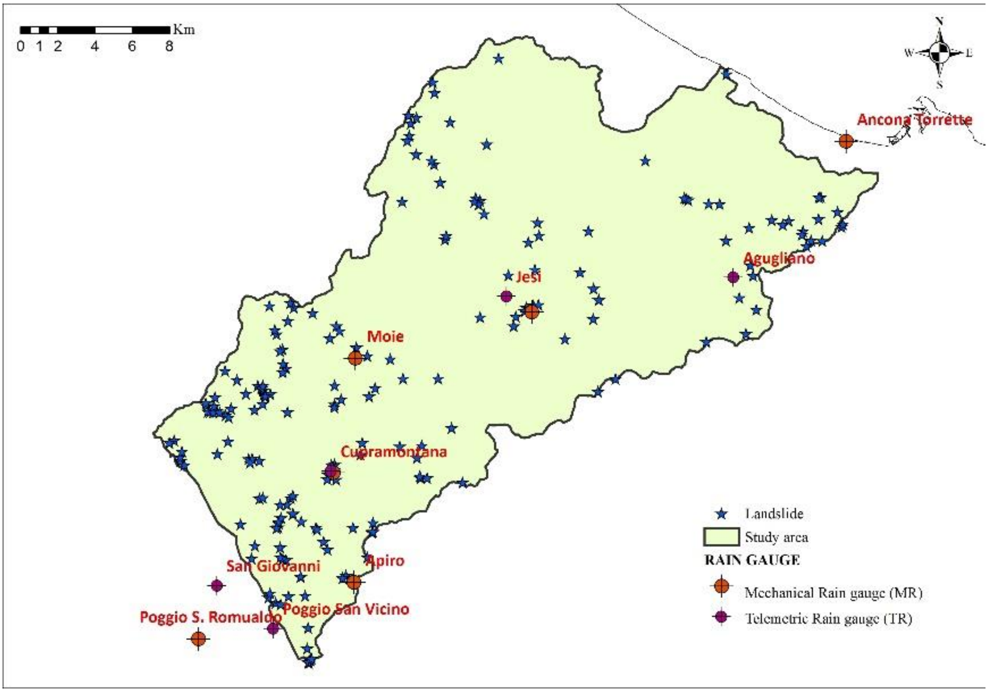

Figure 19 Rain gauges network of the study area

Rain gauge code	Rain gauge name	Height [m]	Network	Data availability [years]
Ag [1220]	Agugliano	170	TR	2003-nowadays
A-T [2009]	Ancona (Torrette)	6	MR	1951-2011
Ap [2066]	Apiro	516	MR	1951-2009
Cu [2062]	Cupramontana	510	TR	2003-nowadays
Cu [1263]	Cupramontana	506	MR	1951-2008
Je [2063]	Jesi	100	TR	2003-nowadays
Je [1213]	Jesi	96	MR	1951-2008
Mo [2067]	Moie	110	MR	1951-2011
PSR [2064]	Poggio S. Romualdo	926	MR	1991-2007
PSV [2848]	Poggio S. Vicino	580	TR	2009-nowadays
SG [1413]	San Giovanni	625	TR	2001-nowadays

Table 4 List of the rain gauges in study area. MR = mechanical rain gauge, TR = telemetric rain gauge

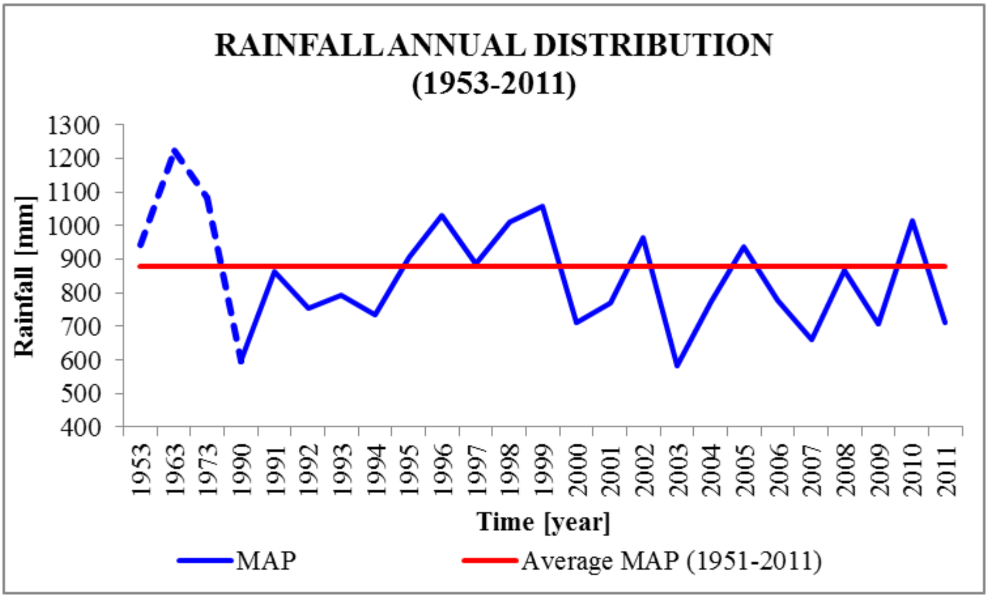

Figure 20 MAP and average precipitation for the years with landslides (1953-2011)

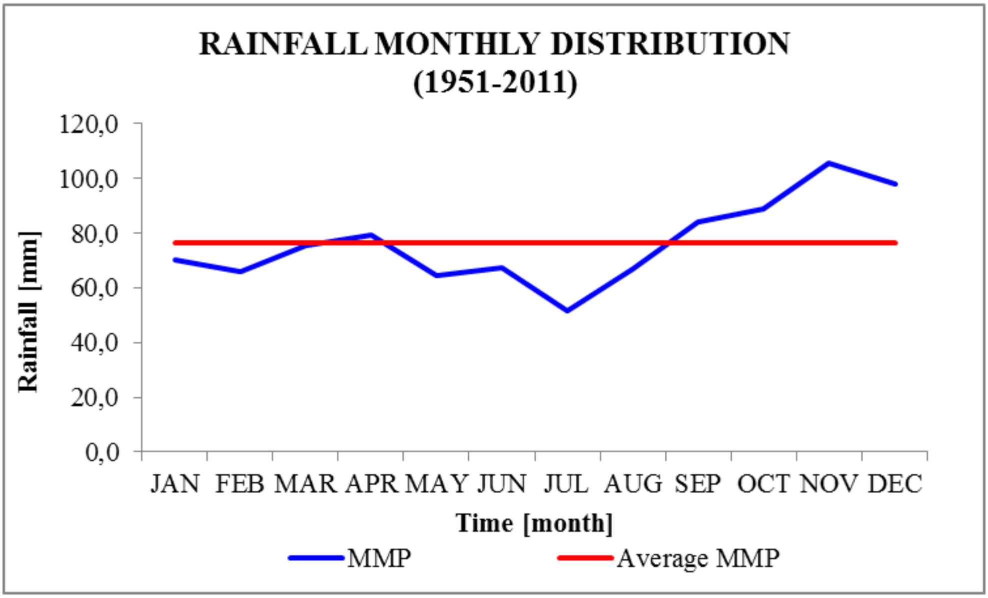

Figure 21 Mean Monthly Precipitation (MMP) for the period 1951-2011

Figure 21 shows the Mean Monthly Precipitation (MMP) of the study area from 1951 to 2011. Here as well, the computations regard the average values of all the rain gauges before mentioned. The rainfall monthly distribution shows a seasonal trend with autumn, winter and spring presenting peaks of precipitation over the mean. In particular, November and December are the rainiest months of the zone. On the contrary, the summer and the second part of the winter usually present rainfall values below the mean. This is confirmed especially in July.

4.1.3 Correlation between landslides and rainfall

The historical series of landslides and rainfalls, thus acquired, were compared both on annual and monthly basis. The purpose was to verify a potential correlation and validate the hypothesis that in the study area the landslides initiation is generally related to the precipitation.
Based on previous studies (e.g. Berti et al. 2003), the statistical method of the correlation function was used to establish the possible existence of a relationship between the above series. The correlation function represents the link between two variables (X and Y) which assume the following values: (X_1, Y_1), (X_2, Y_2)… (X_n, Y_n). The correlation coefficient (r) was calculated with the formula below:

$$r = \frac{\sum_{i=1}^{n}(x_i - \bar{x})(y_i - \bar{y})}{\sqrt{\sum_{i=1}^{n}(X_i - \bar{X})^2 \sum_{i=1}^{n}(Y_i - \bar{Y})^2}} \qquad (11)$$

where x_i is the i^{th} value of the first matrix of data, y_i is the i^{th} value of the second matrix of data, $\bar{x}$ is the medium value of the first matrix of data and $\bar{y}$ is the medium value of the second matrix of data. The result of the correlation function is always between -1 and +1. If the value of the formula tends to one (+1), the link between the two series is positive, which means that both the values increase or vice versa. If the value of the formula tends to minus one (-1), the link between the two series is negative, which means that as the value of one increases the other decreases. Instead, if the value of the formula tends to zero (0), there is no connection between the series, which means that these are not mutually dependent.

First, the annual landslide and rainfall distribution were compared (Figure 22). The diagram shows that, in general, the greater is the cumulated annual rainfall the greater is the number of landslides of the area but the correlation coefficient of the series is very low (*r* = 0.16). In the 1994-1998 and in the 2003-2010 periods, a certain correspondence between the sets is pointed out. In these years, when the MAP of the rain gauges is above the average, a peak of landslide is registered. Contrarily, years particularly dry resulted in few or even none slope failure. The great anomaly is represented by the 1990 in which the rainfall data recorded were below the mean, but the number of landslides remarkably high. In fact, in 1990 the database was affected by the lack of a large number of rainfall data from the rain gauges of Apiro, Cupramontana and Poggio San Romualdo, due to nonfunctional stations.

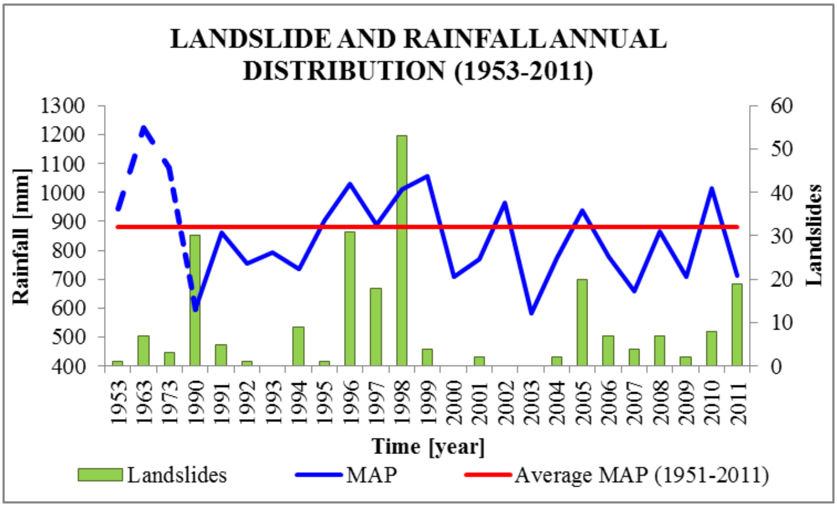

Figure 22 Comparison between landslide and rainfall annual distribution (MAP) within the study area (period 1953-2011)

Then, the monthly frequency of landslides and the series of the mean monthly precipitation were compared (Figure 23). The correspondence in this graph is higher than in the annual chart. The correlation coefficient *r* is equal to 0.43. Overall, the largest number of landslides is activated during one of the rainiest month. In autumn and winter, peaks of landslides are recorded when the precipitation are higher than the mean. Exception is the month of November. Although it shows the highest values of mean precipitation, the highest number of landslides manifests in December.

On the contrary, the months with the lowest number of slope failures (July and August) also correspond to the driest periods.

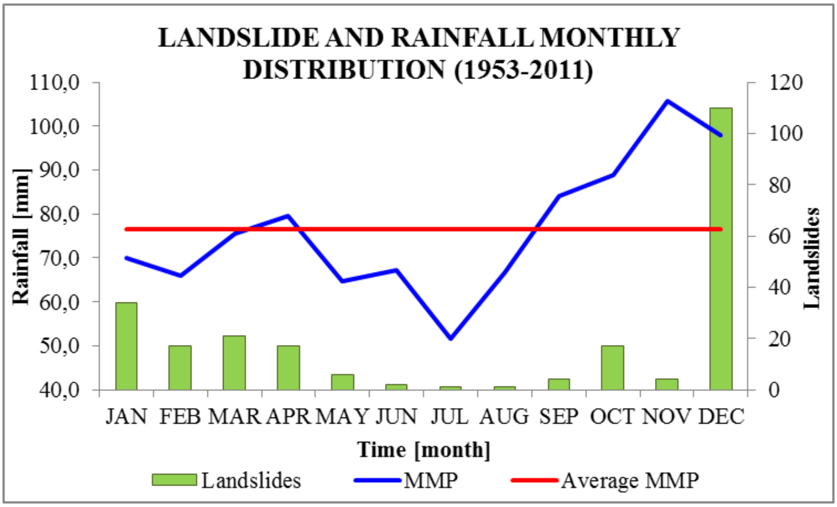

Figure 23 Comparison between landslide and rainfall monthly distribution (MMP) within the study area (period 1953-2011)

4.2 Empirical models

This chapter describes the results of the second phase of the research, which is the application of empirical models for (a) the analysis of the rainfall characteristics that triggered landslides in the post-orogenic complex of the Esino basin and (b) the calculation of rainfall thresholds for the initiation of future failures.
Three statistical approaches are applied: (i) the cumulative event rainfall–duration method, (ii) the intensity – duration method, and (iii) the Bayesian probabilistic method.
The use of these methods in the same bounded area (local scale), containing lithologies with comparable hydrogeological properties, represents an uncommon technique that allows considering the geological features of the application zone.

4.2.1 Cumulative event rainfall – duration (ED) method

The first method consisted in the comparison of the cumulative event rainfall (E) and the rainfall duration (D) of the events that triggered the 234 landslides recorded during the first step (Chapter 4.1).

4.2.1.1 Methodology

In this study, a "rainfall event" is identified as a period of one or more days in which a continuing rainfall, of at least 1mm/day, is registered. The "cumulative event rainfall" is defined as the total rainfall measured from the beginning of the rainfall event to the time of failure (in mm) (Guzzetti et al., 2008). Unfortunately, for this database, the exact hour of landslide initiation is not available. Sometimes, as described before, a range of uncertainty exists also for the day of the triggering. For this reason, the cumulative event rainfall of the study is the total rainfall measured from the beginning to the end of the rainfall event in which one or more landslides are activated. Similarly, the "duration" is defined as the length of the rainfall event (in h) (Caine, 1980).

To compute the rainfall parameters, every mass movement has been related with the nearest rain gauge among the eleven considered in the catchment area. Specific areas of influence were defined using the method of the Thiessen polygons (Croley and Hartmann, 1985) (Figure 24). This method is a simple geometric process, which define an area of influence for each rain gauge wherein the precipitation is considered constant and equal to the value of rainfall measured by the rain gauge itself. Consequently, each rain gauge was connected to the pertaining landslides. When the reference station was not functioning at the time of failure, the second closest gauge was chosen as datum point (and so on).

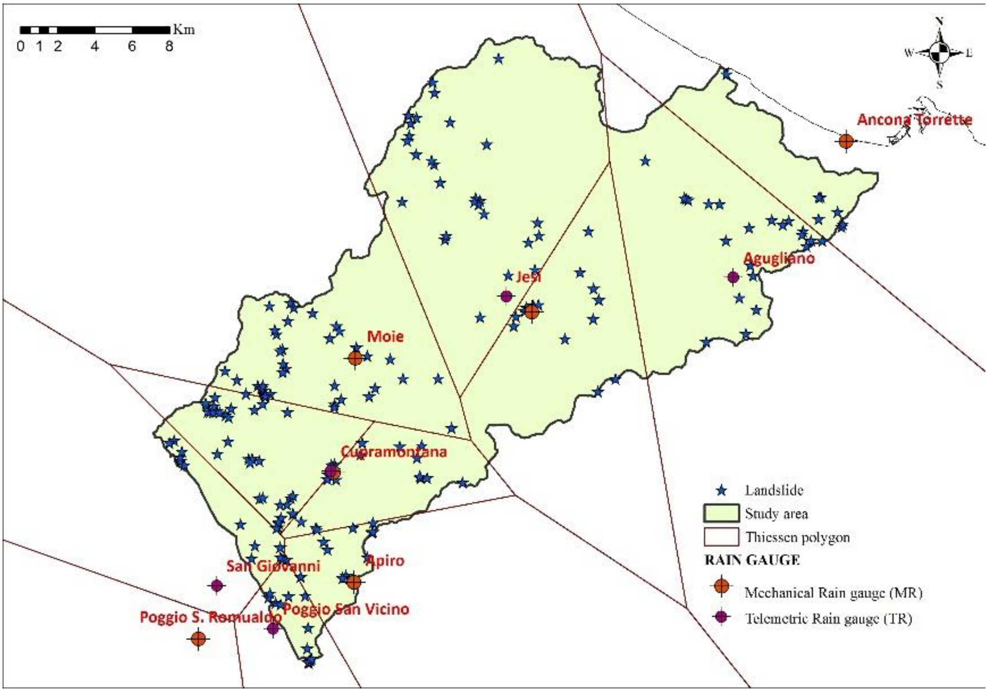

Figure 24 Thiessen polygons obtained through the rain gauges network of the study area. Each landslide was associated to the polygon, thus the rain gauge, in which is located.

Afterwards, the rainfall events that triggered the 234 landslides of the database have been identified. Moreover, these events has been divided in four categories: *main events* (those triggering more than 10 landslides), *secondary events* (those triggering from three to nine landslides), *minor events* (triggering two landslides) and *single events* (triggering one landslide). Following, the cumulative event rainfall and the duration of the specified events that triggered at least one landslide in the study area have been computed and plotted on a logarithmic graph. The points in the graph correspond to the precipitation patterns (ED) of every rain gauge related to a

rainfall event (e.g. the nov-91 event triggered 4 landslides that were referred to 4 different polygons and thus 4 gauges).
Finally, a comparison between the data distribution on the diagram and some multi-scale rainfall thresholds existing in literature is proposed.

4.2.1.2 Results

Results from the Thiessen method shows that the rain gauge stations with the influence on the largest number of failures are Moie (MR) with 64 events, Cupramontana (MR) with 53 events and Jesi (MR) with 45 events (Table 5). These rain gauges are located in the central zone of the post-orogenic complex. Instead, those located outside the basin have been related to less landslides: 18 events for Ancona (Torrette), 2 events for Poggio San Romualdo and Poggio San Vicino, 3 events for San Giovanni (Table 5).

	Ag **[1220]**	**A-T** **[2009]**	**Ap** **[2066]**	**Cu** **[2062]**	**Cu** **[1263]**	**Je** **[2063]**	**Je** **[1213]**	**Mo** **[2067]**	**PSR** **[2064]**	**PSV** **[2848]**	**SG** **[1413]**
Landslides	11	18	27	53	1	45	8	64	2	2	3

Table 5 Number of landslides pertaining to each rain gauge of the study area.

With the values extracted from the rain gauges, 45 rainfall events that triggered the 234 landslides studied were identified. Each event initiated a certain number of slope failures, from one to a maximum of 19 (activated on 10-15 December 1990 in the Mo [2067] area of influence). Particularly, there were documented:

(i) 6 main events (≥ 10 landslides), corresponding to 155 landslides;
(ii) 9 secondary events (3-9 landslides), corresponding to 40 landslides;
(iii) 9 minor events (2 landslides), corresponding to 18 landslides ;
(iv) 21 single events (1 landslide), corresponding to 21 landslides.

The logarithmic ED graph (Figure 25) shows the distribution of the four classes of rainfall events.
First, it is observed that duration ranged between 4 and 167 h, whereas the event rainfall ranged between 1.2 and 191.6 mm/h. It is notable that, except for one outlier, the greater is the duration and the greater is the cumulated

rainfall. Moreover, the main events are characterized by the highest amounts and durations, whereas the single events have the lowest values. Minor and secondary occurrences are situated in the intermediate conditions.

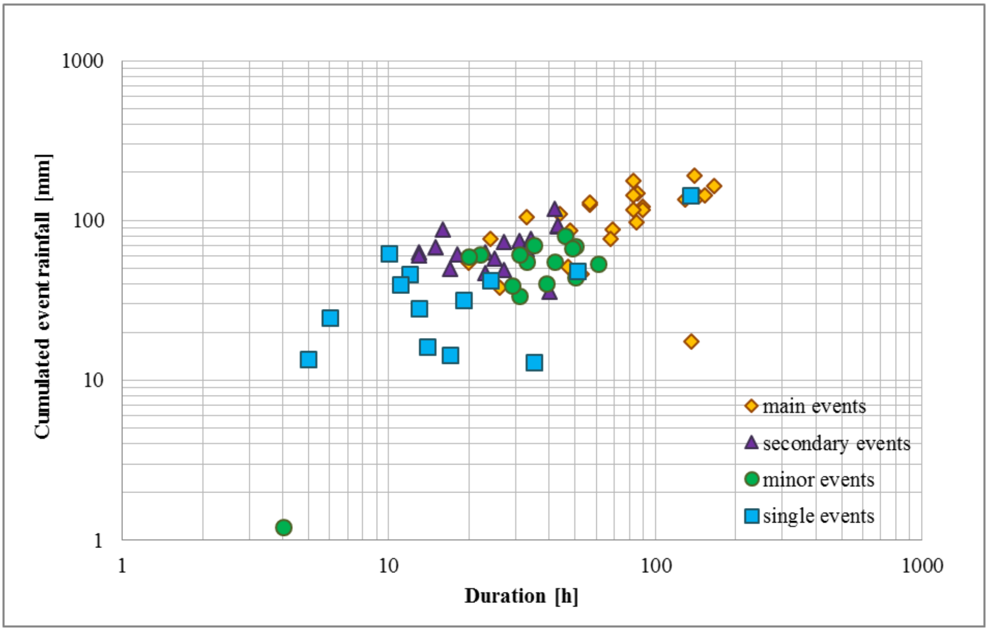

Figure 25 Cumulated event rainfall – duration logarithmic graph. Highlighted also is the difference among the events that triggered only 1 landslide (square), 2 (circle), 3-9 (triangle) or more than 10 (diamond) landslides

Data distribution have been compared to some global (Caine, 1980), regional (Kanji et al., 2003; Peruccacci et al., 2012; Vennari et al., 2014) and local (Annunziati et al., 2000) ED rainfall thresholds (Figure 26). These curves represents the minimum thresholds of the data to which they are referred. In the cases of Peruccacci et al. (2012) and Vennari et al. (2014), the curves show the 1% or 5% exceedance probability levels.

It is observable that the thresholds have slopes similar to the general tendency of the data. In fact, Caine (1980) described a global threshold, Kanji et al. (2003) developed a regional threshold for Brazil and Annunziati et al. (2000) a local threshold for an area in the Apuan Alps. These curves are all located above the data dispersion. Better results are gained with the remaining regional thresholds of Vennari et al. (2014) for Calabria region and most of all with Peruccacci et al. (2012) for the post-orogenic sediments of Abruzzo, Marche and Molise. Nonetheless, these latest curves do not represent the 1% or 5% of exceedance probability of the Esino area data.

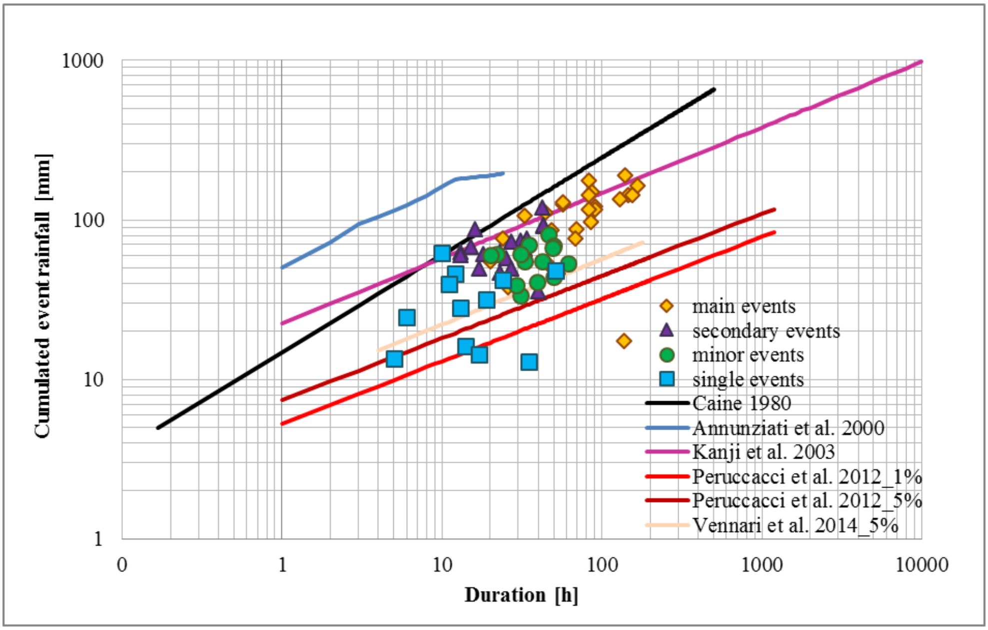

Figure 26 Cumulated event rainfall – duration distribution, compared with some global, regional and local thresholds

4.2.2 Intensity – duration (ID) method

The second empirical method calibrated in the study area is the rainfall intensity (I) and duration (D) model.

4.2.2.1 Methodology

The same methodology of the ED model is adopted for the computation of the rainfall events and parameters of the ID method.
As a result, logarithmic graphs of the mean and maximum intensity compared with the duration of the rainfall events, that triggered at least one landslide in the study area, are plotted. The “mean intensity” (in mm/h) is defined as the average rate of precipitation of the rainfall event and the “maximum

intensity" (in mm/h) is the highest rate of precipitation of the rainfall event. The "duration" (in h) is defined as before.

A threshold for the mean intensity – duration chart is also proposed. Frequently, a rainfall threshold is drawn by adopting a mathematical function that visually fit the lower boundary of the data plotted in the logarithmic graph. The method used for the computation of the threshold in this study involved two steps. First, the equation describing the intensity-duration threshold was computed in the form of the power law regression of the plotted dataset; this has enabled the computing of the β (slope) value of the equation. Second, the curve was shifted along the vertical axis to extract the α (intercept) value that split the cloud of data in two parts: the 90% of the data above the curve and the remaining 10% below the curve. This allowed to exclude from the threshold equation those landslides triggered by very low values of intensity-duration. In fact, particular local condition (e.g. antecedent wetness, slope, human activities) might have a key role for the initiation of landslides.

Furthermore, a technique suggested by Guzzetti et al. (2007) was adopted to portray percentile estimates of the rainfall ID conditions. The purpose was to approximate the values of the mean intensities for the empty logarithmic bins of duration. Starting from the minimum value of duration and up to the maximum, a moving window of 5 data has been identified among the rainfall events. For example, at the n^{th} duration value a range of 5 data, centered in the n^{th} value and including the two before and the two after, has been considered. All the data points in the 5-bin moving window were selected, and the percentiles of the intensity values were computed. The 2^{nd} , 5^{th} , 10^{th} , 20^{th} , 30^{th} , 40^{th} , 50^{th} , 60^{th} , 70^{th} , 80^{th}, and 95^{th} percentiles of the rainfall intensities were calculated and attributed to the central point. Results of the analysis are plotted in a diagram that shows the probability lines drawn by linking equal percentile points.

4.2.2.2 Results

Results of the analysis were first plotted in a logarithmic chart displaying the maximum intensities and the duration of the rainfall events (Figure 27). In the study area, the maximum intensities ranged between 0.4 and 37.4 mm/h. The first observation is that the general trend, excluding the outlier, is opposite to the ED model. The higher is the duration of an event and the smaller is the maximum precipitation rate needed to trigger at least a landslide. Moreover, the main events are characterized by lower maximum intensities than those required to activate secondary and minor events. Despite considerable scattering along the x and y axes, the ID combinations of single events are located below the other events.

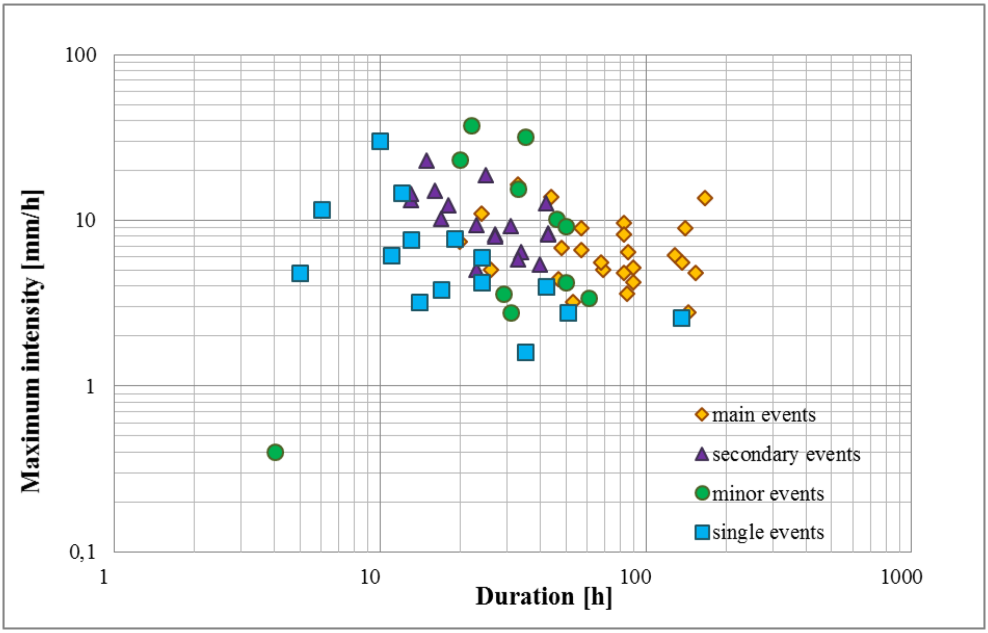

Figure 27 Maximum intensity – duration logarithmic graph.

Figure 28 shows the logarithmic chart of the mean intensities and durations that affected the Esino study area(Gioia et al., 2015b). First, it is notable that the mean intensity ranged between 0.3 to 5.3 mm/h. Second, the graph confirms the findings of Caine (1980), namely that with the increase of rainfall duration, the minimum average intensity likely to trigger shallow slope failures decreases in the logarithmic plot. Additionally, a significant difference exists between the ID values of single and main events. These last events have considerable higher duration and lower mean intensities than the first ones. The secondary and minor events lie in between.

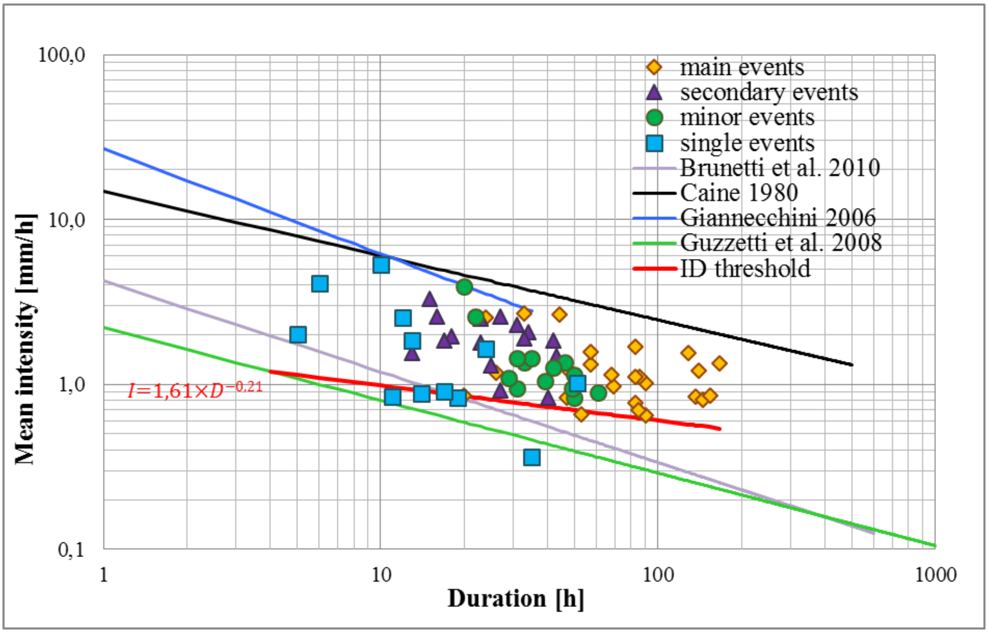

Figure 28 Intensity-duration logarithmic graph with the power-law threshold for this study (red line) and the thresholds developed by Brunetti et al. (2010), Caine (1980), Giannecchini (2006) and Guzzetti et al. (2008).

The trend observed in Figure 28 supports the definition of a minimum rainfall ID threshold for the occurrence of landslides. The threshold curve (red line) has the following power law equation:

$$I = 1.61 \times D^{-0.21} \qquad (12)$$

where I is the mean rainfall intensity (mm/h) and D is the rainfall duration (h) (Figure 28). This equation represents the minimum intensity-duration conditions that activated 90% of the studied landslides over the past decades. Moreover, the comparison of the global (Caine, 1980; Guzzetti et al., 2008), regional (Brunetti et al., 2010) and local (Giannecchini, 2006) thresholds reveals that the local threshold for the study area is systematically lower than the global curve of Caine (1980) and the local curve of Giannecchini (2006). The equation is more comparable with the Brunetti et al. (2010) threshold developed for the Abruzzo region, bordering the southern part of Marche, and the Guzzetti et al. (2008) global threshold.

Finally, Figure 29 shows the probability lines resulted from the computations of the percentiles. These lines support the interpretation of the ID data in Figure 28. For example, for any specific rainfall duration, the second percentile curve represents the probability that the 2% of the known landslide events lays below the line. For the analysis, the outlier was not considered. Inspection of Figure 29 confirms the linear scaling of the minimum level of rainfall intensity likely to trigger landslides. However, for small durations the probability lines are more separated than for durations exceeding 20h.

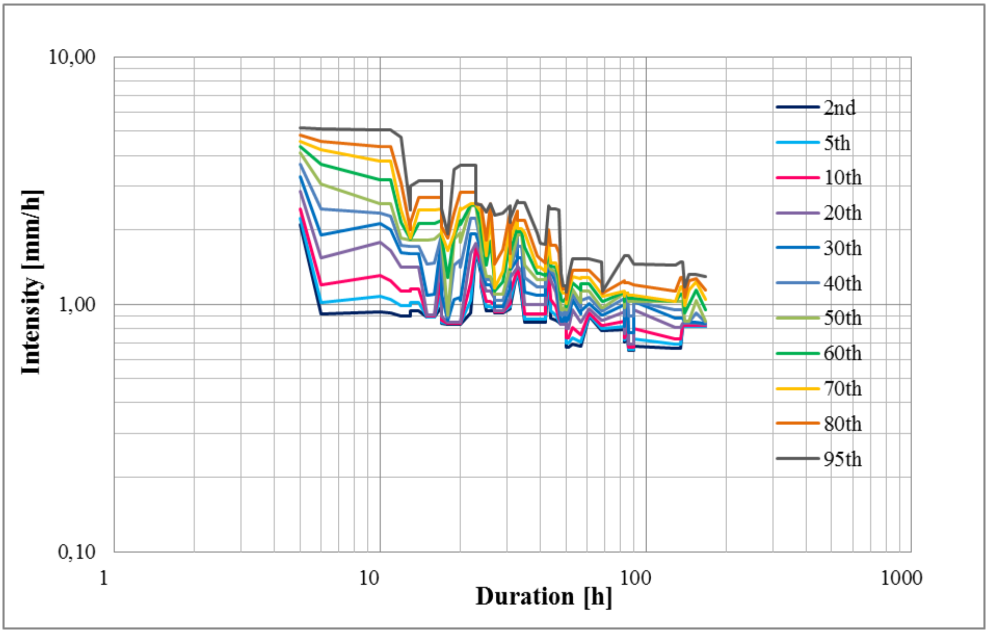

Figure 29 Percentile estimates (2nd, 5th, 10th, 20th, 30th, 40th, 50th, 60th, 70th, 80th, and 95th) of rainfall ID conditions.

4.2.3 Bayesian probabilistic method

The third method applied in the study area is the determination of probabilistic rainfall thresholds based on the Bayes' theorem.

4.2.3.1 Methodology

Of all the landslides that occurred in the study area between 1953 and 2012, only those of the period 1990-2012 are considered for this analysis. The

reason is that this model requires examining a set of data not discontinuous. Consequently, a total number of 210 landslides were conveyed in a GIS environment (Figure 30).
In addition, the operational rain gauges for each year from 1990 to 2012 were selected. Only rain gauges with at least 80% of data available (quality level) were considered. Next, the precipitation data of the stations related to one or more landslides per year were extracted. It was decided not to get the entire rainfall series (from 1990 to 2012) because it is possible that landslides occurred also over the years lacking information, without being reported. A probabilistic analysis, including the distribution of non-triggering rainfall, is much more informative and is capable of assign a reliability to a given threshold. However, analyzing only the years with slope failures helps to overcome the problems of underestimation. The years in which at least one landslide in the study area has been recorded are: 1990, 1991, 1992, 1994, 1995, 1996, 1997, 1998, 1999, 2001, 2004, 2005, 2006, 2007, 2008, 2009, 2010, and 2011.

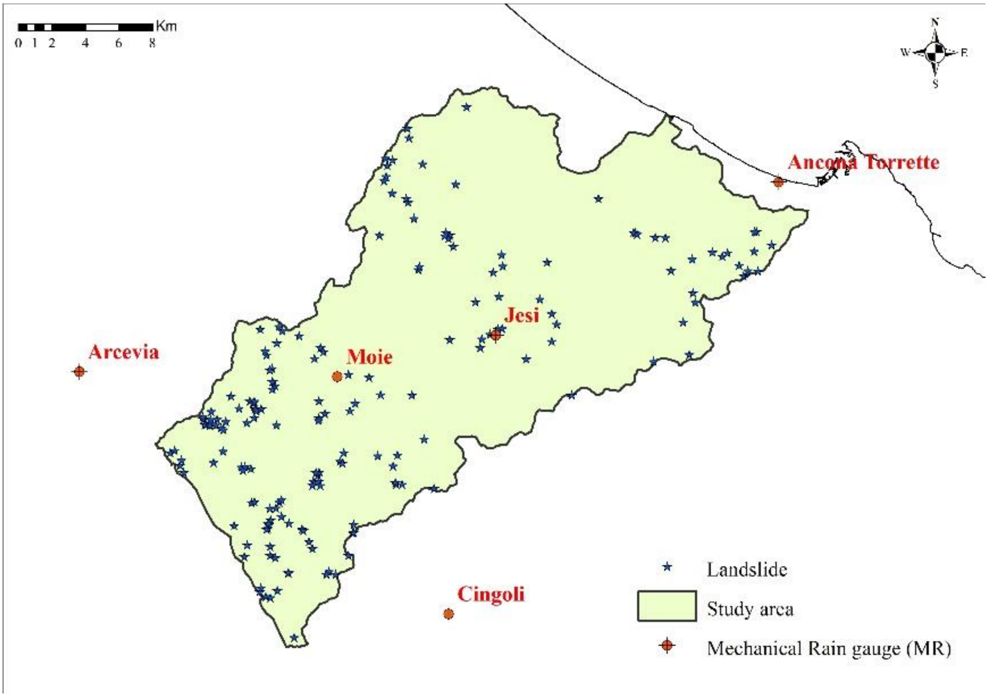

Figure 30 Landslides considered for the Bayesian model. Figure shows also an example of the rain gauges selected for the year 1990 analysis.

For the Bayesian model, the Thiessen polygons technique was not used. A major limitation of that approach is the significance of the data from a statistical point of view. In fact, by dividing the study area ($550 km^2$) in polygons, the number of historical landslides in each area can be very small (1-2 events or even 0), thus leading to inaccurate estimates of landslide probability. One way to pass this problem is to consider the study area as a whole, by calculating a single value of rain interpolated from every gauge functioning at the time analyzed. Consequently, landslides are considered in the totality. To calculate the interpolated data of rain was used the method of Inverse Distance Weighting (IDW). The interpolated precipitation can be compared to the concept of areal average precipitation. The areal rainfall represents the corresponding value of precipitation that equally falls over the entire area of interest.
As a result, the rainfall events were identified. For these events, the cumulated event rainfall has been computed. Moreover, daily and antecedent rainfall of 5, 7, 15, and 30 days were calculated.

Once identified the precipitations parameters, the probability of landsliding, conditional to the characteristics of the rainfall events, was evaluated. In particular, the Bayes' theorem is expressed by the equation (9):

$$P(A|B) = \frac{\cdot P(B|A) \cdot P(A)}{P(B)}.$$

In this study, the method is computed in terms of relative frequencies as proposed by Berti et al. (2012). The probability terms can be approximated to:

- $P(A) = N_A/N_R$;
- $P(B) = N_B/N_R$;
- $P(B|A) = N_{B|A}/N_A$;

where N_R is the total number of rainfall events identified, N_A is the total number of landslides occurred, N_B is the number of rainfall events of magnitude B, and $N_{B|A}$ is the number of rainfall events of magnitude B that resulted in landslides. Thus, equation (9) reduces to:

$$P(A|B) = \frac{\frac{N_{B|A}}{N_A} \cdot \frac{N_A}{N_R}}{\frac{N_B}{N_R}} = \frac{N_{B|A}}{N_B} \qquad (13)$$

In the methodology described so far there is no discrimination between rainfall events that triggered one landslide and those that activated multiple

landslides. At these conditions, in fact, N_A represents the number of events with occurred slope failures and P(A) is the probability of having at least a landslide in the study area. P(A|B), that is the probability that a given quantity of rain triggers at least a landslide, is the result to be obtained.
The method returns a value of landslide probability (from 0 to 1) for each combination of the selected variables (A and B). To rate P(A|B), 4 classes have been used. These classes correspond to a confidence level of low, medium, medium-high and high probability of occurrence (Table 6).

P(A|B) %	Level
0-35	Low
36-50	Medium
51-65	Medium-high
66-100	High

Table 6 Probability intervals and levels of confidence used to classify the results of the Bayesian model

Thus far, the one-dimensional approach of the Bayes' theorem has been adopted. In this case, the only control variable is B, which represents a rainfall event with a certain magnitude. For the study, B has been expressed in terms of cumulated event rainfall (E), daily rainfall (R), and antecedent rainfall (A_5, A_7, A_{15}, and A_{30}). P(A|B) has been computed for all these significance attributed to the variable B.

A further analysis consisted in the application of the two-dimensional approach, in which two control variable (B and C) are considered. The resulting equation is in the form:

$$P(A|B,C) = \frac{\cdot P(B,C|A)\cdot P(A)}{P(B,C)} \qquad (14)$$

where the notation B, C indicates the joint probability of having a certain value (or range of values) of the two variables. Any pair of variables can be considered in the two- dimensional Bayesian analysis. For this study, B and C have been represented by the control variables among the best performing of the one-dimensional case: daily rainfall (R) and five days antecedent rainfall (A_5). The performance of the computed probabilities can be evaluated by comparing the posterior probability P(A|B) to the prior probability P(A). If the conditional event B is significant for the initiation of landslide in the study area, the posterior probability lies above the corresponding prior

(P(A|B)>P(A)). If the conditional event B is irrelevant to the process, the two probability distributions P(B) and P(B|A) would have roughly the same values (P(A|B)≈P(A)).

The two-dimensional model was accomplished by creating a B-C plane divided into 16 regions delimited by intervals of B and C values. Equation (14) is then computed separately for each region obtaining probabilistic information in the B-C space.

4.2.3.2 Results of one-dimensional approach

The Bayesian one-dimensional approach have been applied first to the cumulated event rainfall (E), then to the daily rainfall (R), and finally to the antecedent rainfall (A_5, A_7, A_{15}, and A_{30}). The values of E, R, and A_D are referred to areal averages of the entire study area.
A summary description of the input data for all the analyses is proposed in Table 7. The values of N_B are not specified, because they vary depending on the magnitude of B (i.e. the rainfall parameters and intervals) considered in each test.

CONTROL VARIABLE	E	R	A_5	A_7	A_{15}	A_{30}
N_R	1126	2480	5878	6717	8023	8365
N_A	29	45	57	57	60	60

Table 7 Number of rainfall (N_R) and landslide (N_A) events considered as input for the Bayesian analyses

Results of the Bayesian model applied for the cumulated event rainfall recorded in the Esino post-orogenic complex are presented in Figure 31and Figure 32.
Figure 31 shows the distribution of prior landslide probability P(A), prior rainfall probability P(B), conditional probability P(B|A) and conditional landslide probability P(A|B) for event rainfall (E) values from 10mm to 200mm. Particularly, P(A), P(B), P(B|A), and P(A|B) are calculated for E≥10mm, E≥15mm, and so on. Results reveal descending values of P(B) and P(B|A), whereas the P(A/B) is always ascending. For E≥140mm the case study is just one (147mm), therefore the computation of probabilities has no statistical significance. The figure also shows a P(A|B)>P(A), thus the event rainfall is significant for the initiation of landslides in the study area.

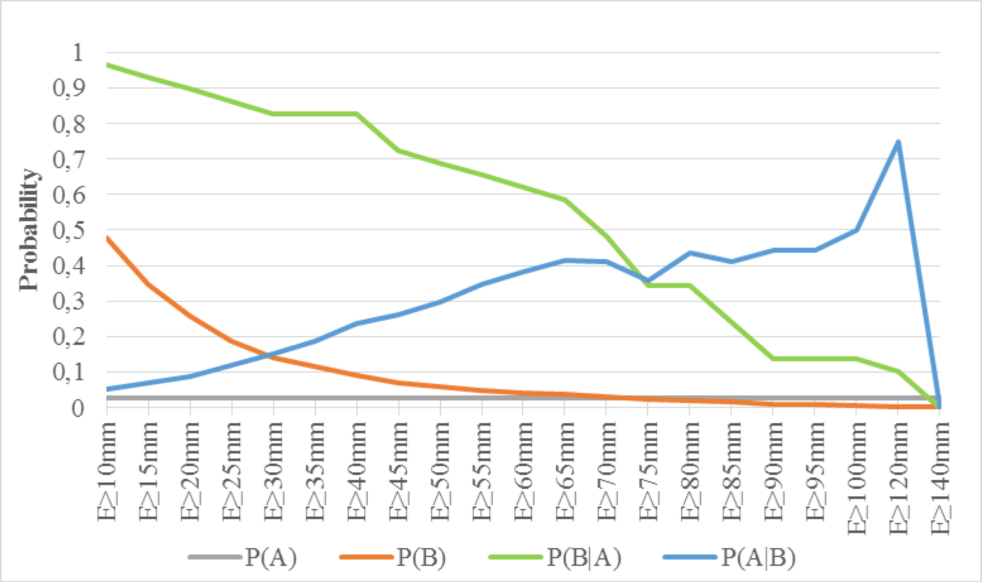

Figure 31 Comparison of P(A), P(B), P(B|A), and P(A|B) for different values of E

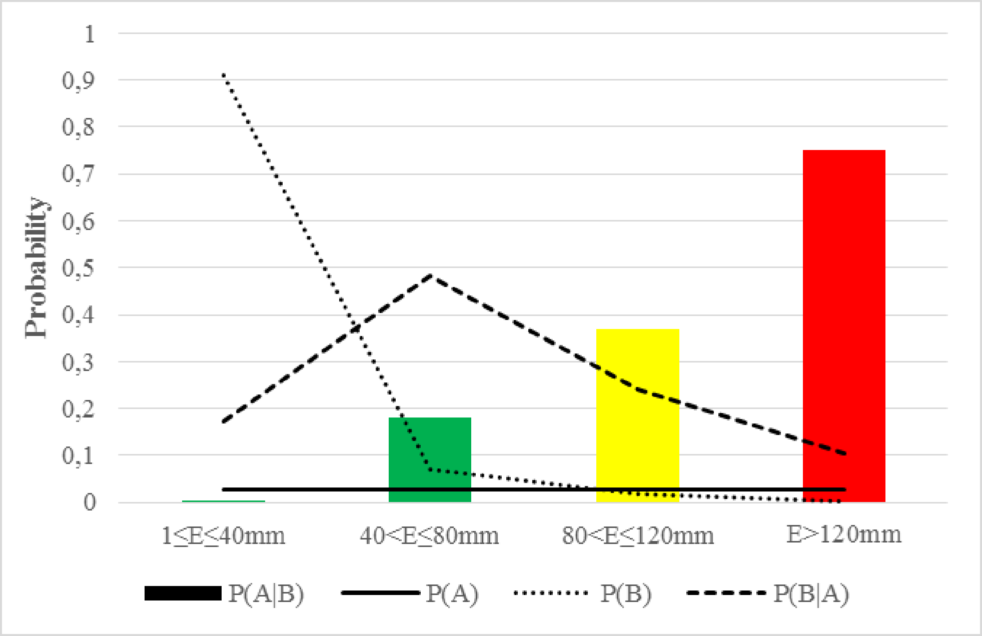

Figure 32 Computed values of P(A), P(B), P(B|A), and P(A|B) for four intervals of E

Figure 32 displays the values of P(A), P(B), P(B|A), and P(A|B) computed for four classes of E: 1-40mm, 40-80mm, 80-120mm, >120mm. In the first two classes, according to Table 6, the probability of occurrence of one or more landslides is low. This probability is medium in the third class and high in the fourth class. It is notable also that P(A|B)>P(A), except for 1≤E≤40mm.

The Bayesian statistic model applied for the daily rainfall (R) provides the results illustrated in Figure 33 and Figure 34.
The same observation made for Figure 31, can be transposed for Figure 33, except for the ascending trend of P(A/B) which continues towards the value of one. Thus, the significance of the daily rainfall is high. In fact, the few events with daily rainfall greater than 65mm all resulted in at least a landslide, thus P(A|B)=1. The maximum value of R in the study area is 68.4mm.
Figure 34 shows the outcomes of P(A), P(B), P(B|A), and P(A|B) computed for four classes of R: 1-20mm, 20-40mm, 40-60mm, >60mm. The first three classes listed display increasing values of P(A|B), but they all conform to a low level of probability. The third class is at the boundary line with the medium level. However, when R exceeds 60mm, P(A|B) decisively increases to high likelihood of occurrence.

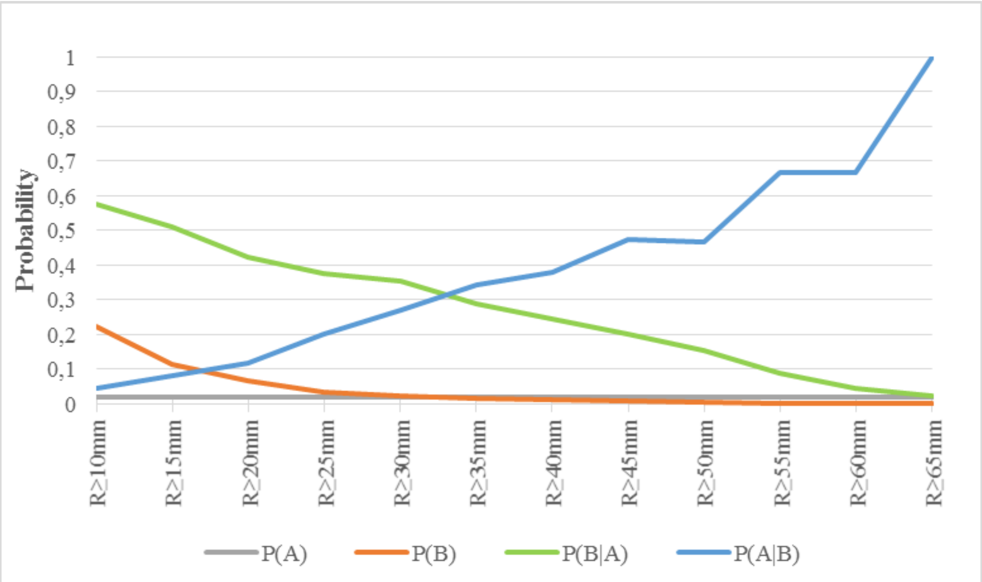

Figure 33 Comparison of P(A), P(B), P(B|A), and P(A|B) for different values of R

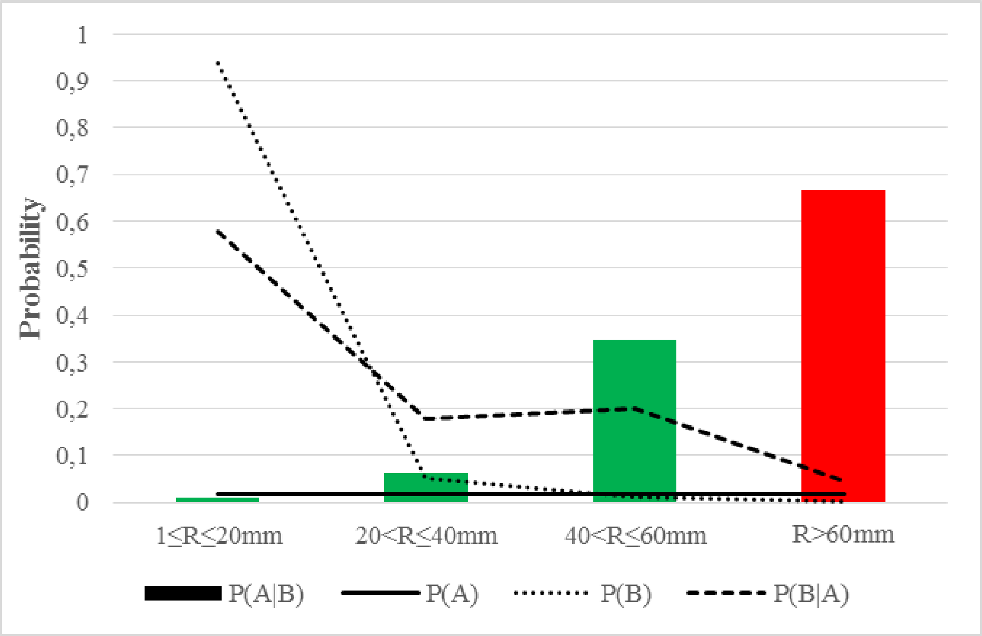

Figure 34 Computed values of P(A), P(B), P(B|A), and P(A|B) for four intervals of R

The Bayesian method has been applied also considering the antecedent rainfall as the control variable. The following figures (from Figure 35 to Figure 42) shows the distributions of P(A), P(B), P(B|A), and P(A|B) considering 5 days (Figure 35 and Figure 36), 7 days (Figure 37 and Figure 38), 15 days (Figure 39 and Figure 40), and 30 days (Figure 41 and Figure 42) of antecedent rainfall. These intervals were considered to verify the best period to be taken into account in the forecast activity.

P(A), P(B), P(B|A), and P(A|B) were computed for antecedent rainfall (A_D) values ranging from 10mm to 200mm and for four classes of A_D: 1-30mm, 30-60mm, 60-90mm, >90mm.

The first remark is that, for all the analyses, even if P(B) and P(B|A) are always decreasing, the increasing of P(A|B) is considerably lower compared to the case of E and R. The P(A|B) increment is quasi null for A_{15} and A_{30}.

More specifically, the analysis carried out for A_5 is the one with the maximum values of resulting P(A|B). In fact, only the third and fourth intervals considered have P(A|B)>P(A) with probability levels corresponding to low (Figure 36). The same notes can be done for A_7, which is a period of antecedent rainfall very close to A_5, but with lower resultant P(A|B) (Figure 38). Moreover, the results of A_{15} shows a slightly increase of P(A|B) for the fourth interval, whereas for A_{30} there is no evidence.

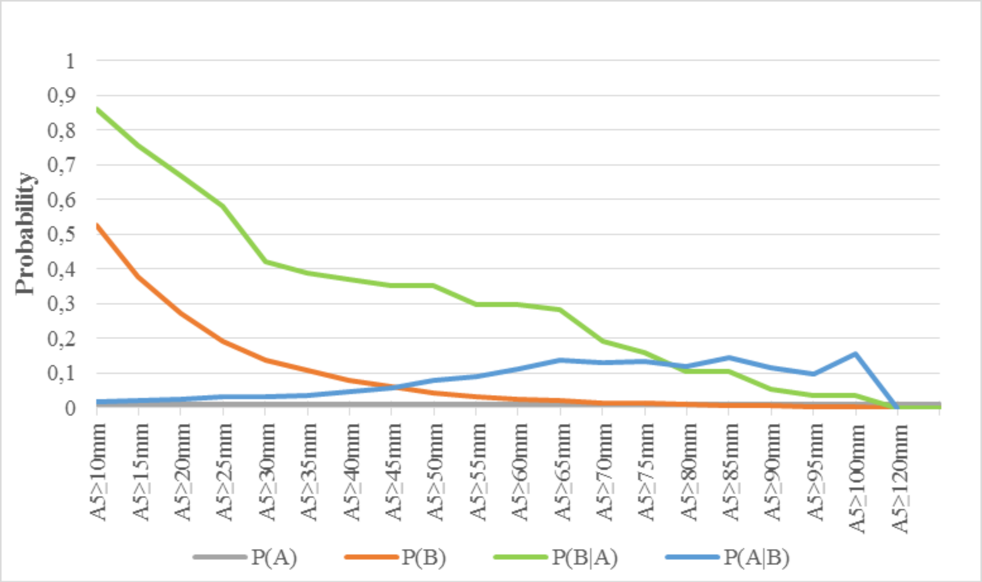

Figure 35 Comparison of P(A), P(B), P(B|A), and P(A|B) for different values of A_5

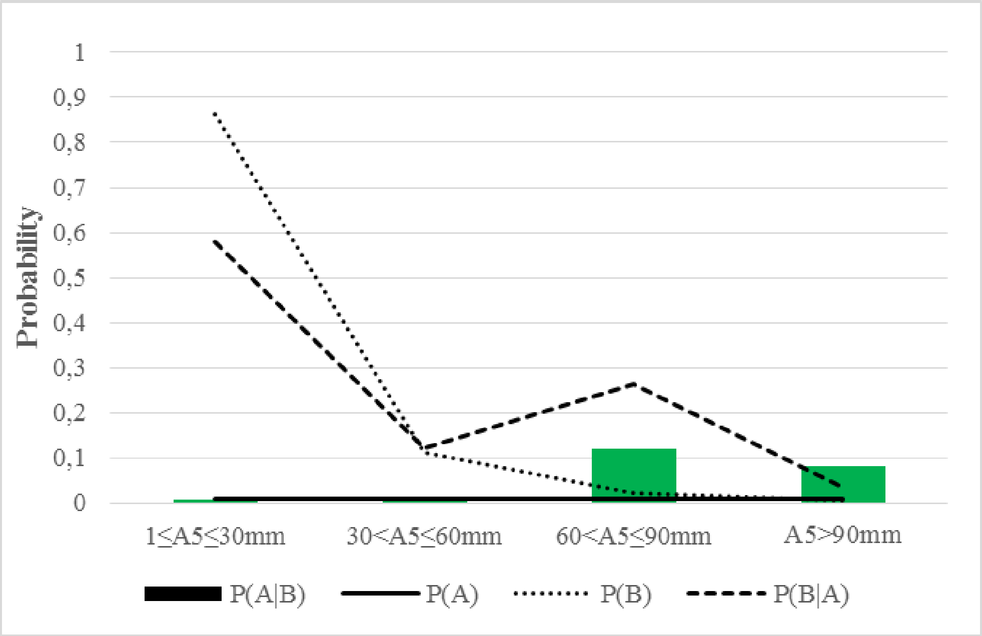

Figure 36 Computed values of P(A), P(B), P(B|A), and P(A|B) for four intervals of A_5

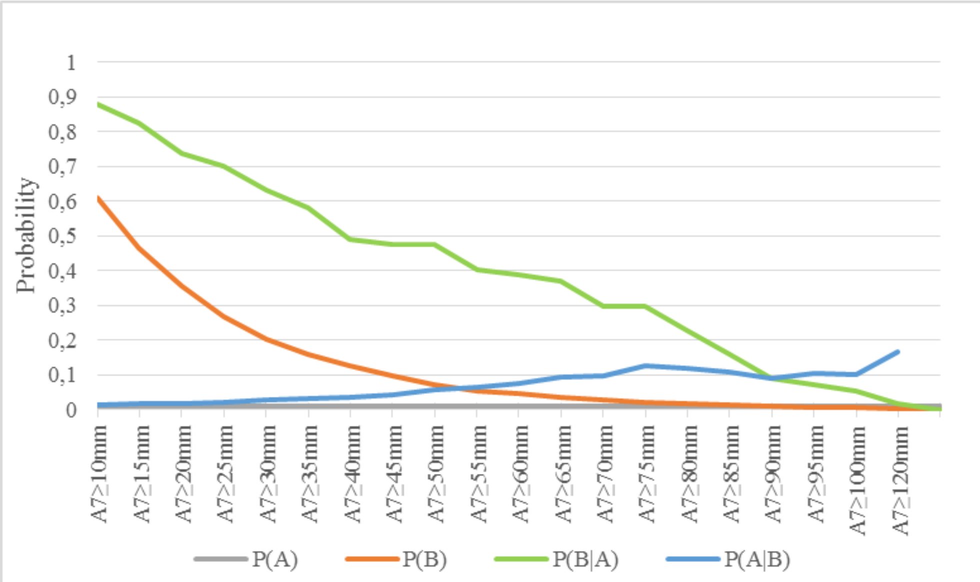

Figure 37 Comparison of P(A), P(B), P(B|A), and P(A|B) for different values of A_7

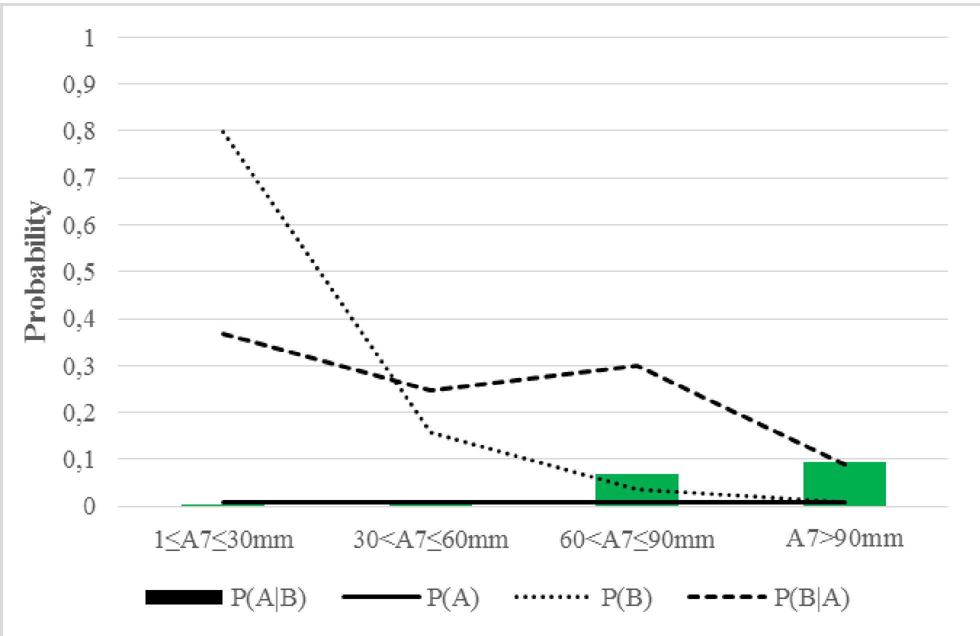

Figure 38 Computed values of P(A), P(B), P(B|A), and P(A|B) for four intervals of A_7

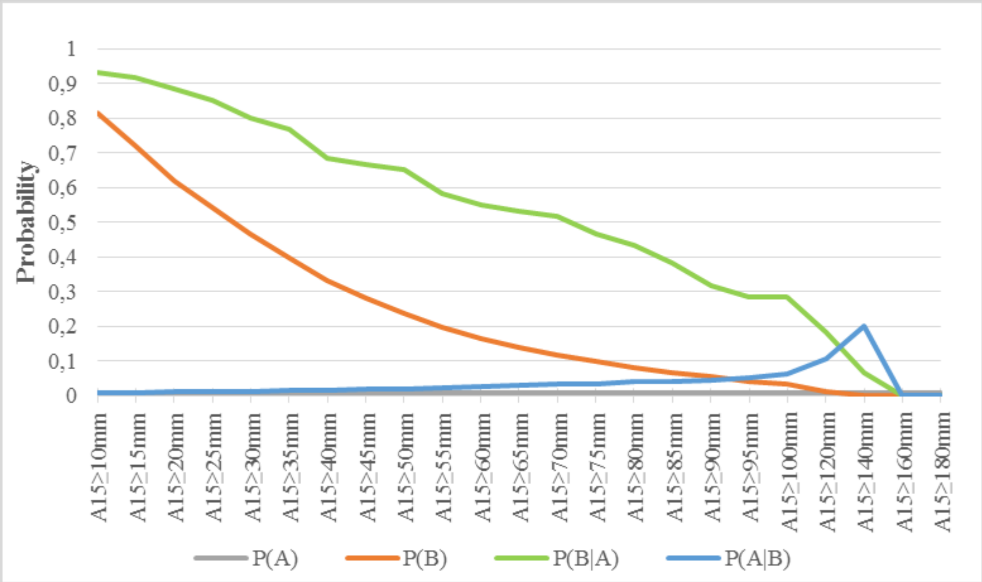

Figure 39 Comparison of P(A), P(B), P(B|A), and P(A|B) for different values of A_{15}

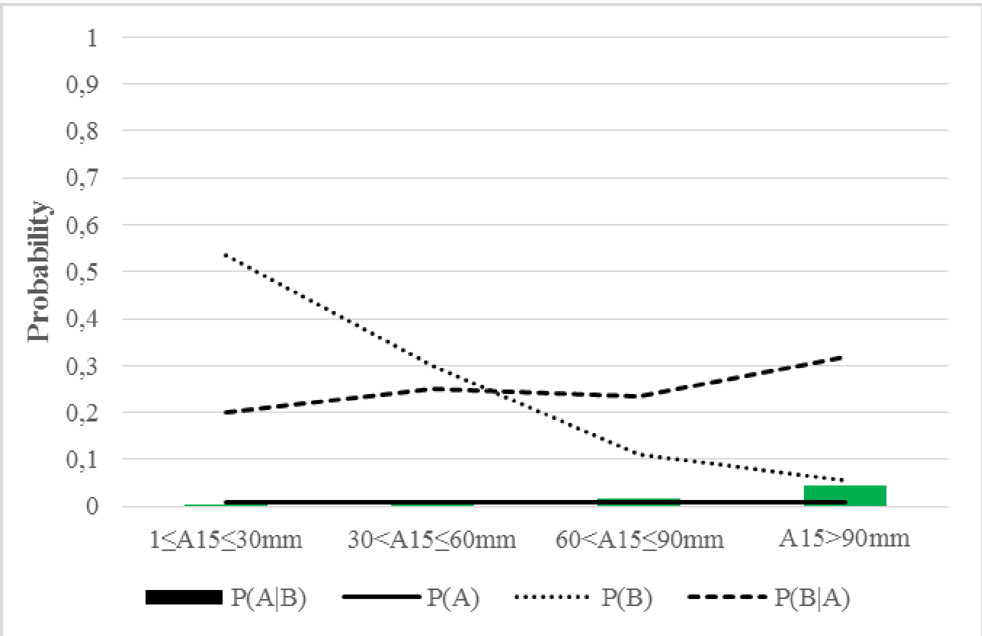

Figure 40 Computed values of P(A), P(B), P(B|A), and P(A|B) for four intervals of A_{15}

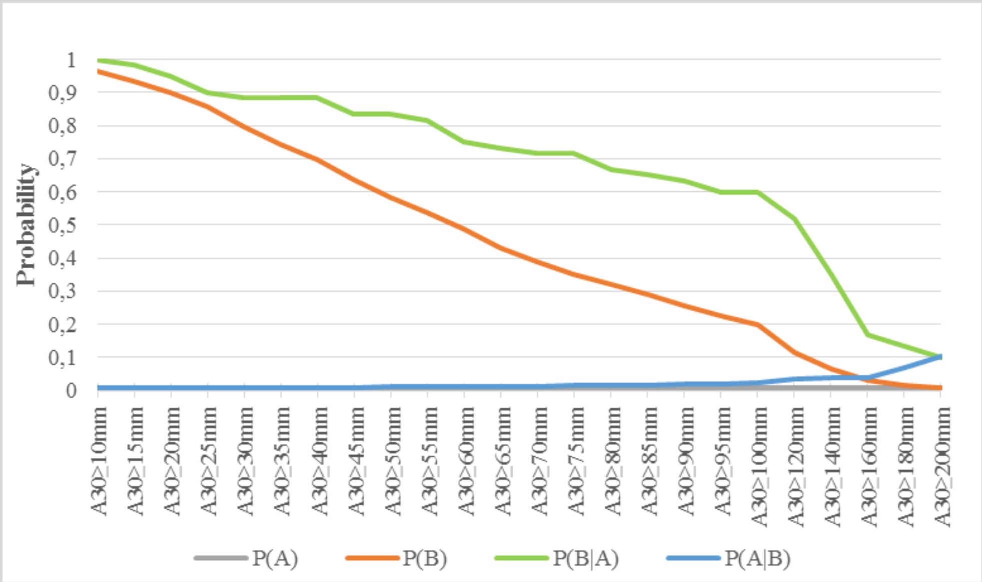

Figure 41 Comparison of P(A), P(B), P(B|A), and P(A|B) for different values of A_{30}

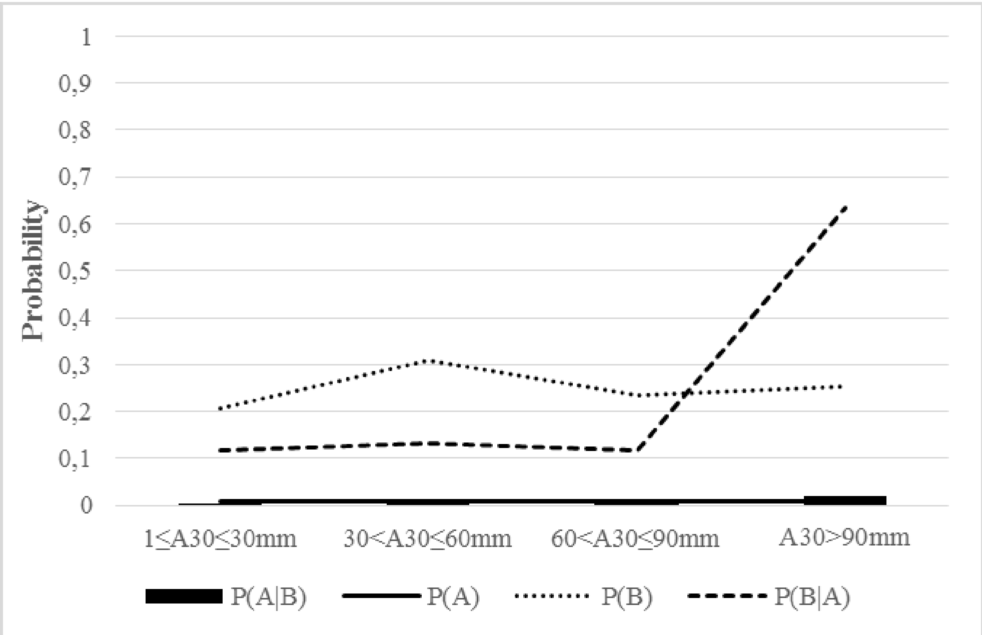

Figure 42 Computed values of P(A), P(B), P(B|A), and P(A|B) for four intervals of A_{30}

The output obtained from the one-dimensional Bayesian model, led to the choice of the two control variables to be tested for the two-dimensional model.

4.2.3.3 Results of two-dimensional approach

The two-dimensional Bayesian approach was applied to two control variables: daily rainfall (R) and five days antecedent rainfall (A_5). The reason of this choice is because, even if R and E are the best performing variables, when considered together the data overlap. Indeed the event rainfall includes also the daily rainfall. Therefore, the two-dimensional method has been applied to the antecedent rainfall variable with more significant results.

The analysis was accomplished by creating a R-A_5 plane divided into 16 regions delimited by intervals of daily rainfall and five days antecedent rainfall (Table 8 and Figure 43). Results of equation (14) have been plotted in the R-A_5 space for every region.

For example, the upper-left quadrant of Table 8 and Figure 43 represents the posterior probability of initiating at least a landslide within the study area, given a rainfall event of $0 \leq A_5 \leq 20$mm and $R \geq 60$mm ($P(A|A_5,R)$). The colors of cells and histograms correspond to the levels described in Table 6. The “no applicable” areas (NA) indicate rainfall conditions that never occurred in the Esino post-orogenic complex during the considered period. The values of $P(A|A_5,R)=0$ represent rainfall conditions which never resulted in landslides during the considered period.

The model’s outputs show that in general landslide probability increases with both daily and antecedent rainfall. The maximum probability value of 1.0 are reached for rainfall events with $20 \leq A_5 \leq 40$mm and $R \geq 60$mm or for rainfall events with $A_5 \geq 60$mm and $40 \leq R \leq 60$mm. Medium-high probability levels characterize rainfall events with $20 \leq A_5 \leq 40$mm and $40 \leq R \leq 60$mm or for rainfall events with $A_5 \geq 60$mm and $20 \leq R \leq 40$mm. The remaining probabilities computed are included in the low probability level.

≥60	0,00	1,00	NA	NA
40-60	0,24	0,57	0,00	1,00
20-40	0,03	0,03	0,09	0,60
0-20	0,00	0,01	0,01	0,09
R / A_5	0-20	20-40	40-60	≥60

Table 8 Values of the computed P(A/A5,R) classified in 16 combinations of A_5 and R (in mm)

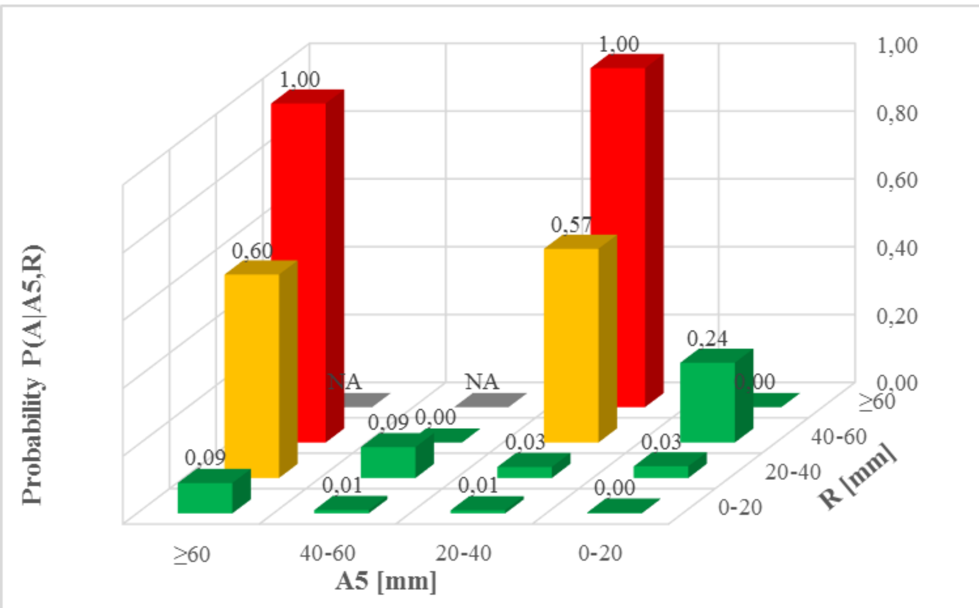

Figure 43 Histograms of conditional landslide probability P(A/A5,R) for 16 different combinations of A_5 and R

4.3 Physical model

This chapter describes the third part of the analysis, which is the application of the U.S. Geological Survey's Transient Rainfall Infiltration and Grid-Based Regional Slope-Stability (TRIGRS) model (Baum et al., 2008, 2002, 2010) to the Esino post-orogenic complex. Previous studies have successfully applied physical models, and particularly the TRIGRS, to compute infiltration-driven changes in the hillslopes' factor of safety on small scales (i.e. tens of square kilometers). Indeed, soil data inputs for such models are difficult to obtain across larger regions. This work describes a novel methodology for the application of TRIGRS over broad areas with relatively uniform hydrogeological properties (Gioia et al., 2016).

4.3.1 Theoretical basis of the TRIGRS model

TRIGRS is a Fortran program designed for modeling the timing and distribution of shallow, rainfall-induced landslides. TRIGRS employs a distributed approach to model transient vertical groundwater flow over a digital landscape. It uses approximate analytical solutions of the Richards equation (Richards, 1931) for saturated (Iverson, 2000; Savage et al., 2003) and variably saturated conditions (Savage et al., 2004; Srivastava and Yeh, 1991) to determine the pressure head, the factor of safety and their spatial and temporal variations.

The governing equations of the TRIGRS model for wet initial conditions are based on a linearized solution of the Richards equation proposed by Iverson (2000) and implemented by Baum et al. (2002). The pressure head time-dependent vertical distribution for infinite depth is so described:

$$\psi(Z,t) = (Z-d)\beta + 2\sum_{n=1}^{N} \frac{I_{nZ}}{K_S}\left\{H(t-t_n)[D_1(t-t_n)]^{\frac{1}{2}}\, ierfc\left[\frac{Z}{2[D_1(t-t_n)]^{\frac{1}{2}}}\right]\right\} - 2\sum_{n=1}^{N} \frac{I_{nZ}}{K_S}\left\{H(t-t_{n+1})[D_1(t-t_{n+1})]^{\frac{1}{2}}\, ierfc\left[\frac{Z}{2[D_1(t-t_{n+1})]^{\frac{1}{2}}}\right]\right\} \qquad (15)$$

where Ψ is the pressure head, t is time, $Z = \frac{z}{\cos\delta}$ is the vertical depth, z is the slope-normal coordinate direction, δ is the slope angle, d is the steady-state depth of the water table, $\beta = cos^2\delta - \left(\frac{I_{ZLT}}{K_S}\right)$ the steady initial surface flux, K_S is the saturated hydraulic conductivity in the Z direction, I_{nZ} is the surface flux at the n^{th} interval, $H(t - t_n)$ is the Heaviside step function, t_n is the time at the n^{th} interval, $D_1 = \frac{D_0}{cos^2\delta}$_$0 = K$_$S/S$_$S$ is the saturated hydraulic diffusivity, S_S is the specific storage and N is the total number of time intervals. The function *ierfc* is of the form $ierfc(\eta) = \frac{1}{\sqrt{\pi}}\exp(-\eta^2) - \eta erfc(\eta)$ where *erfc(η)* is the complementary error function. The first term of equation (15) consists of a steady (long-term) component and the remaining terms a transient (short-term) infiltration component.

The analytical solution for unsaturated groundwater flow considers the soil as a two-layer system consisting of a saturated zone with a capillary fringe above the water table and an unsaturated zone extending from the top of the capillary fringe to the ground surface. The unsaturated zone acts like a filter absorbing part of the infiltrated water from the ground surface; the remaining water accumulates at the base of the unsaturated zone and thus raises the water table conserving a capillary fringe. In this condition TRIGRS uses four parameters (residual water content θ_r, saturated water content θ_s, inverse height of capillary fringe α, and K_S) to approximate the soil-water characteristic curve (SWCC) as suggested by Gardner (1958), and thus approximates the infiltration flux as one-dimensional (Srivastava and Yeh, 1991). The vertical pressure head changes in the unsaturated zone are obtained from the following equation:

$$\psi(Z,t) = \frac{\cos\delta}{\alpha_1}\ln\left[\frac{K(Z,t)}{K_S}\right] + \psi_0 \qquad (16)$$

where $\alpha_1 = \alpha\, cos^2\,\delta_0$ is the pressure head at the water table ($\Psi_0 = 0$) or at the top of the capillary fringe ($\Psi_0 = -1/\alpha$), *K(Z,t)* is the time and depth dependent hydraulic conductivity in the unsaturated zone given by the solution of Srivastava and Yeh (1991) and implemented in Baum et al. (2008) (later corrected in Baum and Godt (2013)). *K(Z,t)* is computed with the ensuing formula:

$$K(Z,t) = \sum_{n=1}^{N} H(t - t_n) \Bigg\{ I_{nZ} - (I_{nZ} - K_S) \exp[-\alpha_1 (d_u - Z)] - 4(I_{nZ} - I_{ZLT}) \exp\left(\frac{\alpha_1 Z}{2}\right) \exp\left[-D_\Psi \frac{(t-t_n)}{4}\right] \cdot \sum_{m=1}^{\infty} \frac{\sin[\Lambda_m \alpha_1 (d_u - Z)] \sin(\Lambda_m \alpha_1 d_u)}{1 + \frac{\alpha_1 d_u}{2} + 2\Lambda_m^2 \alpha_1 d_u} \exp[-\Lambda_m^2 D_\Psi (t - t_n)] \Bigg\} - \sum_{n=1}^{N} H(t - t_{n+1}) \Bigg\{ I_{nZ} - (I_{nZ} - K_S) \exp[-\alpha_1 (d_u - Z)] - 4(I_{nZ} - I_{ZLT}) \exp\left(\frac{\alpha_1 Z}{2}\right) \exp\left[-D_\Psi \frac{(t-t_{n+1})}{4}\right] \cdot \sum_{m=1}^{\infty} \frac{\sin[\Lambda_m \alpha_1 (d_u - Z)] \sin(\Lambda_m \alpha_1 d_u)}{1 + \frac{\alpha_1 d_u}{2} + 2\Lambda_m^2 \alpha_1 d_u} \exp[-\Lambda_m^2 D_\Psi (t - t_{n+1})] \Bigg\} \quad (17)$$

in which d_u is the vertical depth of the top of the capillary fringe, D_Ψ is the decay constant, and the values of Λ_m are the positive roots of a pseudo-periodic characteristic equation.

Below the initial top of the saturated zone and for finite depth basal boundary, TRIGRS computes the pressure head rise using a formula based on a Fourier series solution:

$$\Psi(Z_W, t) = \sum_{n=1}^{N} \Psi_{hn} H(t - t_n) \left\{ 1 - \frac{4}{\pi} \sum_{m=1}^{\infty} (-1)^{m-1} \frac{1}{2m-1} \exp\left[-\frac{(2m-1)^2 \pi^2 D_1 (t-t_n)}{4 d_{LZ}^2}\right] \cos\left[\frac{\pi}{2}(2m-1)\left(\frac{Z_W}{d_{LZ}} - 1\right)\right] \right\} - \sum_{n=1}^{N} \Psi_{hn} H(t - t_{n+1}) \left\{ 1 - \frac{4}{\pi} \sum_{m=1}^{\infty} (-1)^{m-1} \frac{1}{2m-1} \exp\left[-\frac{(2m-1)^2 \pi^2 D_1 (t-t_{n+1})}{4 d_{LZ}^2}\right] \cos\left[\frac{\pi}{2}(2m-1)\left(\frac{Z_W}{d_{LZ}} - 1\right)\right] \right\} \quad (18)$$

where $Z_W = Z - d$ is the vertical depth below the initial water table, $\Psi_{hn} = \beta h_n$ is the pressure head applied after the accumulation of water above the initial water table, d_{LZw} is the vertical height of the saturated layer. For the very early times, formulas based on Fourier series converge poorly so other approximations have been used (Baum et al., 2008, 2010).

To determine the stability of a slope, TRIGRS computes the factor of safety (F_S) using a one-dimensional infinite-slope stability analysis (Taylor, 1948).

F_S is defined as the ratio between the resisting and the driving forces acting on a point along the potential failure plane. The resisting force is the Coulomb shear strength of the soils, a combination of gravity, pore pressure and material properties. The driving force is the shear stress, the slope parallel component of gravity. The equation of F_S is:

$$F_S(Z,t) = \frac{\tan \phi'}{\tan \delta} + \frac{c' - \psi(Z,t)\gamma_W (\tan \phi)'}{\gamma_S Z \sin \delta \cos \delta} \qquad (19)$$

where ϕ' is the soil friction angle for effective stress, c' is soil cohesion for effective stress, γ_w is unit weight of water, and γ_s is unit weight of soil. $\psi(Z,t)$ is the transient pressure head at depth Z and time t, obtained from either equation (15), (16) or (18) depending on the particular conditions modeled. In the unsaturated zone, TRIGRS computes the factor of safety above the water table, multiplying the matric suction $\psi(Z,t)\gamma_W$ by $\chi = ((\theta - \theta\_r\ ))/((\theta\_s - \theta\_r\ )$ as suggested by Vanapalli and Fredlund (2000).
When the shear strength is greater than the shear stress (F_S>1), the slope is predicted to be stable. When the shear stress is greater than the shear strength (F_S<1), the slope is predicted to be unstable. F_S=1 is a state of equilibrium, but inherently unstable.

4.3.2 Methodology

TRIGRS is applied here in the post-orogenic complex of the Esino river catchment, which is about 550km^2 wide, combined with a Geographic Information System (GIS).

The first part of this method consisted in the improvement of the available data.
Hydrogeological, topographic (20m Digital Elevation Model), landslides and rainfall data for this spatial analysis were obtained from government agencies as described before (Chapter 4.1). Usually, shallow landslides are characterized by small thickness, up to 2-3m (Caine, 1980; Crosta and Frattini, 2003). From observational data registered in the field and from reports received by the Marche CFR, an average depth of failure of 1m is reasonably assumed. This depth represents the eluvio-colluvium layer composed of weathered material typical of the clayey Plio-Pleistocene marine deposits (Bisci and Dramis, 1991).

The model requires accurate information on location and timing of the failures. For this reason, from the original database, the events with uncertain date of activation and those related to engineering failures were no longer considered.

The landslides were then associated with one of the local mechanical (MR) or telemetric (TR) rain gauges distributed in the study area or in the proximity. Afterwards, each landslide locations was assigned to a hydrogeological map unit, using a map provided by the National Research Council (Folchi Vici D'Arcevia et al., 2008), and to a land use class, according to the European Corine Land Cover - CLC 2000 (unpublished data, 2002) database, available from the European Environmental Agency (http://www.eea.europa.eu/). A soil texture class was identified for every hydrogeological unit assigned to the landslides of the study area.

In large regions such as the study area, local and detailed data on soil properties and thickness are difficult to obtain. To overcome this limitation an innovative approach has been proposed. The values of the soil physical parameters, required as input for the TRIGRS program, has been gathered from literature review of works related to soil texture classes matching the study area ones. These parameters are:

a) *cohesion* c [kPa], which is a measure of the forces that cement particles of soils; is the non-frictional part of the shear strength that is independent of the normal stress;
b) *angle of internal friction* φ [deg], which is the angle of inclination, measured between the normal and the resultant force, that is attained when failure occurs in response to a shearing stress; it is a measure of the ability of a unit of rock or soil to withstand a shear stress;
c) *unit weight of soil* γ_s [kN/m^3], which is the specific weight of the material per unit volume;
d) *saturated hydraulic conductivity* K_S [m/s], which is a measure of the soil's ability to conduct water when is submitted to a hydraulic gradient; at saturated conditions is a constant value for any given time and location within the soil body.
e) *hydraulic diffusivity* D_0 [m^2/s], which is the ratio between saturated hydraulic conductivity and specific storage (water capacity); it controls the fluid pressure and hence affects the effective normal stress during a rupture;
f) *residual water content* θ_r [-], which is defined as the ratio of the volume of water retained in the soil, after all downward gravity drainage has ceased, to the total volume of the sample;

g) *saturated water content* θ_s [-], which is the soil water content when all pores are filled with water and is equivalent to porosity;
h) *inverse height of capillary fringe* α [1/m], which represents the desaturation rate of the soil water and is related to pore size distribution; it is smaller for finer-textured soils.

Among the physical parameters collected, the best sources considering proximity, data availability, and soil characteristics were chosen for every texture class. The arithmetic mean was derived when the references cited a large range of values. Descriptive statistics, such as the smallest observation (sample minimum), lower quartile (q1), median, upper quartile (q3), and largest observation (sample maximum), has been computed for each set of parameters. These limit values has been used alternately in the model for its calibration.

The second part of the analysis involved the examination of the model's sensitivity to the inputs. The intention was to assess the performance of TRIGRS, calibrated to produce failure, over: (i) timing of the highest pressure head with time of landslide occurrence, and (ii) pore pressure fluctuation in response to rainfall in the different texture classes. These objectives have been achieved by computing the pressure head variation for a single 1-D profile over a range of hydrological property values typical of the soil texture classes previously identified in the Esino river basin area, namely clay, sandy-clay and loam.

The analysis required as input the slope characteristics and the mechanical and hydrogeological properties of the material involved. Once these parameters values were selected, fifteen model runs on a 1-D profile were carried out.

TRIGRS was tested in the opposite cases of saturated condition with infinite depth of the basal boundary (SAT-INF) and unsaturated condition with finite depth of the basal boundary (UNS-FIN). The permeability contrast depth, used in the finite case, was 1m; as described before, this depth was also assumed the average depth of landslide failure. The model was calibrated with representative input values that yield a change in pore-water pressure that reduced the safety factors to one during the simulation. Some input parameters were the same for each test while others were varied.

The storms chosen for the study were picked among those that triggered, in the study area, the largest number of landslides during the past years (1990-2012). The reason of this choice is to analyze the sensitivity of the program to different intensity-duration ratios. The rainfall data concerning these

storms are referred to the rain gauges (MR) with the most number of landslides correlated.
Among the model runs, those with the best results were selected to compare behaviors of different materials and pressure head responses during the storms selected. The best results of the model runs were identified as the tests in which the 1-D profile was stable ($F_S > 1$) at the beginning and unstable ($F_S \leq 1$) at the end of the storm.
Moreover, three parameters were used to examine and compare the different responses of the model to the change in the saturated hydraulic properties: (1) saturated hydraulic conductivity (K_S), (2) saturated hydraulic diffusivity (D_0), and (3) initial depth of the water table (d). Values for these three input variables were varied in the model runs considering saturated and unsaturated conditions for all the above-mentioned soils and storms.

The third part of the research consisted in the application of TRIGRS to the entire study area. TRIGRS was uses for historical storm scenarios to compare model results against the landslide database.
First, every landslide point location was related to a corresponding polygon of the IFFI database (APAT - Dipartimento Difesa del Suolo, 2007) or to a buffer area whose width depended on the information available of the failure. This was done because the physical model requires the specific surface of the landslides to compare the stable with the unstable areas.
The best performing hydrological and mechanical property values, assessed through the calibration (see part 2), represent a portion of the inputs for the application of TRIGRS to the post-orogenic complex. Moreover, for this 2-D profile have been provided: (i) the initial water table positions; (ii) the spatial distribution of topographic slope; (iii) the time-varying rainfall intensities; (iv) the antecedent soil moisture conditions; (v) the spatial distribution of soil depths.
The initial water table depth was considered as assumed during the calibration phase.
The slope was derived from a 20m Digital Elevation Model (DEM), which was also used to divide the study area into a grid of 1376590 cells sized 20m x 20m.
Because of the large number of cells and consequently of data, the hourly precipitation was grouped into intervals with similar rainfall intensity. The mean rainfall has been computed for every interval and those values has been used as input for the model. Therefore, the number of computational steps and the total running time of each simulation decreased.

For the deduction of the soil moisture conditions at the beginning of the storms, the Antecedent Water Index (AWI) was calculated according to Godt et al. (2006). The AWI is zero at the field capacity, defined as the moisture content above which water freely drains from the soil, negative below and positive above (Godt et al. 2006). The field capacity was evaluated through a range of values effective for every texture class: (a) 0.27m for clay (Brady, 1990); 0.13m for sandy-clay (Godt et al., 2006a); 0.26m for loam (Brady, 1990). These values represent the amount of rainfall (in m) needed to reach the field capacity starting from wilting conditions. Thus, the AWI was computed for every rainfall event, since the beginning of the meteorological season or the beginning of consistent rainfall, which was considered as the wilting condition. If the AWI was approximately equal or greater than zero at the beginning of the days of landslides initiation, TRIGRS was run in the form of saturated initial conditions. If the AWI was less than zero for one or more texture classes, TRIGRS was run with unsaturated initial conditions.

The soil depth (Z) was assessed assuming its negative correlation with the profile slope angle, so that the depth decreases with the increase of the slope (DeRose et al., 1991). Based on the strength property values (friction angle, cohesion and unit weight of soil) gathered from the literature review and calibrated in the above described tests, the critical soil depth for $F_S = 1.0$ was calculated. Namely, the inverse form of equation (19) has been used in every texture class, assuming the water table at the ground surface, to compute Z for every slope values from the minimum to the maximum in the study area. The power law regression ($y = a \times x^{-b}$) derived from these computed data, represents the maximum acceptable soil thickness of a slope to become potentially unstable. We considered the power law for the model, because the data regression coefficient (R^2) is higher than in the exponential equation applied by DeRose (1991).

After collecting and computing all the required inputs, TRIGRS was run to provide estimates of the F_S distribution across the study area. As initial conditions, for this simulation we used saturated (SAT) or unsaturated (UNS) settings, depending on the AWI, with a basal boundary at 1m of depth (FIN). Furthermore, the receiver operating characteristics (ROC) technique was used to assess the performance of the model as landslide predictor for the study area. The ROC chart illustrates the outputs of classification models where the response variable is binary; in this case, the states are either "unstable" or "stable". To perform the ROC analysis, the cells with $F_S \leq 1.0$ were considered unstable, whereas the cells with $F_S > 1.0$ were considered stable.

There are four possible outcomes from a binary classifier that can be formulated in a two-by-two contingency table (or confusion matrix) (Fawcett,

2006). If a grid cell is modeled unstable and corresponds to a mapped landslide, it is considered a "true positive" (TP); otherwise, if no landslide is recorded, the cell is considered a "false positive" (FP). If the grid cell is modeled stable and does not match a mapped landslide, it is considered a "true negative" (TN); otherwise, if it fits a slope failure, the cell is considered a "false negative" (FN). The ROC curve is created by plotting the "true positive rate" (TPR) vs. the "false positive rate" (FPR). The TPR (or sensitivity) is the fraction of TP out of the sum TP+FN that represents the total number of landslide cells. The FPR (or fall-out) is the fraction of FP out of the sum FP+TN that represents the total number of non-landslide cells. In a ROC graph the origin point (0, 0) represents a classification model which commits no FP errors but also gains no TP. On the contrary, a classifier which unconditionally predicts the entire area to be unstable would be located at point (1,1). The perfect outcome of a model is represented by the upper left corner (0,1). The closer is a prediction to the point (0,1), the better is the performance of the model. A result that falls along the diagonal is considered random.
Finally, the ROC curves were plotted to evaluate the model outcomes by varying the range of F_S values considered unstable. In the first setting, the cells with $F_S \leq 0.8$ were supposed unstable and those with $F_S > 0.8$ were supposed stable. In the second scenery, the instability limit was at $F_S \leq 0.9$, and so forth up to the value of 2.0. Acceptable prediction are results of the classification falling in the upper left quadrant of the graph, namely the outputs with TPR > 0.5 and FPR < 0.5. These ranges represent the conditions that maximized the sensitivity and minimized the fall-out of the TRIGRS runs.

Interpretation of the model's output in a probabilistic framework accounts for uncertainties in the material properties and rainfall distribution as well as temporal changes in topography or subsurface conditions that are not represented in the available geographical datasets.

4.3.3 Results

The first part consisted initially in the cataloging of landslides with certain timing and location. The remaining number of landslides (82) after the above edits belongs to 25 different rainstorm events (Table 9) from November 1991 to February 2011.

Storm	Starting date	Ending date	Duration (h)	Event rainfall (mm)	Intensity (mm/h)	Landslides
Nov-91	11/23/1991	11/25/1991	72	66.7	15.6	3
Oct-92	10/20/1992	10/21/1992	48	42.0	6.0	1
Jan-94	01/20/1994	01/21/1994	48	71.4	17.2	7
Jul-94	07/20/1994	07/21/1994	48	62.4	30.2	1
Sep-95	09/08/1995	09/08/1995	24	24.6	11.6	1
Mar-96	03/16/1996	03/17/1996	48	16.2	3.2	1
Apr-96	04/02/1996	04/05/1996	96	55.2	15.6	1
Oct-96	10/07/1996	10/09/1996	72	97.6	16.4	7
Dec-96	12/24/1996	01/05/1997	312	125.9	9.0	11
Nov-98	11/30/1998	12/05/1998	144	120.9	9.4	18
Dec-98	12/12/1998	12/12/1998	24	1.2	0.4	2
Dec-99	12/15/1999	12/16/1999	48	76.6	6.4	1
Jan-01	01/28/2001	02/01/2001	120	74.8	10.2	2
Feb-04	02/24/2004	03/02/2004	192	48.9	4.2	2
May-05	05/17/2005	05/19/2005	72	28.2	7.6	1
Oct-05	10/06/2005	10/09/2005	96	80.4	27.8	5
Dec-05	12/31/2005	01/03/2006	96	49.4	8.0	2
May-08	05/18/2008	05/22/2008	120	70.2	32.2	1
Sep-08	09/12/2008	09/16/2008	120	61.4	37.4	1
May-09	05/31/2009	06/02/2009	72	13.0	1.6	1
Dec-09	12/31/2009	01/06/2010	168	48.0	2.8	1
Mar-10	03/09/2010	03/11/2010	72	36.5	3.6	2
May-10	05/11/2010	05/16/2010	144	67.0	5.4	1
Nov-10	11/30/2010	12/03/2010	96	49.4	4.4	2
Feb-11	02/27/2011	03/6/2011	192	137.0	13.6	7
Median			96	61.4	9.0	

Table 9 Storms that triggered one or more landslides during the period 1990-2012. The table shows the starting and ending date of the storms, the storm duration in hours (maximum value of all rain gauges), the storm event rainfall (mean of all rain gauges data), the peak hourly rainfall (maximum value of all rain gauges) and the number of landslides triggered during the storm. Median values of the storms are shown at the bottom of the table.

The values of storm duration vary from 24 h to 312 h, with a median of 96 h. The average total rainfall in the rainstorms ranges between 1.2 mm (distance from nearest gauge is 4 km) and 135 mm (distance from nearest gauge is 3.7 km) with a mean of 91.6 mm, a median of 61.4 mm and a standard deviation of about 41 mm. The maximum intensities, ranging from 0.4 mm/h to 37.4 mm/h, registered a median value of 9 mm/h. The rainfall events triggered from one to 18 landslides. The correlation coefficient (r), computed with the equation (11), shows divergent results. The value of r for the landslide and intensity series is 0.02, for the landslide and duration series is 0.44, for the landslide and event rainfall series is 0.72.

Almost all the landslides are located in clay (44) or sandstone (29) materials (Table 10), in areas where the land use is generally agricultural. Other failures initiated in alluvium (5), limestone (3), and colluvium (1) hydrogeological classes. The soil texture categories appointed to every hydrogeological unit were clay, sandy-clay, loam, and gravel (Table 10).

Hydrogeological Classes	**Landslides**	**Texture**
Alluvium	5	Loam
Chalk	0	-
Clay	44	Clay
Colluvium	1	Loam
Limestone	3	Gravel
Marl	0	-
Sandstone	29	Sandy-Clay

Table 10. Soils and frequency of landslides in the study area. The right column represents the soil texture class associated to the hydrogeological units in which at least one landslide was initiated.

The physical parameters values, collected from published works and referred to every texture class, are listed in Table 11. Statistics of the best matching sources for every texture class was computed. Figure 44 shows the ranges and the central tendencies of all the physical properties thus considered, summarized for each soil texture class.

c (kPa)	φ (deg)	Υ_S (kN m^3)	D_0 (m^2 s^1)	K_S (m s^{-1})	θ_r (-)	θ_s (-)	α (m^{-1})	Reference
Clay								
				1.16 - 6.94·10^{-6}				(Cascini et al., 2010)
					0.17	0.35		(Cassinis et al., 1985)
0 – 5	10 – 20	20	10^{-8} - 10^{-7}	10^{-9} - 10^{-7}				(Cervi et al., 2010)
100	15 – 21				0.10	0.50		(Cotecchia, 2006)
10	15 – 30		10^{-5}					(Montrasio et al., 2011)
4	18		5.0·10^{-6}	10^{-7}	0.07	0.80	5	(Raia et al., 2014)
5 – 10	18 – 22	19 – 19.6						(Salciarini et al., 2006)
20 – 80	26 – 34	19.6 – 22		10^{-8}				(Salciarini et al., 2006)
0	20			10^{-8}-10^{-7}				(Simoni et al., 2004)
Sandy-clay								
0.5	32	19.1 – 19.7		10^{-6}			2	(Casagli et al., 2006)
0 – 10	15 – 25	20	10^{-8}-10^{-7}	10^{-7} - 10^{-5}				(Cervi et al., 2010)
0	12.4	17.09				0.37		(Crescenti et al., 2000)
0	30 – 35		10^{-5}					(Montrasio et al., 2011)
3	31		3.8·10^{-4}	10^{-4}	0.05	0.20	2	(Raia et al., 2014)
Loam								
0	18 – 35	18.4 – 19		1.3·10^{-6}			2.5	(Casagli et al., 2006)
0 – 10	25 – 35	24	10^{-8}-10^{-7}	10^{-7} - 10^{-4}				(Cervi et al., 2010)
4.5	13.5	19.07				0.33		(Crescenti et al., 2000)
2.9	32.5	14.9 – 19		10^{-7}			1	(Dapporto et al., 2001)
0	30 – 32	20						(Luzi and Pergalani, 1996)
3	15		4.7·10^{-3}	10^{-4}	0.10	0.50	1	(Raia et al., 2014)

0	33	19.6		0.5 - $6.0 \cdot 10^{-6}$		0.45		(Rinaldi and Casagli, 1999)
2 – 7	33 – 35	16.1 – 19.3		$1.1 \cdot 10^{-6}$	0.15	0.35	2.5	(Rinaldi et al., 2004)
0 – 10	24 – 34	18 – 19.5		10^{-5} - 10^{-2}				(Salciarini et al., 2006)
0	35	19		$8 \cdot 10^{-6}$	0.28	0.45		(Tofani et al., 2006)
Gravel								
		16 – 24.9		$1.5 \cdot 10^{-7}$ - $3.5 \cdot 10^{-5}$			10	(Cascini et al., 2006)
29.5	14.7	18.82				0.35		(Crescenti et al., 2000)
2 - 3	34 – 45	17 – 19	$2 \cdot 10^{-4}$	$5 \cdot 10^{-5}$ - $2 \cdot 10^{-4}$				(Crosta and Frattini, 2003)
20 – 50	34 – 36	22						(Luzi and Pergalani, 1996)
15	30		$4.0 \cdot 10^{-4}$	10^{-4}	0.10	0.45	5	(Raia et al., 2014)

Table 11. Overview of soil physical parameters values required: c, cohesion; φ, angle of internal friction; γ_s, unit weight of soil; D_0, hydraulic diffusivity; K_s, saturated hydraulic conductivity; θ_r, residual water content; θ_s, saturated water content; α, inverse height of capillary fringe

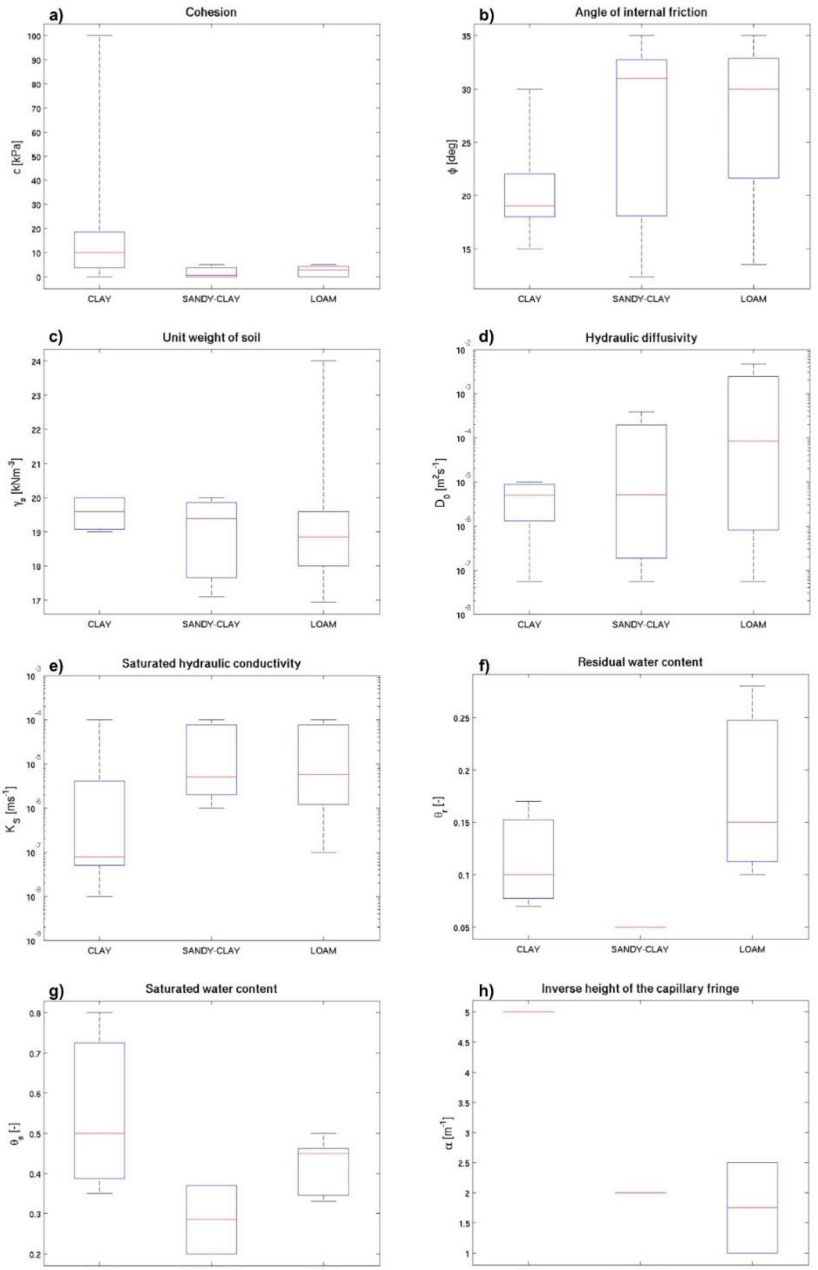

Figure 44 Box plot charts of cohesion (a), angle of internal friction (b), unit weight of soil (c), hydraulic diffusivity (d), saturated hydraulic conductivity (e), residual water content (f), saturated water content (g), inverse height of capillary fringe (h) per each soil texture class. Lower extreme, lower quartile, median (red line), upper quartile and upper extreme values are shown.

The box plots in Figure 44 highlight the trend and the variability of the physical property values selected from the literature review. The wider are the segments (“whiskers”), the higher is the data variability. The parameters with the maximum spread are the angle of internal friction, the hydraulic diffusivity, and the saturated hydraulic conductivity. Furthermore, the cohesion of clay, the soil unit weight of loam, the residual water content of loam, and the saturated water content of clay displays a large variability too. On the contrary, when simply the median is represented it means that only one value or more values with the same measure were collected.
The only value of alpha parameter in clay material found in the literature research, is anomalously high ($\alpha = 5$) for the texture considered, and resulted in non-convergence of the Fourier series’ solutions when tested. For this reason, the next tests are executed using a generic value of $\alpha = 1$ (Table 12). The gravel texture class was not considered in Figure 44 and further, because only three landslides were triggered within it and few data were available, compared with the other soils.

The storms chosen as input for the calibration are: October 7th – 10th 1996 (October 1996) that triggered 7 landslides and November 30th – December 5th 1998 (November 1998) that triggered 18 landslides. The rain gauges considered were Jesi and Montecarotto (Figure 45). In fact, these storms were representative of two different intensity - duration events; the first one was shorter (72 h) than the second (120 h), but more intense (16.4 mm/h vs 9.4 mm/h). On the other hand, the total rainfall was similar and equal to 105.8 mm in the 1996 occurrence and 138.2 mm in the 1998 one.

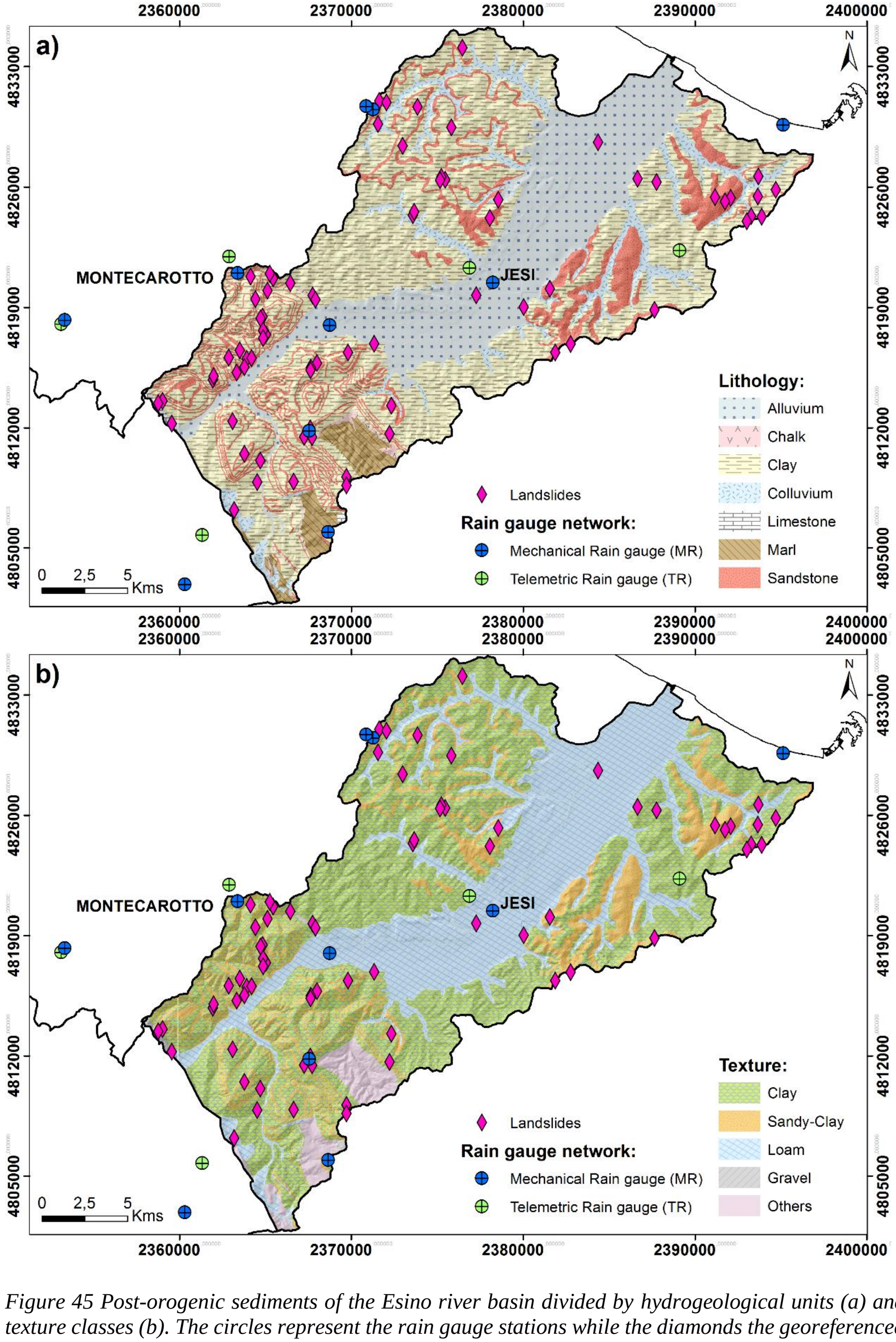

Figure 45 Post-orogenic sediments of the Esino river basin divided by hydrogeological units (a) and texture classes (b). The circles represent the rain gauge stations while the diamonds the georeferenced landslides

The calibration aimed at the selection of the physical parameters that yielded the best results of the model runs. Particularly, the choice referred to results of parameterization on:

- clayey soil landslides, with slope equal to the value of the 95th percentile of the slopes that were recorded on clayey landslides, initial depth of the water table equal to 0.5 m, cohesion equal to the first quartile of the related data collected from the literature, friction angle equal to the minimum value found, inverse of capillary fringe height equal to 1 and median values for the other mechanical and hydrogeological properties (e.g. sat. hyd. conductivity) (Table 12);
- sandy-clayey soil landslides, with slope equal to the value of the 95th percentile of the slopes that were recorded on sandy-clayey landslides, initial depth of the water table equal to 1 m, cohesion equal to the first quartile of the related data collected from the literature, third quartile for the diffusivity and median values for the other mechanical and hydrogeological properties (Table 12);
- loamy soil landslides, with slope equal to the value of the 95th percentile of the slopes that were recorded on loamy landslides, initial depth of the water table equal to 1 m, cohesion and friction angle equal to the first quartile of the related data collected from the literature and median values for the other mechanical and hydrogeological properties (Table 12).

Figure 46 and Figure 47 shows the comparison of TRIGRS's output, run with the input values in Table 12 while changing the saturated hydraulic properties (K_s-D_0-d).
In these figures, each column represents the trend of pressure head at 1 m of depth, for a specific soil texture, throughout the storm. The upper graphs (from (a) to (f)) illustrate the differences in pressure head response when the saturated hydraulic conductivity equals the first quartile, the median, or the third quartile of the values collected, respectively. In the third and fourth rows of charts (from (g) to (l)), the pressure head was computed for a changing saturated hydraulic diffusivity (first quartile, median and third quartile). The fifth and sixth rows of graphs (from (m) to (r)) show the differences in pressure head when the initial depth of the water table is 1 m, 0.5 m or 0 m. The first, third and fifth rows are the output of the infiltration model for saturated conditions and an infinitely deep basal boundary (SAT-INF). The second, fourth and sixth rows show the pressure head variations of the infiltration model for unsaturated soils and impermeable basal boundary at a finite depth of 1 m (UNS-FIN). The red lines in the plots represent the

minimum pressure head for landslide initiation (F_S = 1) computed with the property values indicated in Table 12. Cumulative and hourly rainfall for both the October 1996 (Figure 46) and the November 1998 (Figure 47) storms are plotted in the bottom graphs (from (s) to (u)).

No.	**Slope (°)**	**Depth (m)**	**c (kPa)**	**φ (deg)**	**γ_s (kN m^{-3})**	**D_0 (m^2 s^{-1})**	**K_s (m s^{-1})**	**θ_r (-)**	**θ_s (-)**	**α (m^{-1})**
1	21.4 (95th perc.)	0.5	4 (q1)	15 (min)	19.6 (med)	$5.00\cdot10^{-6}$ (med)	$7.75\cdot10^{-8}$ (med)	0.10 (med)	0.50 (med)	1
2	28.2 (95th perc.)	1	0 (q1)	31 (med)	19.4 (med)	$1.03\cdot10^{-4}$ (q3)	$5.05\cdot10^{-6}$ (med)	0.05 (med)	0.29 (med)	2 (med)
3	12.7 (95th perc.)	1	0 (q1)	23.25 (q1)	18.9 (med)	$8.33\cdot10^{-5}$ (med)	$5.63\cdot10^{-6}$ (med)	0.15 (med)	0.45 (med)	1.8 (med)

Table 12. Soil types and properties used as settings for the tests in clay (1), sandy-clay (2) and loam (3) texture classes

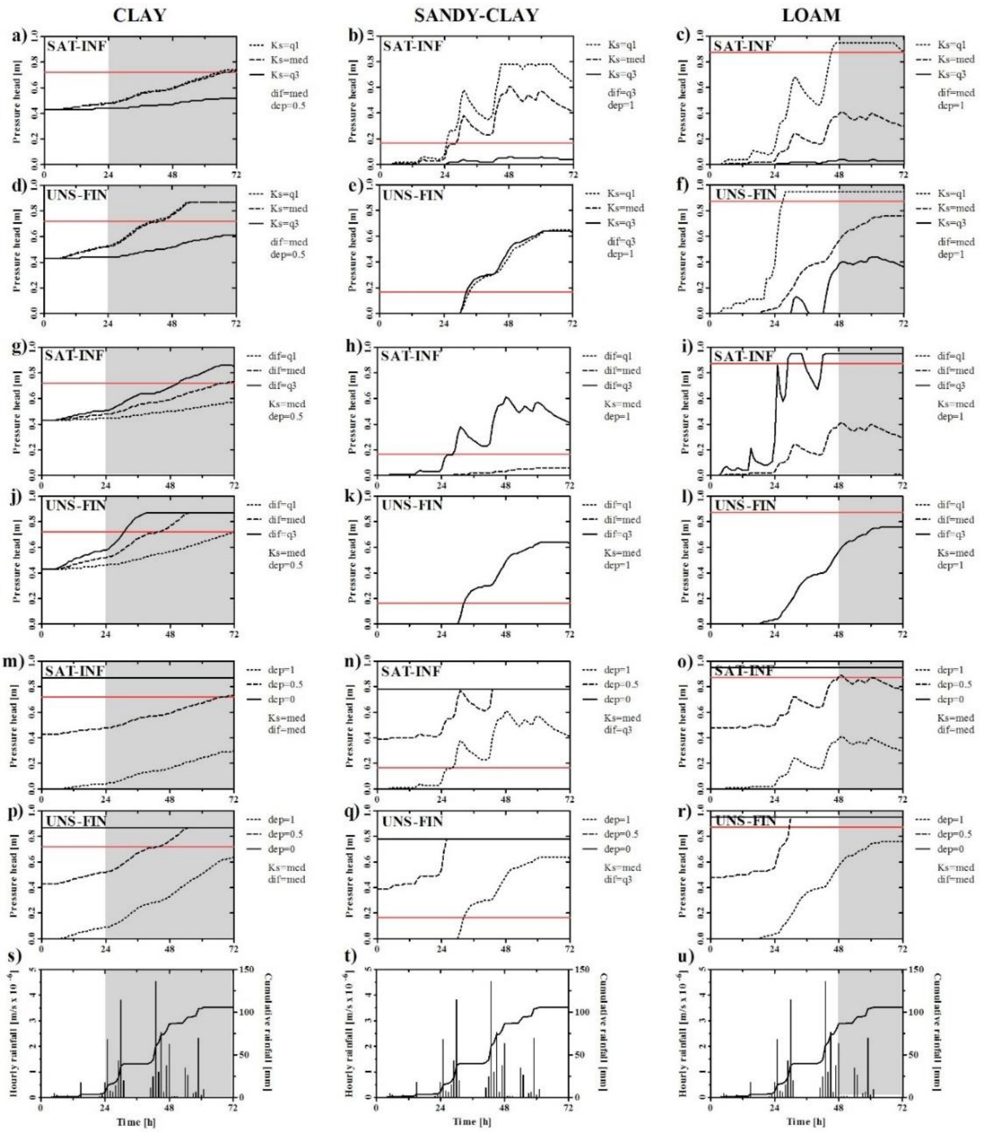

Figure 46 TRIGRS outputs for K_S-D_0-d variation tests. Graphs (a), (d), (g), (j), (m), (p) show the pressure head responses in clayey soils, graphs (b), (e), (h), (k), (n), (q) show the pressure head responses in sandy-clayey soils, and graphs (c), (f), (i), (l), (o), (r) show the pressure head responses in loamy soils during the October 1996 storm ((s), (t), (u)). The red lines indicate the threshold pressure head for landslide initiation ($F_S \leq 1$). Highlighted is the period of landslide activity

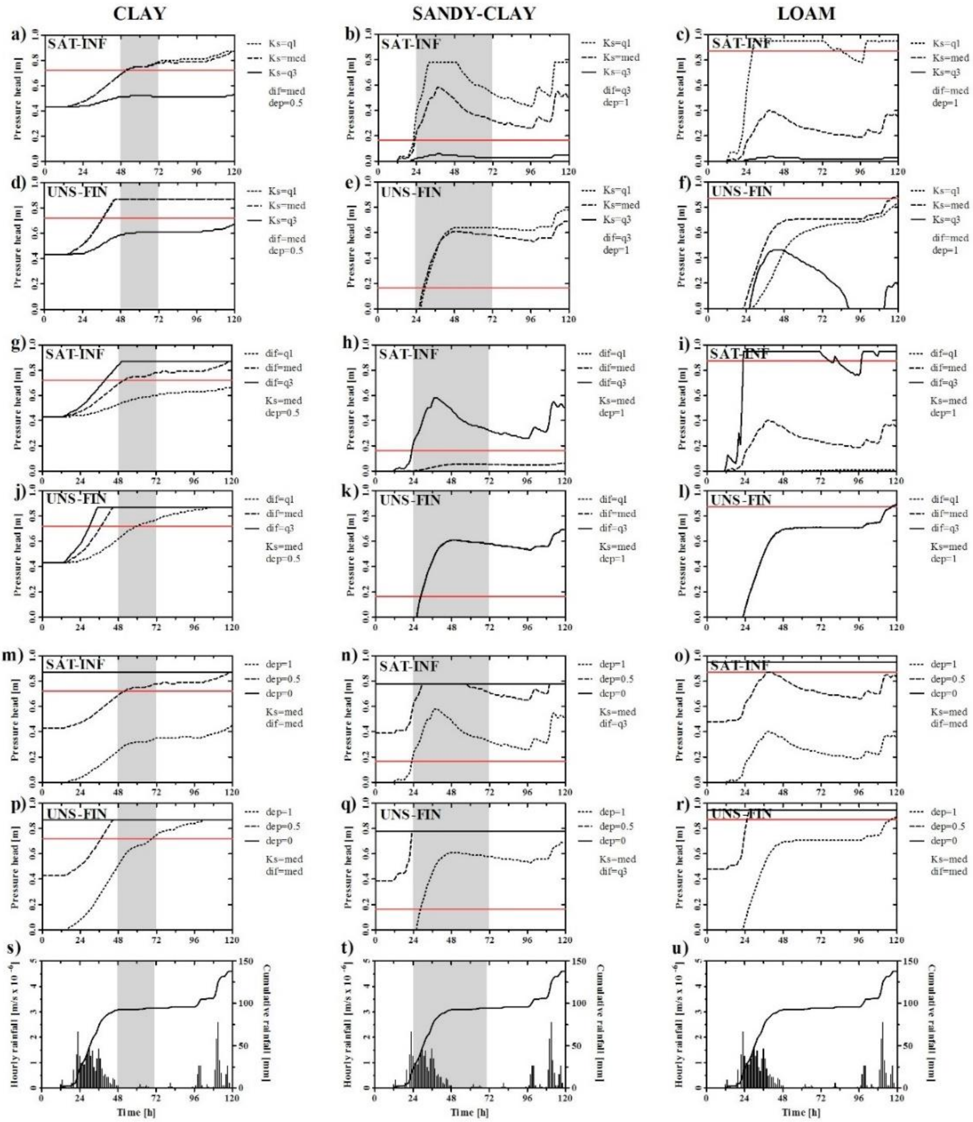

Figure 47 TRIGRS outputs for KS-D0-d variation tests. Graphs (a), (d), (g), (j), (m), (p) show the pressure head responses in clayey soils, graphs (b), (e), (h), (k), (n), (q) show the pressure head responses in sandy-clayey soils, and graphs (c), (f), (i), (l), (o), (r) show the pressure head responses in loamy soils during the November 1998 storm ((s), (t), (u)). The red lines indicate the threshold pressure head for landslide initiation ($F_S \leq 1$). Highlighted is the period of landslide activity

In general, pressure head increases in response to rainfall and peaks at values sometimes considerably minor than the expected ones. The initial pressure head response of the finite depth models is always less sudden than response of the infinite depth models. Among the three texture classes, for hydraulic conductivity and diffusivity that vary over the ranges defined in Table 13, and for both the storms, the pressure head increase is the smallest in clay, larger in sandy-clay and largest in loam. For SAT-INF conditions in sandy-clay and loam, the pressure head drops rapidly when the rainfall stops and even when the rainfall intensity decreases to less than 5 x 10^{-7} m/s. In fact, in this last case, the conductivity is up to 10000 times higher than the rainfall flux. For UNS-FIN conditions, the pressure head declines gradually following long periods of no rainfall. This is evident for the November 1998 storm, where the UNS-FIN pressure head decreases only during a period of drier conditions with 4.6 mm of rainfall distributed in 51 hours. Also, the reduction occurs about 12 h after the SAT-INF settings. In the clay texture class, the pressure head never decreases, even during the November 1998 maximum duration of low-to-null rainfall considered in these models.

Parameters	**Clay**			**Sandy-clay**			**Loam**		
K_S [m/s]	$5.16\cdot 10^{-8}$ (q1)	$7.75\cdot 10^{-8}$ (med)	$3.06\cdot 10^{-6}$ (q3)	$3.03\cdot 10^{-6}$ (q1)	$5.05\cdot 10^{-6}$ (med)	$5.25\cdot 10^{-5}$ (q3)	$1.25\cdot 10^{-6}$ (q1)	$5.63\cdot 10^{-6}$ (med)	$6.25\cdot 10^{-5}$ (q3)
D_0 [m²/s]	$2.53\cdot 10^{-6}$ (q1)	$5.00\cdot 10^{-6}$ (med)	$7.50\cdot 10^{-6}$ (q3)	$2.48\cdot 10^{-7}$ (q1)	$5.16\cdot 10^{-6}$ (med)	$1.03\cdot 10^{-4}$ (q3)	$1.20\cdot 10^{-6}$ (q1)	$8.33\cdot 10^{-5}$ (med)	$1.30\cdot 10^{-3}$ (q3)
d [m]	1	0.5	0	1	0.5	0	1	0.5	0

Table 13. Values of saturated hydraulic properties varied in the model runs

Moreover, changes in the saturated hydraulic diffusivity do not cause dissimilar variation of pressure head in the UNS-FIN computations, except in the clayey soils.

Furthermore, in every texture class the pressure head increases more in lower conductivity and higher diffusivity conditions. That said, it is important to highlight that a factor of 100 difference in saturated hydraulic conductivity for clay soils has smaller effect on pressure head (0.2 m of fluctuation) than a factor of 10 difference in sandy-clay or loamy soils (0.8 m up to 1 m of fluctuation) (Table 13). On the contrary, a factor of 1000 difference in the

sandy-clay and loam saturated hydraulic diffusivity increased the pressure head of 0.6 m and almost 1m respectively, but a maximum factor of 3 difference in clay (between the lowest and highest values of diffusivity) resulted in changing the pressure head up to 0.3 m.
In addition, the pressure head changes its values but not its trends when the initial depth of the water table is modified from 1 m to 0.5 m or vice versa. On the other hand, the pressure head is steady over time, when the initial depth of the water table is equal to 0 m (ground surface).
Finally, the two case studies show different pressure head responses due to the rainfall conditions. The October 1996 storm presented several periods of short duration (less than 20 h) with high intensity rainfall (maximum of 16.4 mm/h) and a shorter total duration (72 h) than the November 1998 storm (120 h). This last event displayed a rather long duration with low intensity rainfall at the beginning (almost 40 h) followed by an equally long dry period and in the end moderate intensity rainfall (maximum of 9.4 mm/h). At the beginning, during the first period of continuous rainfall, the pressure head in every plot of the October 1996 storm increases less sharply than in the November 1998 and reaches values consistently inferior (about 0.2 m lower) to those of the other storm, also because the duration is less than half of the November 1998 storm. Although drainage occurs during the dry periods, pressure head does not fall back to its initial value. After the long dry period of the 1998 storm, the pressure head of the sandy-clayey and loamy soils decreases, especially within infinite depth simulations, enough to almost match the 1996 values, so that after the last rainfall period they have comparable values. On the other hand, as previously mentioned, the pressure head of the clayey soil does not decrease so that in the end in the 1998 storm it is generally higher than in the 1996 one.
Landslide response of the storms also differs. During the 1996 storm, 3 landslides were related to the rain gauge of Jesi, 2 in clay and 1 in loam (Figure 46); during the 1998 event 6 landslides were associated to the rain gauge of Montecarotto, 5 in sandy-clay and 1 in clay (Figure 47). Most of them (7) were triggered the second day of rainfall, generally after the increasing of pressure head above the marked threshold ($F_S \leq 1$).
Figure 48 summarizes the different responses of the soils to the two storms in terms of landslide initiation. Graph shows in the y-axes the pressure head rise as the ratio between the peak and the initial pressure head, while the x-axes represents a measure of the storm rainfall uniformity as the ratio between the average and the peak intensity. The pressure head rise is computed as the maximum change in pressure head with the preferred model inputs (Table 12) from the beginning of the storm until the end of the time-window for landslide

occurrence. The intensity ratio is suggested to characterize the storm rainfall. It tends to one when the rainfall becomes steady. Figure 48 illustrates that during both the rainfall scenarios the clay soil has the lowest pressure head rise, compared to sandy-clay and loam. The chart highlights also that the pressure head total variation is higher, in addition to the delay of about 12 h (Figure 46 and Figure 47), in UNS-FIN conditions compared to SAT-INF settings.

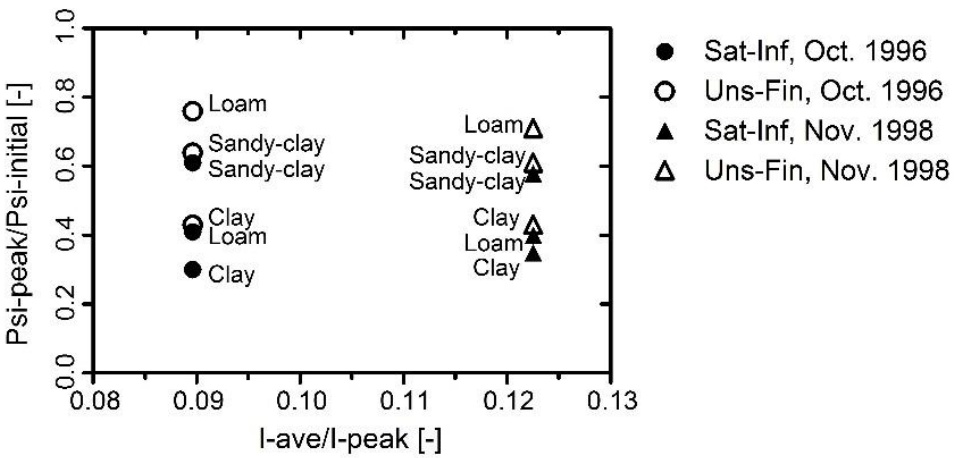

Figure 48 Summary of the soil responses to the October 1996 and November 1998 scenarios (SAT-INF and UNS-FIN).

In the third part of the analysis, the time-varying mean rainfall intensities of every storm has been computed and used as input for the model. Figure 49 shows the example for the October 1996 event in which the total duration has been divided in 5 intervals. The second and the forth periods are characterized by higher intensities, thus greater averages. With this method, it was possible to reduce the number of rainfall intensities in input but still considering their fluctuations.

Moreover, Figure 50 illustrates an example of the AWI trends for the rainfall event of October 1996. All the texture classes reached values greater than or equal to zero (field capacity) during the days of landslides (October 8th-9th). Therefore, the soil was considered saturated in the initial condition of the analysis.

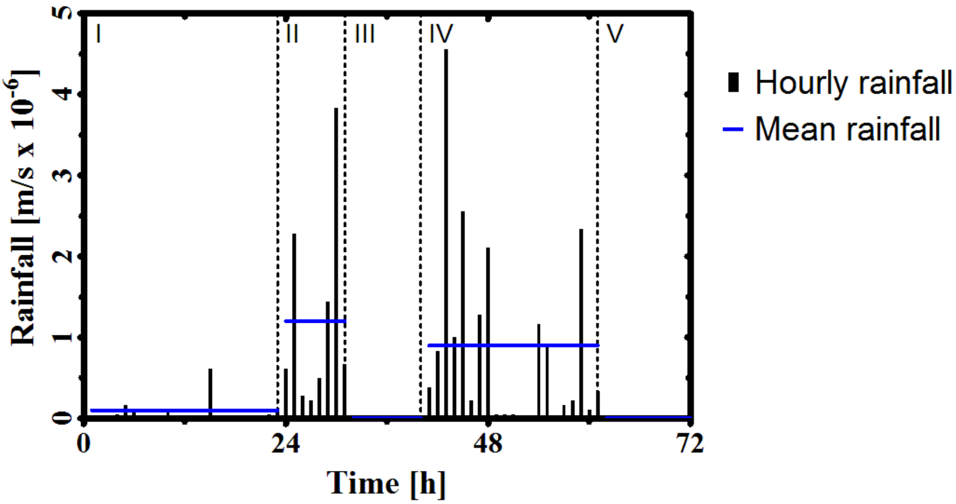

Figure 49 Rainfall intervals identified for the October 1996 event (I to V). Histograms show the hourly rainfall while the horizontal lines represent the mean rainfall of every time step.

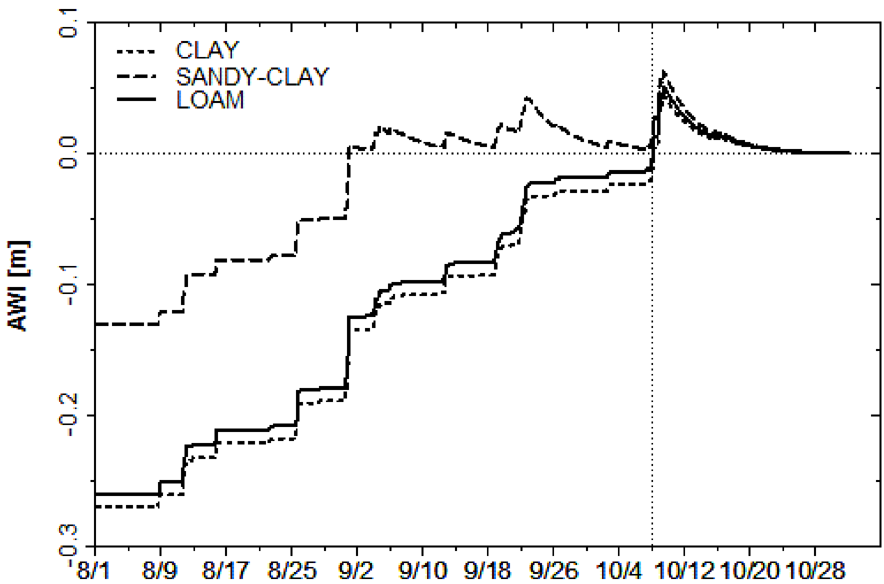

Figure 50 AWI trend for the period August 1st – October 31st 1996.

Additionally, the power law regression used to derive the critical soil thickness of a defined slope is displayed in Figure 51. The R^2 for every texture class is very high. However, for slopes below 9°, the curves reach values of soil thickness too elevated for the study area. Therefore, the maximum value of soil depth is considered as the one resulting at slope=9°.

Figure 52 shows the spatial and the temporal variation of the F_S values during the October 1996 rainfall event. Moreover, the number of cells stable ($F_S \geq 1.3$), unstable ($F_S \leq 1.0$) or with uncertain stability ($F_S = 1.0 – 1.3$) and the trends over time is displayed in Figure 53. As initial conditions, for this simulation saturated settings (equation (13)) with a basal boundary at 1m of depth has been used.

At time 0h, most of the grid cells in the post-orogenic complex are stable (green), very few are unstable (red) and approximately one fourth are in an intermediate state (yellow). Here, the unstable and the uncertain cells are located on the steepest slopes of the area. Moreover, the AWI computation showed that the soil was at the field capacity at the beginning of the October 1996 storm (Figure 50), therefore the terrain was saturated. At the end of the first interval, the red cells increased replacing the green and the yellow ones. The instability was amplified especially in the SW hilly area. At time 32h, the unstable cells increased further and faster throughout the entire study area equaling the uncertain ones. During the following 9h, the rain was over and TRIGRS simulated no variation of the stability conditions. Consequently, the F_S values hold steady. Next, at time 62h, after a long (21h) period of rainfall with lower average intensity, the number of the stable cells again began to decrease while the unstable as well as the uncertain cells started to increase. During the last time step, the rain stopped again until the end of the period considered and so the ratio between the stable, uncertain and stable cells did not vary.

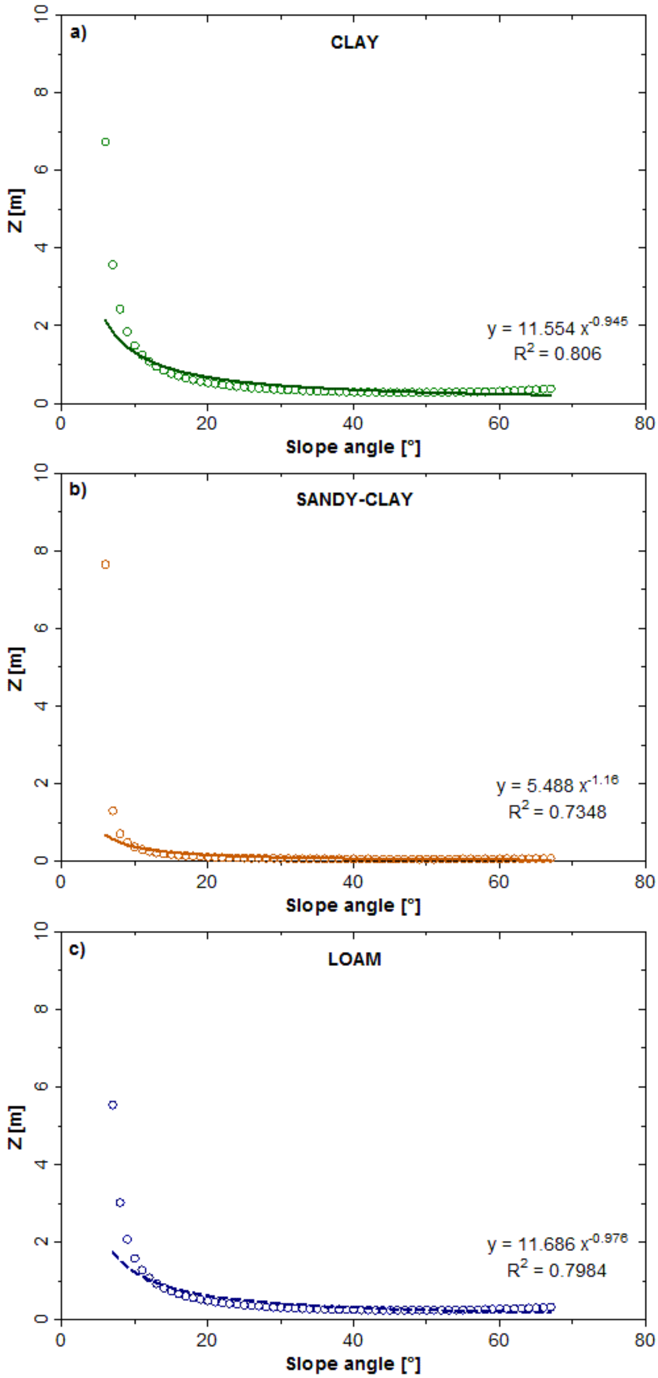

Figure 51 Soil depth profiles per slope angle, computed with the power law regressions, for clay (a), sandy-clay (b) and loam (c)

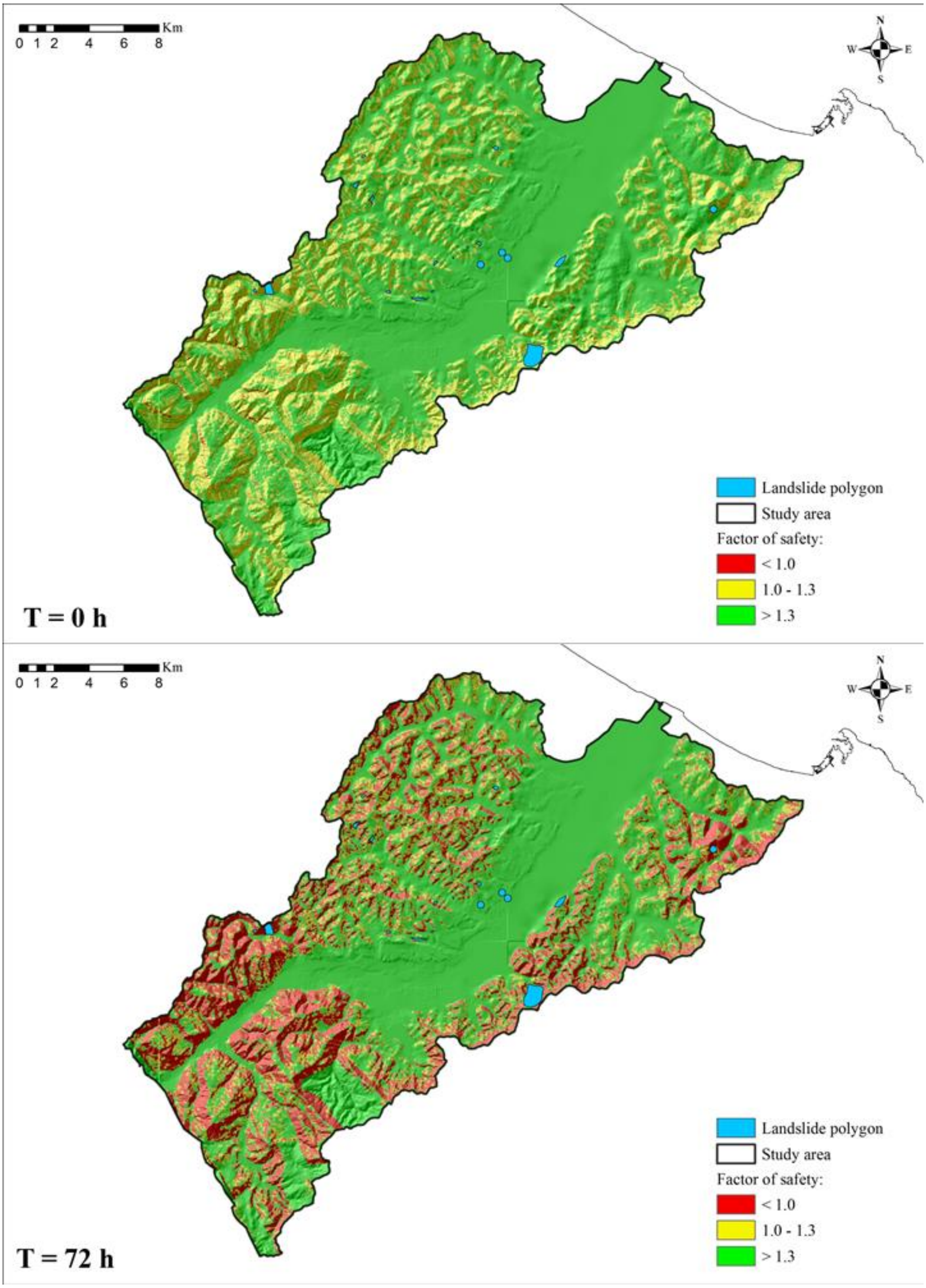

Figure 52 TRIGRS results for the October 1996 event. Figure shows the spatial and temporal distribution of unstable ($F_S \leq 1.0$), uncertain ($F_S = 1.0 – 1.3$), and stable ($F_S \geq 1.3$) cells. The timing (0, 24, 32, 41, 62, 72 h) coincides with the time steps of Fig. 7.

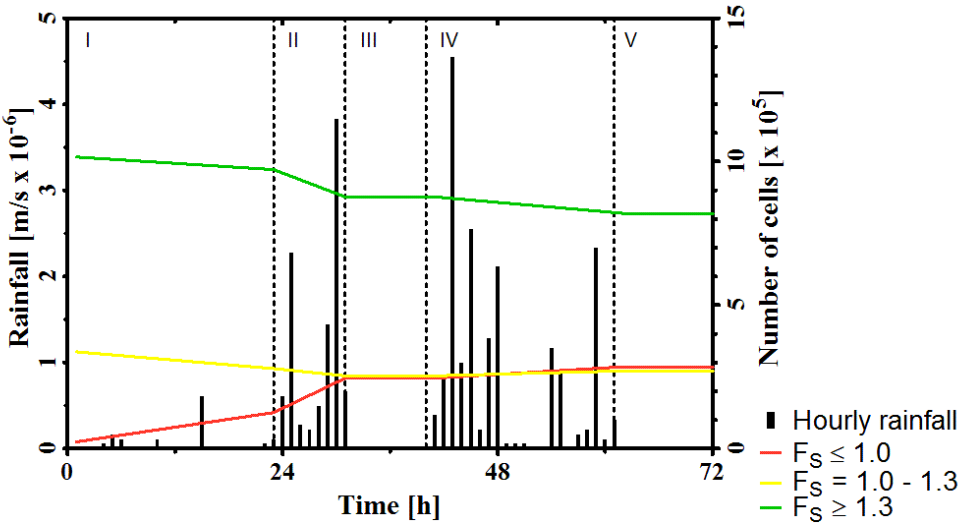

Figure 53 Quantification of TRIGRS results for the October 1996 event. Lines indicate the number of cells unstable ($F_S \leq 1.0$), uncertain (F_S = 1.0 – 1.3), and stable ($F_S \geq 1.3$) over time, compared with the rainfall intervals and intensities

Results of ROC (Figure 54b) shows that the TPR is always greater than the FPR, except for the event of July 1994, which is located in the FPR axis (TPR=0), and for the event of December 2009, which is nearly located in the diagonal (TPR=FPR). Te events with the best output of TRIGRS are October 2005, November 1998, February 2004, and January 2007. In these cases, the TPR is in between 0.4 and 0.5 while the FPR is in between 0.15 and 0.25. Moreover, additional observations can be done with the ROC curves (Figure 54c and Figure 54d). The value in the lower left part of these diagrams, correspond to the analysis of the TRIGRS run when the instability is considered for $F_S \leq 0.8$ and the stability is considered for $F_S > 0.8$. Continuing along the curves, in the following value the unstable points are selected as those with $F_S \leq 0.9$ and the stable points as those with $F_S > 0.9$. And so on. Results of these analyses are all situated above the diagonal, thus TPR > FPR, except for the $F_S \leq 0.8$ in October 1996 that is positioned almost in the origin. The best performance are gained by the $F_S \leq 1.1$-1.3, in which the TPR > 0.5 and the FPR < 0.5.

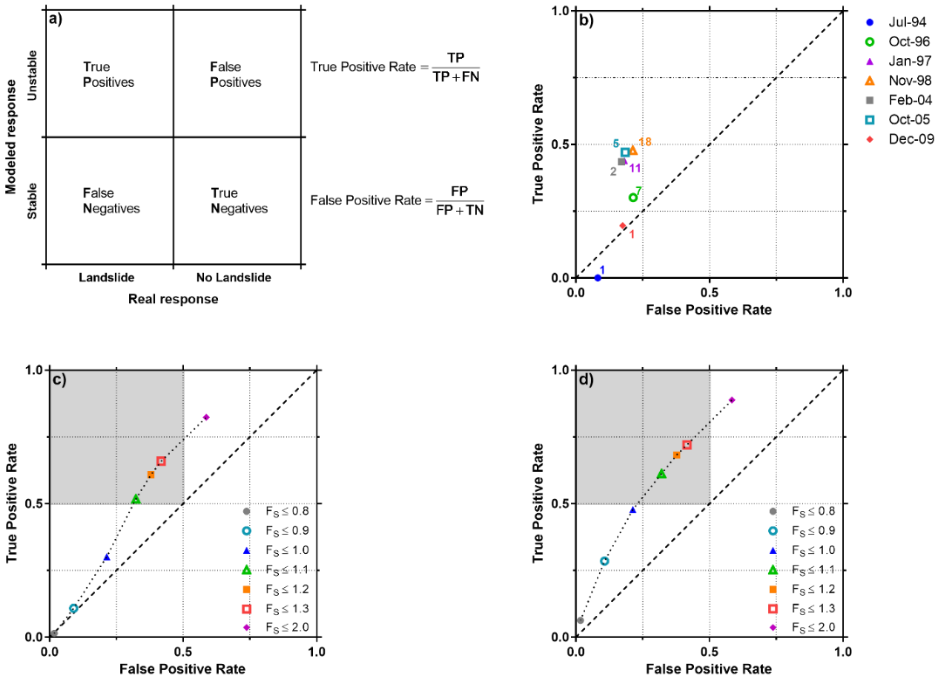

Figure 54 (a) Contingency table (adapted from Fawcett (2006)) for the binary problem of this study and performance metrics calculated from it. (b) ROC analysis for different rainfall scenarios (July 1994, October 1996, January 1997, November 1998, February 2004, October 2005 and December 2009). The labels represent the number of landslides related to each rainfall event. The lower graphs show the ROC curves for the events of October 1996 (c) and November 1998 (d) plotted by varying the range of Fs values considered as TP. The upper left quadrants (highlighted) represent acceptable prediction levels

4.4 Testing the different models: the May 2014 event

This chapter describes the test of the models developed in the previous sections, through the case study of a rainfall event that affected the Esino post-orogenic complex in the period of 2-4 May 2014. First, a description of the event and its effects is provided. Second, the results of the ED, ID, and Bayes (1-D and 2-D) computations are presented. Finally, the outputs of the TRIGRS run, using the features of the May 2014 event, and the ROC chart are shown.

4.4.1 The May 2014 rainfall event and landslide distribution

On 2-4 May 2014, the Marche region has been affected by a particularly severe meteorological event, characterized by widespread rainfalls that occasionally have assumed the character of a strong storm (Centro Funzionale Regionale - CFR, 2014).

The event was preceded by thirty days of approximately 99 mm of average rainfall all over the Region, with higher values in the southern internal portions (Figure 55). This very rainy period led to the saturation of the soil and thus reduced the capacity of water infiltration.

The May 2014 event was characterized by particularly intense rainfall that affected the hilly-coastal portion of the Region on 2 May and intensified from the early hours of 3 May. Figure 56, Figure 57, and Figure 58 show the recorded daily rainfall on 2, 3 and 4 May 2014. The most intense rain have occurred in the first 6 hours of 3 May 2014.

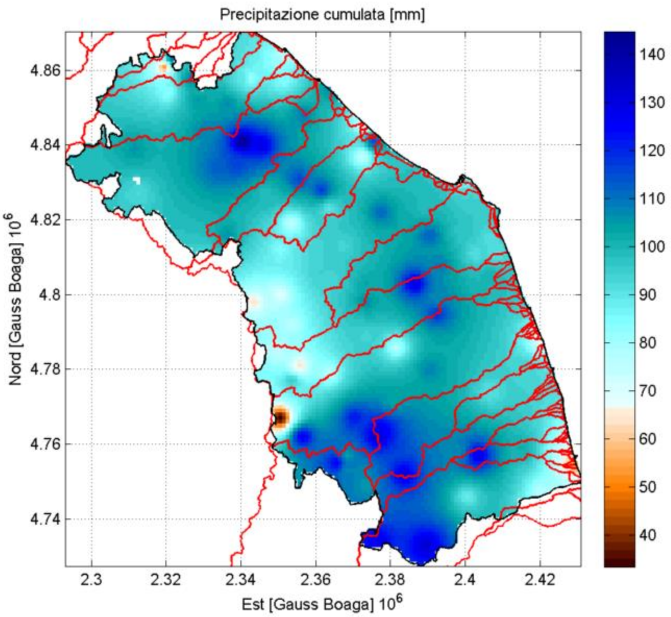

Figure 55 Map of cumulated antecedent rainfall from 2 April to 1 May 2014 throughout the Marche region (Centro Funzionale Regionale - CFR, 2014).

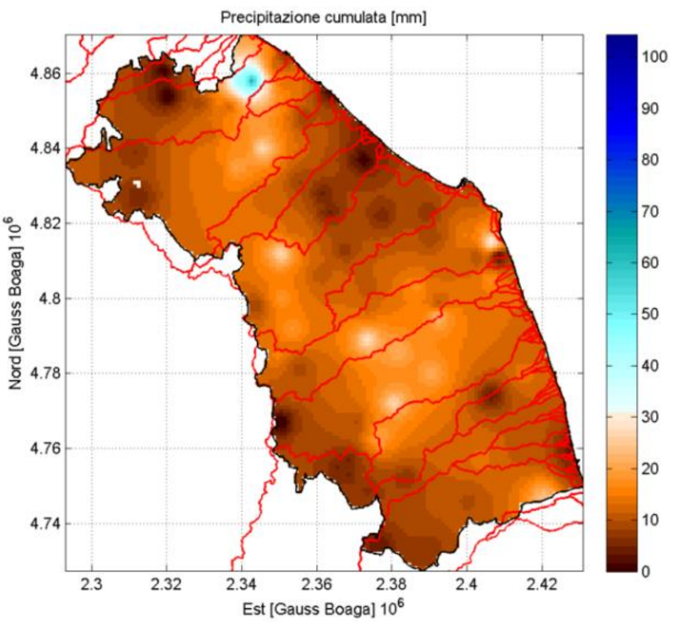

Figure 56 Map of the 2 May 2014 daily rainfall throughout the Marche region (Centro Funzionale Regionale - CFR 2014)

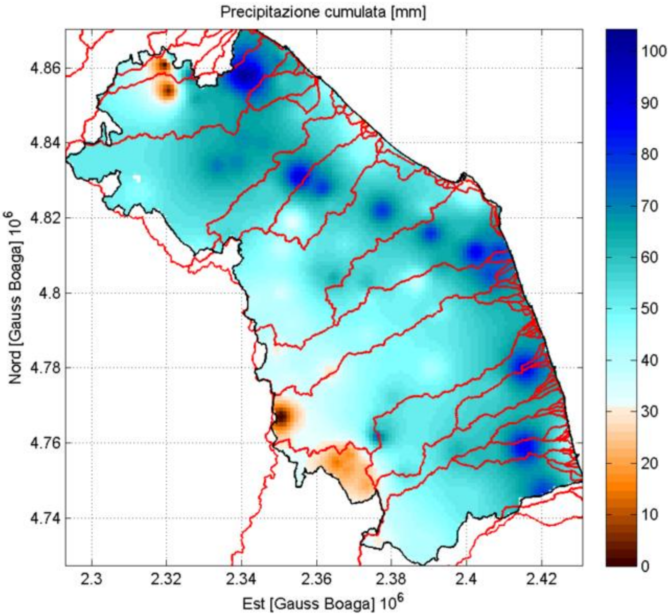

Figure 57 Map of the 3 May 2014 daily rainfall throughout the Marche region (Centro Funzionale Regionale - CFR 2014)

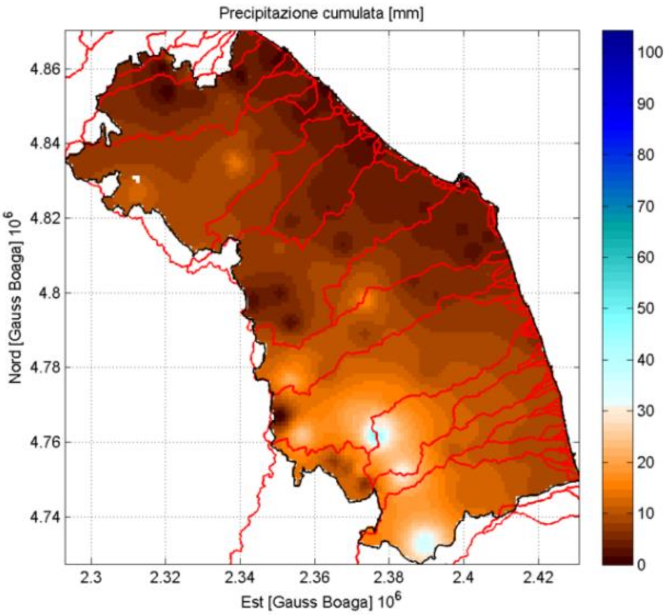

Figure 58 Map of the 4 May 2014 daily rainfall throughout the Marche region (Centro Funzionale Regionale - CFR 2014)

The smaller basins of the Region increased the water levels and subsequently gave rise to the phenomenon of flooding. The main effects were recorded in Senigallia (Ancona province), because of the river Misa flood, and in Chiaravalle (Ancona province), because of the overflowing of the Triponzio, a tributary of the Esino (Figure 59).

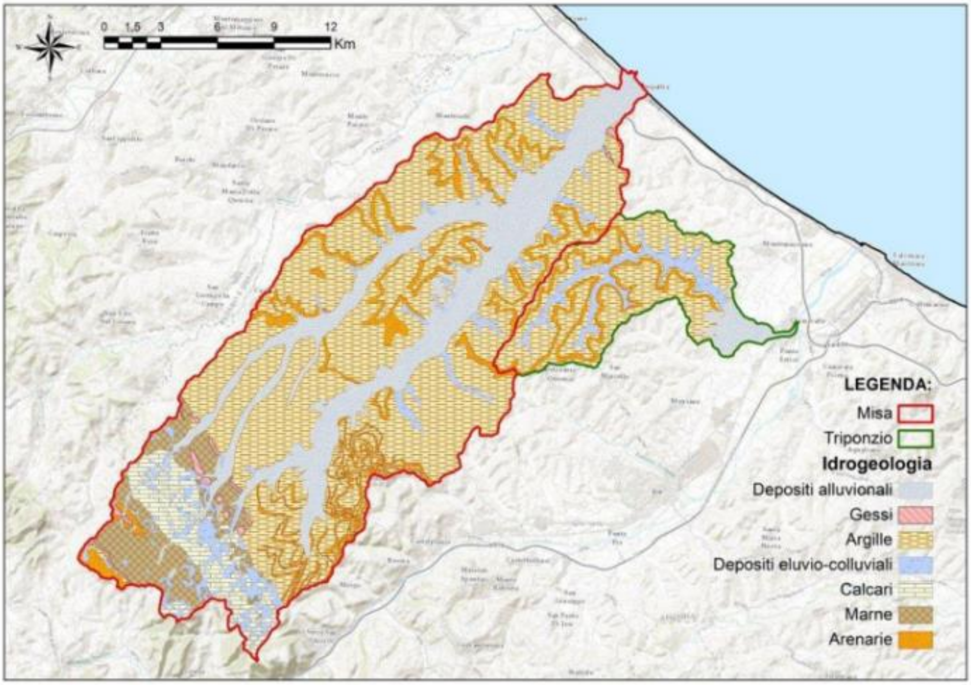

Figure 59 Lithology of the basins of the Misa and Triponzio, characterized by predominantly impermeable formations (Centro Funzionale Regionale - CFR, 2014).

Instability phenomena have been initiated throughout the Region. Numerous landslides have mainly concerned the roads, causing traffic disruption (Figure 60) (Centro Funzionale Regionale - CFR, 2014). The reports received by the CFR shows that the consequences interested particularly the hilly-coastal zone, rather than the inland of the Region. Landslides occurred also in the days following the rainfall event. The most recurrent slope failures have been rock falls, earth flows and debris flows.

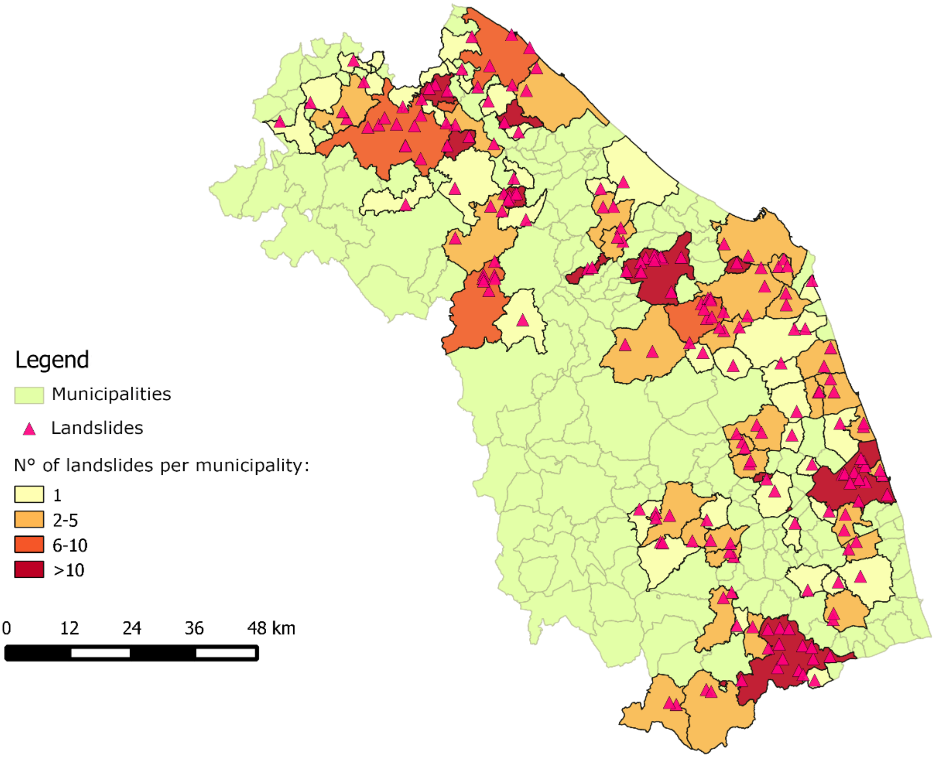

Figure 60 Localization of the reported landslides resulting from the May 2014 rainfall event.

In the study area, a total number of 19 landslides were reported and thus georeferenced in GIS (Figure 61). All of these failures occurred on May 3 within the province of Ancona: 12 phenomena in the municipality of Jesi, 3 in Belvedere Ostrense, 2 in Poggio San Marcello, 1 in Ancona and in Monte San Vito.
The 19 landslides documented were associated to 3 rain gauges available in the study area (Figure 61): Agugliano (Ag [1220]) linked to 2 failures, Jesi (Je [1213]) linked to 15 failures, and Cupramontana (Cu [1263]) linked to 2 failures.

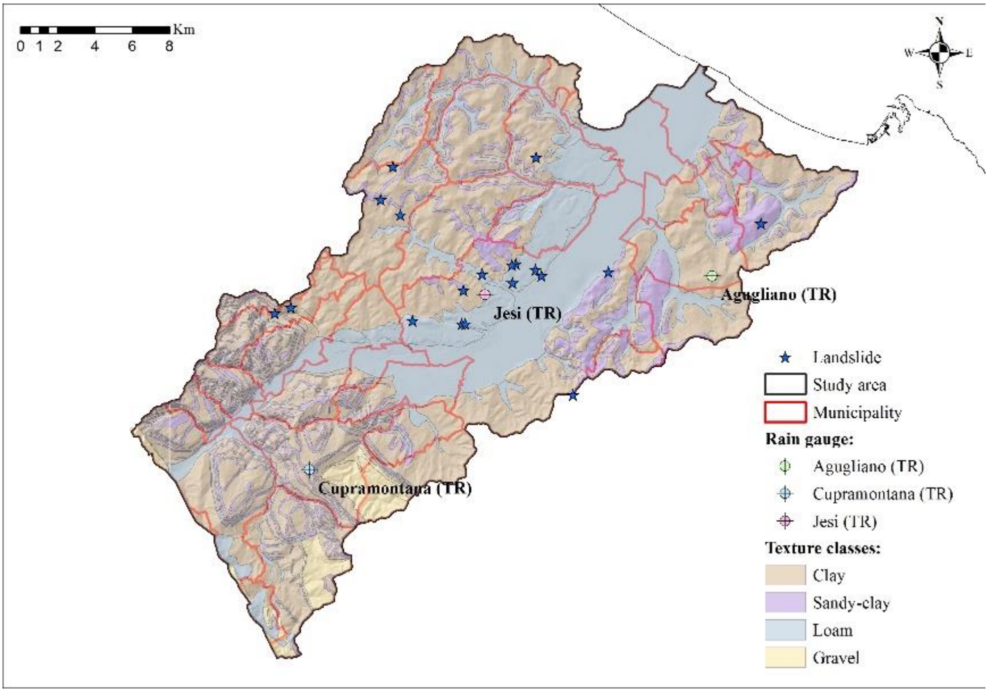

Figure 61 Landslides triggered in the study area during the 2-4 May 2014 rainfall event

4.4.2 Application of the empirical models

The analysis of the event of 2-4 May 2014, for the application of the empirical models developed in Chapter 4.2, resulted in the computation of some rainfall parameters (Table 14): (i) the cumulative event rainfall, (ii) the duration, (iii) the maximum intensity, and (iv) the mean intensity.

Figure 62 shows the logarithmic graph of the values of cumulated event rainfall (E) and duration (D) registered during the event of May 2014 in the rain gauges of Agugliano, Jesi, and Cupramontana. Je [1213] recorded the maximum value of event rainfall (88.4 mm), followed by Cu [1263] with 60.2 mm, and Ag [1220] with 59.8 mm (Table 14). The amount of rainy hours was 43 h for Je [1213], 38 h for Ag [1220], and 35 h for Cu [1263] (Table 14). Landslides related to the event of 2-4 May 2014 are displayed with red crosses.

	Ag [1220]	Cu [1263]	Je [1213]
Event rainfall (mm)	59,8	60,2	88,4
Duration (h)	38	35	43
Maximum intensity (mm/h)	10,6	10,6	25,4
Mean intensity (mm/h)	1,57	1,72	2,06
Landslides	2	2	15

Table 14 Values of cumulative event rainfall, duration, maximum intensity, and mean intensity registered in the rain gauges of Agugliano, Cupramontana, and Jesi during the event of May 2014. Moreover, the number of landslides related to each gauge is shown.

A comparison with the ED distribution related to the historical database of landslides, displays consistence with the minor (Agugliano and Cupramontana) and the main (Jesi) events, which are defined as the rainfall events that triggered respectively 2 and more than 10 failures.

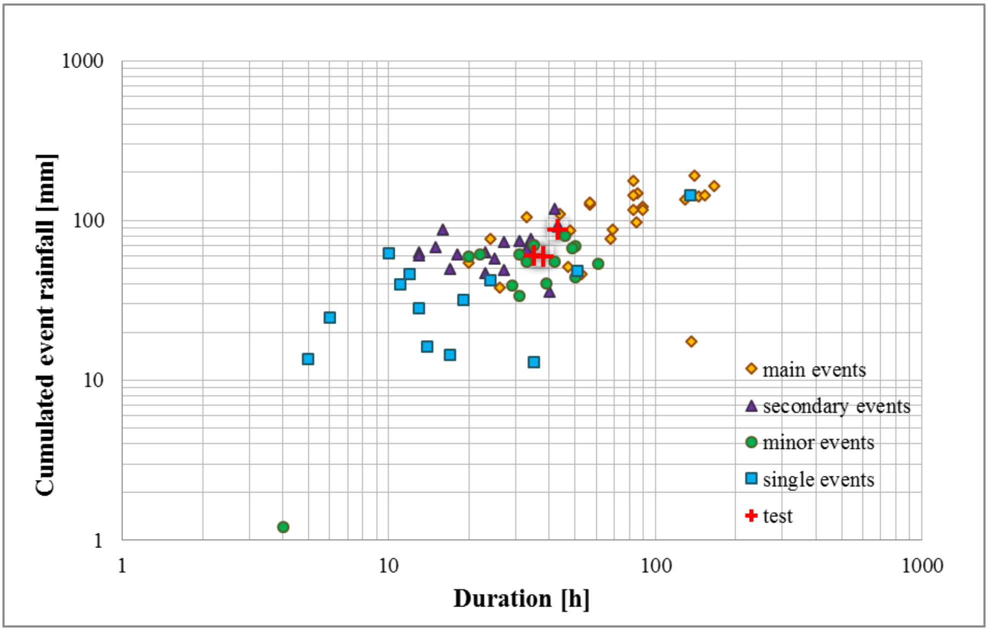

Figure 62 ED graph. Comparison between the values of historical landslides and the test of May 2014.

In the Esino post-orogenic complex, the maximum hourly intensities, all registered on May 3, were particularly high. The Agugliano station recorded a maximum intensity of 10.6mm/h at 2am, Jesi observed 25.4 mm/h at 3am, and Cupramontana registered 10.6 mm/h at 3am (Table 14). Figure 63 illustrates that these values are in line with the historical database. Particularly, records of Agugliano and Cupramontana are similar to those of the minor events, while the Jesi intensity is higher than usual but still in the cloud of data.

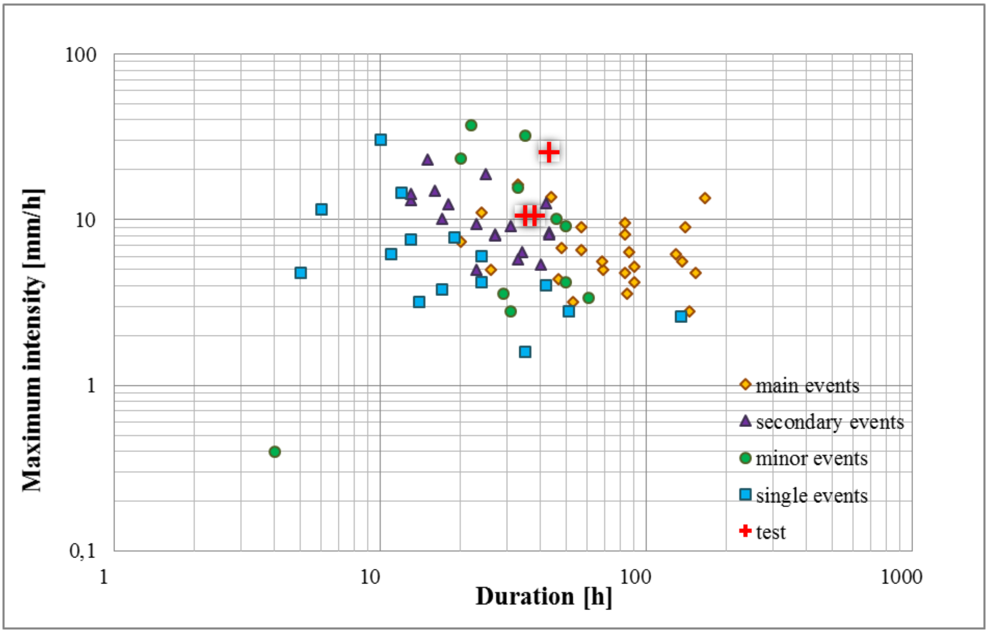

Figure 63 $I_{max}D$ graph. Comparison between the values of historical landslides and the test of May 2014

The graph in Figure 64 represents the average intensities and durations logged by the rain gauges considered for the event of May 2014, in relation with the threshold tested for the study area (equation (12))(Gioia et al., 2015a). All the data are located above the threshold and are comparable with main, secondary, and minor events. In fact, the Jesi station is the one with the highest mean intensity (2.06 mm/h) and is similar to the values of main and secondary events. Agugliano and Cupramontana registered respectively 1.57 mm/h and 1.72 mm/h, which are precipitation rates in between the secondary and the minor events.

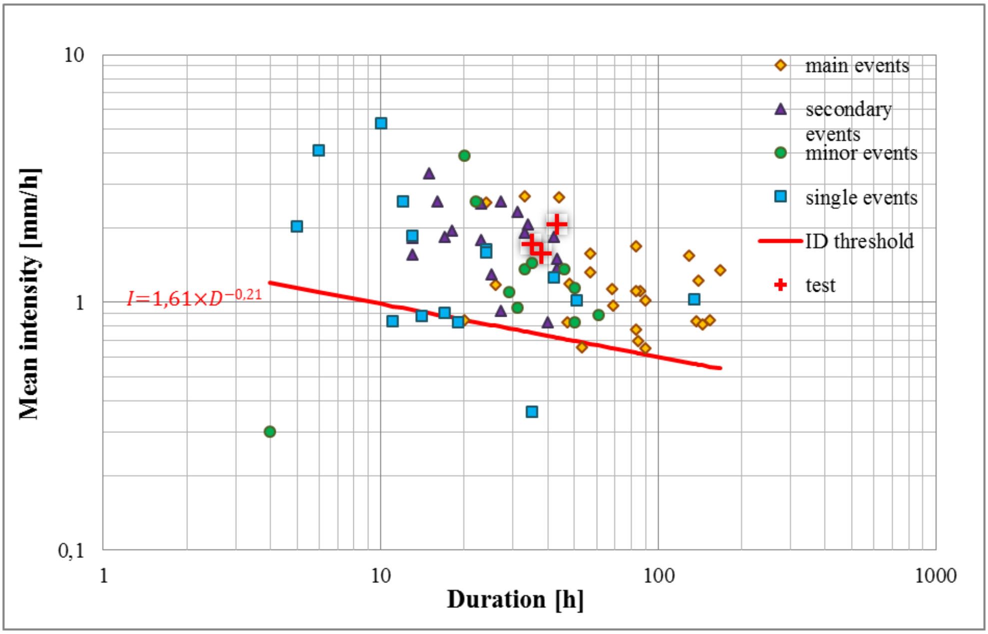

Figure 64 ID graph. Comparison between the values of historical landslides, the threshold and the test of May 2014.

Figure 65 shows the position of the ID values of the test, compared to the percentile curves developed in Chapter 4.2.2.2. According to the graph, the green and the yellow lines correspondingly cross the rainfall ID patterns of Agugliano and Cupramontana rain gauges. This means that their values match the 60th and 70th percentiles, which refers to 60% and 70% probability of landslide occurrence. Furthermore, the ID of Jesi match the orange line that is the 80% probability of landslide initiation.

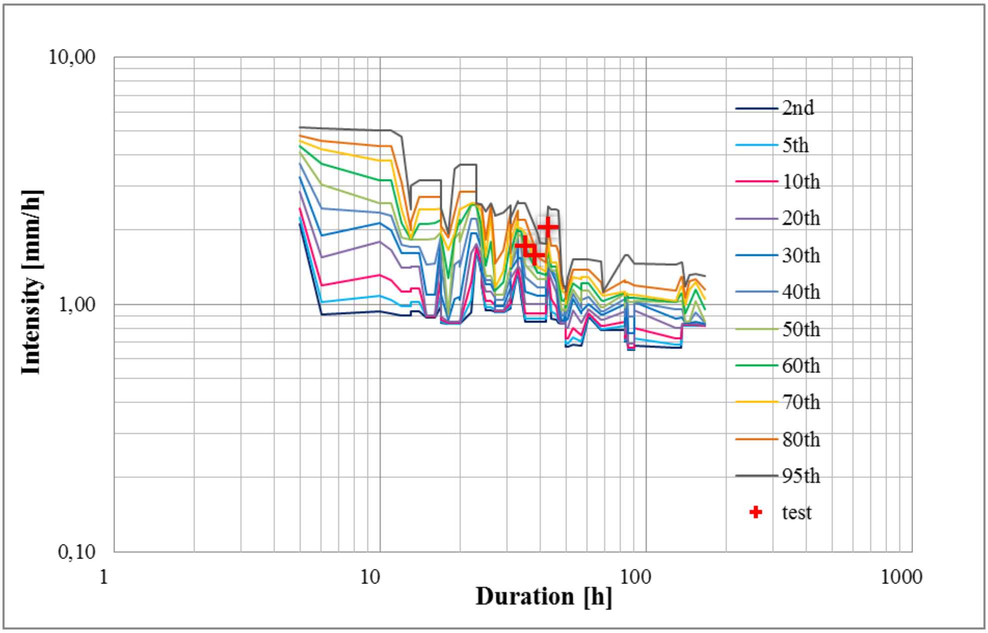

Figure 65 ID probability graph. Comparison between the percentiles based on historical landslides and the values of the May 2014 event.

Additionally, other rainfall parameters were computed for the Bayesian probabilistic test of the May 2014 event (Table 15): (i) the cumulative event rainfall, (ii) the daily rainfall of May 3, (iii) the antecedent rainfall (A_5, A_7, A_{15}, and A_{30}). Every value computed for the entire study area, through an interpolation of the rain gauges data, was compared to the probability intervals illustrated in Chapter 4.2.3.2 and 4.2.3.3. The results are displayed in Table 15.

For the Bayesian monodimensional approach, the conditional probability of activating at least a landslide (P(A|B)) is:

- 41,2% for E = 71.2 mm, which correspond to a medium probability (Table 6);
- 66,7% for R = 61.9 mm, which correspond to a high probability;
- 4,5% for A_5 = 40,5 mm, which correspond to a low probability;
- 7,4% for A_7 = 60,6 mm, which correspond to a low probability;
- 3,5% for A_{15} = 76,5 mm, which correspond to a low probability;
- 2,2% for A_{30} = 108,2 mm, which correspond to a low probability.

For the bidimensional method, the coupled values of R = 61,9 mm and A_5 = 40,5 mm corresponds to a category, in Table 8, which never resulted in the past years. However, to allow a comparison, the 5-days antecedent rainfall is rounded up to 40 mm. The subsequent combination is included in a class with probability P(A|B,C) = 100%.

1-D	Value [mm]	P(A|B)
E	71,2	0,411765
R	61,9	0,666667
A_5	40,5	0,044968
A_7	60,6	0,074074
A_{15}	76,5	0,035132
A_{30}	108,2	0,02157
2-D	**Value [mm]**	**P(A|B,C)**
R	61,9	NA
A_5	40,5	

Table 15 Values of cumulative event rainfall, daily rainfall, and antecedent rainfall registered in the study area during the event of May 2014, and results of Bayesian monodimensional and bidimensional probability

4.4.3 Application of TRIGRS

The TRIGRS program was applied to the May 2014 event to test the feasibility of the model as landslide predictor within the study area.

Figure 66 shows the landslide polygons used for the analysis. Given the location of the slope failures, Jesi [1213] was chosen as reference rain gauge. The rainfall periods selected as inputs of precipitation are shown in Figure 67. The values of the mean intensities are $6.02 \cdot 10^{-08}$ m/s for the interval I, $2.71 \cdot 10^{-06}$ m/s for the interval II, $3.27 \cdot 10^{-07}$ m/s for the interval III, $8.59 \cdot 10^{-08}$ m/s for the interval IV, and 0.00 m/s for the interval V.
The computation of the Antecedent Water Index resulted in the choice of saturated initial conditions. In fact, the sandy-clay texture class reached the field capacity several days before the event and on May 3 the average AWI was 0.05 (Figure 68). The clay and loam texture classes showed similar trends with average AWI on May 3 slightly lower the field capacity (-0.06 in clay and -0.05 in loam) (Figure 68). In all the cases, a significant peak was registered on the days of the landslides.

The values of safety factor (F_S), resulting from the TRIGRS runs, were imported in a GIS environment. The initial conditions, presented in Figure 69, correspond to the 0am of 2 May in which the saturated soil caused widespread cells with “uncertain” stability (F_S = 1.0 – 1.3). Only a little percentage of points with $F_S \leq 1.0$ are located in the steepest slopes. The final conditions, displayed in Figure 70, shows the spatial distribution of the safety factor at the 12pm of 4 May. At this point, a large part of the yellow and green cells in Figure 69 has turned into reds ($F_S \geq 1.3$), affecting also more gentler slopes.

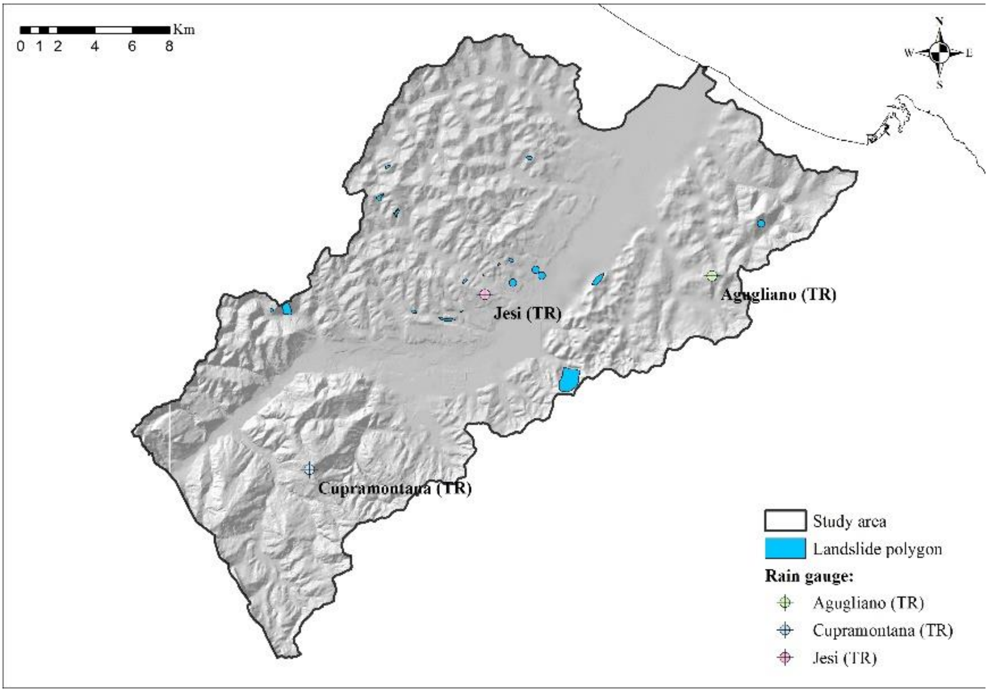

Figure 66 Landslides polygons of the May 2014 event

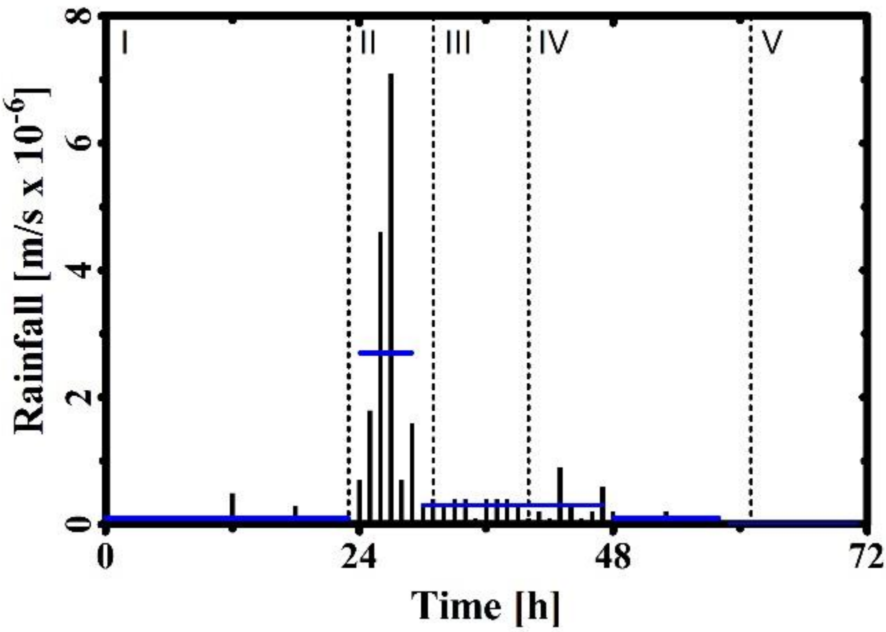

Figure 67 Rainfall intervals identified for the May 2014 event (I to V). Histograms show the hourly rainfall while the horizontal lines represent the mean rainfall of every time step

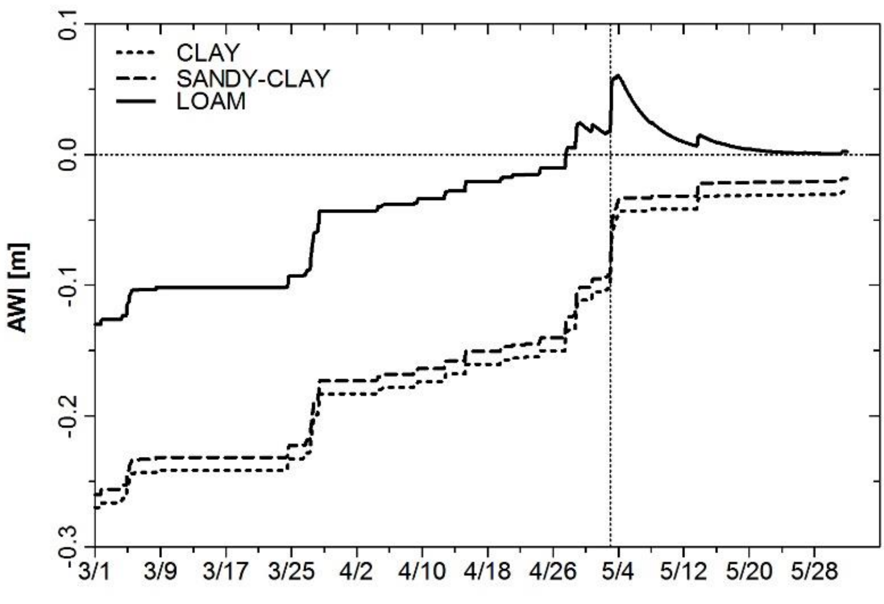

Figure 68 AWI trend for the period March 1st – May 31st 2014.

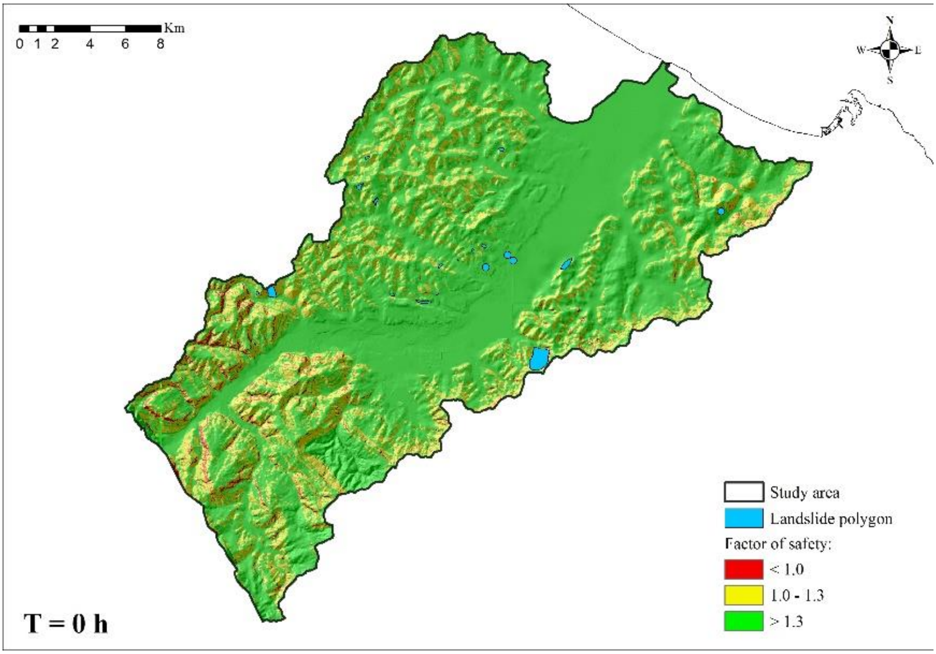

Figure 69 TRIGRS results for the May 2014 event. Figure shows the spatial distribution of unstable ($F_S \leq 1.0$), uncertain ($F_S = 1.0 – 1.3$), and stable ($F_S \geq 1.3$) cells at the initial conditions (T = 0 h).

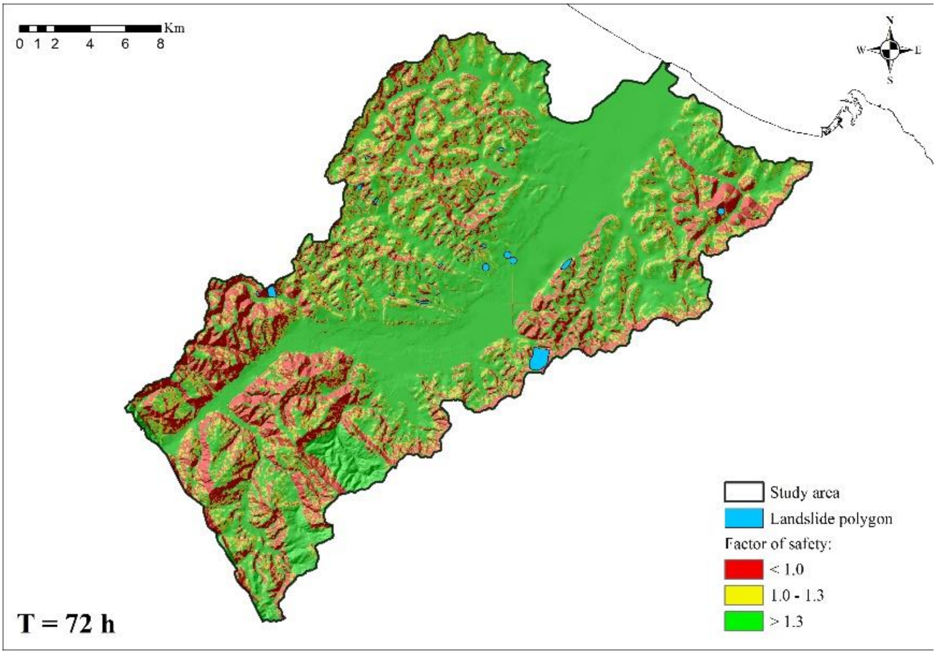

Figure 70 TRIGRS results for the May 2014 event. Figure shows the spatial distribution of unstable ($FS \leq 1.0$), uncertain ($FS = 1.0 – 1.3$), and stable ($FS \geq 1.3$) cells at the final conditions (T = 72 h).

The ROC analysis indicated that, at the end of the storm, the TPR is greater than the FPR (Figure 71). The graph shows also that TPR>FPR is always verified, even when the range of cells defined stable and unstable varies.

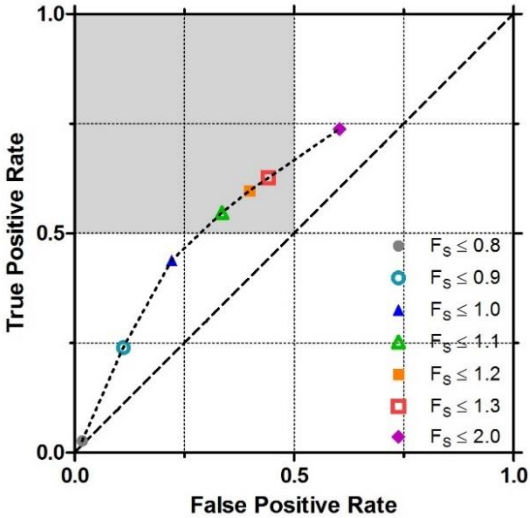

Figure 71 ROC curve for the events of May 2014 plotted by varying the range of F_s values considered as TP. The upper left quadrant (highlighted) represents acceptable prediction levels.

5 Discussion

The present study consisted in the application of empirical and physical models for the determination of potential landslide rainfall thresholds in the post-orogenic complex of the Esino river basin.

The following chapters are intended to interpret the outcomes of the described investigations. The results of this work can be grouped in 4 sections, corresponding to the parts in which the analyses were performed.

5.1 Landslides and rainfall data

The first result obtained shows that the landslide annual distribution in the study area is not constant over the years (Figure 10), rather some years have been more affected by landslides than others. This wide difference can be explained by attributing the slope failures not only to the predisposing factors (e.g., slope angle, soil thickness), which are assumed fixed or slightly variable from year to year. On the contrary, the triggering factors (e.g., rainfall, erosion) are largely mutable over time, thus they can cause very fluctuating effects on the soils.
Furthermore, the initiation of landslides has a strong connection with the rainfall monthly distribution (Figure 11) and the meteorological season (Figure 13). The high percentage of failures in the winter season (December, January, and February) and, in contrast, the low initiation rate in summer (June, July, and August) demonstrate the connection between landslides and climatic factors. However, it must be highlighted that information on 79 phenomena has uncertainty of the triggering day, which affected especially the number of landslides occurred on November 1998. Therefore, data may be underestimated in the autumn months.
Moreover, Figure 14 shows that many landslides occurred in the same period, indicating a widespread triggering cause, not limited to the worsening of specific conditions, although the final spatial distribution of landslides depends on the local settings.
Additionally, data recorded within the study area indicate little proximity to the polygons cataloged by the PAI (Figure 16 and Figure 17). In fact, the National Plan for the governance of Hydrogeological Hazard (PAI) is based

on information contained in the municipal plans, in the provincial plans and other specific studies developed before 2001, which is the year of its first adoption. This reveals the need of a supplementary analysis of landslide hazard within the study area, besides the work done for the PAI.
Finally, Figure 18 displays that the soil most prone to landslides is the terrain with agricultural use. This may be due to the vast extent of the farmland in the post-orogenic complex of the Esino and to the agricultural practices (e.g., soil tillage, residue management, planting) that affect the slope stability conditions (Ayalew, 1999; Fell et al., 2008; Strudley et al., 2008; Wasowski et al., 2010).

The rainfall data were collected from a list of rain gauges spatially and temporally distributed, which therefore can significantly represent the rainfall patterns of the post-orogenic complex.
The MAP series from 1953 to 2011 (Figure 20) is discontinuous and oscillating from the average MAP. This demonstrate a cyclic (a little decreasing) annual trend that may depends on an extremely wide range of physical, climatic, and even human factors.
The MMP series from 1951 to 2011 (Figure 21) shows also a cyclic trend, but conditioned by the season. This proves that in the study area the autumn, and part of the winter and the spring months, are normally the rainiest periods of the year. On the other hand, the summer months are the driest.

The comparison between rainfall and landslides series indicates that, in general, the number of landslides are not directly related to the annual cumulated rainfall of the study area (Figure 22). The correlation coefficient tends to 0, thus the series are not mutually dependent. This outcome is probably due to the fact that a single rainfall datum is an excessively raw parameter over a year of variable meteorological conditions and does not allow a proper comparison between precipitation and slope failures.
Different considerations can be done for the monthly-based evaluation. Here, the correlation coefficient is higher and the correspondence between the series more visible. Accordingly, the months with the highest average precipitation are responsible for the activation of the highest number of landslides. This is in agreement with the hypothesis that rainfall is one of the key triggering factor of landslides within the selected area. The exception of November is maybe due to the mentioned adjustment of 24 landslides, initiated between 30 November and 1 December 1998, into the month of December. Another source of data alteration are the wet soil conditions. This denotes the importance of the antecedent rainfall, remarks that are essentially valid for

the months of January and February. These winter months follows a rainy period lasting from September to December, thus the soil in January is generally already saturated and easy to destabilize. Moreover, the lengthy melting of the snow, due to the low temperature, maybe tends to saturate the terrain slowly for prolonged periods and the ground effects may occur over a longer time scale.

5.2 Empirical models

The application of empirical models to the study area led to several significant results.

First, the majority of the landslides were triggered during the main events. This is perhaps due to the nature of the available database of landslides, which mainly refers to reports of circumstances that caused widespread damages to the citizens and the territory.

Second, Figure 25 shows that the correlation between cumulative event rainfall (E) and duration (D) is positive; the higher is the duration of an event and the greater is the total amount of precipitation needed to trigger at least one landslide in the study area. This general trend is confirmed except for a value out of scale, which is located in the lower left corner of the graph, close to the x-axis. This datum may represents two landslides that are not directly related to precipitation or that depend on antecedent rainfall..
Moreover, from the distribution of main, secondary, minor, and single events is noticeable that different cumulative rainfalls and durations correspond to different number of landslides occurred in the territory (Figure 25). For example, abundant and widespread landslides are generally caused by a rainfall event that last at minimum 20 h and is characterized by a total amount of precipitation higher than 38 mm. The large scattering of data concerning single events makes difficult to generalize the ED bounds accountable for those activations. On the other hand, the minor and the secondary events, which are gathered in the middle of the graph, present evident minimum values of ED (20 h and 34 mm for minor events, 13 h and 36 mm for secondary events) which in the forecast activity can be considered as threshold values.
From the comparison with data of the analysis and the thresholds curves found in the literature, it is observable that the thresholds are representative of the general tendency of the data (Figure 26). However, not all the curves can be considered as minimum thresholds for the study area. In fact, the more the area involved in the analysis is large and generalized (e.g. the global thresholds of Caine 1980) and the more the lines overestimates the distribution of data and thus the probability of landslide. The curves more feasible for the study area are those of Peruccacci et al. (2012), developed for the post-orogenic sediments of the Marche, Abruzzo, and Umbria regions. However, these thresholds does not represents the 1% and 5% probability

exceedance, giving significance to the choice of selecting circumscribed areas along with similar lithological settings.

Third, the analysis computed with the maximum intensities and durations (Figure 27) displays a large scattering along the y-axis. This indicates that the maximum intensities, which characterize the event that triggered landslides in the study area, present a large variability. The reason is due to the different meteorological conditions that are responsible of landslide initiation, which strongly depends on the season. For example, the storms commonly affecting the spring or the summer have higher intensities and shorter durations if compared to the autumn and winter ones. In fact, the general trend of the $I_{max}D$ graph is that low intensities and long-term precipitations trigger the main events, whereas a wider range of rainfall parameters initiates the single events. Excluding the outlier, the minor and secondary events present limited durations but scattered intensities. As described before, this spreading can make the landslide prevision difficult to calibrate.
In the case of mean intensities and durations, the descending trend and the distribution of the events are confirmed (Figure 28). The negative value of the β parameter in the developed threshold proves that longer rainfall events require lower intensity to trigger at least one landslide in the study area. However, the distribution of data is more confined within the y-axis. For this reason, the ID method is more suitable for landslide forecasting than the $I_{max}D$. Moreover, it is easier to identify for each class of events the range of rainfall ID conditions likely to result in hillslope failures, excluding the single failures that are diffused along the duration axis.
The developed threshold is valid only in the range of duration in which was inferred, namely between 4 h and 167 h. The low steep of this curve highlights that the duration of the event is not as significant as the mean intensity, which discriminates the condition of slope failure (Guzzetti et al. 2008). In fact, the low intensities necessary to trigger landslides attributes importance also to the antecedent precipitation. This suggests that slope failures triggered after long periods of low rainfall intensity are the result of processes not accounted for by the simple ID model adopted. Deriving from the comparison with the other thresholds, the variances among the curves denote the importance of the hydrogeological setting of the area for the application of such model.
Finally, Figure 29 shows that the general trend of the curves is descending, and the shape of the threshold is largely preserved. The probability curves associate the row data of the database to a detailed probability of occurrence, valid for every combination of intensity and duration in the range of effectiveness of the ID threshold ($4h<D<167h$). Moreover, the different

distances between the lines, attribute elevated importance to the values of intensities when the duration of the storm is shorter than 20 h, whereas for longer rainfalls a small range of mean intensity values (about 0.70-2 mm/h) is likely to trigger landslides independently of rainfall duration. This result allows considering the seasonal variability of the rainfall ID patterns, along with the possible effects on the ground in the post-orogenic complex of the Esino basin.

Forth, the Bayesian analysis enabled to evaluate in a probabilistic framework the significance of a rainfall variable in explaining the initiation of a landslide event. Bayes contemplates that the same rainfall event may or may not result in a landslide, depending on a large number of factors. In the Bayes' theorem, if $P(A|B)$ objectively differs from $P(A)$, the variable B has a significant influence on A; if $P(A|B) \approx P(A)$ there is no mutual influence. Moreover, a large difference between $P(B|A)$ and $P(B)$ results in high landslide probability and stresses the importance of the variable B.

The results of the analyses are shown from Figure 31 to Figure 42. The charts clearly display that cumulative event rainfall and daily rainfall are strongly significant. In these cases the distributions of $P(B|A)$ and $P(B)$ are markedly different and the corresponding landslide probability $P(A|B)$ is well above the prior probability $P(A)$ (from Figure 31 to Figure 34). The cumulative event rainfall, in particular, seems to be the most significant variable, showing values of $P(A|B)$ as high as 0.75 for $E > 120$ mm (Figure 32). In fact, the probability of landsliding rises with the severity of the event, namely with increased daily or cumulative rainfall, except for the highest values of E ($E > 120$ mm) in which $P(A|B)$ decreases (Figure 31). This unexpected outcome is mainly due to the small number of samples of such magnitudes, which affect the statistical computation of the probability.

In the case of five days antecedent rainfall, the differences between the marginal ($P(B)$) and the likelihood ($P(B|A)$) probabilities, therefore between the prior ($P(A)$) and the posterior ($P(A|B)$) probabilities, are reduced. $P(A|B)$ never exceeds 0.16 in the expanded analysis (Figure 35) and 0.12 when considering rainfall intervals (Figure 36). This means that the sole five days of antecedent rainfall are not statistically significant for the initiation of landslides in the post-orogenic complex considered. The same evaluation can be done for the seven days antecedent rainfall in which $P(A|B)$ never exceed 0.17 in the expanded analysis (Figure 37) and 0.09 when considering the rainfall intervals (Figure 38). Results are even poorest for 15 and 30 days of antecedent rainfall: the maximum values of $P(A|B)$ is respectively 0.04 in the rainfall intervals of Figure 40 and 0.01 in the rainfall intervals of Figure 42.

In these cases, $P(A|B) \approx P(A)$, thus the A_{15} and A_{30} control variables appear statistically irrelevant for the initiation of landslides in the study area, which means they are randomly related with landslides. Consequently, apparently, landslides in the study area are not correlated with the antecedent precipitation of the 15 or 30 days before the event. A possible explanation of this result may lie in the criterion used for rainfall identification or in the fact that the analysis provides the probability of having at least one landslide and does not consider multiple events. In fact, antecedent saturated conditions are usually related to widespread (multiple) landsliding (Godt et al., 2006).

The two-dimensional Bayesian analysis supply additional information to improve the knowledge on how effective are the variables in local landslide activity. The advantage of the 2-D model is to consider that two (or more) rainfall variables can reciprocally influence the conditional probability of landslide and thus they can enhance or worsen the consequences on slope stability. In the example of the study, the posterior probability is deeply conditioned by the joint probability of daily and antecedent rainfall. This can be demonstrated by the different values of $P(A|B)$ in Figure 43 compared to Figure 34 and Figure 36. Particularly, an antecedent five days of rainfall shorter than 20 mm reduce the probability of rainfall in every interval considered for the 1-D daily rainfall. Overall, the influence of antecedent rainfall on $P(A|B)$ rises with both the increase of the antecedent rainfall itself and the increase of the daily rainfall. On the other hand, the lower than expected landslide probability observed for rainfall events characterized by $40 \leq A_5 \leq 60$mm and $20 \leq R \leq 40$mm or $40 \leq R \leq 60$mm, may be due to the lack of landslide data or to a bias caused by rainfall data interpolation.

5.3 Physical model

Results of the application of the TRIGRS model to the post-orogenic section of the Esino catchment area have numerous significances.

First, the variability in rainfall amount and intensity among the refined landslide-inducing storms confirms that conditions related to landslide initiation in the study area are complex. Table 9 shows that neither peak hourly rainfall intensity, nor duration are strongly correlated with the number of landslides, although the database could be refined by considering specific timing of landslides related to each storm and more precise duration (to the nearest hour, rather than rounding up to the nearest day). On the other hand, the relationship between slope failures and cumulative rainfall is high. Because of this high variability, for a better understanding of the landslide initiation in the study area, an approach that is capable of considering a wider range of variables seems justified.

Second, almost all the landslides of the database were triggered in fine-grained soils (Table 10), which usually are more characterized by short-term responses to rainfall.

Next, the review of the physical parameter values found in literature shows results consistent with the characteristics of the soils in the study area (Figure 44). As expected, the median values of cohesion are higher for clay and smaller for sandy-clay, while the loam texture is in the middle. The range for cohesion is large because it vary considerably, depending on the compactness and the saturation. The angle of internal friction also reflects the estimates, because the values of clay are lowermost, whereas the loam and the sandy-clay are upmost (with a higher median for sandy-clay). The soil unit weight usually varies depending on the amount of water contained in the pores, thus is strongly connected with the diffusivity and the conductivity of the soil. In fact, while the unit weight resulted averagely higher in clay and progressively lower in sandy-clay and loam, the trends of saturated hydraulic diffusivity and conductivity is opposite. Furthermore, the value of the storage parameter S_S (K_S/D_0) is higher for clay, followed by loam and finally sand, which is consistent with the greater ability of clay to accumulate water. Results of the analysis of residual water content indicate that the mean percentage of water, retained by the soil after drainage, is higher in loamy then in sandy-clay soils. In fact, the void volume in the loamy soils is elevated, because the particle size is more variable. On the other hand, the average saturated water content is highest in clay and lowest in sandy-clay. This is in accordance with the common values of porosity in these soils. Finally, the inverse height of the capillary fringe present anomalies in the values, because generally the height of capillary rising is higher in clay, medium in loam and low in sandy-clay. Results of the data collection shows instead an elevated inverse height of capillary fringe in clay soils. However, the significance of these values is slight due to the lack of data from literature.

Furthermore, the calibration of TRIGRS and the analysis of its sensitiveness to hydraulic property values (Figure 46 and Figure 47) induced several observations.
First, the pressure head peaks at definite values because under downward gravity-driven flow, it cannot exceed the value resulting with the water table at ground surface (Iverson, 2000). For this reason, TRIGRS automatically set the maximum pressure head as the value for slope-parallel flow.
Second, the slow decreasing of pressure head in UNS-FIN conditions is in agreement with the water absorption of the unsaturated media that delays the rise of pressure head at 1 m depth. In addition, the hypothetical less permeable bedrock is responsible for the slower drainage during dry periods as compared with the INF-SAT model. However, in the clay texture class the pressure head does not decrease. Indeed, the low hydraulic conductivity of the clay, which in the runs ranges between 10^{-8} and 10^{-6}, plays an important role reducing the drainage of the infiltration flux.
Furthermore, the variations of saturated hydraulic diffusivity in UNS-FIN conditions led to no difference in the pore pressure trends (graphs j-k-l in Figure 46 and Figure 47), except in the clayey soils. In fact, in sandy-clay and loam the point of view of the analysis coincides with the initial water-table depth so that the linearized Richards equation for the above-unsaturated zone is solved using only the soil-water diffusivity D_{Ψ} (equation (16) and equation (17)). In the clay example, on the other hand, the initial water table is at 0.5 m and the point of view of the analysis is below the water table, in the saturated zone, where the Fourier series' solution requires the saturated hydraulic diffusivity D_0 (equation (18)).
Additionally, results display that the increase of pressure head is higher with lower conductivity, which denotes a greater ability to impede drainage, and with higher diffusivity on equal conductivity settings, which indicates a lower specific storage.
Moreover, the comparison of the October 1996 and November 1998 storms indicated that the pressure head in every plot of the October 1996 storm rises less sharply and reaches values consistently inferior than November 1998.

The reason is that, even if the intensity is higher in the first storm, the total amount of precipitation is greater in the second one. However, even though the raising of pressure head was lower in October 1996, it was sufficient to affect the slope stability of clayey areas probably due to the low permeability of those soils. Conversely, the higher number of landslides triggered in November 1998 are probably due to the larger amount and duration of the rainfall, which in the first days was able to saturate even a soil with high conductivity (Figure 47). These results reveal that, beyond the different total amount of rainfall (105.8 mm in October 1996 and 138.2 mm in November 1998) and duration (72 h and 120 h respectively), the soil properties strongly influence landslide initiation.
Finally, the comparison of pressure head in the different textures, summarized in Figure 48, confirms that the responses of the soil in sandy-clay and loam textures are quicker than in clay. As a matter of fact, several investigators (Baum et al., 2010; Biavati et al., 2006; Casagli et al., 2006; Hewlett and Hibbert, 1963; Tofani et al., 2006; Von Ruette et al., 2013) have observed that the pressure head rises more quickly in soils with greater saturated hydraulic conductivity. Iverson (2000) observed: i) a negligible pressure head rise in a clay-rich soils after 10 days of low-intensity rainfall, and ii) a sudden increase in a sandy-loam soils after 10 minutes of high-intensity rainfall. Berti and Simoni (2012) also noted that (a) in sandy soil the pressure head increase can be very significant despite a low pre-storm water level, and (b) in clay soil the pore pressure rises faster than it falls afterwards. Godt et al. (2008) found that the deeper s the initial water table, the higher is the required rainfall intensity or duration to initiate a landslide. Therefore, in addition to the intensity and the duration of the storm, an elevated initial water table in the clay is needed to explain slope instability during the storms. Figure 48 highlights also that the pressure head total variations are higher in UNS-FIN conditions. The peculiar findings of this study can be explained as the consequence of the impermeable boundary layer at 1m depth in the UNS-FIN model, as reported by Tofani et al. (2006) and Godt and McKenna (2008).
Summarizing, results shows TRIGRS to be consistently sensitive to the variations of the initial soil properties and moisture. The model confirms that, for the same rainfall flux, the pressure head increases more with lower conductivity and higher diffusivity conditions but the soil properties in the different texture classes modify the magnitude of the responses. Moreover, TRIGRS proves that unsaturated conditions delay the rise of pressure head at 1 m depth and an impermeable basal boundary reduces the total drainage. The model comparison between the two storms highlights the rapidity of the sandy-clayey and loamy soils responses to the infiltration compared to those

of the clayey ones. This stresses also the importance of the rainfall hyetograph shape for the development of the landslide scenarios. In fact, pressure head variation and rainfall rate have a direct relationship but the greater is the duration of the storm, the more marked are the changes. However, TRIGRS sensitivity to the saturated hydraulic properties, and nonetheless to the rainfall intensity and duration attests the importance of having well-defined initial scenarios to achieve results as close as possible to the local conditions.

The final part, which is the spatial application of TRIGRS (Figure 52 and Figure 53), showed the temporal and spatial distribution of the safety factor values over the study area. At the beginning of the October 1996 event, there were already intrinsic conditions of possible instability. These conditions are represented by for example local physical conditions that can affect the slopes. Moreover, the saturation of soil at the beginning of the storm (Figure 50) caused the worsening of the initial settings. At 24 h, the $F_S \leq 1.0$ cells increased even with small amounts of rainfall, probably because the soil wetness had made the terrain very fragile and prone to changes in stability. At 32h, the steep increase of unstable cells is due to the 8h of intense rainfall with the highest average intensity of the event. At 40 h, the storm stopped and the distribution of F_S did not vary, due to the presence of an impermeable boundary in the soil that prevented the water from draining and the pressure head from decreasing. At 62h, the gentle increase of points with $F_S \leq 1.0$ was caused by the long period with lower intensity rainfall (Figure 49) that probably infiltrate in the soil and affected the values of pressure head at greater depths (Figure 46). In fact, the F_S considered as output of TRIGRS is the value correspondent to the soil surface. At this time, both reds and yellows replaced the green cells, thus demonstrating the deteriorating of the stability conditions throughout the whole area and extended to the gentler slopes. Indeed, this interval coincided with the highest variation in pressure head (Figure 46) often resulting in the surpassing of the instability threshold (the red line). At the end of the storm, the F_S remained identical to those at 62 for the same reasons described before at 40 h.
Results of ROC (Figure 54) indicate that for the events that triggered a single landslide TRIGRS tends to minimize both FPR and TPR, thus it over predicts the extent of the unstable cells and the performance is low. In fact, the lowest data represents one landslide activated at the end of July, when the soil parameters could sensibly vary from the rest of the year. Moreover, to simplify the computations, a uniform value of rainfall has been used for the analysis, which is largely simplistic for an area of 550 km^2 especially in summer, when the storms are often sudden and confined. On the other hand,

for scenarios that are more acute, TRIGRS increases the TPR and so the sensitivity. Results showed also that the simulations with instability boundaries within the interval 1.1 - 1.3 maximizes the agreement between known and predicted landslides for both the events. This range coincided with the values of the yellow cells previously classified with uncertain instability. Thus, accounting as unstable the uncertain data would improve the effectiveness of the model.

In the application of the physical model, three factors were considered responsible for landslide susceptibility in the study area: (i) soil texture, (ii) rainfall, and (iii) slope. Indeed, refining the zoning with additional factors that control landslide distribution, would enhance the discriminatory power of distinguish landslide from non-landslide areas and thus of susceptibility mapping. However, more detailed and confined zones would decrease the number of physical parameters values available for every area and necessary for the statistical analyses executed during the phase of calibration. Therefore, the refinement of the approach would require the collection of supplementary information on the study area that might be difficult to access. Additionally, for this area of smooth, rolling hills, with the available data, making better assessment of the landslide susceptibility would be challenging regardless of the method used. In fact, from the historical database, there is not any well-defined relationship between landslides and topographic variables, such as a narrow range of slope angles, or slope curvature (e.g. concave slopes).

5.4 Test

The event of 2-4 May 2014 was used to test the empirical and physical models developed for the study area.

Results of the ED distribution (Figure 62), compared to the historical database of landslides, displays values included in the ranges of duration and cumulative rainfall typical of the minor (Agugliano and Cupramontana) and the main (Jesi) events. Indeed, the number of landslides related to the rain gauges are 2 for Agugliano and Cupramontana, therefore these are considered minor events, and 15 for Jesi, which is considered a main event (Table 14). Likewise, the $I_{max}D$ and the ID values of the landslides triggered during the May 2014 event (Figure 63 and Figure 64) are in agreement with the historical database. Particularly, records of Agugliano and Cupramontana are similar to those of the minor events, while the Jesi intensity is higher than usual but still in the cloud of data. These results suggest that the rainfall parameters of the test are comparable with the distribution of previous events. Moreover, the coupled values of E, I_{max}, I, and D demonstrated to be representative of the magnitude of the effects within the study area, namely the number of landslides associated to every rainfall event.
Additionally, all the ID data recorded for the test are located above the threshold (Figure 64). Also, according to the Figure 65, the values registered in the Agugliano and Cupramontana stations match 60% and 70% probability, whereas the ID of Jesi match the 80% probability of landslide initiation. The implication of these results is that the distributions of ID that triggered landslides in the past are still representative nowadays. Moreover, the threshold computed in this study is validated for the post-orogenic complex of the Esino river basin. Finally, the probability graph further distinguishes the events that can cause a higher number of landslides from those that are likely to trigger fewer failures, by attributing to the rainfall parameters a different value of landslide probability.

The Bayesian test showed which parameters are more effective for the landslide forecast activity in the study area. The one-dimensional approach demonstrated that for the event of May 2014 only the cumulative event rainfall and the daily rainfall revealed landslide probability levels higher than the low class (Table 15). The event rainfall was associated to a medium probability, while the daily rainfall to a high probability. Indeed, an event that trigger 19 landslides has to be related at least to a medium conditional probability for considering the rainfall parameter reliable. This confirms the

considerations made during the development of the model, for which the antecedent rainfall seems not critical in the post-orogenic lithologies. On the other hand, the two-dimensional approach demonstrated that the combination of daily and five days antecedent rainfall computed is higher than ever occurred in the past years considered for the model design (Table 15). For this reason, the conditional probability could not be computed. This could indicates that the magnitude of the event of May 2014 was particularly significant. Additionally, this limit can be attributed to the consistency of information related to failures occurred in the territory (lack of information in some years and for some events) and then to the low density of rain gauges in the area.
After rounding up the value of antecedent rainfall, to allow the computation of P(A|B,C), the result obtained was a high probability level. The value of P(A|B) for R was 0.67. When coupled with A_5, the value of P(A|B,C) raised to 1. Therefore, the test demonstrated that the 2-D Bayes' theorem helps in attributing importance to the antecedent rainfall, in term of probability of occurrence, when coupled with the daily precipitation. This correlated R-A_D effect is possibly explained by the medium-low permeability of the soils, which keeps the water table close to the ground surface, especially throughout the wet season, and consequently causes a sudden connection between the rainfall and pore-pressure increase (Berti and Simoni, 2010). Additionally, this test highlighted the importance of keeping updated the database of landslides and rainfall for adapting the thresholds to the present rainfall patterns, also in the light of the current climatic trends.

Results of TRIGRS test for the May 2014 event showed that the model effectively predicts the spatial distribution of landslide with an acceptable level of performance (Figure 70). The ROC analysis indicated that, at the end of the storm, TPR>FPR is always verified (Figure 71). The outputs are comparable to those of the November 1998 event (Figure 53), which triggered 18 landslides. Results are maximized when the valuation of instability is extended to the points with F_S between 1.1 and 1.3 (highlighted area in Figure 71). This means that the areas with uncertain conditions may represent a geologic hazard as much as the cells with $F_S \leq 1.0$. This test validates the physical model as useful tool for landslide susceptibility assessment over broad regions and, nonetheless, as landslide spatial predictor in the study area.

6 Conclusion

The main objective of this study was to provide some methodologies for the determination of possible landslide rainfall thresholds to implement in the warning system of the Regional Functional Center of the Marche Civil Protection. In order to accomplish this, both empirical and physical predictive models has been applied in a particular area located in the hilly-coastal part of the Esino River Valley (Marche region, central Italy). This area was chosen for several reasons: (i) is characterized by lithologies with similar hydrogeological features, such as medium-low permeability, which makes it subject to rainfall-induced landslides; (ii) is high populated, compared to the rest of the Region, thus the exposure to the landslide hazard is significant; (iii) information on past landslides are more readily available, given the presence of human settlements in the area; (iv) is subject to shallow landslides, which are suitable for both empirical and physical models.
Every technique has intrinsic advantages and limitations. For example, the empirical models consider the history of the territory in order to design the future trends but do not take into account of the change in the hydrogeological features or in the rainfall patterns over time. On the other hand, the physical models contemplate the current spatial distribution of the input parameters (e.g. geomorphological, geotechnical, and hydrological data), but they are over detailed for an application on broad areas. The core assumption of the research was that the estimates of shallow failures in the study area is enhanced when empirical and physical models are jointly used and run simultaneously. This, during the delicate phase of forecast conducted by the Marche CFR, allows (i) the individuation and the comparison of the main triggering factors because the methods are applied in the same region, (ii) the use of the advantages of one model for the implementation of the other, and (iii) the attenuation of the weaknesses because they are run in parallel.

The *first part* of the research demonstrated that the correlation between landslides and rainfall in the study area is positive. Results are thus in line with the literature, which mainly attributes the slope failure occurrence to the precipitation factor. However, the high variability of the local conditions makes extremely important the weather monitoring as well as a further knowledge of the rainfall patterns that triggered landslides, to predict the possible effects on the ground.

The correlation between landslides and temporal distribution of rainfall, in the post-orogenic sediments of the Esino river basin, was verified by the data gathered for this research. Although the comparison between MAP an annual landslide frequency was very low, the cross-correlation coefficient of the MMP series and the monthly landslide frequency was equal to 0.43. Considering some approximation, such as the uncertainty of the exact triggering day for some landslides or the effect of the snow melting on the soil, the correlation value is sufficient to evaluate the rainfall one of the key triggering factors of slope failures.

The *second part* of the study proved that the application of empirical models at a local scale, in an area with approximatively similar hydrogeological properties, enhance the prediction of landslide occurrence. The selection of these input features made the methods and the rainfall thresholds more effective for the study area. This observation was done through the comparison of the critical rainfall data distribution with other global, regional or local thresholds. Results displays that, even if the curves fit the general trend of data, they do not represent the minimum thresholds, possibly due to the variability of the environmental (hydrological, geological and climate) settings. The variances among the curves denote the importance of the hydrogeological setting of the area for the application of empirical models.

Moreover, the most effective parameters for the definition of rainfall thresholds, for the initiation of landslides in the Esino post-orogenic sediments, are (i) cumulative event rainfall (E), (ii) mean rainfall intensity (I), (iii) duration (D), (iv) daily rainfall (R), and (v) five days antecedent rainfall (A_5), only if considered with daily rainfall.

The event rainfall resulted highly significant both in the Bayesian and in the ED method. The Bayesian analysis, which attributed importance also to the daily rainfall, enabled to compute the conditional probability of landslide, when a particular rainfall event occurs within the study area. Compared to the other empirical analysis applied, the improvement of this model is the consideration of all the rainfall events, whether they resulted in landslides or not. The ED method correlated the cumulative rainfall and the duration of those events that triggered landslides in the past years, finding that the greater is the duration of a rainfall event and the greater is the amount of precipitation needed to activate at least one landslide in the study area. Furthermore, different ranges of ED can cause different frequencies of landslides per rainfall event.

The mean rainfall intensity showed strong significance, especially when coupled with the duration parameter in the ID model. As opposed to the ED

approach, the greater is the duration of a rainfall event the lower is the mean intensity necessary to trigger one or more landslides. The classification of the rainfall events, based on the number of landslides occurred is still possible in this model. Additionally, the rainfall threshold in the form of a power law was developed to represent the ID settings with a greater than 10% likelihood of landslide initiation in the study area. The low slope of this curve highlights also that the mean intensity is more decisive than the duration for the stability conditions, whereas the low intercept of the equation indicates the importance of antecedent conditions. The significance of the intensity values is confirmed also from the probability ID graph, especially for durations shorter than 20 h, in which the seasonality of the rainfall patterns play a key role.
The five days antecedent rainfall resulted significant only when coupled with daily rainfall in the two-dimensional Bayesian analysis. Apparently, the one-dimensional approach showed that landslides in the study area are not correlated with the antecedent precipitation in the 5, 7, 15 or 30 days before the event. This finding is rather surprising because it is generally observed that antecedent rainfall conditions strongly affect slope stability in fine-grained soils. However, the two-dimensional Bayesian analysis shows that the conditional probability intensifies with both the increase of the antecedent rainfall and the increase of the daily rainfall. The reason is probably due to the oversimplification of the Bayes' theorem when merely one variable is considered to affect the stability of such a large area.

The *third part* of the investigation aimed at describing an innovative methodology for the application of a deterministic model for shallow landslide forecasting at a regional scale. The USGS TRIGRS physical model, which is an infinite slope stability model coupled with 1-D infiltration models, demonstrated that a deterministic method can be applied over large areas by considering the historical landslide and rainfall databases and by statistically infer the physical property values. To achieve this result, a complex analysis was accomplished.
First, the mechanical and hydrological properties (cohesion, friction angle, soil unit weight, saturated hydraulic conductivity, saturated hydraulic diffusivity, saturated water content, residual water content, and inverse height of capillary fringe) of the soil textures that characterize the study area were collected from a literature review. Consequently, the sample minimum, the lower quartile, the median, the upper quartile, and the sample maximum of each set of considered parameter has been tested in the model for its calibration in a single representative cell. The combination of values that led to instability conditions, during two of the historical rainfall events that

triggered several landslides in the post-orogenic area (October 1996 and November 1998), were selected. After picking these parameters, a comparative analysis of the pressure head variation in the soil texture classes (clay, sandy-clay and loam) was performed to simulate the groundwater conditions throughout October 1996 and November 1998 rainfall events. TRIGRS was used to simulate variation in pressure head in a representative profile of the study area. Saturated hydraulic conductivity, hydraulic diffusivity and initial depth of the water table were varied, as well as the hillslope conditions (saturated-unsaturated, infinite-finite depth boundary). This simulation aimed at quantifying the sensitivity of the TRIGRS model to these variations and its ability to discriminate effects of variable rainfall on slope stability in different soil types. Results revealed that TRIGRS enable to successfully simulate the condition of the hillslopes during two different rainfall scenarios.
Afterwards, the feasibility of TRIGRS as landslide predictor was verified by applying the model over the entire study area and comparing the results of the computation of safety factors against the inventory of local landslides triggered during the period 1990-2012. Input data selected during the calibration, along with a soil moisture and a soil depth model, were tested for some storm scenarios that triggered the historical landslides. The ROC technique applied to the results showed that, despite all the limitations inherent the application of a deterministic approach in an area with little information about the soil properties, TRIGRS effectively simulated the instability conditions in the post-orogenic complex. The analysis presented here, with simple assumptions and inferred input data, represents an example for scientists and decision makers that need to assess the stability condition of an area at regional scale with limited financial supports. Furthermore, TRIGRS outcomes were enhanced when the upper limit condition for the instability were extended to the uncertain values (F_S = 1.0-1.3). The reason is maybe due to local circumstances, such as for instance a road cut or a fallow land, which can facilitate the initiation of a landslide, especially on slopes with factor of safety close to the failure conditions. Therefore, this study also proved the importance of considering a level of uncertainty as a confidence interval to improve the landslide forecasting activity within the study area.

The *fourth* part of the research consisted in the test of the empirical and physical models previously developed, on the rainfall event of 2-4 May 2014 that affected the study area and a large portion of the Region. The validation allowed a comparison of the methodologies applied in the study area for

choosing the best model to be applied in the forecast system of the Marche CFR.
In fact, the test demonstrated that all the methods proposed are reliable and effective for the post-orogenic section of the Esino basin. Moreover, each technique highlighted a particular feature of the rainfall and landslide correlation, so that the concurrently use of all the models could permit an enhanced forecast. Particularly, the ED and the ID models considered the extent of the storm effects in term of number of landslides possibly triggered. The ID probability graph showed the likelihood of slope failure, depending on the mean intensity and duration of the historical events. The Bayesian approach estimated the most effective rainfall parameters for the study area, which are the cumulative event and the daily rainfall, and emphasized the importance of the antecedent rainfall, in term of probability of occurrence. Lastly, the application of TRIGRS allowed the forecast of the real-time spatial distribution of potentially unstable zones within the study area.

A number of possibilities were opened from the results of this study. This suggest a variety of research directions that may be pursued to make the methodology feasible for a direct application in the warning system of the Marche CFR.
One direction already undertaken has been the study of the effects of climate change on landslide initiation in the study area, which findings demonstrate show an overall increase in projected landslide occurrence over the twenty-first century, especially in summer (Sangelantoni et al., 2018).
Moreover, it would be interesting to investigate how to develop a decisional algorithm for the landslide forecast in the study area. This step-by-step well defined instructions could encourage the parallel or the consequential use of both empirical or physical model to help the Civil Protection decision maker in solving the problem of early warning issues.
Another possibility would be to improve the predictive power of the models. For example, the landslides and rainfall databases could be updated with reports of the 2013- 2014 landslides occurred and with the assistance of remote sensing techniques to obtain more precise data on landslides location, type and extension. Moreover, the ED and ID approaches could be further refined by normalizing the cumulative event and the intensity values with the mean annual precipitation (MAP), thus emphasizing the regionalization of the thresholds, or by considering also the rainfall events that did not triggered landslides. Additionally, these models could be coupled with the land use information to guide the efforts of hazard monitoring and risk mitigation, because, once exceeded the triggering threshold in the weather forecast, the

most fragile areas of the region may be individuated. Furthermore, the Bayesian method could be enriched by extending the analysis to other independent variables (e.g. number of landslides effectively triggered, land use, soil moisture, slope angle). Besides, the TRIGRS model could be improved by a real-time monitoring system that could mines the current physical property values in few key points (e.g. one for each textural class) within the study area.
Finally, the methodology described possibly will be extended to other zones of the Marche region, even in the mountains where the hydrogeological characteristics are different, to support the forecasting activity in those areas and compare the results with this study.

In conclusion, this research developed a methodology for the concurrently application of empirical and physical landslide predictive models, in a 550km^2 area of comparable hydrogeological features. The empirical models were calibrated at local scale and using similar geologic settings. The physical model was implemented by the historical landslide and rainfall series and by a statistical computation of the physical properties values. The encouraging results obtained in the framework of the activities carried out in this project have shown that a diversified methodological approach is the best way to study a complex problem as the landslide hazard in the Marche region.

Acknowledgments

This book is the result of a 3-year project performed under the agreement between the Polytechnic University of Marche, the Marche Region Civil Protection Service, and the National Civil Protection Department.
For all the work, authors have benefited from the kindness and help of many professors, experts, and technicians that we had the pleasure to work with.
We express our thankfulness to all the staff of the **Marche Civil Protection Multi-risk Functional Center** (Ancona, Italy). They have been unconditionally willing in providing all the data necessary for the study and in assisting when technical support was needed. A very special thanks goes to Dr. **Gabriella Speranza** for her guidance and help in developing landslide forecasting thresholds.
We are also grateful Dr. **Rex Baum** and Dr. **Jonathan Godt** of the **United States Geological Survey - Geologic Hazards Science Center** (Golden, Colorado, USA) and Prof. **James Kendra** of the **Disaster Research Center** at the University of Delaware (Newark, Delaware, USA) for providing invaluable support and guidance during the analysis and data interpretation.
Last, but not least, we would like to thank our invaluable collaborators of the **Disaster Lab** at the Università Politecnica delle Marche (Ancona, Italy).

References

Aleotti, P., 2004. A warning system for rainfall-induced shallow failures. Eng. Geol. 73, 247–265. https://doi.org/10.1016/j.enggeo.2004.01.007

Aleotti, P., Balzelli, P., Bellardone, G., Quaranta, N., Tresso, F., Troisi, C., Zani, A., 2002. Soil slips triggered by October 13-16, 2000 flooding event on the Piedmont Region (North West Italy): criticall analysis of rainfall data. Geol. Tec. e Ambient. Anno X, Ge, 15–25.

Aleotti, P., Chowdhury, R., 1999. Landslide hazard assessment: summary review and new perspectives. Bull. Eng. Geol. Environ. https://doi.org/10.1007/s100640050066

Alexander, D., 1992. On the causes of landslides: Human activities, perception, and natural processes. Environ. Geol. Water Sci. 20, 165–179. https://doi.org/10.1007/BF01706160

Ali, A., Huang, J., Lyamin, A. V., Sloan, S.W., Griffiths, D. V., Cassidy, M.J., Li, J.H., 2014. Simplified quantitative risk assessment of rainfall-induced landslides modelled by infinite slopes. Eng. Geol. 179, 102–116. https://doi.org/10.1016/j.enggeo.2014.06.024

Almagià, R., 1910. Studi Geografici sopra le frane in Italia. Volume II, L'Appennino centrale e meridionale - Conclusioni generali. Società Geografica Italiana, Roma.

Amici, M., Spina, R., 2002. Campo medio della precipitazione annuale e stagionale sulle Marche per il periodo 1950-2000.

Anderson, M.G., Burt, T.P., Speight, J.G., 1978. The role of topography in controlling throughflow generation. Earth Surf. Process. 3, 187–195. https://doi.org/10.1002/esp.3290030402

Anderson, M.G., Lloyd, D.M., 1991. Using a combined slope hydrology-stability model to develop cut slope design charts, in: ICE Proceedings. pp. 705–718. https://doi.org/10.1680/iicep.1991.17486

Annunziati, A., Focardi, A., Focardi, P., Martello, S., Vannocci, P., 2000. Analysis of the rainfall thresholds that induced debris flows in the area of Apuan Alps – Tuscany, Italy (19 June 1996 storm), in: EGS Plinius Conference on Mediterranean Storms. Maratea, Italy, pp. 485–493.

Antonini, G., Cardinali, M., Guzzetti, F., Reichenbach, P., Sorrentino, A., 2003. Carta Inventario dei Movimenti Franosi della Regione Marche ed aree limitrofe. https://doi.org/Pubblicazione Consiglio Nazionale delle Ricerche (CNR) – Gruppo Nazionale per la Difesa dalle Catastrofi Idrogeologiche

APAT - Dipartimento Difesa del Suolo, 2007. Rapporto sulle frane in Italia. Il progetto IFFI: metodologia, risultati e rapporti regionali. Roma.

Armaş, I., Vartolomei, F., Stroia, F., Braşoveanu, L., 2014. Landslide susceptibility deterministic approach using geographic information systems: application to Breaza town, Romania. Nat. Hazards 70, 995–1017. https://doi.org/10.1007/s11069-013-0857-x

Ayalew, L., 1999. The effect of seasonal rainfall on landslides in the highlands of Ethiopia. Bull Eng Geol Env 58, 9–19.

Bacchini, M., Zannoni, A., 2003. Relations between rainfall and triggering of debris-flow: case study of Cancia (Dolomites, Northeastern Italy). Nat. Hazards Earth Syst. Sci. 3, 71–79. https://doi.org/10.5194/nhess-3-71-2003

Baum, R., Savage, W., Godt, J., 2008. TRIGRS- A Fortran Program for Transient Rainfall Infiltration and Grid-Based Regional Slope-Stability Analysis, Version 2.0. https://doi.org/Open-File Report 2008–1159

Baum, R., Savage, W., Godt, J., 2002. TRIGRS- A Fortran Program for Transient Rainfall Infiltration and Grid-Based Regional Slope-Stability Analysis. https://doi.org/Open-file Report 02-424

Baum, R.L., 1995. Contribution of artesian water to progressive failure of the upper part of the Delhi Pike landslide complex, Cincinnati, Ohio, International Journal of Rock Mechanics and Mining Sciences & Geomechanics Abstracts. Washington, D.C. https://doi.org/10.1016/0148-9062(95)90054-9

Baum, R.L., Godt, J.W., 2013. Correction to “Estimating the timing and location of shallow rainfall-induced landslides using a model for transient, unsaturated infiltration.” J. Geophys. Res. Earth Surf. 118, 1. https://doi.org/10.1002/jgrf.20100

Baum, R.L., Godt, J.W., Savage, W.Z., 2010. Estimating the timing and location of shallow rainfall-induced landslides using a model for transient, unsaturated infiltration. J. Geophys. Res. 115, 1–26. https://doi.org/10.1029/2009JF001321

Baum, R.L., McKenna, J.P., Godt, J.W., Harp, E.L., McMullen, S.R., 2005. Hydrologic monitoring of landslide-prone coastal bluffs near Edmonds and Everett, Washington, 2001–2004.

Baum, R.L., Reid, M.E., 2000. Ground water isolation by low-permeability clays in landslide shear zones, in: Bromhead, E.N., Dixon, N., Ibsen, M.L. (Eds.), Landslides in Research, Theory and Practice, 8th Int. Symp. on Landslides. Cardiff, Wales, pp. 139–144.

Baum, R.L., Reid, M.E., 1995. Geology, hydrology and mechanics of a slow-moving, clay-rich landslide, Honolulu, Hawaii. Rev. Eng. Geol. 10, 79–105.

Bean, M.A., 2009. Probability: The Science of Uncertainty With Applications to Investments, Insurance, and Engineering, Am. Math. ed. Providence, R.I.

Berti, M., Ghirotti, M., Simoni, A., 2003. Analisi statistica dei rapporti precipitazioni-frane in un'area dell'Appennino bolognese, in: Biancotti, A., Motta, M. (Eds.), Risposta Dei Processi Geomorfologici Alle Variazioni Ambientali. Bologna, Italy, pp. 99–109.

Berti, M., Martina, M.L. V., Franceschini, S., Pignone, S., Simoni, A., Pizziolo, M., 2012. Probabilistic rainfall thresholds for landslide occurrence using a Bayesian approach. J. Geophys. Res. 117, 20. https://doi.org/10.1029/2012JF002367

Berti, M., Simoni, A., 2012. Observation and analysis of near-surface pore-pressure measurements in clay-shales slopes. Hydrol. Process. 26, 2187–2205. https://doi.org/10.1002/hyp.7981

Berti, M., Simoni, A., 2010. Field evidence of pore pressure diffusion in clayey soils prone to landsliding. J. Geophys. Res. Earth Surf. 115, 1–20. https://doi.org/10.1029/2009JF001463

Berti, M., Simoni, A., 2005. Experimental evidences and numerical modelling of debris flow initiated by channel runoff. Landslides. https://doi.org/10.1007/s10346-005-0062-4

Beven, K.J., Kirkby, M.J., 1979. A physically based, variable contibution area model of basin hydrology. Hydrol. Sci. Bull. 24, 43–69. https://doi.org/10.1080/02626667909491834

Bhandari, R., Senanayake, K., Thayalan, N., 1991. Pitfalls in the prediction on landslide through rainfall data, in: Bell, D. (Ed.), Landslides. A.A. Balkema, Rotterdam, Netherlands, pp. 887–890.

Biavati, G., Godt, J.W., McKenna, J.P., 2006. Drainage effects on the transient, near-surface hydrologic response of a steep hillslope to rainfall: Implications for slope stability, Edmonds, Washington, USA. Nat. Hazards Earth Syst. Sci. 6, 343–355. https://doi.org/10.5194/nhess-

6-343-2006

Bisci, C., Dramis, F., 1991. La geomorfologia delle Marche. L'ambiente Fis. delle Marche.

Bishop, A.W., 1959. The principle of effective stress. Tek. Ukebl. 106, 859–863.

Bishop, A.W., 1955. The use of slip circle in the stability analysis of slopes. Géotechnique 5, 7–17.

Boni, C., Mastrorillo, L., 1995. Valutazione delle risorse idriche sotterranee dei bacini dei fiumi Esino e Potenza (Appennino marchigiano) e considerazioni sul loro uso. Quad. di Geol. Appl. 1, 257–266.

Bonnard, C., Noverraz, F., 2001. Influence of climate change on large landslides: assessment of long term movements and trends, in: Proceedings of the International Conference on Landslides Causes Impact and Countermeasures. Gluckauf, Essen, Davos, pp. 121–138.

Borga, M., Dalla Fontana, G., Da Ros, D., Marchi, L., 1998. Shallow landslide hazard assessment using a physically based model and digital elevation data. Environ. Geol. 35, 81–88. https://doi.org/10.1007/s002540050295

Bovis, M.J., Jones, P., 1992. Holocene history of earthflow mass movements in south-central British Columbia: the influence of hydroclimatic changes. Can. J. Earth Sci. 29, 1746–1755.

Brady, N.C., 1990. The nature and properties of soils, 10th editi. ed. Macmillan, New York.

Brand, E.W., 1992. Slope instability in tropical areas, in: VI International Symposium on Landslides. Christchurch, New Zealand, pp. 2031–2051.

Brand, E.W., Premchitt, J., Phillipson, H., 1984. Relationship between rainfall and landslides in Hong Kong, in: 4th International Symposium on Landslides. Toronto, pp. 377–384.

Bronstert, A., 1994. Modellierung der Abflussbildung und der Bodenwasserdynamik von Hangen. Universitat Karlsruhe.

Brooks, R., Corey, A., 1964. Hydraulic properties of porous media. Hydrol. Pap. Color. State Univ. 3, 37 pp.

Brunetti, M.T., Peruccacci, S., Rossi, M., Luciani, S., Valigi, D., Guzzetti, F., 2010. Rainfall thresholds for the possible occurrence of landslides in Italy. Nat. Hazards Earth Syst. Sci. 10, 447–458.

https://doi.org/10.5194/nhess-10-447-2010

Buchanan, P., Savigny, K., 1990. Factors controlling debris avalanche initiation. Can. Geotech. J. 27, 659–675.

Busslinger, M., 2009. Landslide time-forecast methods, a literature review towards reliable prediction of time to failure. HSR University of Applied Science, Rapperswil.

Caine, N., 1980. The Rainfall Intensity: Duration Control of Shallow Landslides and Debris Flows, Geografiska Annaler. Ser. A. Phys. Geogr. 62, 23–27. https://doi.org/10.2307/520449

Calcaterra, D., Parise, M., Palma, B., Pelella, L., 2000. The influence of meteoric events in triggering shallow landslides in pyroclastic deposits of Campania, Italy, in: Bromhead, E., Dixon, N., Ibsen, M.L. (Eds.), 8th Int. Symp. On Landslides. Cardiff, p. 209214.

Campbell, R., 1974. Debris flows originating from soil slips during rainstorms in Southern California. Q. J. Eng. Geol. 7, 339–349.

Campbell, R.H., 1975. Soil slips, debris flows, and rainstorms in the Santa Monica Mountains and Vicinity, Southern California.

Cancelli, A., Nova, R., 1985. Landslides in soil debris cover triggered by rainstorms in Valtellina (Central Alps - Italy), in: 4th International Conference and Field Workshop on Landslide. Tokyo.

Cannon, S., Ellen, S., 1985. Rainfall conditions for abundant debris avalanches, San Francisco Bay region, California. Calif Geol 38, 267–272.

Cannon, S.H., 1988. Regional rainfall-threshold conditions for abundant debris-flow activity, in: Ellen, S.D., Wieczorek, G.F. (Eds.), Landslides, Floods and Marine Effects of the Storm of January 3-5, 1982 in the San Francisco Bay Region, California. US Geological Survey Professional Paper 1434, pp. 35–42.

Cannon, S.H., Boldt, E.M., Laber, J.L., Kean, J.W., Staley, D.M., 2011. Rainfall intensity–duration thresholds for postfire debris-flow emergency-response planning. Nat. Hazards 59, 209–236. https://doi.org/10.1007/s11069-011-9747-2

Canuti, P., Focardi, P., Garzonio, C.A., 1985. Correlation between rainfall and landslides . Bull. Eng. Geol. Environ. 32, 49–54.

Capecchi, F., Focardi, P., 1988. Rainfall and landslides: Research into a critical precipitation coefficient in an area of Italy, in: Proceedings of the

Fifth International Symposium on Landslides. Lausanne, pp. 1131–1136.

Cardinali, M., Galli, M., Guzzetti, F., Ardizzone, F., Reichenbach, P., Bartoccini, P., 2006. Rainfall induced landslides in December 2004 in Southwestern Umbria, Central Italy. Nat Hazard Earth Syst Sc 6, 237–260.

Caris, J., 1991. Geophysical, geotechnical and hydrological investigations of a small landslide in the French Alps. Eng. Geol. https://doi.org/10.1016/0013-7952(91)90011-9

Carone, M.T., Gioia, E., Ferretti, M., Marincioni, F., 2015. Linking vegetation patterns and landslide occurrence: An empirical method. Eng. Geol. Soc. Territ. - Vol. 2 Landslide Process. https://doi.org/10.1007/978-3-319-09057-3_209

Casagli, N., Dapporto, S., Ibsen, M.L., Tofani, V., Vannocci, P., 2006. Analysis of the landslide triggering mechanism during the storm of 20th–21st November 2000, in Northern Tuscany. Landslides 3, 13–21. https://doi.org/10.1007/s10346-005-0007-y

Cascini, L., Calvello, M., Grimaldi, G.M., 2010. Groundwater Modeling for the Analysis of Active Slow-Moving Landslides. J. Geotech. Geoenvironmental Eng. 136, 1220–1230. https://doi.org/10.1061/(asce)gt.1943-5606.0000323

Cascini, L., Gullà, G., Sorbino, G., 2006. Groundwater modelling of a weathered gneissic cover. Can. Geotech. J. 43, 1153–1166. https://doi.org/10.1139/T06-066

Cassinis, R., Tabacco, I., Bruzzi, G.F., Corno, C., Brandolini, A., Carabelli, E., 1985. The contribution of geophysical methods to the study of the great Ancona landslide (December 13, 1982). Geoexploration 23, 363–386. https://doi.org/10.1016/0016-7142(85)90003-1

Catenacci, V., 1992. Il dissesto geologico e geoambientale in Italia dal dopoguerra al 1990. Mem. Descr. Cart. Geol. D’Italia 47, 301.

Centamore, E., Micarelli, A., 1991. Stratigrafia, in: Regione Marche - Assessorato Urbanistica-Ambiente (Ed.), L’ambiente Fisico Delle Marche. SELCA, Firenze, Italy, pp. 1–58.

Centro Funzionale Regionale - CFR, 2014. Rapporto di evento 2-4 maggio 2014. Ancona, Italy.

Cepeda, J., Nadim, F., Høeg, K., Elverhøi, A., 2009. A new function for estimating local rainfall thresholds for landslide triggering (Abstract). Geophys. Res. Abstr. 11.

Cepeda, J.M., Malet, J.P., Remaître, A., 2011. Empirical estimates of precipitation conditions for landslide triggering in France and Norway. Geophys. Res. Abstr. 13.

Ceriani, M., Lauzi, S., Padovan, N., 1994. Rainfalls thresholds triggering debris-flows in the Alpine area of Lombardia Region, Central Alps - Italy, in: Man and Mountain, 1st Conv. Intern. Per La Protezione e Lo Sviluppo Dell'ambiente Montano. Ponte di Legno (BS), pp. 123–139.

Cervi, F., Berti, M., Borgatti, L., Ronchetti, F., Manenti, F., Corsini, A., 2010. Comparing predictive capability of statistical and deterministic methods for landslide susceptibility mapping: a case study in the northern Apennines (Reggio Emilia Province, Italy). Landslides 7, 433–444. https://doi.org/10.1007/s10346-010-0207-y

Chen, H.X., Zhang, L.M., 2014. A physically-based distributed cell model for predicting regional rainfall-induced shallow slope failures. Eng. Geol. 176, 79–92. https://doi.org/10.1016/j.enggeo.2014.04.011

Chien-Yuan, C., Tien-Chien, C., Fan-Chieh, Y., Wen-Hui, Y., Chun-Chieh, T., 2005. Rainfall duration and debris-flow initiated studies for real-time monitoring. Environ. Geol. 47, 715–724. https://doi.org/10.1007/s00254-004-1203-0

Chleborad, A., Baum, R., Godt, J., 2006. Rainfall thresholds for forecasting landslides in the Seattle, Washington, area- exceedance and probability. Reston, Virginia. https://doi.org/Open-File Report 2006–1064

Chleborad, A.F., 2000. Preliminary Method for Anticipating the Occurrence of Rainfall-induced Landslides in Seattle, Washington. Washington, D.C. https://doi.org/Open-File Report, vol. 00-469

Cho, S.E., 2009. Infiltration analysis to evaluate the surficial stability of two-layered slopes considering rainfall characteristics. Eng. Geol. 105, 32–43. https://doi.org/10.1016/j.enggeo.2008.12.007

Clarizia, M., Gullà, G., Sorbino, G., 1996. Sui meccanismi di innesco dei soil slip, in: International Conference, Prevention of Hydrogeological Hazards: The Role of Scientific Research. pp. 585–597.

Coe, J., Michael, J., Crovelli, R.A., Savage, W.Z., Laprade, W.T., Nashem, W.D., 2004. Probabilistic assessment of precipitation-triggered landslides using historical records of landslide occurrence, Seattle, Washington. Environ. Eng. Geosci. X, 103–122.

Coe, J.A., Ellis, W.L., Godt, J.W., Savage, W.Z., Savage, J.E., Michael, J.A., Kibler, J.D., Powers, P.S., Lidke, D.J., Debray, S., 2003. Seasonal movement of the Slumgullion landslide determined from global positioning system surveys and field instrumentation, July 1998-March 2002. Eng. Geol. 68, 67–101. https://doi.org/10.1016/S0013-7952(02)00199-0

Coe, J.A., Kinner, D.A., Godt, J.W., 2008. Initiation conditions for debris flows generated by runoff at Chalk Cliffs, central Colorado. Geomorphology 96, 270–297. https://doi.org/10.1016/j.geomorph.2007.03.017

Collins, B.D., Znidarcic, D., 2004. Stability Analyses of Rainfall Induced Landslides. J. Geotech. Geoenvironmental Eng. https://doi.org/10.1061/(ASCE)1090-0241(2004)130:4(362)

Coltorti, M., Nanni, T., 1987. La bassa valle del Fiume Esino: geomorfologia, idrogeologia e neotettonica. Boll. della Soc. Geol. Ital. 106, 35–51.

Consiglio Nazionale dei Geologi (Ed.), 2010. Terra e Sviluppo - Decalogo della Terra 2010, Rapporto sullo stato del territorio italiano. Roma.

Corominas, J., 2001. Landslides and Climate, in: Keynote Lectures from the 8th International Symposium on Landslides. pp. 1–33.

Corominas, J., Moya, J., 1999. Reconstructing recent landslide activity in relation to rainfall in the Llobregat River basin, Eastern Pyrenees, Spain. Geomorphology 30, 79–93. https://doi.org/10.1016/S0169-555X(99)00046-X

Corominas, J., Moya, J., 1996. Historical landslides in the Eastern Pyrenees and their relation to rainy events, in: Chacon, J., Irigaray, C., Fernandez, T. (Eds.), Landslides. A. A. Balkema, Rotterdam, Netherlands, pp. 125–132.

Corominas, J., Moya, J., Hürlimann, M., 2002. Landslide rainfall triggers in the Spanish Eastern Pyrenees, in: Proceedigns of 4th EGS Plinius Conference. Mallorca, Spain.

Cotecchia, V., 2006. The Second Hans Cloos Lecture. Experience drawn from the great Ancona landslide of 1982. Bull. Eng. Geol. Environ. 65, 1–41. https://doi.org/10.1007/s10064-005-0024-z

Crescenti, U., Favali, P., Rainone, M., Sciarra, N., Signanini, P., 2000. About Landslide Risk Evaluation: The Example Of Numana Cliff (Central Italy). ISRM Int. Symp. 5–10. https://doi.org/ISRM-IS-2000-519

Croley, T.E., Hartmann, H.C., 1985. Resolving Thiessen polygons. J. Hydrol. https://doi.org/10.1016/0022-1694(85)90143-X

Crosta, G., 1998. Regionalization of rainfall thresholds: an aid to landslide hazard evaluation. Environ. Geol. 35, 131–145. https://doi.org/10.1007/s002540050300

Crosta, G.B., 1989. A study of slope movements caused by heavy rainfall in Valtellina (Italy - July 1987), in: Cancelli A. (Ed.), Proceedings 6th International Conference and Field Workshop on Landslides ALPS 90. Milano, pp. 247–258.

Crosta, G.B., Dal Negro, P., 2003. Observations and modelling of soil slip-debris flow initiation processes in pyroclastic deposits: the Sarno 1998 event. Nat. Hazards Earth Syst. Sci. https://doi.org/10.5194/nhess-3-53-2003

Crosta, G.B., Frattini, P., 2003. Distributed modelling of shallow landslides triggered by intense rainfall. Nat. Hazards Earth Syst. Sci. 3, 81–93. https://doi.org/10.5194/nhess-3-81-2003

Crosta, G.B., Frattini, P., 2000. Rainfall thresholds for triggering soil slips and debris flow, in: 2nd EGS Plinius Conference on Mediterranean Storms. Siena, Italy, pp. 463–487.

Crovelli, R.A., 2000. Probability Models for Estimation of Number and Costs of Landslides.

Crozier, M., Eyles, R., 1980. Assessing the probability of rapid mass movement, in: Technical Groups (Ed.), 3rd Australia-New Zealand Conference on Geomechanics. Wellington, pp. 247–251.

Crozier, M.J., 1999. Prediction of rainfall-triggered landslides: A test of the antecedent water status model. Earth Surf. Process. Landforms 24, 825–833. https://doi.org/10.1002/(SICI)1096-9837(199908)24:9<825::AID-ESP14>3.0.CO;2-M

Crozier, M.J., 1996. The climate-landslide couple: a Southern Hemisphere perspective. Paleoclimate Res. 19, 329–350.

Crozier, M.J., 1986. Landslides: causes, consequences and environment. Croom Helm, London.

Crozier, M.J., Glade, T., 1999. Frequency and magnitude of landsliding. Zeitschrift für Geomorphol.

Cruden, D.M., 1991. A simple definition of a landslide. Bull. Int. Assoc. Eng. Geol. - Bull. l’Association Int. G??ologie l’Ing??nieur 43, 27–29.

https://doi.org/10.1007/BF02590167

Cruden, D.M., Varnes, D.J., 1996. Landslides Types and Processes, in: Turner, A.K., Schuster, R.L. (Eds.), Landslides: Investigation and Mitigation. Transportation Research Board Special Report 247. National Academy Press, Washington, DC, pp. 36–72.

Cuomo, S., Della Sala, M., 2013. Rainfall-induced infiltration, runoff and failure in steep unsaturated shallow soil deposits. Eng. Geol. 162, 118–127. https://doi.org/10.1016/j.enggeo.2013.05.010

D'Amato Avanzi, G., Falaschi, F., Giannecchini, R., Puccinelli, A., 2009. Soil slip susceptibility assessment using mechanical–hydrological approach and GIS techniques: an application in the Apuan Alps (Italy). Nat. Hazards 50, 591–603. https://doi.org/10.1007/s11069-009-9357-4

Dahal, R.K., Hasegawa, S., 2008. Representative rainfall thresholds for landslides in the Nepal Himalaya. Geomorphology 100, 429–443. https://doi.org/10.1016/j.geomorph.2008.01.014

Dahal, R.K., Hasegawa, S., Yamanaka, M., Dhakal, S., Bhandary, N.P., Yatabe, R., 2009. Comparative analysis of contributing parameters for rainfall-triggered landslides in the Lesser Himalaya of Nepal. Environ. Geol. 58, 567–586. https://doi.org/10.1007/s00254-008-1531-6

Dapporto, S., Rinaldi, M., Casagli, N., 2001. Failure mechanisms and pore water pressure conditions: analysis of a riverbank along the Arno River (Central Italy). Eng. Geol. 61, 221–242. https://doi.org/10.1016/S0013-7952(01)00026-6

Darcy, H., 1856. Les fontaines publiques de la ville de Dijon : exposition et application des principes à suivre et des formules à employer dans les questions de distribution d'eau, Recherche.

De Vita, P., 2000. Fenomeni di instabilità delle coperture piroclastiche dei Monti Lattari, di Sarno e di Salerno (Campania) ed analisi degli eventi pluviometrici determinanti. Quad. di Geol. Appl. 7, 213–235.

De Vita, P., Reichenbach, P., 1998. Rainfall-triggered landslides: a reference list. Environ. Geol. 35, 219–233. https://doi.org/10.1007/s002540050308

DeGraff, J. V., 2012. Solving the dilemma of transforming landslide hazard maps into effective policy and regulations. Nat. Hazards Earth Syst. Sci. 12, 53–60. https://doi.org/10.5194/nhess-12-53-2012

Della Sala, M., Cuomo, S., 2013. Analisi su area vasta di frane superficiali e fenomeni erosivi indotti da pioggia, in: Incontro Annuale Dei Ricercatori Di Geotecnica IARG. Perugia, Italy, p. 6.

DeRose, R., Trustrum, N., Blaschke, P., 1991. Geomorphic change implied by regolith—slope relationships on steepland hillslopes, Taranaki, New Zealand. Catena 18, 489–514.

Dhakal, A.S., Sullivan, K., 2014. Shallow groundwater response to rainfall on a forested headwater catchment in northern coastal California: Implications of topography, rainfall, and throughfall intensities on peak pressure head generation. Hydrol. Process. 28, 446–463. https://doi.org/10.1002/hyp.9542

Di Crescenzo, G., De Falco, M., Iervolino, V.E., Rinaldi, S., Santangelo, N., Santo, A., 2008. Proposal of a new semiquantitative methodology for flowslides triggering susceptibility assessment in the carbonate slope contexts of Campania (Southern Italy). Ital. J. Eng. Geol. Environ. 1, 61–79. https://doi.org/10.4408/IJEGE.2008-01.O-04

Dir.P.C.M. 27 febbraio 2004 "Indirizzi operativi per la gestione organizzativa e funzionale del sistema di allertamento nazionale, statale e regionale per il rischio idrogeologico ed idraulico ai fini di protezione civile.," n.d.

Dramis, F., 1984. Aspetti geomorfologici e fattori genetici delle deformazioni gravitative profonde. Boll. della Soc. Geol. Ital. 103.

Dripps, W.R., Bradbury, K.R., 2007. A simple daily soil-water balance model for estimating the spatial and temporal distribution of groundwater recharge in temperate humid areas. Hydrogeol. J. 15, 433–444. https://doi.org/10.1007/s10040-007-0160-6

ENEA, 1990. L'archivio storico del Progetto Giano. Frane ed inondazioni in Italia nei secoli XVIII e XIX [WWW Document]. URL http://www.gndci.cnr.it/si/it/pag/giano.htm

EU-FP7, 2012. SafeLand - living with landslide risk in Europe: assessment, effects and global change, and risk management strategies, Deliverable 1.1 Landslide triggering mechanisms in Europe – Overview and State of the Art.

Fawcett, T., 2006. An introduction to ROC analysis. Pattern Recognit. Lett. 27, 861–874. https://doi.org/10.1016/j.patrec.2005.10.010

Feddes, R.A., Kowalik, P., Kolinska-Malinka, K., Zaradny, H., 1976. Simulation of field water uptake by plants using a soil water dependent root extraction function. J. Hydrol. https://doi.org/10.1016/0022-1694(76)90017-2

Fell, R., Corominas, J., Bonnard, C., Cascini, L., Leroi, E., Savage, W.Z., 2008. Guidelines for landslide susceptibility, hazard and risk zoning for land use planning. Eng. Geol. 102, 85–98. https://doi.org/10.1016/j.enggeo.2008.03.022

Fiorillo, F., 2004. Blue clay slope angle in relation to some geological and geotechnical characteristics, Italy. Q. J. Eng. Geol. Hydrogeol. 37, 49–59. https://doi.org/10.1144/1470-9236/03-027

Floris, M., Bozzano, F., 2008. Evaluation of landslide reactivation: A modified rainfall threshold model based on historical records of rainfall and landslides. Geomorphology 94, 40–57. https://doi.org/10.1016/j.geomorph.2007.04.009

Folchi Vici D'Arcevia, C., Nanni, T., Palpacelli, S., Siciliani, A., Vita, F., Vivalda, P., 2008. Schema Idrogeologico della Regione Marche, Foglio Nord, Scala 1:100.000. Regione Marche – Servizio Ambiente e Paesaggio, Italy.

Frattini, P., Crosta, G.B., Fusi, N., Dal Negro, P., 2004. Shallow landslides in pyroclastic soils: A distributed modelling approach for hazard assessment. Eng. Geol. 73, 277–295. https://doi.org/10.1016/j.enggeo.2004.01.009

Fredlund, D.G., Rahardjo, H., 1993. Soil Mechanics for Unsaturated Soils, Stress The International Journal on the Biology of Stress. John Wiley and Sons, New York.

Freeze, R.A., 1971. Three-Dimensional, Transient, Saturated-Unsaturated Flow in a Groundwater Basin. Water Resour. Res. https://doi.org/10.1029/WR007i002p00347

Freeze, R.A., Cherry, J.A., 1979. Groundwater. Prentice-Hall, Englewood Cliffs, NJ.

Gabet, E.J., Burbank, D.W., Putkonen, J.K., Pratt-Sitaula, B. a., Ojha, T., 2004. Rainfall thresholds for landsliding in the Himalayas of Nepal. Geomorphology 63, 131–143. https://doi.org/10.1016/j.geomorph.2004.03.011

Galliani, G., Pomi, L., Zinoni, F., Casagli, N., 2001. Analisi meteoclimatologica e soglie di innesco delle frane nella regione Emilia-Romagna negli anni 1994–1996. Quad. di Geol. Appl. 8.

Gardner, W., 1958. Some steady-state solutions of the unsaturated moisture flow equation with application to evaporation from a water table. Soil Sci. 85, 228–232. https://doi.org/10.1097/00010694-195804000-00006

Gentili, B., Dramis, F., 1997. Geomorphology and Quaternary Evolution of Central Italy - Guide for the excursion. Suppl Geogr Fis Dinam Quat 3, 79–103.

Geo-Slope, 2003a. SEEP/W model and User manual 2000.

Geo-Slope, 2003b. SLOPE/W model and User manual 2000.

Giannecchini, R., 2006. Relationship between rainfall and shallow landslides in the southern Apuan Alps (Italy). Nat. Hazards Earth Syst. Sci. 6, 357–364. https://doi.org/10.5194/nhess-6-357-2006

Giannecchini, R., 2005. Rainfall triggering soil slips in the southern Apuan Alps (Tuscany, Italy). Adv. Geosci. 2, 21–24.

Giannecchini, R., Galanti, Y., D'Amato Avanzi, G., 2012. Critical rainfall thresholds for triggering shallow landslides in the Serchio River Valley (Tuscany, Italy). Nat. Hazards Earth Syst. Sci. 12, 829–842. https://doi.org/10.5194/nhess-12-829-2012

Gillham, R.W., 1984. The capillary fringe and its effect on water-table response. J. Hydrol. https://doi.org/10.1016/0022-1694(84)90248-8

Gioia, E., Carone, T., Marincioni, F., 2015a. Rainfall and land use empirically coupled to forecast landslides in the Esino river basin, central Italy. Nat. Hazards Earth Syst. Sci. 15. https://doi.org/10.5194/nhess-15-1289-2015

Gioia, E., Speranza, G., Appiotti, F., Ferretti, M., Marincioni, F., 2015b. Rainfall threshold and landslides in the post-Orogenic complex of the Esino River Basin, Central Italy. Eng. Geol. Soc. Territ. - Vol. 2 Landslide Process. https://doi.org/10.1007/978-3-319-09057-3_275

Gioia, E., Speranza, G., Ferretti, M., Godt, J.W., Baum, R.L., Marincioni, F., 2016. Application of a process-based shallow landslide hazard model over a broad area in Central Italy. Landslides 13, 1197–1214. https://doi.org/10.1007/s10346-015-0670-6

Glade, T., 2012. Landslide-triggering rainfall thresholds - a review of concepts and some examples, in: Sediment-Related Disasters: Mechanism, Prediction and Assessment. Taichung, Taiwan, p. 46.

Glade, T., Crozier, M., Smith, P., 2000. Applying Probability Determination to Refine Landslide-triggering Rainfall Thresholds Using an Empirical Antecedent Daily Rainfall Model. Pure Appl. Geophys. https://doi.org/10.1007/s000240050017

Godt, J.W., Baum, R.L., Chleborad, A.F., 2006a. Rainfall characteristics for shallow landsliding in Seattle, Washington, USA. Earth Surf. Process. Landforms 31, 97–110. https://doi.org/10.1002/esp.1237

Godt, J.W., Baum, R.L., Chleborad, A.F., 2006b. Rainfall characteristics for shallow landsliding in Seattle, Washington, USA. Earth Surf. Process. Landforms 31, 97–110. https://doi.org/10.1002/esp.1237

Godt, J.W., Baum, R.L., Savage, W.Z., Salciarini, D., Schulz, W.H., Harp, E.L., 2008. Transient deterministic shallow landslide modeling: Requirements for susceptibility and hazard assessments in a GIS framework. Eng. Geol. 102, 214–226. https://doi.org/10.1016/j.enggeo.2008.03.019

Godt, J.W., McKenna, J.P., 2008. Numerical modeling of rainfall thresholds for shallow landsliding in the Seattle, Washington, area. Geol. Soc. Am. Rev. Eng. Geol. XX, 121–135. https://doi.org/10.1130/2008.4020(07)

Godt, Jonathan W, Schulz, W.H., Baum, R.L., Savage, W.Z., 2008. Modeling rainfall conditions for shallow landsliding in Seattle, Washington. Geol. Soc. Am. Rev. Eng. Geol. XX, 137–152. https://doi.org/10.1130/2008.4020(08)

Godt, J.W., Şener-Kaya, B., Lu, N., Baum, R.L., 2012. Stability of infinite slopes under transient partially saturated seepage conditions. Water Resour. Res. 48. https://doi.org/10.1029/2011WR011408

Govi, M., Mortara, G., Sorzana, P., 1985. Eventi idrologici e frane. Geol. Appl. Ing. 20, 359–375.

Govi, M., Sorzana, P.F., 1980. Landslide susceptibility as function of critical rainfall amount in Piedmont basin (North-Western Italy). Stud. geomorphol. Carpatho-Balc 14, 43–60.

Greco, R., Comegna, L., Damiano, E., Guida, A., Olivares, L., Picarelli, L., 2013. Hydrological modelling of a slope covered with shallow pyroclastic deposits from field monitoring data. Hydrol. Earth Syst. Sci. 17, 4001–4013. https://doi.org/10.5194/hess-17-4001-2013

Green, W.H., Ampt, G.A., 1911. Studies on Soil Phyics. J. Agric. Sci. https://doi.org/10.1017/S0021859600001441

Grelle, G., Soriano, M., Revellino, P., Guerriero, L., Anderson, M., Diambra, A., Fiorillo, F., Esposito, L., Diodato, N., Guadagno, F., 2013. Space–time prediction of rainfall-induced shallow landslides through a combined probabilistic/deterministic approach, optimized for initial water table conditions. Bull. Eng. Geol. Environ. 14. https://doi.org/10.1007/s10064-013-0546-8

Guidicini, G., Iwasa, O.Y., 1977. Tentative correlation between rainfall and landslides in a humid tropical environment. Bull. Int. Assoc. Eng. Geol. 16, 13–20. https://doi.org/10.1007/BF02591434

Guzzetti, F., Cardinali, M., Reichenbach, P., 1994. The AVI project: A bibliographical and archive inventory of landslides and floods in Italy. Environ. Manage. 18, 623–633. https://doi.org/10.1007/BF02400865

Guzzetti, F., Carrara, A., Cardinali, M., Reichenbach, P., 1999. Landslide hazard evaluation: a review of current techniques and their application in a multi-scale study, Central Italy. Geomorphology 31, 181–216. https://doi.org/10.1016/S0169-555X(99)00078-1

Guzzetti, F., Peruccacci, S., Rossi, M., 2005. Definition of critical threshold for different scenarios (WP 1.16) 36.

Guzzetti, F., Peruccacci, S., Rossi, M., Stark, C., 2007. Rainfall thresholds for the initiation of landslides in central and southern Europe. Meteorol. Atmos. Phys. 98, 239–267. https://doi.org/10.1007/s00703-007-0262-7

Guzzetti, F., Peruccacci, S., Rossi, M., Stark, C.P., 2008. The rainfall intensity–duration control of shallow landslides and debris flows: an update. Landslides 5, 3–17. https://doi.org/10.1007/s10346-007-0112-1

Guzzetti, F., Salvati, P., Rossi, M., Bianchi, C., 2012. Rischio geo-idrologico per la popolazione in Italia, in: Atti Dei Convegni Lincei n. 270. Roma, pp. 197–203.

Hammond, C., Hall, D., Miller, S., Swetik, P., 1992. Level I Stability Analysis (LISA) documentation for version 2.0, Gen. Tech. Rep. INT-285. U.S. Department of Agriculture, Forest Service, Intermountain Research Station, Ogden, UT.

Haneberg, W.C., 1991. Observation and analysis of pore pressure fluctuations in a thin colluvium landslide complex near Cincinnati, Ohio. Eng. Geol. https://doi.org/10.1016/0013-7952(91)90004-5

Harr, R.D., 1977. Water flux in soil and subsoil on a steep forested slope. J. Hydrol. https://doi.org/10.1016/0022-1694(77)90097-X

Hewlett, J., Hibbert, A., 1963. Moisture and energy conditions within a sloping mass during drainage. J. Geophys. Res. 68, 1081–1087.

Heyerdahl, H., Harbitz, C., Domaas, U., Sandersen, F., Tronstad, K., Nowacki, F., Engen, A., Kjekstad, O., Dévoli, G., Buezo, S., Diaz, M., Hernandez, W., 2003. Rainfall induced lahars in volcanic debris in Nicaragua and El Salvador: practical mitigation, in: International

Conference on Fast Slope Movements – Prediction and Prevention for Risk Mitigation, IC-FSM2003. Patron Pub, Naples, Italy, pp. 275–282.

Hodge, R.A.L., Freeze, R.A., 1977. Groundwater flow systems and slope stability. Can. Geotech. J. 14, 416–466.

Hong, Y., Hiura, H., Shino, K., Sassa, K., Suemine, A., Fukuoka, H., Wang, G., 2005. The influence of intense rainfall on the activity of large-scale crystalline schist landslides in Shikoku Island, Japan. Landslides 2, 97–105. https://doi.org/10.1007/s10346-004-0043-z

Hungr, O., Leroueil, S., Picarelli, L., 2013. The Varnes classification of landslide types, an update. Landslides 11, 167–194. https://doi.org/10.1007/s10346-013-0436-y

Hutchinson, J.N., 1988. Morphology and geotechnical parameters of landslides in relation to geology and hydrogeology, in: 5th Int. Symp. on Landslides. Balkema, Lousanne, pp. 3–35.

Innes, J.L., 1983. Debris flows. Prog. Phys. Geogr. 7, 469–501.

International Geotechnical Societies UNESCO Working Party on World Landslide Inventory (WP/WLI), 1993. Multilingual landslide glossary. Bitech Publishers, Vancouver, Canada.

Iverson, R.M., 2000. Landslide triggering by rain infiltration. Water Resour. Res. 36, 1897–1910. https://doi.org/10.1029/2000WR900090

Iverson, R.M., 1997. The physics of debris flows. Rev. Geophys. https://doi.org/10.1029/97RG00426

Iverson, R.M., Lahusen, R.G., 1989. Dynamic pore-pressure fluctuations in rapidly shearing granular materials. Science 246, 796–799. https://doi.org/10.1126/science.246.4931.796

Iverson, R.M., Major, J.J., 1987. Rainfall, ground-water flow, and seasonal movement at Minor Creek landslide, northwestern California: physical interpretation of empirical relations. Geol. Soc. Am. Bull. https://doi.org/10.1130/0016-7606(1987)99<579:RGFASM>2.0.CO;2

Iverson, R.M., Major, J.J., 1986. Groundwater seepage vectors and the potential for hillslope failure and debris-flow mobilization. Water Resour. Res. 22, 1543–1548.

Jaiswal, P., van Westen, C.J., 2009. Estimating temporal probability for landslide initiation along transportation routes based on rainfall thresholds. Geomorphology 112, 96–105. https://doi.org/10.1016/j.geomorph.2009.05.008

Jakob, M., Weatherly, H., 2003. A hydroclimatic threshold for landslide initiation on the North Shore Mountains of Vancouver, British Columbia. Geomorphology 54, 137–156. https://doi.org/10.1016/S0169-555X(02)00339-2

Jenkins, A., Ashworth, P.J., Ferguson, R.I., Grieve, I.C., Rowling, P., Stott, T.A., 1988. Slope failures in the Ochil hills, Scotland, November 1984. Earth Surf. Process. Landforms 13, 69–76.

Jibson, R.W., 1989. Debris flows in southern Puerto Rico. Geol. Soc. Am. Spec. Pap. 236, 29–56. https://doi.org/10.1130/SPE236-p29

Kanji, M.A., Massad, F., Cruz, P.T., 2003. Debris flows in areas of residual soils: occurrence and characteristics, in: International Workshop on Occurrence and Machanisms of Flows in Natural Slopes and Earthfills. Sorrento, Italy, pp. 1–11.

Keim, R.F., Skaugset, A.E., 2003. Modelling effects of forest canopies on slope stability. Hydrol. Process. 17, 1457–1467. https://doi.org/10.1002/hyp.5121

Kim, S., Hong, W., Kim, Y., 1991. Prediction of rainfall triggered landslides in Korea, in: Bell, D. (Ed.), Landslides. A.A. Balkema, Rotterdam, Netherlands, pp. 989–994.

L. 24 febbraio 1992 , n. 225 “Istituzione del Servizio nazionale della protezione civile,” n.d.

Lanni, C., Borga, M., Rigon, R., Tarolli, P., 2012. Modelling shallow landslide susceptibility by means of a subsurface flow path connectivity index and estimates of soil depth spatial distribution. Hydrol Earth Syst Sc 16, 3959–3971. https://doi.org/10.5194/hess-16- 3959-2012

Larsen, M.C., Simon, A., 1993. A rainfall intensity-duration threshold for landslides in a humid- tropical environment, Puerto Rico. Geogr. Ann. 75A, 13–23.

Lee, M.L., Ng, K.Y., Huang, Y.F., Li, W.C., 2014. Rainfall-induced landslides in Hulu Kelang area, Malaysia. Nat. Hazards 70, 353–375. https://doi.org/10.1007/s11069-013-0814-8

Lehmann, P., Or, D., 2012. Hydromechanical triggering of landslides: From progressive local failures to mass release. Water Resour. Res. 48. https://doi.org/10.1029/2011WR010947

Leroueil, S., 2001. Natural slopes and cuts: movement and failure mechanism. Géotechnique 51, 197–243.

Li, W.C., Lee, L.M., Cai, H., Li, H.J., Dai, F.C., Wang, M.L., 2013. Combined roles of saturated permeability and rainfall characteristics on surficial failure of homogeneous soil slope. Eng. Geol. 153, 105–113. https://doi.org/10.1016/j.enggeo.2012.11.017

Lu, N., Godt, J.W., 2013. Hillslope Hydrology and Stability. Cambridge University Press.

Lumb, P., 1975. Slope failures in Hong Kong. Q. J. Eng. Geol. Hydrogeol. 8, 31–65. https://doi.org/10.1144/GSL.QJEG.1975.008.01.02

Luzi, L., Pergalani, F., 1996. Applications of statistical and GIS techniques to slope instability zonation (1:50.000 Fabriano geological map sheet). Soil Dyn. Earthq. Eng. 15, 83–94. https://doi.org/10.1016/0267-7261(95)00031-3

Malet, J.-P., van Asch, T.W.J., van Beek, R., Maquaire, O., 2005. Forecasting the behaviour of complex landslides with a spatially distributed hydrological model. Nat. Hazards Earth Syst. Sci. https://doi.org/10.5194/nhess-5-71-2005

Marchi, L., Arattano, M., Deganutti, A.M., 2002. Ten years of debris-flow monitoring in the Moscardo Torrent (Italian Alps). Geomorphology 46, 1–17. https://doi.org/10.1016/S0169-555X(01)00162-3

Mark, R.K., Newman, E.B., 1985. Rainfall totals before and during the storm distribution and correlation with damaging landslides.

Martelloni, G., Segoni, S., Fanti, R., Catani, F., 2011. Rainfall thresholds for the forecasting of landslide occurrence at regional scale. Landslides 9, 485–495. https://doi.org/10.1007/s10346-011-0308-2

Matsushi, Y., Matsukura, Y., 2007. Rainfall thresholds for shallow landsliding derived from pressure-head monitoring: Cases with permeable and impermeable bedrocks in Boso Peninsula, Japan. Earth Surf. Process. Landforms 32, 1308–1322. https://doi.org/10.1002/esp.1491

Mercogliano, P., Segoni, S., Rossi, G., Sikorsky, B., Tofani, V., Schiano, P., Catani, F., Casagli, N., 2013. Brief communication A prototype forecasting chain for rainfall induced shallow landslides. Nat. Hazards Earth Syst. Sci. 13, 771–777. https://doi.org/10.5194/nhess-13-771-2013

Ministry of Environment Territory and Sea, 2008. Il Rischio Idrogeologico in Italia.

Mirus, B.B., Ebel, B.A., Loague, K., Wemple, B.C., 2007. Simulated effect of a forest road on near-surface hydrologic response: Redux. Earth Surf. Process. Landforms 32, 126–142. https://doi.org/10.1002/esp.1387

Mitchell, J.K., 1976. Fundamentals of soil behavior. John Wiley and Sons, New York.

Montgomery, D.R., Dietrich, W.E., 1994. A physically based model for the topographic control on shallow landsliding. Water Resour. Res. https://doi.org/10.1029/93WR02979

Montgomery, D.R., Dietrich, W.E., Torres, R., Anderson, S.P., Heffner, J.T., Loague, K., 1997. Hydrologic response of a steep, unchanneled valley to natural and applied rainfall. Water Resour. Res. https://doi.org/10.1029/96WR02985

Montrasio, L., 2000. Stability analysis of soil slip, in: Brebbia, C.A. (Ed.), Proceedings of International Conference “Risk 2000.” Wit Press, Southampton.

Montrasio, L., Valentino, R., Losi, G.L., 2011. Towards a real-time susceptibility assessment of rainfall-induced shallow landslides on a regional scale. Nat. Hazards Earth Syst. Sci. 11, 1927–1947. https://doi.org/10.5194/nhess-11-1927-2011

Motamedi, M., Liang, R.Y., 2013. Probabilistic landslide hazard assessment using Copula modeling technique. Landslides 565–573. https://doi.org/10.1007/s10346-013-0399-z

Muzylo, A., Llorens, P., Valente, F., Keizer, J.J., Domingo, F., Gash, J.H.C., 2009. A review of rainfall interception modelling. J. Hydrol. https://doi.org/10.1016/j.jhydrol.2009.02.058

National Institute of Statistics - ISTAT, 2014. Population by age, sex and marital status on 1 January 2014 [WWW Document]. URL https://www.istat.it/it/archivio/132669

Nilsen, T., Turner, B., 1975. Influence of rainfall and ancient landslide deposits on recent landslides (1950- 1971) in urban areas of Contra Costa County, California.

O’Loughlin, E., 1986. Prediction of surface saturation zones in natural catchments by topographic analysis. Water Resour. Res. 22, 794–804.

O’Loughlin, E.M., 1981. Saturation regions in catchments and their relations to soil and topographic properties. J. Hydrol. https://doi.org/10.1016/0022-1694(81)90003-2

Onodera, T., Yoshinaka, R., Kazama, H., 1974. Slope failures caused by heavy rainfall in Japan, in: 2nd International Congress of the International Association of Engineering Geology. Sao Paulo, Brazil, pp. 11:1–10.

Pack, R.T., Tarborton, D., Goodwin, C., 1998. The SINMAP Approach to Terrain Stability Mapping, in: 8th Congress of the International Association of Engineering Geology and the Environment. A.A. Balkema, Vancouver, British Columbia, Canada, pp. 1157–1165.

Papa, M.N., Medina, V., Ciervo, F., Bateman, A., 2013. Derivation of critical rainfall thresholds for shallow landslides as a tool for debris flow early warning systems. Hydrol. Earth Syst. Sci. 17, 4095–4107. https://doi.org/10.5194/hess-17-4095-2013

Pasuto, A., Silvano, S., 1998. Rainfall as a trigger of shallow mass movements. A case study in the Dolomites, Italy. Environ. Geol. 35, 184–189. https://doi.org/10.1007/s002540050304

Pereira, S., Zêzere, J.L., Bateira, C., 2012. Technical Note: Assessing predictive capacity and conditional independence of landslide predisposing factors for shallow landslide susceptibility models. Nat. Hazards Earth Syst. Sci. 12, 979–988. https://doi.org/10.5194/nhess-12-979-2012

Peruccacci, S., Brunetti, M.T., Luciani, S., Vennari, C., Guzzetti, F., 2012. Lithological and seasonal control on rainfall thresholds for the possible initiation of landslides in central Italy. Geomorphology 139–140, 79–90. https://doi.org/10.1016/j.geomorph.2011.10.005

Picarelli, L., Vinale, F., 2007. Analisi della bibliografia. Napoli.

Pierson, T.C., 1983. Soil Pipes and Slope Stability. Q. J. Eng. Geol. Hydrogeol. 16, 1–11. https://doi.org/10.1144/GSL.QJEG.1983.016.01.01

Pignone, S., Del Maschio, L., Gozza, G., Pizziolo, M., 2005. Determinazione di soglie pluviometriche per innesco di fenomeni franosi nell'Appennino settentrionale. Bologna, Italy.

Ponziani, F., Pandolfo, C., Stelluti, M., Berni, N., Brocca, L., Moramarco, T., 2012. Assessment of rainfall thresholds and soil moisture modeling for operational hydrogeological risk prevention in the Umbria region (central Italy). Landslides 9, 229–237. https://doi.org/10.1007/s10346-011-0287-3

Principi, M., Bettucci, C., Carotti, A., 2007. Analisi del dissesto da frana nelle

Marche, in: Rapporto Sulle Frane in Italia. Il Progetto IFFI: Metodologia, Risultati e Rapporti Regionali. APAT - Dipartimento Difesa del Suolo, Servizio Geologico d'Italia, Roma, pp. 425–444.

Quintavalla, C., Montrasio, L., Valentino, R., 2009. Utilizzo di osservazioni satellitari per la stima del grado di saturazione di terreni superficiali, in: Incontro Annuale Dei Ricercatori Di Geotecnica 2009 - IARG 2009. Roma, p. 6.

Raia, S., Alvioli, M., Rossi, M., Baum, R.L., Godt, J.W., Guzzetti, F., 2014. Improving predictive power of physically based rainfall-induced shallow landslide models: a probabilistic approach. Geosci. Model Dev. 7, 495–514. https://doi.org/10.5194/gmd-7-495-2014

Rappelli, F., 2008. Definizione delle soglie pluviometriche d'innesco di frane superficiali e colate torrentizie: accorpamento per aree omogenee, IRER, Milano. Milano. https://doi.org/Codice IReR: 2007B023

Regionale, S., Protezione, D.I., Ufficiale, B., Regione, D., Marche, N., 2001. L.R. 11 Dicembre 2001, n. 32 "Sistema regionale di protezione civile."

Regione Marche - Autorità di Bacino Regionale, 2004. Piano stralcio di bacino per l'Assetto Idrogeologico dei bacini di rilievo regionale (PAI) Relazione.

Reichenbach, P., Cardinali, M., De Vita, P., Guzzetti, F., 1998. Regional hydrological thresholds for landslides and floods in the Tiber River Basin (central Italy). Environ. Geol. 35, 146–159. https://doi.org/10.1007/s002540050301

Reid, M.E., 1994. A pore-pressure diffusion model for estimating landslide-inducing rainfall. J. Geol. 102, 709–717.

Reid, M.E., La Husen, R.G., Iverson, R.M., 1997. Debris-flow initiation experiments using diverse hydrologic triggers, in: First International Conference on Debris- Flow Hazards Mitigation: Mechanics, Prediction, and Assessment: ASCE. pp. 1–11.

Rianna, G., Pagano, L., Urciuoli, G., 2014. Rainfall patterns triggering shallow flowslides in pyroclastic soils. Eng. Geol. 174, 22–35. https://doi.org/10.1016/j.enggeo.2014.03.004

Richards, L.A., 1931. Capillary conduction of liquids through porous mediums. J. Appl. Phys. 1, 318–333. https://doi.org/10.1063/1.1745010

Rigon, R., Bertoldi, G., Over, T.M., 2006. GEOtop: A Distributed Hydrological Model with Coupled Water and Energy Budgets. J.

Hydrometeorol. https://doi.org/10.1175/JHM497.1

Rinaldi, M., Casagli, N., 1999. Stability of streambanks formed in partially saturated soils and effects of negative pore water pressures: the Sieve River (Italy). Geomorphology 26, 253–277. https://doi.org/10.1016/S0169-555X(98)00069-5

Rinaldi, M., Casagli, N., Dapporto, S., Gargini, A., 2004. Monitoring and modelling of pore water pressure changes and riverbank stability during flow events. Earth Surf. Process. Landforms 29, 237–254. https://doi.org/10.1002/esp.1042

Rossi, G., Catani, F., Leoni, L., Segoni, S., Tofani, V., 2013. HIRESSS: a physically based slope stability simulator for HPC applications. Nat. Hazards Earth Syst. Sci. 13, 151–166. https://doi.org/10.5194/nhess-13-151-2013

Rubin, J., Steinhardt, R., 1963. Soil Water Relations During Rain Infiltration: I. Theory1, 2. Soil Sci. Soc. Am. J. https://doi.org/10.2136/sssaj1963.03615995002700030011x

Salciarini, D., Godt, J.W., Savage, W.Z., Conversini, P., Baum, R.L., Michael, J.A., 2006. Modeling regional initiation of rainfall-induced shallow landslides in the eastern Umbria Region of central Italy. Landslides 3, 181–194. https://doi.org/10.1007/s10346-006-0037-0

Salciarini, D., Tamagnini, C., Ponziani, F., Berni, N., 2013. Defining Physically-Based Rainfall Thresholds for Early Warning Systems, in: Margottini, C., Canuti, P., Sassa, K. (Eds.), Landslide Science and Practice. pp. 651–657. https://doi.org/10.1007/978-3-642-31445-2_85

Sangelantoni, L., Gioia, E., Marincioni, F., 2018. Impact of climate change on landslides frequency: the Esino river basin case study (Central Italy). Nat. Hazards 93, 849–884. https://doi.org/10.1007/s11069-018-3328-6

Savage, W.Z., Godt, J.W., Baum, R.L., 2004. Modeling time dependent aerial slope stability, in: Lacerda, W.A., Erlich, M., Fontoura, S.A.B., Sayao, A.S.F. (Eds.), Landslides-Evaluation and Stabilization, International Symposium on Landslides, Vol. 1. A. A. Balkema, London, pp. 23–36.

Savage, W.Z., Godt, J.W., Baum, R.L., 2003. A model for spatially and temporally distributed shallow landslide initiation by rainfall infiltration, in: Rickenmann, D., Chen, C. (Eds.), Debris-Flow Hazards Mitigation: Mechanics, Prediction and Assessment. Millpress, Rotterdam, Netherlands, pp. 179–187.

Segoni, S., Leoni, L., Benedetti, a. I., Catani, F., Righini, G., Falorni, G., Gabellani, S., Rudari, R., Silvestro, F., Rebora, N., 2009. Towards a definition of a real-time forecasting network for rainfall induced shallow landslides. Nat. Hazards Earth Syst. Sci. 9, 2119–2133. https://doi.org/10.5194/nhess-9-2119-2009

Sengupta, A., Gupta, S., Anbarasu, K., 2010. Rainfall thresholds for the initiation of landslide at Lanta Khola in north Sikkim, India. Nat. Hazards 52, 31–42. https://doi.org/10.1007/s11069-009-9352-9

Sidle, R.C., Ochiai, H., 2006. Landslides: Processes, Prediction, and Land Use, Water Resources Monograph. American Geophysical Union Water Resources Monograph 18, Washington, D. C. https://doi.org/10.1029/WM018

Sidle, R.C., Swanston, D.N., 1982. Analysis of a small debris slide in coastal Alaska. Can. Geotech. J. https://doi.org/10.1139/t82-018

Sidle, R.C., Tsuboyama, Y., Noguchi, S., Hosoda, I., Fujieda, M., Shimizu, T., 2000. Stormflow generation in steep forested headwaters: A linked hydrogeomorphic paradigm. Hydrol. Process. 14, 369–385. https://doi.org/10.1002/(SICI)1099-1085(20000228)14:3<369::AID-HYP943>3.0.CO;2-P

Simoni, A., Berti, M., Generali, M., Elmi, C., Ghirotti, M., 2004. Preliminary result from pore pressure monitoring on an unstable clay slope. Eng. Geol. 73, 117–128. https://doi.org/10.1016/j.enggeo.2003.12.004

Simoni, S., Zanotti, F., Bertoldi, G., Rigon, R., 2008. Modelling the probability of occurrence of shallow landslides and channelized debris flows using GEOtop-FS. Hydrol. Process. 22, 532–545. https://doi.org/10.1002/hyp.6886

Skempton, A., DeLory, F., 1957. Stability of natural slopes in London clay, vol 2, in: 4th International Conference on Soil Mechanics and Foundation Engineering. London, pp. 378–381.

Sorriso-Valvo, M., Agnesi, V., Gullà, G., Merende, L., Antronico, L., Di Maggio, C., Filice, E., Petrucci, O., Tansi, C., 1994. Temporal and spatial occurrence of landsliding and correlation with precipitation time series in Montaldo Uffugo (Calabria) and Imera (Sicilia) areas, in: Casale, R., Fantechi, R., Flageollet, J. (Eds.), Temporal Occurrence and Forecasting of Landslides in the European Community. pp. 825–869.

Srivastava, R., Yeh, T.C.J., 1991. Analytical solutions for one dimensional, transient infiltration toward the water table in homogeneous and layered soils. Water Resour. Res. 27, 753–762.

https://doi.org/10.1029/90WR02772.

Staley, D.M., Kean, J.W., Cannon, S.H., Schmidt, K.M., Laber, J.L., 2013. Objective definition of rainfall intensity–duration thresholds for the initiation of post-fire debris flows in southern California. Landslides 10, 547–562. https://doi.org/10.1007/s10346-012-0341-9

Strudley, M., Green, T., Ascoughii II, J., 2008. Tillage effects on soil hydraulic properties in space and time: State of the science. Soil Tillage Res. 99, 4–48. https://doi.org/10.1016/j.still.2008.01.007

Tacher, L., Bonnard, C., Laloui, L., Parriaux, A., n.d. Modelling the behaviour of a large landslide with respect to hydrogeological and geomechanical parameter heterogeneity. Landslides 2, 3–14. https://doi.org/10.1007/s10346-004-0038-9

Tan, C., Ku, C., Chi, S., Chen, Y., Fei, L., Lee, J., Su, T., 2008. Assessment of regional rainfall-induced landslides using 3S-based hydro-geological model. Landslides Eng. Slopes 1639–1645. https://doi.org/10.1201/9780203885284-c225

Tao, J., Barros, A.P., 2014. Coupled prediction of flood response and debris flow initiation during warm- and cold-season events in the Southern Appalachians, USA. Hydrol. Earth Syst. Sci. 18, 367–388. https://doi.org/10.5194/hess-18-367-2014

Taylor, D.W., 1948. Fundamentals of Soil Mechanics, Soil Science. John Wiley and Sons, New York. https://doi.org/10.1097/00010694-194808000-00008

Terlien, M., 1998. The determination of statistical and deterministic hydrological landslide-triggering thresholds. Environ. Geol. 35, 124–130. https://doi.org/10.1007/s002540050299

Terlien, M., 1996. Modelling spatial andtemporal variations in rainfall-triggered landslides. ITC Publ. 32, Enschede, Netherlands.

Terzaghi, K., 1943. Theoretical soil mechanics, Géotechnique. John Wiley and Sons, New York.

Tiranti, D., Rabuffetti, D., Salandin, A., Tararbra, M., 2013. Development of a new translational and rotational slides prediction model in Langhe hills (north-western Italy) and its application to the 2011 March landslide event. Landslides 10, 121–138. https://doi.org/10.1007/s10346-012-0319-7

Tofani, V., Dapporto, S., Vannocci, P., Casagli, N., 2006. Infiltration, seepage and slope instability mechanisms during the 20–21 November 2000 rainstorm in Tuscany, central Italy. Nat. Hazards Earth Syst. Sci. 6, 1025–1033. https://doi.org/10.5194/nhess-6-1025-2006

Torres, R., Dietrich, W.E., Montgomery, D.R., Anderson, S.P., Loague, K., 1998. Unsaturated zone processes and the hydrologic response of a steep, unchanneled catchment. Water Resour. Res. https://doi.org/10.1029/98WR01140

U.S. Geological Survey, 2004. Landslide types and processes, Fact Sheet 2004-3072 (No. Fact Sheet 2004-3072). U.S. Geological Survey.

Uchida, T., Kosugi, K., Mizuyama, T., 2001. Effects of pipeflow on hydrological process and its relation to landslide: A review of pipeflow studies in forested headwater catchments. Hydrol. Process. 15, 2151–2174. https://doi.org/10.1002/hyp.281

UNISDR, 2010. Early warning practices can save lives: selected examples 67.

USSCS - U.S. Soil Conservation Service, 1964. Section 4: Hydrology, in: SCS National Engineering Handbook. USDA Soil Conservation Service, Washington, D.C.

Van Asch, T.W.J., Buma, J.T., 1997. Modelling Groundwater Fluctuations and the Frequency of Movement of a Landslide in the Terres Noires Region of Barcellonnette (France). Earth Surf. Process. Landforms 22, 131–141. https://doi.org/10.1002/(SICI)1096-9837(199702)22:2<131::AID-ESP679>3.0.CO;2-J

Van Beek, L.P.H., Van Asch, T.W.J., 2004. Regional assessment of the effects of land-use change on landslide hazard by means of physically based modelling. Nat. Hazards 31, 289–304.

Van Genuchten, M.T., 1980. A Closed-form Equation for Predicting the Hydraulic Conductivity of Unsaturated Soils1. Soil Sci. Soc. Am. J. https://doi.org/10.2136/sssaj1980.03615995004400050002x

Vanapalli, S.K., Fredlund, D.G., 2000. Comparison of different procedures to predict unsaturated soil shear strength, in: Shackelford, C.D., Houston, S.L., Chang, N.-Y. (Eds.), Advances in Unsaturated Geotechnics (Proceedings of Geo-Denver 2000, Denver, Colo., August 5-8, 2000). Reston, Virginia.

Varnes, D.J., 1984. Landslide hazard zonation: a review of principles and practice. Nat. Hazards.

Varnes, D.J., 1978. Slope movement types and processes, in: Schuster, R.L., Krizek, R.J. (Eds.), Special Report 176: Landslides: Analysis and Control. Washington, DC, pp. 11–33.

Vennari, C., Gariano, S.L., Antronico, L., Brunetti, M.T., Iovine, G., Peruccacci, S., Terranova, O., Guzzetti, F., 2014. Rainfall thresholds for shallow landslide occurrence in Calabria, southern Italy. Nat. Hazards Earth Syst. Sci. 14, 317–330. https://doi.org/10.5194/nhess-14-317-2014

Vieira, B.C., Fernandes, N.F., Filho, O. a., 2010. Shallow landslide prediction in the Serra do Mar, São Paulo, Brazil. Nat. Hazards Earth Syst. Sci. 10, 1829–1837. https://doi.org/10.5194/nhess-10-1829-2010

Von Ruette, J., Lehmann, P., Or, D., 2013. Rainfall-triggered shallow landslides at catchment scale: Threshold mechanics-based modeling for abruptness and localization. Water Resour. Res. 49, 6266–6285. https://doi.org/10.1002/wrcr.20418

Walker, B., 2007. Rainfall Data Analysis at Newport and the Relationship to Landsliding in Pittwater. Aust. Geomech. 42, 197–212.

Wasowski, J., Lamanna, C., Casarano, D., 2010. Influence of land-use change and precipitation patterns on landslide activity in the Daunia Apennines, Italy. Q. J. Eng. Geol. Hydrogeol. 43, 387–401. https://doi.org/10.1144/1470-9236/08-101

Weyman, D.R., 1973. Measurements of the downslope flow of water in a soil. J. Hydrol. 20, 267–288.

White, I.D., Mottershead, D.N., Harrison, J.J., 1996. Environmental Systems, Second Edi. ed. Chapman & Hall, London.

White, J.A., Singham, D.I., 2012. Slope stability assessment using stochastic rainfall simulation, in: Procedia Computer Science. pp. 699–706. https://doi.org/10.1016/j.procs.2012.04.075

Wieczorek, G., 1996. Landslide triggering mechanisms, in: Turner, A., Schuster, R. (Eds.), Landslides, Investigation and Mitigation. National Academy Press, Washington, DC, pp. 76–90.

Wieczorek, G., Guzzetti, F., 2000. A review of rainfall thresholds for triggering landslides, in: Claps, P., Siccardi, F. (Eds.), Mediterranean Storms, Proceedings of the EGS Plinius Conference ’99. Maratea, Italy, pp. 404–414.

Wieczorek, G.F., 1987. Effect of rainfall intensity and duration on debris flows in central Santa Cruz Mountains., in: Costa, J., Wieczorek, G. (Eds.), Debris Flow/Avalanches: Process, Recognition, and Mitigation. Geological Society of America, Reviews in Engineering Geology, p. 93.

Wieczorek, G.F., Morgan, B.A., Campbell, R.H., 2000. Debris flow hazards in the Blue Ridge of Central Virginia. Environ. Eng. Geosci. 6, 3–23.

Wilcock, P.R., Schmidt, J.C., Wolman, M.G., Dietrich, W.E., Doyle, M.W., Grant, G.E., Iverson, R.M., David, R., Pierson, T.C., Schilling, S.P., Wilson, R.C., 2003. When Models Meet Managers : Examples from Geomorphology. Geophys. Monogr. Ser. 1–14. https://doi.org/10.1029/135GM03.

Wilks, D.S., 2011. Statistical methods in the atmospheric sciences, Third Edit. ed. Academic Press. https://doi.org/10.1002/1521-3773(20010316)40:6<9823::AID-ANIE9823>3.3.CO;2-C

Wilson, R., Jayko, A., 1997. Preliminary maps showing rainfall thresholds for debris-flow activity, San Francisco Bay Region, California. https://doi.org/Open-File Report 97-745 F

Wilson, R.C., 2000. Climatic variations in rainfall thresholds for debris-flows activity, in: P. Claps, Siccardi, F. (Eds.), Plinius Conference on Mediterranean Storms. Maratea, Italy, pp. 415–424.

Wilson, R.C., 1989. Rainstorm, pore pressures, and debris flows: a theoretical framework. Publ. Inl. Geol. Soc. 2, 101–117.

Wilson, R.C., Wieczorek, G.F., 1995. Rainfall thresholds for the initiation of debris flows at La Honda, California. Environ. Eng. Geosc. 1, 11–27.

Wu, W., Sidle, R.C., 1995. A distributed slope stability model for steep forested basins. Water Resour. Res. https://doi.org/10.1029/95WR01136

Zêzere, J., Trigo, R., Trigo, I., 2005. Shallow and deep landslides induced by rainfall in the Lisbon region (Portugal): assessment of relationships with the North Atlantic Oscillation. Nat. Hazards Earth Syst. Sci. 5, 331–344. https://doi.org/SRef-ID: 1684-9981/nhess/2005-5-331 European Geosciences Union

Zêzere, J.L., Trigo, R.M., Trigo, I.F., 2005. Shallow and deep landslides induced by rainfall in the Lisbon region (Portugal): Assessment of relationships with the North Atlantic Oscillation. Nat. Hazards Earth Syst. Sci. 5, 331–344. https://doi.org/10.5194/nhess-5-331-2005

Zhang, L.L., Zhang, J., Zhang, L.M., Tang, W.H., 2011. Stability analysis of rainfall- induced slope failure : a review. Proc. ICE Geotech. Eng. 164, 299–316.

Zimmermann, U., Münnich, K.O., Roether, W., Kreutz, W., Schubach, K., Siegel, O., 1966. Tracers determine movement of soil moisture and evapotranspiration. Science 152, 346–347. https://doi.org/10.1126/science.152.3720.346

Modeling landslide hazard is among the forecast activities of the Civil Protection system. Usually, scientific literature that aims to determine rainfall thresholds for the possible occurrence of landslides, tends to rely on two main separate approaches: empirical and physical models. This research contributes to such debate by adopting both the approaches, after integrating some of the each other features. This novel methodology has been applied to the landslides affecting the eastward Esino River Valley, located in the Marche region (central Italy). Post-orogenic quaternary sediments, with approximatively similar hydrogeological properties and prone to rainfall-induced shallow landslides, characterize this 550 km2 wide area.

This volume is divided in four sections focusing on: i) the validation of the correlation between historical landslides and rainfall series; ii) the application of empirical models, namely the cumulative event – duration, the maximum intensity – duration, the mean intensity – duration, and the Bayesian methods; iii) the application of the US Geological Survey's Transient Rainfall Infiltration and Grid-based Regional Slope-stability (TRIGRS) physical model; iv) the testing of all the above models, during a rainfall event that affected the study area on 2-4 May 2014 and triggered several landslides.

Results of this research are proposed as possible decision support tools for landslide warning.

Eleonora Gioia is a research fellow and lecturer at the Università Politecnica delle Marche (Ancona, Italy). She holds a PhD in Civil and Environmental Protection at UNIVPM, for which completion she collaborated with the Civil Protection of the Marche Region and the United States Geological Survey (USGS) in Golden Colorado (USA). She worked on the European project "Landslide", with the University of Camerino, to develop landslide forecasting models, and on the European projects LIFE "PRIMES" and Interreg Italy-Croatia "RESPONSe", with UNIVPM. She is currently working on the analysis of the perception and responses of local communities to climate change impacts.

Fausto Marincioni is an associate professor at the Università Politecnica delle Marche (Ancona, Italy), where he teaches and carries out research on disaster risk reduction. He holds a Ph.D. in geography from the University of Massachusetts (USA) and is an editor of the International Journal of Disaster Risk Reduction. Previously, he has worked with the United States Geological Survey, in Woods Hole, Massachusetts, and taught human and environmental geography at Long Island University (LIU Post) in New York.

Maurizio Ferretti is a geologist, graduated from the University of Urbino (Italy). He is an official of the Marche Region Civil Protection for which, over the years, he managed and directed several complex organizational structures including the Functional Center and the Emergency Operations Room. For more than a decade he has been Adjunct Professor at the Università Politecnica delle Marche (Ancona, Italy). He has also been a member of the Italian National Operational Committee of Civil Protection. He is currently directing the service of the Single European Emergency Number NUE 112 for the Marche and Umbria Regions.

ISBN 979-12-80064-11-0

Il Sileno Edizioni

Geographies of the Anthropocene